



**Université de Strasbourg (UdS)**

**Discipline: Physique des Polymères**

**Thèse de doctorat de l'UdS**

# **Improving the scratch resistance of PMMA**

**MUHAMMAD Mansha**

**Thèse soutenue publiquement, le 29 Septembre 2011**



## **Membres du jury**

<b>Rapporteur</b>	<b>: Mme Noëlle Billon</b> Professeur, CEMEF, Ecole des Mines de Paris, Paris
<b>Rapporteur</b>	<b>: M. Chateauinois Antoine</b> Directeur de Recherches, Ecole Supérieure de Physique et Chimie industrielles (E.S.P.C.I), Paris
<b>Examineur</b>	<b>: M. Pierre Gerard</b> Ingénieur R&D, Laboratoire Mécanique des Polymères et Nanomatériaux au Centre de Recherches de Lacq, Arkema, Lacq
<b>Examineur</b>	<b>: M. Philippe Mesini</b> Chargé de Recherche, ICS (UPR 22), Strasbourg
<b>Directeur de thèse</b>	<b>: Mr. Christian Gauthier</b> Professeur UdS, ICS (UPR 22), Strasbourg
<b>Membre invité</b>	<b>: M. Hervé Pelletier</b> Maitre de Conference, INSA, Strasbourg



To my parents

*Who always encouraged and facilitated me thorough out my academic carrier although they could not get proper education even at primary level.*

To my teachers

*(from my primary school teachers to PhD supervisor Pr Christian Gauthier)*

*Whose superb contribution and guidance to transform me from a child to a doctor cannot be expressed truely in words.*





## **Acknowledgments**

Taking first foot steps towards presenting new understandings is a worthy experience. The dream of this lifetime experience cannot be seen without the help and support of some earnest people. I would like to express my deepest gratitude to the project director Pr. Christian Gauthier for his full support, precious advices and great contribution. Indeed, I feel honoured to work under his learned supervision. His in time availability throughout my research work is a fascination that i will never forget. His unsurpassed knowledge, piercing insight and taste of good research enabled or honestly speaking, forced me to develop an intellectual understanding of the subject. Of course, the responsibility is entirely my own for any errors and inadequacies that remained in this work. It will not be wrong if I admit that the reward goes totally to him for the successful completion of the research work. I don't know how much difficult he found working with an average student like me but I really enjoyed his supervision and learned a lot of things covering many aspects of life. I will remember extensively his perpetual encouragement and motivation on both an academic and a personal level without which this work would not be possible. The free hand given by him to manage the lengthened hospitalisation of my son for the bone marrow transplantation is a worthy aspect that I cannot ignore.

I am extremely grateful to all of the jury members Prof. Noëlle Billon, Dr. Antoine Chateauinois, Dr. Pierre Gerard, Dr. Philippe Mesini and Dr. Hervé Pelletier for dedicating their valuable time and energies for this dissertation and taking interest in evaluating this work. The critical observations, comments and suggestions from all of jury members are priceless. Their contribution will remain an honour for me.

I owe my sincere thanks to Dr. Robert Schirrer, Mr. Pierre Gerard, Dr. Hervé Pelletier, Mr. Damien Favier, Dr. Vincent Le Houerou, and Dr. Anne-Lise Durier for their generous help and fruitful suggestions during my thesis. Their consistent efforts and urge for in depth knowledge are precious trait of their personality and without doubt, they remained a source of encouragement for me. The excellent time i passed in their wise company is surely a valuable part of my life especially the presence of Damien Favier to resolve the various problems faced during experimental work cannot be ignored. I cannot quote a single problem faced during my experimentation whom he hasn't a solution.

I would also like to express my gratitude to Pr. Yves Holl, Dr. Pascal Marie, Dr Christian Blanck, Dr. Anne Rubin and all others for sharing their knowledge and extending their assistance in completing this task.

I owe my appreciation to the humble favour and cooperation shown by Mohamad Alchikh, Chauvelot Jean-Marc, Katia Bruzzone Herbener, Thibaud Chatel, Magali Meyer, Paule Vannson, Sisouk Sivongsay and Mathieu Solar. Despite of my secluding personality, they forged good relationship with me. I would never forget their kind, cordial and warm hospitality throughout my stay in the laboratory. I appreciate and offer my regards and blessings to my Pakistani friends in France and back at home whom I found with me in thin and thick.

I would like to acknowledge the financial assistance provided by Higher Education Commission (HEC) of Pakistan in collaboration with Government of France by awarding me a postgraduate scholarship through an Overseas Research Scholarship Program and that provided by Arkema, Lacq, France. My integration in the Institute Charles Sadron offered me a great opportunity to acquire advance technical knowledge as well as to polish my skills.

Finally, I am indebted to my parents for their unconditional love and support. I would also like to express my heartfelt gratitude, love and admiration to my wife and children for their perseverance, patience, incredible support and sacrifice throughout my PhD studies without which I would not have made it through smoothly. Above all, thanks to Almighty Allah the most merciful the most gracious.

Strasbourg, October 2011

## Abstract

Industrial use of polymers ranges across a broad field of structural, mechanical, electrical and optical applications [1, 2]. Scratch durability of polymer surfaces and coatings is becoming critical for the increasing use of these materials in new applications, replacing other materials with harder surfaces [3]. An understanding of abrasion resistance and the associated surface deformation mechanisms is of primary importance in the material engineering and design of many important industrial components undergoing wear and abrasion [4]. There is a lot of work available regarding various aspects of general mechanical properties of the polymers. The effect of application of different additives on the friction of various materials like films and different parts of various mechanical assemblies has been also understood. On the other hand, there are many researchers who investigated in detail various aspects of friction at appropriate scales. A large number of authors have worked on scratch and nano-indentation of various polymer surfaces. It is well understood that lower friction coefficient and lower modulus is required to increase the scratch resistance of the polymers. Moreover, the effect of addition of various plasticizers/additives, fillers and different types of fibres on overall mechanical properties of various polymers have been also investigated in detail. But the research on the development of the methods to reduce the friction coefficient of the polymers is still lacking. In addition, the effect of various additives on the friction of polymers in order to improve their scratch resistance is yet to be studied. These important issues are addressed in this report.

The manuscript consists of three sections. The first section gives the theoretical background about the appropriate aspects of the scratching process of materials with an emphasis on scratching of polymers. First chapter gives a general idea about the diverse aspects of relevant mechanical properties of materials highlighting the surface properties. It describes also the different aspects of PMMA and that of plasticization of polymers. Second chapter deals with various features of the scratching and sliding process in detail. Third chapter describes various scales and types of friction along with different factors affecting the friction coefficient.

Next section provides different experimental and simulation results for the modification of surface and mechanical properties of PMMA. It starts with the depiction of the effects of various plasticizers on different surface and bulk mechanical properties of PMMA. The experimental work is terminated with an analysis of the experimental results by modelling the scratch behaviour of PMMA by numerical simulation using finite element method. Last section deals with the general discussion on experimental and simulation results along with the concluding remarks and future prospective.



# Summing up the work in French

## I Résumé court

Les polymères deviennent attrayants pour un nombre croissant d'applications industrielles. Leur faible coût, la facilité et la simplicité de fabrication et de transformation, leur faible masse volumique ainsi que l'aspect « fini » qu'ils fournissent sur toute surface ont amplifié leurs utilisations. Cependant, leur durée de vie est souvent réduite par leurs propriétés mécaniques faibles. L'abrasion et l'usure sont la cause de la perte de leurs performances optiques et tribologiques. Les surfaces de matériaux polymères sont surtout sensibles aux rayures, qui entravent leurs utilisations dans les dispositifs optiques de hautes performances. Dans d'autres applications, ces matériaux sont utilisés pour les pièces mécaniques où les propriétés de frottement sont importantes. C'est pourquoi il y a un besoin fort pour rechercher la meilleure résistance à la rayure pour des applications où l'aspect esthétique ou optique est important. Différents processus physico-chimiques (techniques de plantation d'ion...) généralement appliqués pour améliorer les propriétés de surface ne peuvent pas être utilisés sur des polymères transparents comme le PMMA en raison des pertes de transparence engendrés.

L'amélioration de la résistance à la rayure va être étudiée dans sa relation avec la diminution du coefficient de frottement, en analysant le bénéfice apporté par différents plastifiants. Il sera prouvé que cette amélioration du comportement surfacique n'est pas acquise au détriment du comportement volumique. Le travail expérimental est complété par une analyse utilisant la modélisation du comportement à la rayure à l'aide de la simulation par la méthode des éléments finis.

La première partie du mémoire présente l'analyse bibliographique. Le premier chapitre donne une introduction sur les propriétés volumiques et surfaciques qui contrôlent le comportement à la rayure. La fin du premier chapitre présente les effets des plastifiants sur les propriétés volumiques et lubrifiantes. Le deuxième chapitre traite plus précisément des acquis sur l'analyse du comportement à la rayure sur surfaces de polymères. Le troisième chapitre présente l'analyse du frottement sur surfaces de polymères.

La deuxième partie du mémoire présente les travaux réalisés, dans un premier temps les mesures des propriétés volumiques et le comportement surfacique des échantillons PMMA et PMMA avec plastifiants. Le chapitre suivant analyse par simulation numérique l'influence du coefficient de frottement sur le niveau de déformation plastique lors du contact, puis les résultats de simulation sont comparés avec les résultats expérimentaux. Une discussion et des perspectives sont données en fin de cette mémoire.

## II Travaux expérimentaux

### II.I Matériaux testés

L'étude de l'amélioration du comportement à la rayure d'un PMMA par ajout de plastifiant a dans un premier temps été centrée sur l'utilisation de Crodamide et de PEG. Le PMMA étudié est un grade standard (V825), ayant un poids moléculaire de 100K, fourni par Arkema sous forme de plaques de 3 mm d'épaisseur. L'effet du pourcentage de ces plastifiants a été étudié en testant les propriétés surfaciques et volumiques d'échantillons contenant 0, 1, 3, et 5 % de ces plastifiants. En raison de la compatibilité avec la plupart de polymères, les amides d'acides gras sont très utiles

pour surmonter les problèmes de glissement et jouer le rôle d'antibloquant lors de la mise en œuvre des polymères [60, 81, 82]. Le PEG est reconnu comme un agent lubrifiant interne et est très utilisé en raison de son coût bas [60]. Le Crodamide, également un amide d'acide gras, a une stabilité thermique supérieure qui permet une utilisation à des températures plus élevées [82, 83]. Le PEG [(C<sub>2</sub>H<sub>4</sub>O) nH<sub>2</sub>O] employé a une masse Mol. Wt. 3350 et a été acheté chez Sigma-Aldrich. Le Crodamide utilisé est le Crodamide-212 (stearyl erucamide, C<sub>40</sub>H<sub>79</sub>N<sub>0</sub>) de masse Mol. Wt. 590 et a été acheté chez Croda Chemicals.

Trois autres plastifiants ont été étudiés, associés à un grade standard de PMMA: l'Erucamide, le Behenamide et le Stearamide. Ces matériaux ont été polymérisés dans le laboratoire. Comme pour les autres amides d'acides gras, l'Erucamide est utilisé pour sa haute résistance à la chaleur et sa stabilité de couleur. Pour les bas taux de concentration, l'Erucamide commence à jouer sa fonction de plastifiant sans perturber les autres caractéristiques physiques du polymère [84]. L'influence de l'Erucamide [C<sub>22</sub>H<sub>43</sub>NO, Mol. Wt. 337,59 g/mol] a été étudiée en testant des échantillons contenant 0, 0,05, 0,1, 0,15 et 0,2 % en masse d'Erucamide. Autre amide d'acide gras, le Behenamide est classiquement utilisé pour diminuer l'abrasion et le frottement sur les surfaces de polymère [60, 85]. Des échantillons de PMMA contenant différents pourcentages (0, 0,05 et 0,1 % en masse) de Behenamide [CH<sub>3</sub>(CH<sub>2</sub>)<sub>20</sub>CONH<sub>2</sub>, Mol. Wt. 339,6 g/mol] ont été étudiés. Le dernier plastifiant étudié est le Stearamide, utilisé pour améliorer la processabilité, diminuer l'abrasivité et le frottement des surfaces de polymère [60]. Des échantillons contenant 0,1, et 0,3 % en masse de Stearamide [C<sub>18</sub>H<sub>37</sub>NO, Mol. Wt. 283,5 g/mol] ont été testés. Un échantillon contenant 0,1% de Behenamide et 0,2% d'Erucamide a aussi été testé pour examiner la possible synergie entre les deux plastifiants. Les pourcentages de plastifiants ont été limités en raison des problèmes de solubilité dans la solution de monomère de MMA à température ambiante. Ces limites sont celles également données dans la littérature. Les trois plastifiants et les monomères MMA [C<sub>5</sub>H<sub>8</sub>O<sub>2</sub>, Mol. Wt. 100,12 g/mol] ont été achetés de Sigma-Aldrich.

L'effet d'un additif (Crodamide-212 et Crodamide-Er ou Erucamide raffiné) sur les propriétés de surface et volumique des deux grades différents de PMMA (deux catégories standards V825 et HT121) a été étudié. Ils ont été fournis par Arkema sous forme des plaques de 3 mm d'épaisseur. Le PMMA HT121 a la plus grande stabilité thermique (comparé au PMMA V825). Sa température de transition vitreuse est 15°C plus haut que celle du PMMA V825. De plus, HT121 a le groupe fonctionnel acide à la chaîne de polymère principale. Enfin, l'influence d'une réticulation sur le comportement surfacique a également été étudiée en comparant un PMMA non-réticulé de degré standard (496), et un PMMA réticulé (495) ayant 0,6 % en masse de buthanediol diméthacrylate (BDMA) comme un agent réticulation. Ces deux échantillons fournis par Arkéma contenaient 10% de poly (n-butyl acrylate) (PBA) nano-structuré comme élastomère de la phase caoutchouteuse.

## **II.II Résultats expérimentaux**

### **II.II.I Comparaison entre les PMMA plastifiés par le PEG et le Crodamide**

Les résultats expérimentaux indiquent que le Crodamide est plus efficace que PEG pour la réduction de coefficient de frottement. La diminution du coefficient de frottement augmente avec le pourcentage de Crodamide dans le PMMA (Figure I). En revanche, dans le cas du PEG, le coefficient de frottement diminue avec l'introduction de PEG (jusqu'à 1 %), mais l'addition supplémentaire de PEG n'apporte aucune réduction supplémentaire du coefficient de frottement. De plus, à température plus élevée, aucun effet significatif de l'ajout de PEG sur la réduction du coefficient de frottement de PMMA n'est observé. En raison de poids moléculaire plus élevé du

PEG, il semble difficile à ce dernier de migrer vers la surface et former un film abaissant le frottement.

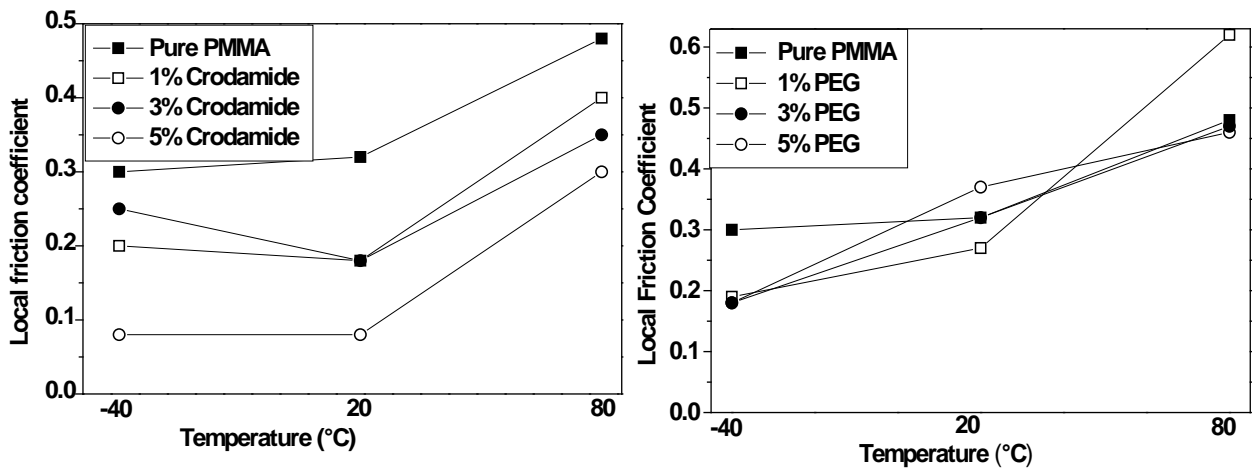


Figure I L'effet de Crodamide (du côté gauche) et de PEG (du côté droit) sur le coefficient de frottement local de PMMA à -40°C, à 20°C et à 80°C (la vitesse de glissant = 0,03 mm/s, rayon de bille = 116  $\mu$ m, charge normale = 1N).

L'effet d'un cycle de chauffage à 80°C pendant une demi-heure sur le comportement de surface a été également étudié. Il est intéressant de noter que le PMMA plastifié par le Crodamide et par le PEG affiche deux comportements très différents après avoir ce cycle (Figure II). Un cycle de chauffage affecte le coefficient de frottement des échantillons plastifiés par le Crodamide, en augmentant le coefficient de frottement. On peut supposer que les petites molécules d'acides gras s'évaporent lors du cycle thermique. En opposition, le PMMA plastifié par le PEG réduit son coefficient de frottement après avoir été chauffé.

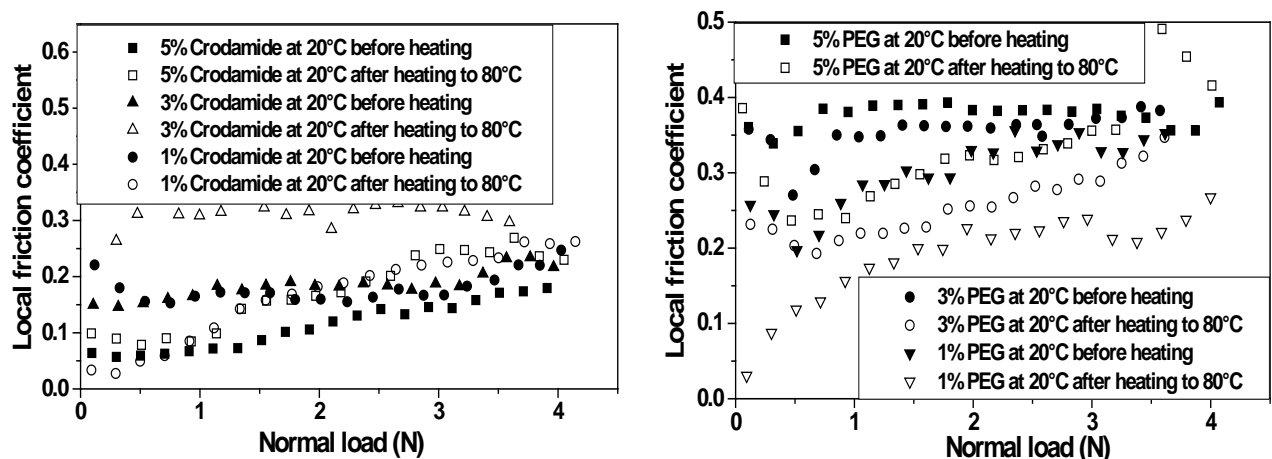


Figure II L'effet du cycle de la chaleur à 80°C pendant 30 minutes sur le coefficient de frottement local de PMMA plastifié par Crodamide (du côté gauche) et de PEG (du côté droit) mesuré à la température ambiante. (La vitesse de glissant = 0,03 mm/s, rayon de bille = 116  $\mu$ m)

La forme de l'aire du contact entre une pointe rigide et la surface de l'échantillon donne des indications sur le taux de plasticité lors du contact; cette forme peut être quantifiée par l'angle de retour de contact ( $\omega$ ). Les résultats expérimentaux montrent que l'introduction de Crodamide dans le PMMA modifie la nature du contact et améliore le retour (la décharge) viscoélastique après

contact (Figure III). Ceci est bien illustré par l'augmentation de la valeur de l'angle de retour et par les photographies in-situ du contact. Pour des déformations moyennes de contact de l'ordre de 0.22, la valeur de l'angle omega est changée de manière significative par l'introduction de Crodamide: cet angle vaut environ 0.9 radian, à comparer au 0.4 radian obtenu lors du contact glissant sur PMMA pur. En première approche, la diminution du coefficient de frottement en lien avec l'ajout de plastifiant entraîne l'augmentation de la valeur de l'angle de retour ce qui traduit moins de plasticité dans le contact glissant pour une déformation géométrique imposée identique. Lorsque la déformation imposée augmente, le contact sur surface PMMA + Crodamide finit par être plastifié. Il est alors intéressant de noter qu'aux mêmes conditions de température et déformation de contact imposée, la nature de contact pour les échantillons de PMMA + PEG est relativement proche de celle du PMMA pur, c.-à-d. presque plastique (Figure IV). La faible diminution du coefficient de frottement pour l'échantillon qui contient 1% PEG entraîne un faible gain dans la résistance à la rayure.

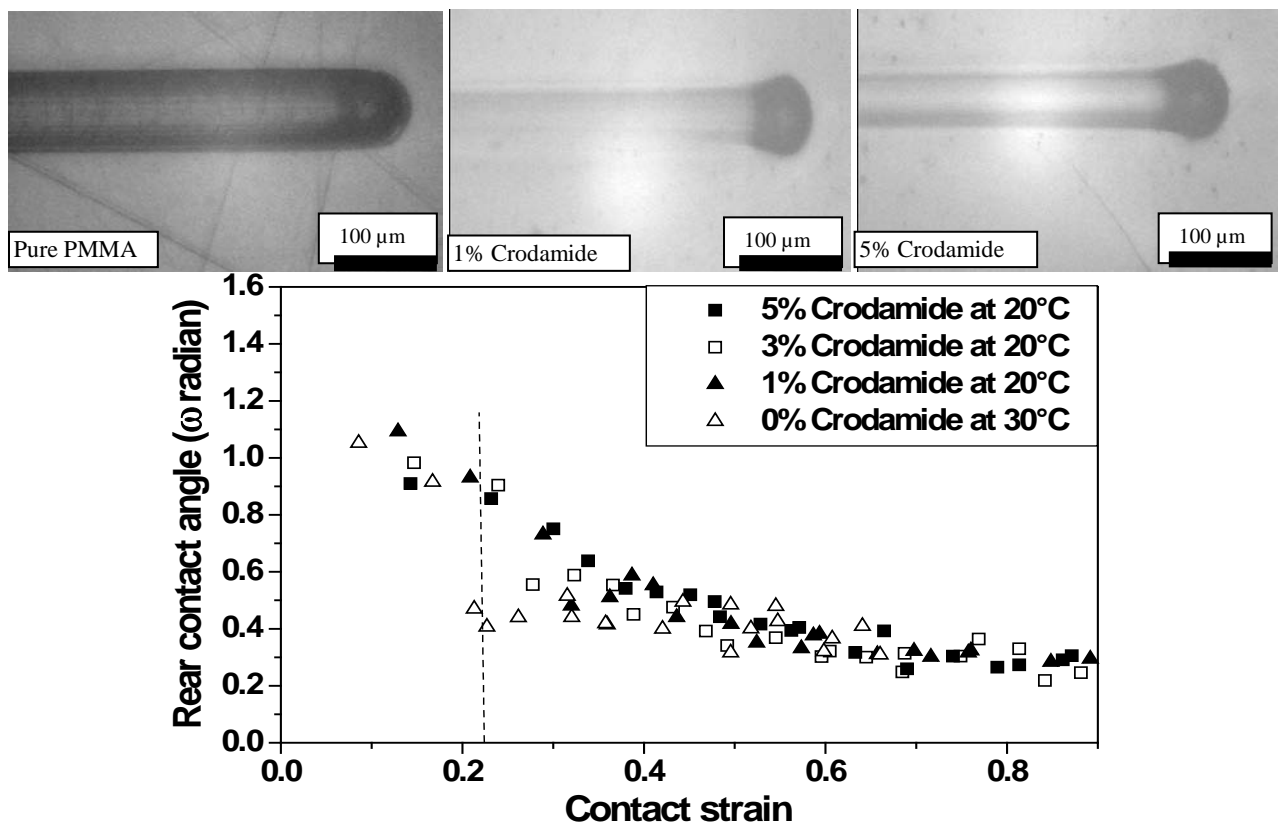


Figure III La variation d'Omega (radian) avec la déformation de contact (défini par le rapport  $\frac{a}{\sqrt{R^2-a^2}}$ , où a est le rayon moyen de contact et R est le rayon de tip) pour différents pourcentages de Crodamide dans PMMA à la température ambiante (la vitesse de glissement/rayant = 0,03 mm/s, rayon de bille = 116 μm). (Seulement quelques images choisies concernant à la déformation de contact = 0,22 sont montrées).

Nous savons que la pente de la courbe de pression - déformation de contact dans le domaine du comportement élastique est proportionnelle au module de Young et fonction du coefficient de frottement car bornée par la déformation seuil du contact plastique. De plus la pression de contact maximale sera obtenue pour l'aire de contact minimale, donc en lien avec la déformation géométrique imposée et le coefficient de frottement. Les résultats expérimentaux indiquent que cette pente est comparable pour les échantillons qui montrent les plus hauts coefficients de



frottement (PMMA pur et échantillons contenant 5% en masse PEG). Cette pente diminue de manière significative pour les échantillons présentant les coefficients de frottement plus bas (PMMA contenant 5 % en masse Crodamide). Dans le premier cas, comme le coefficient de frottement est presque même pour le PMMA pur et pour l'échantillon contenant 5 % en masse PEG, il est possible de supposer que les propriétés massiques comme le module de Young et la contrainte seuil de plasticité ne changent pas aussi de manière significative par l'introduction de PEG. Un raisonnement comparable peut être réalisé pour l'échantillon contenant du Crodamide.

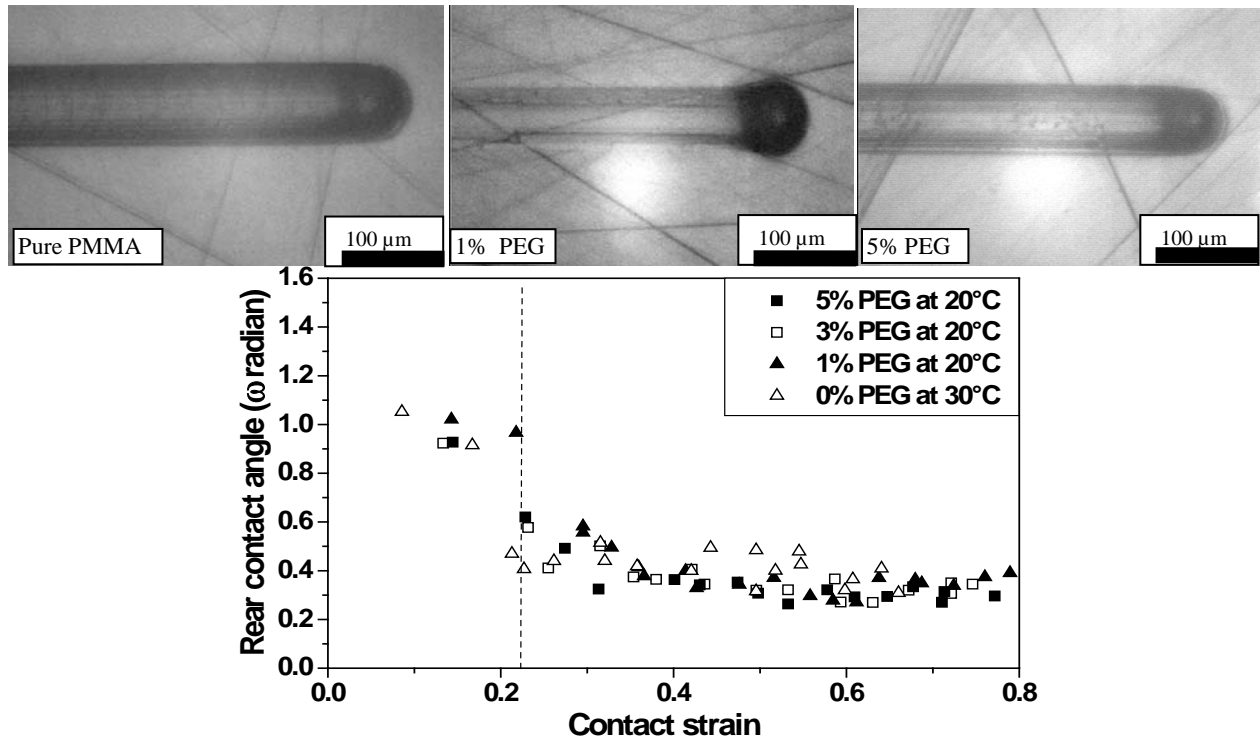


Figure IV La variation d'Omega (radian) avec la déformation de contact pour différents pourcentages de PEG dans PMMA à la température ambiante (la vitesse de glissement/rayant = 0,03 mm/s, rayon de bille = 116 μm). (Seulement quelques images choisies concernant à la déformation de contact = 0,22 sont montrées).

L'énergie libre de surface a été estimée pour le PMMA pur, les échantillons qui contiennent 1 % en masse et 5 % en masse de Crodamide, et pour les échantillons contenant 1 % en masse et 5 % en masse de PEG. Les valeurs d'énergies de surface estimées pour le PMMA pur sont en accord avec les valeurs de la littérature [20, 23, 25, 26, 79, 86, 89]. Les énergies libres des surfaces estimées pour les échantillons plastifiés ne montrent aucun changement considérable (Figure). Ce résultat est contre avec [21] qui montre que le coefficient de frottement et l'énergie libre de surface sont directement proportionnels. Selon Tabor [90], le frottement entre deux corps solides dépend de nombreux facteurs comme les énergies de surface, la rugosité de la surface, la mécanique des surfaces. Le coefficient de frottement local est égal au frottement adhésif pour un contact élastique entre surfaces complètement lisses. Pour une surface rugueuse, le frottement local sera supérieur au frottement adhésif, car les contacts peuvent être localement plastiques. Toutefois, un plastifiant approprié peut diminuer le coefficient de frottement, soit en modifiant l'énergie libre de surface, soit en diminuant la rugosité « apparente » d'un frotteur rugueux de part l'existence d'une couche lubrifiante ce qui aura pour effet de rendre la surface de ce frotteur plus lisse et le contact plus élastique. Les amides d'acides gras peuvent donc réduire le coefficient de frottement en diminuant la rugosité « apparente des frotteurs », en changeant le comportement mécanique de matériau testé

(ce qui peut avoir comme résultat le changement de nature du contact avec moins de plasticité locale).

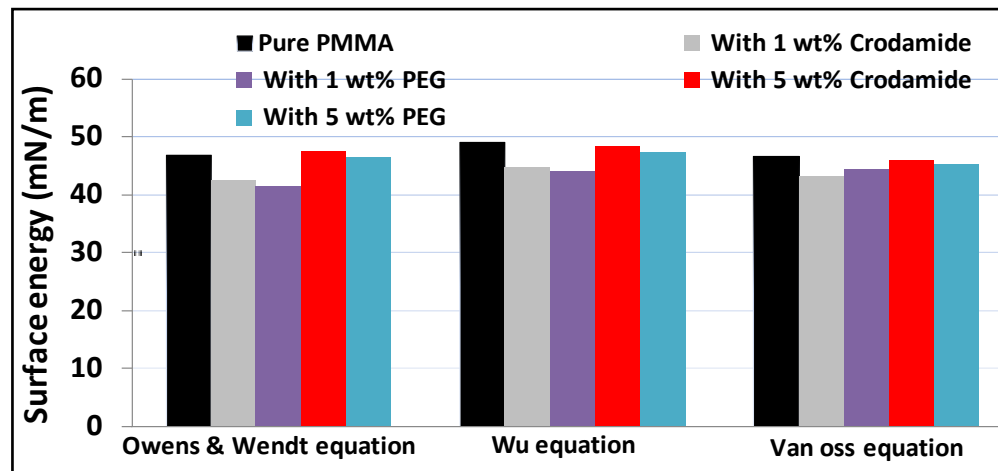


Figure V L'effet de Crodamide et de PEG sur l'énergie libre de surface de PMMA à 20°C.

Compte tenu du fait que le pourcentage de plastifiant reste faible, les conséquences sur les propriétés mécaniques volumiques sont mineures. Le Crodamide et le PEG n'ont eu aucun effet remarquable sur les propriétés mécaniques volumiques comme module de Young (Figure VI). Cependant, le PEG perturbe ces propriétés un peu plus que le Crodamide et cet effet est attribué à la tendance accrue de la migration des Crodamide du volume vers la surface de la matière. En raison de poids moléculaire plus élevé de PEG, la migration vers la surface reste faible et accentue la modification du comportement volumique. L'effet du Crodamide et du PEG sur la contrainte de traction et la déformation à rupture n'est pas très clair. Les deux plastifiants augmentent un peu ces valeurs par rapport à celles mesurées sur PMMA pur.

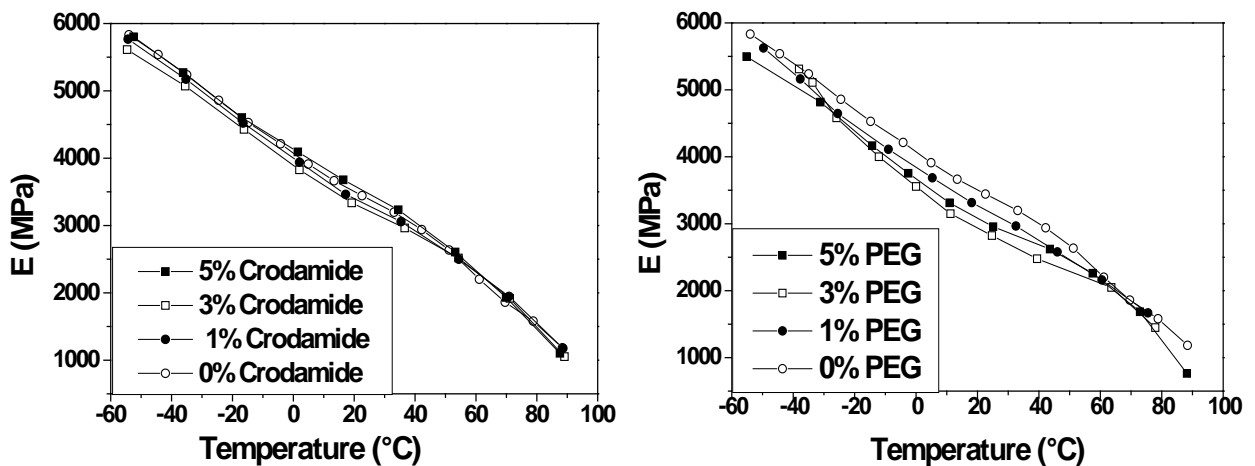


Figure VI L'effet de Crodamide (du côté gauche) et de PEG (du côté droit) sur le module de Young (E) de PMMA.

En résumé, aucun effet significatif des deux plastifiants n'est trouvé sur les propriétés volumiques du PMMA même pour les échantillons qui montrent un coefficient de frottement plus bas. La déformation de contact au seuil du contact entièrement plastifié a été augmentée pour les échantillons ayant le coefficient de frottement le plus bas. Comme les additifs de glissement migrent à la surface, il pouvait être supposé que le comportement volumique pourrait être modifié

sur un très petit volume près de la surface (en raison de la présence de quantité excessive d'additif de glissement près de la surface). Pour vérifier cette hypothèse, quelques échantillons ont été analysés par essai de nano indentation. Cependant, aucune différence significative n'a été observée entre les échantillons qui présentent les coefficients de frottement les plus bas et ceux qui présentent les coefficients de frottement les plus hauts. Par exemple, le module de Young et la dureté estimée par nano indentation pour le PMMA pur et l'échantillon qui contient 5 % de Crodamide évoluent de manière comparable en fonction de la profondeur, bien qu'il y ait une différence significative dans le coefficient de frottement (Figure VII). De même l'échantillon qui contient 5 % PEG et qui présente quasiment le même coefficient de frottement que le PMMA pur montre une valeur plus basse de module de Young et de dureté estimées par nano indentation. Nous pouvons cependant observer une légère augmentation dans le recouvrement élastique après nano indentation, pour les échantillons qui affichent un coefficient de frottement le plus bas, sans pouvoir préciser si cette différence de comportement est due à la diminution du coefficient de frottement, ou si la différence de comportement volumique pour les premiers 100 -200 nm d'enfoncement accentue la diminution du coefficient de frottement en rendant la surface du matériau testée plus élastique à l'échelle des nano rugosité.

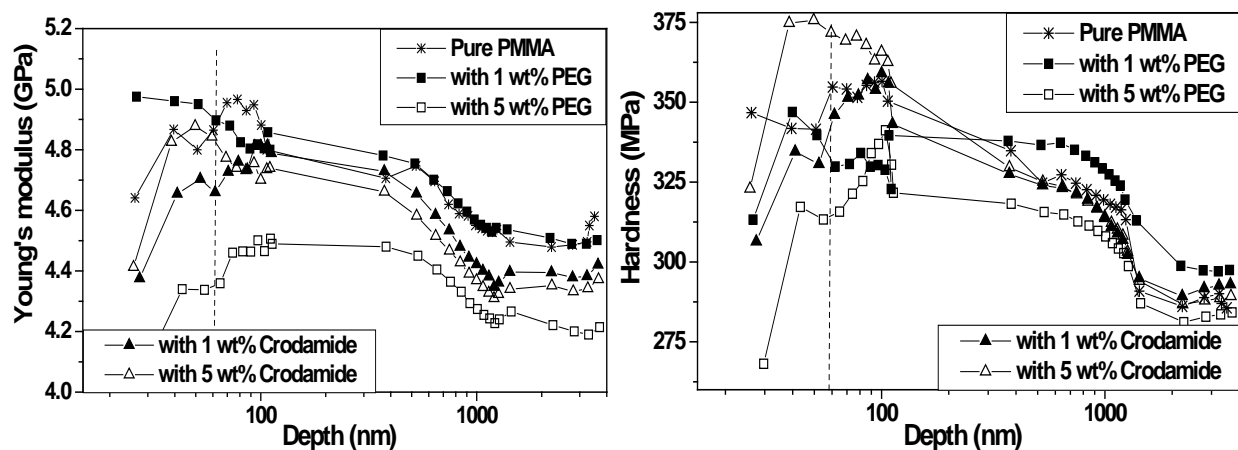


Figure VII La variation du module de Young (du côté gauche) et de la dureté (du côté droit) avec la profondeur pour PMMA à la température ambiante mesuré par nano indentation.

### II.II.II Comparaison entre les PMMA plastifiés par l'Erucamide, le Behenamide et le Stearamide

La comparaison entre les effets d'ajout d'Erucamide, de Behenamide et de Stearamide a été étudiée pour des échantillons de PMMA polymérisés dans le laboratoire. Des échantillons contenant 0, 0,05, 0,1, 0,15 % et 0,2 % d'Erucamide, des échantillons contenant de 0, 0,05 et 0,1 % de Behenamide, des échantillons contenant de 0, 0,1 et 0,3 % de Stearamide et un échantillon contenant 0,1 % Behenamide et 0,2 % d'Erucamide ont été préparés et testés. Les seuils en plastifiants ont été retenus en raison des problèmes de solubilité dans la solution de monomère de MMA à température ambiante. Les résultats expérimentaux indiquent que l'Erucamide est l'amide d'acide gras le plus efficace parmi ces trois amides testés pour réduire le coefficient de frottement du PMMA (Figure VIII). Dans les trois cas, l'amide d'acide gras se révèle un bon agent lubrifiant uniquement s'il est présent en petite quantité car il réduit le coefficient de frottement significativement. Une augmentation du pourcentage donne un effet préjudiciable: à des teneurs élevées en pourcentage d'amide d'acide gras, aucun effet significatif sur le coefficient de frottement n'est observé. Le pourcentage optimal d'Erucamide se trouve à 0,05 %, et il est 0,1 % pour le Behenamide et le Stearamide. La combinaison de 0,1 % Behenamide (montrant une

diminution considérable du coefficient de frottement lorsqu'il est présent seul) et 0,2 % Erucamide n'a pas d'effet sur le coefficient de frottement.

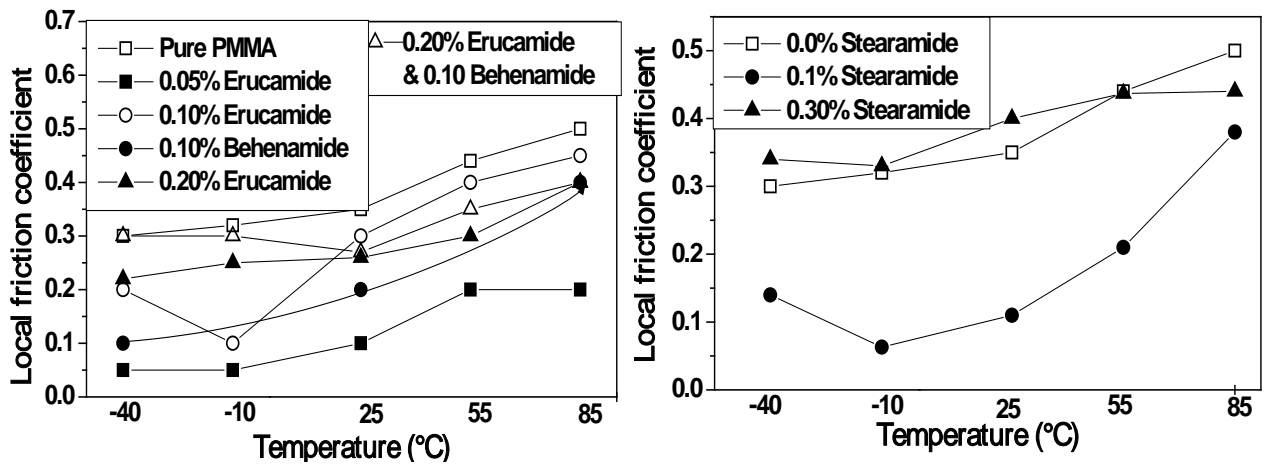


Figure VIII L'effet de Erucamide et de Behenamide (du côté gauche) et de Stearamide (du côté droit) sur le coefficient de frottement local de PMMA aux températures différentes (la vitesse de glissant = 0,03 mm/s, rayon de bille = 116  $\mu$ m, charge normale = 2N).

Les résultats des essais de rayure montrent que l'introduction d'amide d'acide gras dans le PMMA modifie la nature du contact et augmente l'angle de retour de contact. La présence en très petite quantité (Erucamide (0,05 % en masse), Behenamide (0,1 % en masse) et Stearamide (0,1 % en masse)) améliore la viscoélasticité dans le contact. Toutefois, une augmentation de ce pourcentage annule le gain en glissement car le contact redevient plastique. L'amélioration de la viscoélasticité dans le contact est illustrée par les valeurs des angles de retour de contact et par les photographies in-situ du contact. Par exemple, pour une déformation moyenne de contact de 0,3; l'angle de retour de contact à température ambiante pour les échantillons contenant différents pourcentages d'Erucamide vaut environ 0,3 rad pour PMMA pur et pour les échantillons qui contiennent 0,1 % en masse d'Erucamide (tous deux montrant un haut coefficient de frottement), tandis que cette valeur augmente à près de 0,7 rad pour les échantillons qui contiennent 0,05 % en masse Erucamide (Figure IX). Cette dernière valeur de 0,7 rad est également obtenue pour l'échantillon contenant 0,1 % en masse de Behenamide (échantillon ayant également un bas coefficient de frottement). Comme précédemment, pour ce niveau de déformation de contact de 0,3 à température ambiante, les photographies in-situ du contact montrent que la nature du contact est plastique pour PMMA pur et pour les échantillons contenant 0,1 % en masse d'Erucamide, et que les contacts sont bien viscoélastiques pour les échantillons qui contiennent 0,05 % en masse Erucamide et 0,1 % en masse Behenamide. Les résultats identiques ont été obtenus aux températures plus basses et plus hautes. La diminution du coefficient de frottement est bien à l'origine d'une diminution du taux de plasticité dans le contact et d'une augmentation de la valeur de l'angle de retour de contact. Les résultats analogues ont été observés en cas de Stearamide où l'échantillon contenant 0,1 % en masse de Stearamide (affichant le coefficient de frottement plus bas) a montré une augmentation de la valeur de l'angle de retour de contact. Ces résultats intéressants pour une déformation moyenne de contact ne doivent pas faire oublier qu'à déformation dans le contact imposée supérieure le contact est entièrement plastifié et ceci pour tous les cas (quelque soit le % et le type du plastifiant).

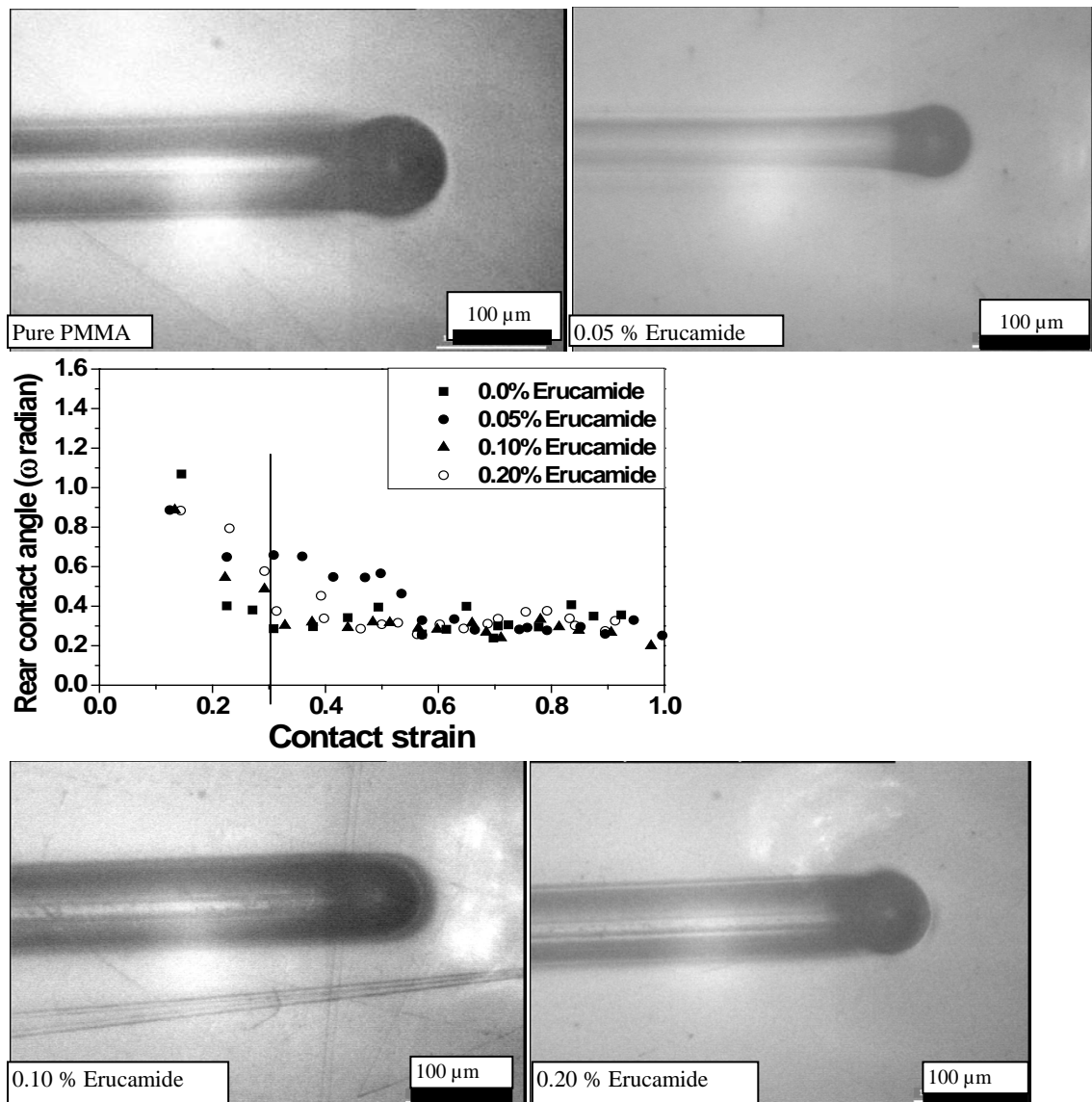


Figure IX La variation d'Omega (radian) avec la déformation de contact pour différents pourcentages d'Erucamide dans PMMA à la température ambiante (la vitesse de glissement/rayant = 0,03 mm/s, rayon de bille = 116 μm). (Seulement quelques images choisies concernant à la déformation de contact = 0,3 sont montrées).

Les courbes pressions de contact en fonction de la déformation géométrique montrent à nouveau que les échantillons présentant les coefficients de frottement les plus hauts (PMMA pur et les échantillons contenant les taux d'amides d'acides gras les plus importants) ont un comportement plastique pour de faibles déformations. A l'opposé les PMMA ayant les coefficients de frottement les plus bas (l'échantillon qui contient 0,05 % en masse d'Erucamide) restent élastoplastiques plus longtemps. Comme le coefficient de frottement est presque même pour le PMMA pur et pour l'échantillon qui contient 0,10 % en masse d'Erucamide, il est légitime de supposer que les propriétés volumiques sont peu affectées en volume par l'introduction d'amide d'acide gras.

L'énergie libre de surface a été estimée pour le PMMA pur et les échantillons contenant 0,05% Erucamide et 0,1% Behenamide. Les valeurs des énergies libres de surface estimées par trois approches différentes pour le PMMA pur sont dans bien en accord avec les valeurs de

littérature [20, 23, 25, 26, 79, 86]. Les résultats expérimentaux ne montrent aucun changement considérable de l'énergie libre de la surface pour les échantillons plastifiés en phase avec la réduction du coefficient de frottement.

L'effet de la présence d'amides d'acides gras sur les contraintes et les déformations n'est pas très clair: les amides d'acides gras testés n'ont pas d'effet majeur sur les propriétés mécaniques volumiques testées comme le module de Young ou les contraintes seuil de plasticité. Cependant, le Stearamide perturbe ces propriétés comparativement un peu plus que ne le font l'Erucamide et le Behenamide. Il est également intéressant de noter que les échantillons présentant une valeur basse de coefficient de frottement (Erucamide (0,05 %), Behenamide (0,1 %) et Stearamide (0,1 %)) ont des modules d'Young un peu plus faibles.

On pouvait supposer que les amides d'acide gras réduisent le coefficient de frottement en formant une couche très mince au comportement plus élastique que dans le volume, qui permet de diminuer les déformations plastiques à l'échelle des nanorugosités des pointes. Il est aussi établi que les additifs de glissement migrent à la surface et forment un film très mince pour réduire le coefficient de frottement et ceci en lien avec l'évolution de l'énergie libre de la surface. Ce mécanisme expliquerait que la déformation de contact au seuil de plasticité est augmentée pour les échantillons ayant le coefficient de frottement plus bas. Pour vérifier que le comportement volumique pouvait être modifié sur un très petit volume près de la surface, quelques échantillons ont été testés par nano indentation. Aucune différence significative n'a été trouvée entre les échantillons qui présentent les coefficients de frottement les plus bas et plus hauts. Le changement dans le coefficient de frottement fait par la très petite quantité d'amides d'acides gras n'est à priori pas en lien avec une variation de propriété volumique (déformation élastique admissible augmentée) sur une petite épaisseur, où qu'elle n'affecte au maximal que quelques dizaines de nanomètres.

### **II.II.III Comparaison de l'effet d'un plastifiant sur deux grades de PMMA**

Deux amides d'acides gras, le Crodamid-212 et le Crodamid-Er ont été testés sur deux grades de PMMA commerciaux pour étudier l'effet sur les coefficients de frottement. Les résultats expérimentaux indiquent qu'un additif de glissement spécifique, efficace pour un grade de polymère peut être inutile pour un autre grade de ce même polymère. Les deux Crodamides diminuent les coefficients de frottement du PMMA-V825, avec un facteur de diminution différents (pour des températures différentes). Dans l'autre cas, pour le PMMA-HT121, le coefficient de frottement reste presque insensible à la présence des deux amides d'acides gras.

### **II.II.IV Influence de la réticulation du PMMA**

Les résultats expérimentaux indiquent que la réticulation n'est pas favorable pour réduire le coefficient de frottement du PMMA. Dans cette comparaison, les PMMA testés contenaient des nano particules de PBA (poly (n-butyl acrylate)). Dans ces conditions, les résultats ne sont pas forcément transposables à des PMMA pur réticulés ou de hautes masses. Le PMMA réticulé testé a présenté un coefficient de frottement supérieur au PMMA non-réticulé. Il est important de noter que les deux PMMA (non-réticulé et réticulé) ont présenté un coefficient de frottement plus bas à plus haute température ce qui est contraire à ce qui est classiquement attendu. De même un cycle de chauffage à 90°C pendant une demi heure a réduit le coefficient de frottement de PMMA réticulé et non-réticulé avec un effet plus significatif pour le PMMA réticulé. Ce comportement inattendu peut être attribué à la présence de PBA, avec des nano particules d'élastomère qui

migraient à la surface avec la température engendrant une diminution dans le coefficient de frottement.

### II.III La discussion générale sur les essais

La diminution du coefficient de frottement des polymères plastifiés par ajout d'un faible pourcentage d'amides d'acides gras évolue au cours du temps. La diminution du coefficient de frottement est maximale immédiatement après la fabrication. Dans un premier temps, le coefficient de frottement reste à cette valeur initiale, tant que la quantité d'amide d'acides gras disponible à la surface est « suffisante ». Puis, les résultats expérimentaux montrent qu'après plusieurs mois de conservation le coefficient de frottement commence à retrouver sa valeur de référence du PMMA pur. Un cycle thermique de courte durée à haute température permet de faire évaporer l'amide d'acide gras de la surface du polymère et donc l'avantage qu'il apporte au coefficient de frottement.

Lors d'un essai de rayure, l'énergie mécanique dissipée par frottement peut générer un échauffement de la surface. La température de contact peut s'élever pour les hautes vitesses de glissement pendant le test de rayure, ce qui aurait comme résultat une variation des propriétés mécaniques volumiques et affecter donc le comportement à la rayure. Dans nos essais, la vitesse tangentielle n'est pas très élevée (0.03 mm/s) et l'augmentation de la température résultante serait inférieure à 1°C (Figure X). Cette estimation est basée sur 'analyse de Bonne [67]:

$$\Delta T = \frac{2}{\pi} \frac{\tan \beta \left( \frac{W}{2L} \right) v}{\sqrt{\lambda \rho c v L}} \quad \text{I}$$

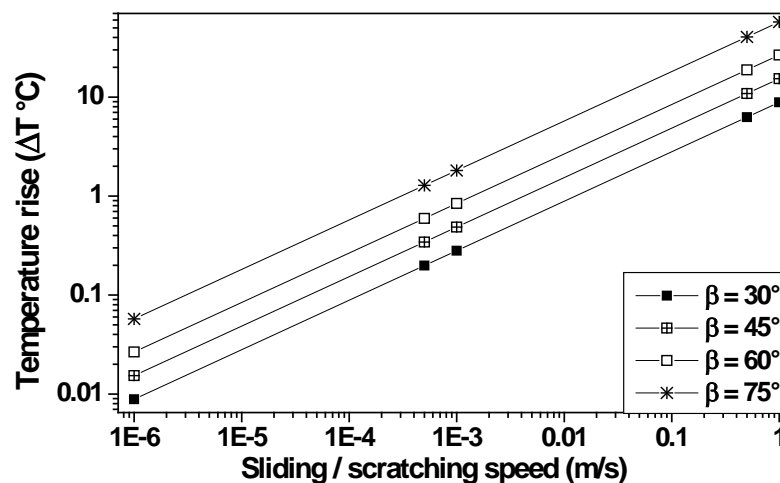


Figure X L'élévation de la température ( $\Delta T$ ) pour différents angles d'attaque ( $\beta$ ) et pour différentes vitesses de glissantes ( $v$ ) pour le rayon de contact = 10  $\mu\text{m}$  pendant l'essai de glissement/rayant.

La relation entre la vitesse de glissement  $v$  et les élévations de la température  $\Delta T$  lors d'un test de rayure peut s'exprimer de la manière suivante:

$$\log \Delta T = m \log v + c \quad \text{II}$$

où  $m$  et  $c$  sont les constantes qui dépendent des propriétés de l'indenter et du matériau. Dans un essai de rayure à grande vitesse, la température pourrait s'élever de 100°C. Le fait que les courbes maîtresses de la pression moyenne de contact obtenues en balayant, pour différentes températures, une gamme de vitesse de 1  $\mu\text{m/s}$  à 10 mm/s permettent de trouver à la bonne équivalence temps

/température la  $T_g$ , permet de confirmer que la procédure d'essai utilisée ne génère pas d'auto échauffement important.

### III Simulation par la méthode des éléments finis

#### III.I Modèle numérique

Les transitions entre un glissement élastique et un contact élastoplastique, et entre un contact élastoplastique et une rayure plastique, ont été analysées numériquement en utilisant les simulations par éléments finis. Dans le contexte de cette thèse, l'objectif principal des simulations était d'étudier l'effet du coefficient de frottement et la déformation géométrique imposée dans le contact sur les paramètres mécaniques du contact (pression, forme du contact) et d'essayer de relier ces transitions de comportement à des valeurs seuils du rapport  $a/R$  définissant la déformation géométrique moyenne de contact et le coefficient de frottement local  $\mu_{loc}$ .

La modélisation par éléments finis utilisée a été développée et validée lors de travaux antérieurs réalisés avec le logiciel MSC Marc<sup>®</sup> [2, 70, 92]. Le maillage à trois dimensions a la forme d'un quart de cylindre, avec un maillage optimisé pour limiter les effets de bords et les problèmes de convergence numérique, sur lequel une pointe sphérique rigide indente puis raye la surface. Bien que le comportement élastique des polymères soit souvent non-linéaire, le comportement élastique est modélisé par une loi linéaire définie par module de Young  $E$  et un coefficient de Poisson, tous les deux constants comme précédemment utilisé par H. Pelletier et al. [92]. Les essais sont réalisés à vitesse constante, et la loi utilisée est une loi de type G'Sell Jonas avec un écrouissage exponentiel, et le seuil des déformations plastiques est défini par un critère de von Mises. Les grandeurs matériaux (module d'Young, contrainte seuil d'écoulement plastique et paramètre d'écrouissage) sont calés sur les essais de compression réalisés ( $E = 3,2$  GPa,  $\sigma_{yield} = 100$  MPa,  $\nu = 0,39$ )

Les paramètres géométriques pour décrire la géométrie du contact et la forme du sillon résiduel ont été définis dans le modèle, pour être analysé en fonction du rapport ( $a/R$ ) et du coefficient de frottement, donc d'une déformation moyenne de contact imposé pendant la rayure. Le maillage développé est composé d'éléments à 8 noeuds permettant l'interpolation linéaire. Les simulations ont exigé 24,045 éléments et 21,240 noeuds. Le maillage est raffiné dans la zone du contact, et environ 95 éléments sont dans le contact, sous l'indenteur, et ce pour toutes les conditions de rayage étudiées. Pendant les phases d'indentation et de rayage, l'épaisseur du plus petit élément dans la zone de contact était d'au moins 0,3 fois la profondeur de pénétration imposée. Le rayon de pointe  $R$  et la profondeur de pénétration  $h_i$  sont choisis pour obtenir des rapports  $a/R$  variant entre 0.025 et 0.6, et pour conserver le même nombre d'éléments pendant le contact. La distance de l'indentation au bord de l'échantillon est supérieure à 5 fois le rayon de contact de l'indentation, la rayure se termine à 5 fois le rayon de contact de l'autre bord, et l'épaisseur de l'échantillon est supérieure à 23 fois la profondeur de pénétration. La longueur de rayage est choisie pour que les chargements normaux et tangentiels appliqués à l'indenter atteignent un état constant: cette longueur correspond à plus de 6 fois le rayon de contact. Le post traitement permet d'analyser la vraie profondeur de contact (tenant compte des écoulements plastiques et de la déflexion élastique) et ainsi le vrai rayon de contact pendant les phases d'indentation et rayage.

Compte tenu que les résultats expérimentaux sont obtenus à une température constante et que la vitesse de glissement est également constante lors d'un essai, l'analyse numérique est réalisée dans un cadre élastoplastique. Ce choix est licite compte tenu que dans le domaine vitreux



la contrainte seuil d'écoulement plastique et le module d'Young varient dans le même rapport. Par ailleurs, cette première série de simulations numériques est destinée à mettre en place les outils d'analyse et ne balayera pas en vitesse et température. Le frottement est pris en compte dans l'analyse, au moyen d'un modèle de Coulomb. Ainsi, le maximum de la contrainte de cisaillement locale  $\tau_c$  agissant à l'interface vaut:

$$\tau_c = \mu_{loc} p \quad \text{III}$$

où  $p$  est la pression normale locale et  $\mu_{loc}$  le coefficient de frottement local entre les surfaces dans le contact [2, 70]. Le modèle de contact a été appliqué dans le contexte d'une formulation glissante finie, où un glissement et une rotation entre les surfaces pouvaient arriver. Pour chaque rapport  $a/R$ , les simulations ont été réalisées pour les valeurs du coefficient de frottement local compris entre 0 et 1,3 pour identifier les conditions de frontière pour les transitions entre les natures différentes de contact. Pour les rapports  $a/R$  et les coefficients de frottement les plus élevés, une attention particulière a été portée sur les déformations du maillage. Pour tous les rapports  $a/R$ , la précision des simulations est tout à fait similaire car le nombre d'éléments et de noeuds dans la zone de contact est quasiment constant. Les simulations réalisées n'utilisent pas de boîte de remaillage. Les données extraites des simulations sont les coefficients de frottement apparent et d'obstacle, l'angle de retour de contact, la pression moyenne de contact, la pression maximum de contact, les contraintes de cisaillement interfacial, la décharge élastique, les champs de déformation plastique équivalente, les tracés des cartes des déformations longitudinales et horizontales.

### III.II Nature du contact selon les conditions de glissement/rayure

Trois critères différents ont été utilisés pour différencier les frontières entre les différents types de contact, en fonction des conditions de glissements/rayure. Ces trois critères peuvent être énumérés comme suit:

#### ***1. Le critère 1 fondé sur l'existence de déformation plastique dans l'aire de contact et dans le plan de symétrie***

Ce critère est fondé sur l'existence de déformation plastique équivalente (déformation  $>0,03$ ) autour et sous le contact. Un contact est dit élastique s'il n'a pas de déformation plastique équivalente à la surface et dans la section longitudinale. Si les déformations plastiques équivalentes sont localisées dans cette section longitudinale et minima dans la zone arrière de l'aire de contact, le contact est appelé plastique. Le contact est qualifié d'élastique plastique si la déformation plastique équivalente est présente partiellement en volume et / ou en surface.

#### ***2. Le critère 2 fondé sur une aire de contact totalement déformée plastiquement***

La base de ce critère est similaire au critère 1 mais est un peu plus strict dans la définition du contact plastique. Les conditions pour déclarer un contact élastique (absence totale de plasticité) ou élastique plastique (plasticité partielle dans les deux sections analysées) sont exactement les mêmes que pour le critère 1. Par contre, avec ce critère, un contact sera plastique si la déformation plastique équivalente est présente sur une toute la surface de contact, donc sur un disque dont le rayon est égal au rayon de contact.

#### ***3. Le critère 3 fondé sur le profil des contraintes de traction dans et autour du contact***

Ce critère diffère des précédents critères car il prend en compte le profil des contraintes horizontales de traction au lieu de considérer la localisation des déformations plastique équivalentes dans et autour du contact. Selon ce critère, dans un contact élastique, la contrainte de traction au centre du contact, pour un rapport  $a/R$  donné, doit être identique et indépendant du

coefficient de frottement. En effet les résultats donnés par G M Hamilton [96] montrent que les profils des contraintes de traction passent tous par la même valeur au centre du contact. De plus, ces contraintes redeviennent nulles après passage du contact. Un contact sera dit plastique si les contraintes horizontales ne sont pas nulles après passage de la pointe, et un contact sera qualifié d'élastique plastique si la contrainte de traction ne respecte plus les profils donnés par G.M. Hamilton tout en pouvant redevenir nulle après passage de la pointe.

L'application de ces trois critères donne des frontières entre les différents domaines de comportement relativement similaires (surtout pour les critères 2 et 3), et permet de tracer des cartes de comportement comparables. Ces cartes et les frontières sont des aides dans l'analyse des comportements observés. Un des cartes est montrée dans le tableau suivant.

a/R ratio	0.025	0.05	0.075	0.1	0.15	0.2	0.3	0.4	0.5	0.6
$\mu_{loc}$										
0	Elastic	Elastic	Elastic	EP	EP	EP	EP	EP	Plastic	Plastic
0.05	Elastic	Elastic	Elastic	EP	EP	EP	EP	EP	Plastic	Plastic
0.1	Elastic	Elastic	Elastic	EP	EP	EP	EP	EP	Plastic	Plastic
0.15	Elastic	Elastic	Elastic	EP	EP	Plastic	Plastic	Plastic	Plastic	Plastic
0.2	Elastic	Elastic	Elastic	EP	EP	Plastic	Plastic	Plastic	Plastic	Plastic
0.25	Elastic	Elastic	Elastic	EP	Plastic	Plastic	Plastic	Plastic	Plastic	Plastic
0.3	Elastic	Elastic	Elastic	EP	Plastic	Plastic	Plastic	Plastic	Plastic	Plastic
0.35	Elastic	Elastic	Elastic	EP	Plastic	Plastic	Plastic	Plastic	Plastic	Plastic
0.4	Elastic	Elastic	Elastic	EP	Plastic	Plastic	Plastic	Plastic	Plastic	Plastic
0.45	Elastic	Elastic	EP	Plastic	Plastic	Plastic	Plastic	Plastic	Plastic	Plastic
0.5	Elastic	Elastic	EP	Plastic	Plastic	Plastic	Plastic	Plastic	Plastic	Plastic
0.55	Elastic	Elastic	Plastic	Plastic	Plastic	Plastic	Plastic	Plastic	Plastic	Plastic
0.575	Elastic	Elastic	Plastic	Plastic	Plastic	Plastic	Plastic	Plastic	Plastic	Plastic
0.6	Elastic	Elastic	Plastic	Plastic	Plastic	Plastic	Plastic	Plastic	Plastic	Plastic
0.65	Elastic	EP	Plastic	Plastic	Plastic	Plastic	Plastic	Plastic	Plastic	Plastic
0.7	Elastic	Plastic	Plastic	Plastic	Plastic	Plastic	Plastic	Plastic	Plastic	Plastic
0.9	Elastic	Plastic	Plastic	Plastic	Plastic	Plastic	Plastic	Plastic	Plastic	Plastic
1.1	Elastic	Plastic	Plastic	Plastic	Plastic	Plastic	Plastic	Plastic	Plastic	Plastic
1.2	Elastic	Plastic	Plastic	Plastic	Plastic	Plastic	Plastic	Plastic	Plastic	Plastic
1.25	Elastic	Plastic	Plastic	Plastic	Plastic	Plastic	Plastic	Plastic	Plastic	Plastic
1.3	Plastic	Plastic	Plastic	Plastic	Plastic	Plastic	Plastic	Plastic	Plastic	Plastic

Tableau I Nature du contacts pour différents coefficients de frottement locaux et différents rapports a/R basés sur le deuxième critère. (EP = élastique plastique)

#### IV Comparaison entre les données expérimentales et les données obtenues par simulations

La comparaison entre les données de simulations numériques et les données expérimentales est correcte pour les grandeurs géométriques. Ainsi les valeurs expérimentales de l'angle de retour de contact en fonction de la déformation moyenne de contact pour différents coefficients de frottement sont encadrées par les résultats numériques. Les transitions de comportement entre les différents types de contacts sont localisées pour les mêmes ordres de grandeurs de déformations

moyennes de contact (Figure XI). Les évolutions de l'angle de retour de contact en fonction de la pression moyenne de contact normée sont aussi comparables. Toutefois, pour le plus haut coefficient de frottement ( $\mu_{loc} = 0,4$ ), les simulations numériques présentent quelques incohérences sans pour autant remettre en cause les tendances.

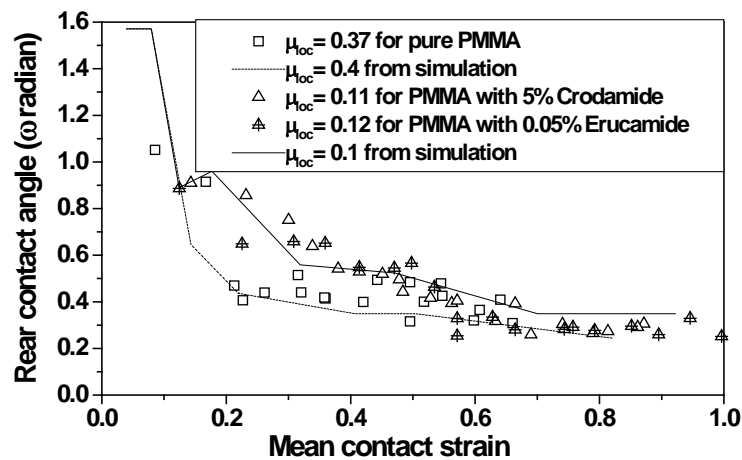


Figure XI La comparaison entre les valeurs expérimental et numérique (obtenues à partir des simulations) du l'angle de retour de contact pour quelques coefficients de frottement choisis.

Il est intéressant de noter que les mesures des pressions moyennes de contact en fonction de la déformation moyenne obtenues pour les expériences sur les surfaces à bas coefficient de frottement valident les résultats numériques des simulations de rayure pour un coefficient de frottement local bas de 0.1. Mais contre toute attente, les simulations numériques réalisées pour un coefficient de frottement de 0.4 ne permettent pas de retrouver le bon niveau de pression de contact.

Cet écart est surprenant et pour l'instant non clairement expliqué; le temps ayant manqué pour réaliser toutes les études de sensibilité aux différentes variables.

- Est-ce que le fait que la loi ne soit pas viscoplastique introduit un écart dans les résultats?
- Est-ce que des simulations numériques à enfoncement imposé et non à force imposée peuvent justifier cette différence?
- Les simulations numériques ont été réalisées avec une pointe sphérique. Or les essais ont été réalisés avec une pointe sphérico-conique dont l'angle du cône est 60°. Les résultats pour les rapports a/R les plus importants supérieurs à 0,4/0,5 sont donc obtenus pour des conditions géométriques différents. Par ailleurs, l'influence d'un coefficient de frottement sur ces profils géométriques différents n'est pas connue.

## V Conclusions & Perspective

Les techniques de rayures instrumentées ont gagné en intérêt en ingénierie des surfaces en raison d'un besoin croissant de surfaces ayant des comportements mécaniques renforcés. Les techniques de rayure fournissent un moyen commode et fiable pour examiner les propriétés mécaniques de polymères sous les conditions diverses de contact, et des sollicitations proches des endommagements rencontrés en service. Les polymères présentent une grande variété de comportements surfaciques avec des mécanismes de déformation et de dissipation d'énergie sont encore mal maîtrisés ou totalement expliqués [33].

Les traitements physico-chimiques et les techniques d'implantation ionique ont prouvé leurs utilités pour modifier et améliorer les propriétés de surface des matériaux polymères mais leurs applications sont limitées à quelques polymères non transparents en raison de leurs effets assombrissants. L'objectif de ces travaux de thèse était d'étudier le gain en résistance à la rayure que peut procurer les plastifiants. L'amélioration de la résistance à la rayure peut être analysée comme un effet dû à une diminution du coefficient de frottement. L'étude de la réduction du frottement par l'usage de plastifiants est donc un sujet de recherche pouvant avoir des applications innovantes.

Les résultats expérimentaux confirment que les amides de différents acides gras sont efficaces en petites quantités pour réduire le coefficient de frottement sur surfaces de PMMA, et qu'un excès affecte ce bénéfice probablement en raison de leur effet « gommant » sur la surface. L'exception à cette généralisation est le stearyl erucamide (Crodamide-212) qui confirme par les données expérimentales que le coefficient de frottement du PMMA diminue lorsque le pourcentage augmente. Ces travaux ont montré et confirmé que la déformation au cours du contact glissant est diminuée de manière significative pour les échantillons qui présentent le coefficient de frottement plus bas, toutes choses étant égales par ailleurs. Nous avons vu aussi que cette diminution du coefficient de frottement par l'introduction d'amides d'acides gras est effective jusqu'à un certain point, et ne peut pas corrélérer par le changement de l'énergie libre de surface du PMMA, mais sans affecter le comportement volumique à l'échelle macroscopique voire submicronique. Il peut être supposé que le frottement est réduit en affectant le comportement volumique seulement pour une très faible épaisseur (quelques dizaines ou une centaine de nanomètres) qui ne sont pas détectable par les techniques de nano indentation. Il est intéressant à noter que l'énergie libre de surface de l'Erucamide pur est beaucoup basse que celle du PMMA pur, mais que, ajouté au PMMA dans une faible quantité, il diminue le coefficient de frottement de PMMA sans changer l'énergie libre de surface.

Les données expérimentales indiquent que l'efficacité d'un additif de glissement peut être très grande pour réduire le coefficient de frottement d'un polymère et ne pas apporter de bénéfice pour un autre grade du même polymère. Les résultats expérimentaux montrent qu'il n'y a pas de synergie dans l'action entre l'Erucamide et le Behenamide pour diminuer le coefficient de frottement de PMMA. Un antagonisme a plutôt été trouvé: 0.1% Behenamide permet de diminuer le coefficient de frottement du PMMA mais cette diminution dans le coefficient de frottement est annulée par la présence de 0.2 % d'Erucamide. Plus de travaux seront nécessaires pour identifier les meilleures combinaisons d'amides d'acides gras (nature et quantité) et trouver si d'autres matériaux comme les particules de nano de silice, les nanoclay comme la laponite pourraient être aussi employés pour trouver une combinaison efficace pouvant réduire le coefficient de frottement.

Même si il peut être conclu que le plastifiant réduit le coefficient de frottement des polymères sans modifiant l'énergie libre de la surface du polymère et en modifiant le comportement mécanique dans un volume de matière proche de la surface, le lien entre frottement, propriété mécanique de la proche surface et énergie libre nécessite encore des travaux pour comprendre les liens. L'avantage procuré par la présence d'un plastifiant reste valide tant que le plastifiant reste disponible à la surface. Mais la plupart des plastifiants reste dans le polymère pendant une durée limitée et, de fait, la diminution du coefficient de frottement n'est pas durable. Des travaux sont nécessaires pour déterminer quelles combinaisons de plastifiants et de polymères permettent de réduire au mieux le coefficient de frottement, et découvrir les méthodes pour augmenter la durée de ce bénéfice. Le bénéfice apporté par les plastifiant lors des contacts glissant/rayure est d'augmenter la déformation au seuil du contact élastoplastique et au seuil de contact

plastique, sans dégrader les propriétés volumiques et donc les forces exercées sur les pointes rigides.

La relation entre l'angle de retour de contact, déformation et le coefficient de frottement local révèle que l'effet maximal de coefficient de frottement local sur l'angle de retour de contact se trouve principalement dans le domaine plastique de contact (Figure XII). L'effet de coefficient de frottement local sur l'angle de retour de contact pendant le domaine élastique plastique et entièrement plastique est presque négligeable. Comme le domaine en plastique du matériel (dépend principalement des propriétés mécaniques en gros (vrac), donc pour améliorer la résistance à la rayure de polymères, il faudrait souligner pour modifier le comportement en gros (vrac) des matériels (matières). Le travail numérique commencé a permis d'identifier les domaines de comportement entre contact glissant élastique, contact élastoplastique et contact plastique. Ce travail pourra être étendu à la cicatrization des sillons, en intégrant des lois élasto viscoélastique plastique /viscoplastique et permettra d'identifier les rapports entre propriétés volumiques et coefficient de frottement pour maximiser la résistance à la rayure.

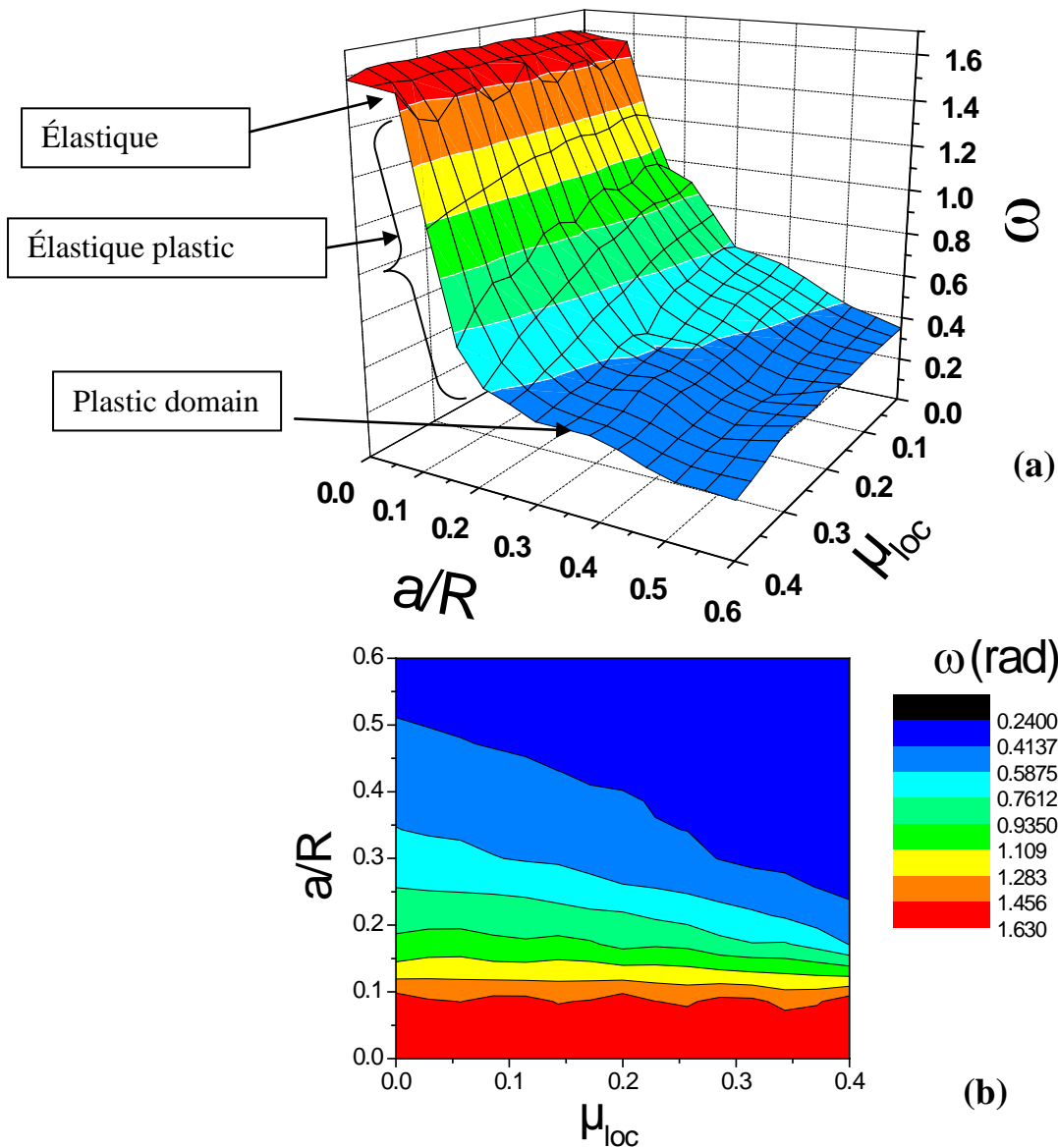


Figure XII Le rapport entre l'angle de retour de contact  $\omega$ , la déformation moyenne de contact imposée et le de coefficient de frottement local  $\mu_{loc}$  comme obtenu à partir des données numériques.



# Contents

Acknowledgments .....	i
Abstract .....	iii
Summing up the work in French .....	v
Section one Important aspects covering the subject.....	1
1 General .....	3
1.1 Introduction .....	3
1.2 Friction coefficient .....	3
1.3 Surface free energy .....	3
1.4 The elastic modulus of amorphous polymers .....	4
1.5 Hardness .....	5
1.6 Different aspects of PMMA .....	6
1.7 Plasticization of polymers .....	11
1.8 Slip additives .....	13
2 Scratching of polymer surfaces .....	19
2.1 Introduction .....	19
2.2 Historical background.....	20
2.3 Indentation & scratching hardness/processes .....	21
2.4 Experimental studies of scratching process.....	25
2.5 Different aspects of scratching of polymers .....	29
2.6 Material properties that affect the scratch damage .....	43
2.7 Improvement in scratch resistance .....	45
2.8 Conclusions .....	46
3 Friction analysis of polymers .....	47
3.1 Introduction .....	47
3.2 Different scales in friction mechanism.....	47
3.3 Different types of friction .....	49
3.4 Parameters controlling the friction coefficient .....	53
3.5 Effect of friction on different parameters .....	54
3.6 Conclusions .....	58
Section two Experimental and simulation results .....	61
4 Experimental work and discussion.....	63
4.1 Materials and methodology .....	63
4.2 Experimental results and discussion.....	67
4.3 Gratifying findings .....	101
5 Simulations by finite element method.....	103
5.1 Introduction .....	103
5.2 Finite element modelling .....	103
5.3 Simulation results and discussion.....	107
5.4 Gratifying findings .....	123
Section three General discussion on results and concluding part .....	125
6 General discussion on the results .....	127
6.1 General discussion on experimental work.....	127
6.2 Comparison between experimental and numerical data obtained from FE simulations .	129
6.3 The best approach to improve the scratch resistance.....	131
6.4 Gratifying findings .....	134
7 Conclusion & Perspective .....	135
8 References .....	139





## **Section one**

# **Important aspects covering the subject**



# 1 General

## 1.1 Introduction

In the past century, engineering plastics have progressed from novel invention to a major component in numerous industries. In recent years, engineering plastics have penetrated markets once dominated by metals and continue to grow in popularity with an average annual consumption growth rate of 5.09%. Because of the nearly limitless polymer structures and formulations that can be designed, the field of plastics is continually marked with technical innovations [5]. Polymers are more and more attractive for an increasing number of industries. Their low cost, ease of manufacture and processing, low weight as well as the appealing look they give to any surface have increased their use. Nevertheless, their lifetime is often reduced by their poor mechanical properties. Abrasion and scratching are often the cause of the loss of their optical and tribological performances [2, 6-11]. Plastics are relatively soft and can be easily scratched. Scratches on plastic surfaces greatly reduce their surface aesthetics and also lead to stress concentration, making them prone to premature failure. There is a strong need to improve scratch resistance in plastics for automotive and other applications demanding high surface quality [6].

Amorphous polymers such as polymethylmethacrylate (PMMA), polystyrene (PS), and polycarbonate (PC) are attractive for many engineering applications because of their excellent transparencies, high moduli, and relative ease of processing. However, these polymers exhibit shortcomings in their mechanical properties. PMMA tends to be brittle material that is damaged at small strains when unoriented. It has been toughened successfully with rubber particles, but high rubber contents (>30 wt %) are generally required, leading to large reductions in both the yield stress (50–75%) and the modulus (50–60%); and in most cases the optical transparency is also compromised [12].

## 1.2 Friction coefficient

The apparent friction coefficient is the ratio between the tangential and the normal load applied to a moving scratching tip [13-18]. It includes a “true local” friction coefficient, which is the scission at the interface between the tip and the surface being scratched, and a “geometrical” friction coefficient, which is the ploughing effect due to the wave front created ahead of the moving tip and depends upon the shape of the tip. Like in any other mechanical test, three basic types of behavior of the material at the interface (purely elastic, elastic-plastic & fully plastic) are observed in friction testing [13]. Different aspects of friction analysis will be discussed in detail in chapter 3.

## 1.3 Surface free energy

Surface free energy (or surface tension)  $\gamma$  is a basic property of the surfaces of materials and is linked directly to adhesion, wetting, adsorption, and other surface and interface phenomena [19, 20]. The attractive force between two bodies in contact is directly proportional to their surface energies. One can control the friction coefficient by modifying the surface free energies of the solids involved. Surface energy is also one of the factors responsible for the removal of the polymer material as wear debris [21]. Surface free energy originates from uneven forces acting on molecules and is defined as the Gibbs surface free energy per unit area. Apparently, the surface area, and eventually the molecular area, plays an important role in the determination of the surface energy [19]. It is well known that the surface composition differs from that of the bulk due to

preferential surface adsorption of one constituent. This process is driven, in part, by differences in surface energies and can be expressed through the Gibbs adsorption isotherm [22]:

$$-d\gamma = \sum_i \Gamma_i d\mu_i \quad 1.1$$

where  $\Gamma_i$  is the surface excess of the component  $i$ , and  $\mu_i$  is the chemical potential of that component. It is apparent from above equation that any difference in the surface energy  $d\gamma$  of the constituents of a multicomponent system results in relative enrichment of the air-interface in the lower-surface-energy component. Surface enrichment with the lower-surface-energy component has been reported for many blends. The compatibility between the blend constituents plays a significant role in surface enrichment [22].

According to Fowkes, surface free energy of a solid and a liquid can be expressed in the form [23]:

$$\gamma = \gamma^d + \gamma^i + \gamma^{Pl} + \gamma^h + \gamma^\pi + \gamma^e + \gamma^{ad} \quad 1.2$$

where index  $d$  refers to dispersion,  $i$  to induced dipole-dipole,  $Pl$  to dipole-dipole,  $h$  to hydrogen bonding,  $\pi$  to  $\pi$  bonding,  $e$  to electrostatic, and  $ad$  to acceptor-donor interaction [23]. From a practical point of view and according to Owens–Wendt theory, the total free surface energy ( $\gamma_s$ ) is the sum of its dispersive ( $\gamma_s^d$ ) and polar ( $\gamma_s^p$ ) components [9, 20, 22-26]:

$$\gamma_s = \gamma_s^d + \gamma_s^p \quad 1.3$$

Practically, this polar component is the sum of one or more nondispersion components arising from different types of molecular interactions. It cannot be stated for certain that the dispersion component of surface free energy results from London forces only, and that the nondispersion component results directly from the action of non-London forces. Rather, it may be assumed that the dispersion component of surface free energy of a liquid and a solid includes the part due to dipole induced-dipole interaction, and the polar component is the result of specific and nonspecific forces [20, 23].

The second point of view is represented by Good, Neumann, and co-workers. They did not divide surface free energy of a solid and liquid into components but expressed the work of adhesion by the geometric mean of the total surface free energies contacting the phase corrected by a parameter  $\Phi$ , which is a unique property of the pair of substances. However, for many solid-liquid systems the calculation of  $\Phi$  is impossible or very difficult [23].

## 1.4 The elastic modulus of amorphous polymers

In many applications, polymer materials undergo a large variety of mechanical loading conditions, wherein the influences of temperature and strain rate are of prime importance. Young's modulus is also strongly influenced by temperature and strain rate. In the glassy region, the initial Young's modulus  $E$  of amorphous polymers is found to decrease with increasing temperature in the following manner [27, 28]:

$$\log E(T) = \log E(T_{ref}) - a(T - T_{ref}) \quad 1.4$$

where  $E(T_{ref})$  is the Young's modulus at the reference temperature  $T_{ref}$  and  $a$  is a parameter characterizing the temperature sensitivity of the material. However, this equation is not valid in the

vicinity of the glass transition region due to the abrupt drop in stiffness between the glassy and the rubbery state. To take into account the effect of the glass transition, Drozdov proposed the following temperature dependence for E [28, 29]:

$$E(T) = E_0 - E_1 / (T_g - T) \quad 1.5$$

where  $E_0$  and  $E_1$  are material parameters and  $T_g$  is the glass transition temperature. However, this equation is only slightly better than Equation 1.4, as it can only be used to describe the very beginning of the glass transition, but not the rubbery plateau. The only model to be valid from fully glassy to fully rubbery is due to the work of Mahieux and Reifsnider. The basis of their approach is the influence of temperature on secondary bonding in polymers. Their concept can be summarized as:

Any transition in the polymer (secondary relaxation, glass transition, flow) requires breakage of secondary bonds (e.g. van der Waals, polar attraction). Breakage means cessation of the attractive interaction between the specific atoms involved in the molecular motion corresponding to the specific relaxation, i.e. rotation of a side group (e.g. beta relaxation), reptation of the main chains (e.g. glass transition) or global translations (e.g. flow). A distribution of strengths exists for the bonds between the macromolecules due to the different nature of bonds present in the material (e.g. Van der Waals, crosslinking) and the spatial arrangement of the molecules (Van der Waals interactions depending on the proximity of atoms) [28]. Amorphous polymers undergo three main transitions ( $\beta$  transition, glass transition and flow). The storage modulus is given by:

$$E(T) = (E_1 - E_2) \exp \left[ - \left( \frac{T}{T_\beta} \right)^{m_1} \right] + (E_2 - E_3) \exp \left[ - \left( \frac{T}{T_g} \right)^{m_2} \right] + E_3 \exp \left[ - \left( \frac{T}{T_f} \right)^{m_3} \right] \quad 1.6$$

where  $T_\beta$  is the  $\beta$  transition temperature,  $T_g$  is the glass transition temperature and  $T_f$  is the temperature marking the beginning of the flow region. The moduli,  $E_i$ , are the instantaneous stiffness of the material at the beginning of each region. The parameters  $m_i$  are the Weibull moduli, corresponding to the statistics of the bond breakage [28].

## 1.5 Hardness

The hardness of material may be simply defined as its ability to resist local deformation [30]. It is defined qualitatively as the characteristic ability of a material to resist penetration or abrasion by other bodies. However, any quantitative measure of this feature of material behaviour depends on the technique used for its measurement. It is an extrinsic property of a material rather than a fundamental or intrinsic property such as density or thermal conductivity. The ability of one material to abrade or scratch another material has a long history as the basis of a scale of hardness and now is clearly related to the more common measure of hardness as the resistance of a material to indentation. However, there is no simple relation between the values of hardness from these two tests. Producing an abraded groove in the surface of a specimen involves large plastic strains, and a number of analytical models have been proposed for this process based on such techniques as slip line field theory and the theorems of plastic load bounding. The scratch testing of brittle solids can also involve plastic behaviour facilitated by the high local hydrostatic compressive stresses generated close to the tip of a sharp indenter [31].

The hardness is traditionally measured by performing an indentation at a certain indentation load, removing the load and optically examining the surface to determine the area of the plastic residual imprint. The hardness is then defined as the ratio of the maximum indentation load and the measured area. A Vickers indenter is typically used, however, spheres and other geometries like conical or pyramidal are also used [32].

Hardness tests provide very simple and non-destructive means of measuring the resistance of a material to plastic deformation (and not the elastic deformation). There is a straightforward relation between the indentation pressure  $P_m$  (or  $H$ ) and the yield stress in simple compression  $Y$  or shear yield stress  $k$ . For an idealized rigid perfectly-plastic material which obeys the von Mises yield criterion, this relation is of the form:

$$P_m = C \cdot Y = \sqrt{3}C \cdot k \quad 1.7$$

where  $C$  is a constant whose value is about 3, depending to some extent on the shape of the indenter [30, 31, 33]. For a wide range of metals,  $P \approx 3Y$ . If the material shows appreciable elasticity, the factor of proportionality between  $P$  and  $Y$  will be less than 3.  $P \approx 1.5 Y$  where  $E/Y \approx 10$  (compared with a value of 100~1000 for metals) and for glasses,  $P \approx 2 Y$  where  $E/Y \approx 20$  [30]. By thoroughly analyzing the spherical indentation data, Tabor concluded that  $C$  is generally known as the constraint factor whose value varies from 2.8 to 3.1 if the substrate is rigid-perfectly plastic and from 1 to 3 if the substrate is elasto-plastic [34]. For polymers and rubber-like materials, the elastic and plastic properties depend on the chain length, the degree of cross-linking and the crystallinity of the material. Short chains are associated with low modulus and low hardness: long chains with increased modulus and hardness [30].

## 1.6 Different aspects of PMMA

### 1.6.1 General

PMMA is an amorphous glass below 110 °C and exhibits a particular damage mode of brittle fracture under normal conditions below 80°C [35]. It has the secondary transition ( $T_\beta$ )  $\approx$  10°C [36]. PMMA has a wide range of applications, which are principally concerned with its excellent transparency and light transfer, its good weathering resistance, and its high surface hardness and durability. These applications include glazing in aircraft and other transport, transparent guards and covers, lenses, baths, washbasins and sanitary ware, and rear-light assemblies for road transport [35]. It is also used in out-door electrical applications, high voltage applications, as transparent neutron stopper, standard broad cast television waves, radar bands, electrochemical windows, magnifiers, automotive tail lights because of its good compatible nature with other polymers, high resistance, non-tracking characteristics, surface resistance and optical properties [37]. The use of PMMA as the substrate material has several advantages. The PMMA sheet is a non-porous solid and therefore contamination caused by biomolecule adsorption is diminished. In addition, PMMA is inert in neutral aqueous solution and no hydrolysis occurs during the application [38].

Distinguished by the preparation method, there are two types of PMMA sheet commercially available. They are cast and extruded PMMA. The cast PMMA has higher softening temperature than that of the extruded PMMA.

### 1.6.2 Molecular mechanics studies on PMMA

The relationship between the physical properties and the chemical constitution of polymers can be better known with the help of polymer chain flexibility. Flory enunciated the interplay between polymer properties and chain flexibility. With the advent of metallocene catalysts, it is possible to prepare and control the stereo chemical sequence of polymers. With this control, it is possible to prepare pure isotactic and syndiotactic polymers. PMMA is one of the typical polymers

whose tacticity can be widely controlled by changing the reaction conditions. The properties of polymers in bulk and in solution depend on tacticity. Therefore, the control of stereo regularity of PMMA provides a promising way for controlling the properties. The glass transition temperature ( $T_g$ ) of PMMA depends on the tacticity and is lower in the isotactic form compared with the syndiotactic form.  $T_g$  of PMMA also depends on the structure of the ester group and generally increases with the increase in bulkiness of the side chain. On the other hand, the flexibility of polymers decreases. It is a linear, thermoplastic and about 70–75% syndiotactic. PMMA can be prepared in both isotactic and syndiotactic forms. Structural characteristics at molecular and super molecular levels greatly affect the relevant properties of macromolecular materials. Before looking at the bulk properties of polymers, an understanding of the individual structure and properties of a single chain is necessary. Based on the properties of a single chain one can select a sequence, which gives properties different from others. The bulk properties of a polymer can be simulated based on the selected new sequence [39].

### 1.6.3 Shear stress & strain rate in PMMA during scratching

The apparent interfacial shear stress on polymeric materials may be taken as the ratio of the tangential force to the normal contact area,  $\tau_{app} = F_t / S_n$ . The apparent shear stress may be split into a ploughing component and a true shear component. The latter is the product of the true local friction coefficient and the contact pressure

$$\tau_{true} = \mu_{local} \times p \quad 1.8$$

and the ploughing shear stress may then be defined as

$$\tau_{plough} = \tau_{app} - \tau_{true} \quad 1.9$$

At low strain rate (or high temperature), the contact is relatively symmetric and the ploughing stress is low. At high strain rate (or low temperature), the contact is asymmetric and both the ploughing stress and the shear stress increase with the logarithm of  $d\varepsilon/dt$ . At intermediate strain rate or temperature, the effect of the tack leads to a local peak in the shear stress. The master curve for the ploughing and true shear stresses for PMMA plotted as a function of strain rate at 20°C displays these three domains as shown in Figure 1.1.

### 1.6.4 Stress-strain relationship in PMMA demonstrating its bulk behaviour

Polymeric materials present a more complex behaviour and a finer analysis is required in order to understand the influence of bulk mechanical properties on the scratch resistance and on the overall surface durability [3, 17]. The viscoelastic–viscoplastic properties as well as the difference between the tensile and compressive behaviour need to be taken into account in the scratch analysis of polymers. The elastic modulus decreases with temperature, as does the yield strength (Figure 1.2). A clear transition in the failure mechanism occurs around 45°C for PMMA. At low temperature, we observe a brittle behaviour while the material remains in an elastic deformation under small strains. Above 45 °C, the strain at break is increased suddenly while a necking deformation mechanism occurs in the material, allowing these larger strains. This ductile/brittle transition may also depend on the strain rate applied during the test [3]. The ductile/brittle transition occurs when the ductile strength becomes less than the brittle strength. These strengths are a function of the temperature. When the strain rate is increased, both ductile and brittle strengths are increased, and the temperature at which the ductile strength becomes less than the

brittle strength also increases. Therefore, the ductile/brittle transition temperature increases as a function of strain rate [3].

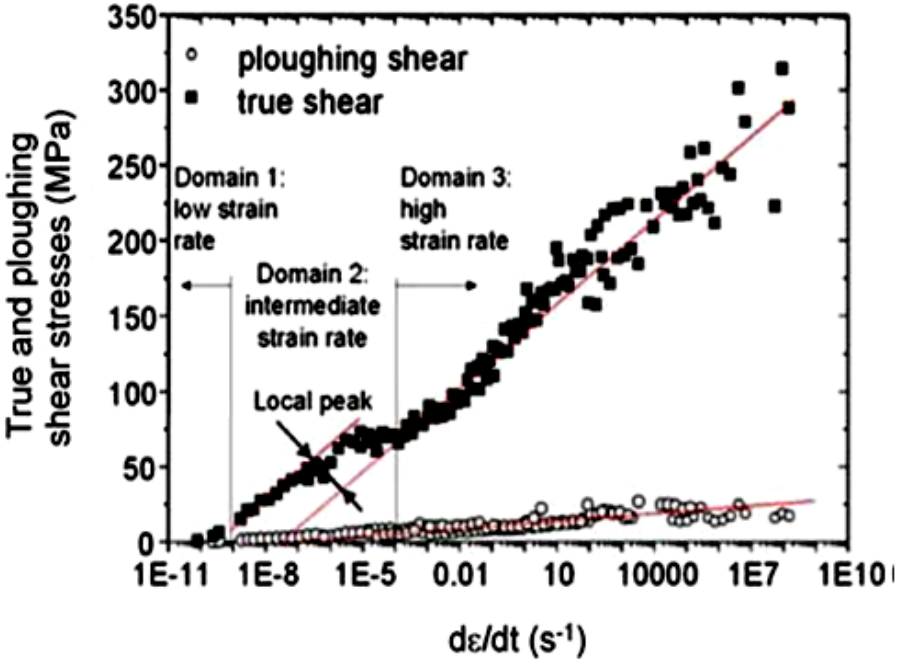


Figure 1.1 Master curves for the ploughing and true shear stresses plotted at room temperature for PMMA with scratch test with a conical tip [13].

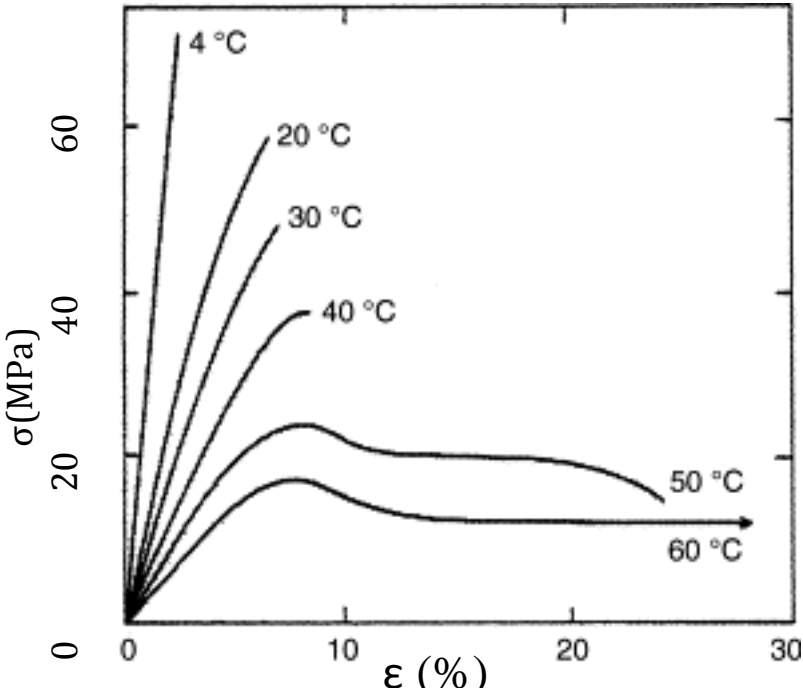


Figure 1.2 Stress–strain relationship for PMMA under uniaxial tensile testing conditions [3].

**1.6.5 Tensile properties of PMMA**

The bulk mechanical properties of PMMA are strongly strain rate sensitive. The effect of strain rate on the mechanical properties of the PMMA can be summarised as follows [40]:



- (1) PMMA changes its tensile behaviour from ductile to brittle one as the strain rate increases.
- (2) Strength and elastic modulus increase with increasing strain rate, which shows strain rate strengthening and strain rate hardening. Fracture initiation strain decreases with increasing strain rate, which exhibits high-rate embrittlement.
- (3) The tensile properties of PMMA show greater strain rate sensitivity when strain rate reaches about  $18.6 \text{ s}^{-1}$  [40].

During the fracture process, the periodical energy accumulation and its release at the crack tip results in the alternate changes of crack speed, which leaves the rib morphology on the fracture surface. Increasing strain rate reduces the energy accumulation time and the crack is appropriate to extend at a high speed, thus increase the gap of the ribs. When the strain rate rises to a certain value, the crack extends unsteadily at a high speed until the specimen fractures, and no rib can be observed. This is coincident with the high-rate embrittlement [40].

Fracture is a dissipative process during which either plastic work is converted partly into heat and/or heat is released during the fracture process itself. When the process is adiabatic, the released heat causes a local temperature elevation which can markedly alter the mechanical characteristics of the material.

### **1.6.6 Influence of water on mechanical behaviour of PMMA**

PMMA is often used as a material in submarine applications. Therefore, the mechanical properties of dry and wet PMMA in water and/or under hydrostatic pressure are of great importance [41]. The specific work for fracture in PMMA in water is about four times higher than in air with unstable propagation, and that the loading rate and crack speed are important parameters. It is also known that water acts like a mild crazing agent, lowering crazing stress, and leading to faster craze growth. The brittleness increases at high water content, due to the appearance of water clusters in the material. From the small-strain mechanical behavior point of view, PMMA containing water shows a small increase in internal friction at very low temperature ( $-100$  to  $-150^\circ\text{C}$ ), 50% of the water being taken up by swelling and the remaining 50% being accommodated in microvoids. Experiments on stretched PMMA showed that the water sorption depends on the molecular orientation, and the relaxation experiments show that the glass transition temperature decreases by about  $25^\circ\text{C}$  [41]. The tensile stress–strain response is shown in Figure 1.3 for individual test samples having 0, 0.40, and 0.80 wt% of sorbed water. The trend of the change in average stress at fracture  $\sigma_f$  and that of the strain to fracture  $\varepsilon_f$  as a function of water concentration are shown in Figure 1.4 and Figure 1.5 respectively. These graphs are based on the experimental data reported by Hamouda [35].

At water contents up to 0.80%, the strain to fracture increases and there is a significant reduction in the modulus. This behaviour is indicative of water acting as a mild plasticizer for PMMA [35, 41]. However, the behaviour of stress to fracture and strain to fracture above 0.80% water concentration cannot be obtained since the highest water concentration was 0.80%. However, as the water concentrations reach 1% or so, it is suggested that some water molecules may begin to cluster and act more as filler particles than as a plasticizer which leads to stress concentration effects, accentuates craze development and causes early fracture [35].

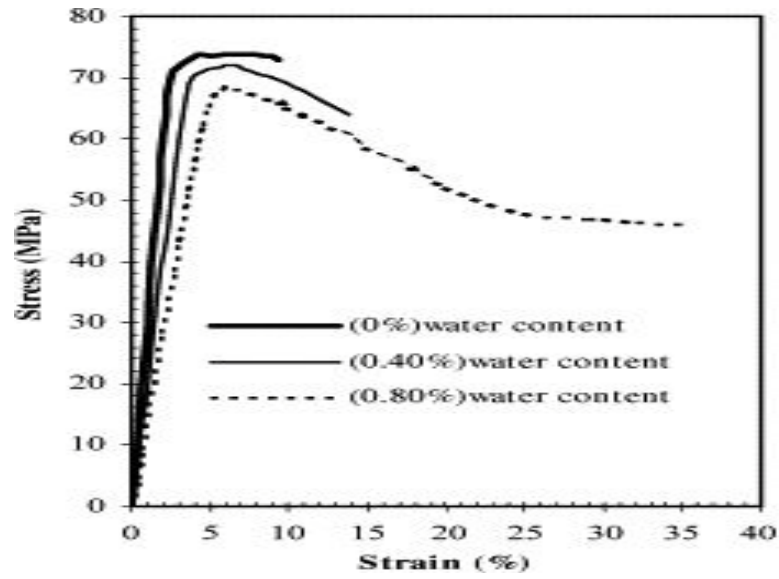


Figure 1.3 The tensile strength response of PMMA at different humidity levels [35].

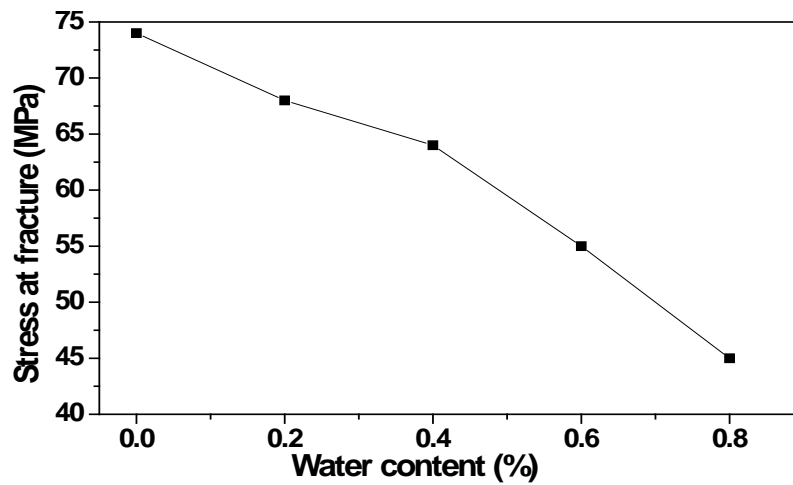


Figure 1.4 Average stress at fracture of PMMA versus its water content.

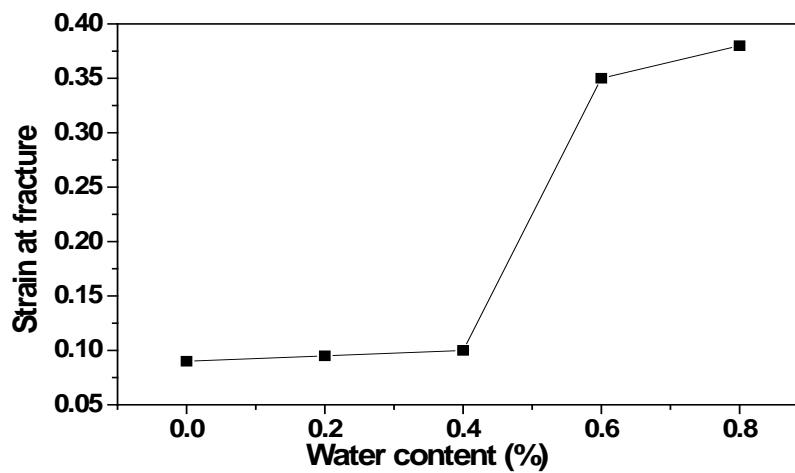


Figure 1.5 Average strain at fracture of PMMA versus its water content.

The general fashion of the influence of absorbed water on tensile strength of the PMMA is shown in Figure 1.6 that is based upon the experimental results reported by Hamouda [35].

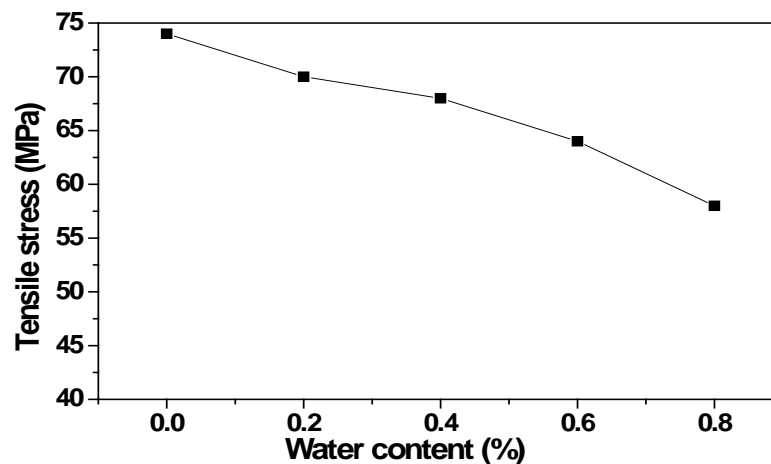


Figure 1.6 Average tensile strength of PMMA versus its water content.

As the water content increases from 0 to 0.80%, there was a significant change in deformation behaviour for PMMA from brittle mode to ductile mode as shown in Figure 1.3. The area under the stress–strain curve up to fracture for PMMA, which indicates the toughness, increases with increasing water content in PMMA from 0 to 0.80%. This means that the increase of water content in PMMA has led to the increment of toughness. With higher water content, ability of PMMA to absorb energy up to fracture will be improved [35].

The following conclusions can be drawn:

1. The strain to fracture for PMMA increases with increasing water content.
2. The tensile strength for PMMA decreases with increasing water content.
3. The water acts as a mild plasticizer for PMMA.
4. The fracture toughness of PMMA increases as the water content increases indicating that the ability of energy absorbing up to fracture is increased.
5. PMMA samples with higher water content have tendency to deform plastically before fracture.

## 1.7 Plasticization of polymers

Industrial use of polymers ranges across a broad field of structural, mechanical, electrical and optical applications. Polymer blends are gaining practical importance and scientific interest, as a result of the current emphasis on modifying the existing synthetic polymers, rather than manufacturing the new ones [22, 42]. Both technically and economically, additives form a large and increasingly significant part of the polymer industry. Plasticizers account for about one third of the global plastic additives market in terms of consumption. Plasticizers have recently been scrutinized for environmental and health related problems [5]. Besides health-related issues, other driving forces for the development of new plasticizing agents include improving the high temperature stability (so that plastics can be used effectively at high temperatures without loss in flexibility), increasing the flexibility of polymers at low temperatures, decreasing the photo-oxidation of polymers in the presence of ultraviolet light, and reducing the leaching of plasticizer from products in contact with various fluids [43].

The definition of an ideal plasticizer changes with each application. The primary role of plasticizers is to improve the flexibility and processability of polymers by lowering the second order transition temperature. Plasticizers are normally low molecular weight (MW) resins or liquids, which form secondary bonds to polymer chains and spread them apart. Thus, plasticizers reduce polymer-polymer chain secondary bonding and provide more mobility for the macromolecules, resulting in a softer, more easily deformable mass [5, 37, 44-49].

Plasticizers can be either internal or external, where external plasticizer molecules are not attached to polymer chains by primary bonds and can therefore be lost by evaporation, migration or extraction. On the other hand, internal plasticizers are inherently part of the plastic and remain part of the product. For both types of plasticizers, there is often a marked temperature dependence of material properties, though this is more pronounced with internal plasticizers. Internal plasticizers also have problems with retaining dimensional stability at elevated temperatures [5].

Plasticizers may also be divided into primary and secondary types. Primary plasticizers are used as the sole plasticizer or as the major component of plasticizer, while secondary plasticizers are typically blended with primary ones to improve certain performance properties and/or to lower cost [5].

Plasticizers are incorporated in the amorphous parts of polymers while the structure and size of any crystalline part remains unaffected. Plasticizers are expected to reduce the modulus, tensile strength, hardness, density, melt viscosity, glass transition temperature, electrostatic chargeability and volume resistivity of a polymer, while at the same time increasing its flexibility, elongation at break, toughness, dielectric constant and power factor. Ideal plasticizers should be highly compatible with polymers, stable in both high and low temperature environments, sufficiently lubricating over a wide temperature range, insensitive to solar ultraviolet (UV) radiation and leaching, migration resistant, inexpensive and should fulfil health and safety regulations [5, 43, 50].

The driving forces for development of speciality plasticizers come from the extensive use of plastics in a wide range of applications, increased quality requirements, the need for materials that meet increasing rigorous product specifications and compatibility problems relating to particular products. Food legislation, health and industrial safety and commercial aspects play an important role and, over last 50 years, have led to the development of the vast range of plasticizers currently available. A large number of high performance plasticizers are produced now by systematic esterification of aliphatic or aromatic carboxylic acids.

The degree of plasticization of polymers is largely dependent on the plasticizer's chemical structure including chemical composition, MW and functional groups. Plasticizers that have low MW and a small number of polar groups generally provide higher flexibility and plasticization. Plasticizers are generally chosen on the basis of the following criteria [5, 43]:

- compatibility of the plasticizer with a given polymer,
- processing characteristics of the plasticizer,
- desired thermal, electrical and mechanical properties of the end product,
- resistance to water, chemicals, solar radiation, weathering, dirt, micro organisms,
- effect of plasticizer on the rheological properties of polymer,
- toxicity, and
- volume-cost analysis.

## 1.8 Slip additives

### 1.8.1 Introduction

The plasticizer used to reduce the friction coefficient of the polymeric surfaces is termed as a slip agent. Modifying the surface of polymer film and sheet through the use of slip and antiblock additives can either improve performance in fabrication or the end-use performance of the polymer [51]. Formulating of slip additives is often a trial-and-error procedure. For example, a processor may need to adjust slip level first to obtain the desired friction coefficient, then add other additive and see what effect it has [51].

Surface blocking was a historical obstacle as long as humans began to process materials. In ancient times natural products such as bees' waxes, plant waxes, natural resins, oils etc were used to improve technological output and quality. The first paper on improvement of friction coefficient of polypropylene film was published in 1966 that included polymer selection, concentration of fatty acid amides, its migration to the film surface and the friction coefficient of the resultant polymer film. However, some related studies and inventions were already reported in 1950s [52].

### 1.8.2 Expectations from commercial slip additives

Table 1.1 presents the general characteristics expected from slip additives [52]:

Sr. No.	Performance indicator of slip additives	Effecting characteristics of polymers
1	Purity	Degradation, toxicity
2	Colour	Cost of colour correction
3	Homogeneity	Handling
4	Compatibility with polymer	Optical properties, migration to surface
5	Low transfer to material in contact	Migration to moulds etc
6	Surface tension	Wetting, migration to surface
7	Oxidation and thermal stability	Oxygen permeability reduced
8	Weathering	Protective layer
9	Non-interference with polymerization	Properties of the product
10	Residue on product	Adhesion, welding
11	Toxicity	Health and safety
12	Price	Cost
13	Water repellency	Hydrophobic properties
14	Abrasion and scratch resistance	Surface modification
15	Reduced friction coefficient	Surface modification
16	High efficiency	Low concentration required
17	Low volatility	Loss from melt, bubbling
18	Non-staining	Inert layer on surface, low adhesion
19	Food contact approval	Health and safety

Table 1.1 Performance indicators and their potential effects on acceptance of slip additives

### 1.8.3 Chemical compositions of some important slip additives

Some important chemical compositions used as slip agents are [52]:

- |                                      |                                     |                        |
|--------------------------------------|-------------------------------------|------------------------|
| i. Carbon nanotubes                  | ii. Fatty acid amides               | iii. Fatty acid esters |
| iv. Fatty acids                      | v. Fatty acid salts                 | vi. Flour compounds    |
| vii. Graphite                        | viii. Molybdenum sulfide            | ix. Secondary amides   |
| x. Lignosulfonates                   | xi. Polytetrafluorethylene          |                        |
| xii. Silicones (oil and crosslinked) | xiii. Waxes (natural and synthetic) |                        |

#### 1.8.4 Mechanism of action of slip agents

When a slip agent is added in a polymer melt, it is absorbed in the polymer amorphous region and remains there till the material remains in melt form. When the material is cooled, the slip agent becomes incompatible due to difference in surface free energy and begins to migrate to the material surface [52]. The rate of migration depends upon the difference in the surface energies of the polymer and the additive (the larger the difference, the faster the migration) as discussed earlier in section 1.3 [22, 52].

The arrangement of the molecules on surface is not muddled but it has a structure resulting from the affinity of two segments contained in the slip agent. Fatty acid amides have two structural units: the amide group and a hydrocarbon chain. Hydrocarbon chain of the fatty acid amides has high affinity to the hydrocarbon chain of the polymer and thus fatty acid amides are embedded in the polymer firstly with their amide groups facing air. On arriving more amide molecules onto the surface, they form second layer on the surface orienting themselves with amide groups facing each other (that is natural as similar functional groups have affinity to each other especially in presence of oxygen and hydrogen due to the capability of forming hydrogen bonding). The friction is not reduced until doubled layer is formed as weak hydrogen bonding is easy to break (does not require substantial energy to break bonds). The presence of such lubricated layers (that slide on each other with ease) on the surface contributes to the slip properties expected from these materials [52].

X-ray photoelectron spectroscopy (XPS) indicated that the surface concentration of Oleamide increases for 30 days and then it becomes constant. However, Stearamide shows 3 times lower concentration on the surface than Oleamide at this time. Oleamide undergoes surface oxidation due to presence of double bond in its structure [52].

#### 1.8.5 Synergy in action between surface additives

It is a very common practice to use a combination of two or more additives, for example a slip additive and an antiblocking agent. Such a combination may include fatty acid amide as slip additive and silica as antiblocking agent. Synergy of action of two or more components may give better combined result than can be expected from a sum of actions of each components action alone as is clear from Figure 1.7. Talc reduces the coefficient of friction to as lesser degree than silica, but adding silica to a material containing Erucamide increases the coefficient of friction. On the other hand, talc and Erucamide form synergetic mixture, but at least both additives are not antagonistic to each other. However, silica and Erucamide form antagonistic mixture which is ineffective combination for reduction in friction. The result of such combinations depends upon the structure of the components. Combination of three additives silica, Oleamide and Stearamide is explained in Figure 1.8 [52]. Silica decreases the block force relative to its concentration without affecting the coefficient friction decreased by the Oleamide. On the other hand, silica decreases the coefficient of friction without affecting the blocking force decreased by the Stearamide. Thus silica acts as antiblock and Oleamide acts as slip agent in the first case whereas it acts as a slip agent and Stearamide acts as an antiblock agent in the second case. Thus it is clear from this example that the complex nature of synergy of action of additives may not only improve the performance of each

other, but may also change the mechanism and nature of action of the other additive in combination (a general antiblocking agent may acts as a slip agent and vice versa) [52].

In addition to synergy (or antagonism) of additives, the polymer type also plays an important role. For example several hundred ppm of Erucamide or Oleamide make the low density polyethylene slippery but 3-4 times more additive is required to obtain the same effect with linear low density polyethylene [52].

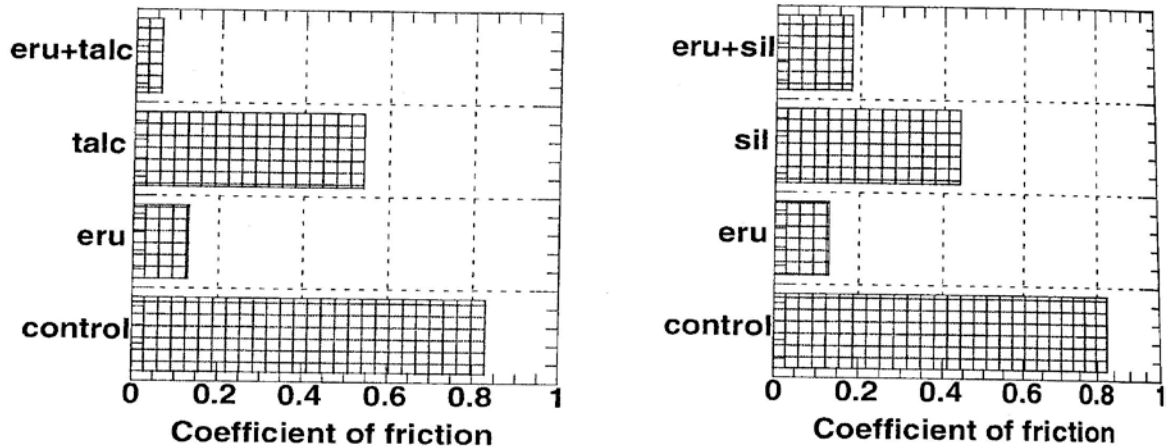


Figure 1.7 Coefficient of friction of LLDPE film (measured after 1 hour) with and without 500 ppm Erucamide and 1000 ppm talc (on the left) or 1000 ppm silica (on the right) [52].

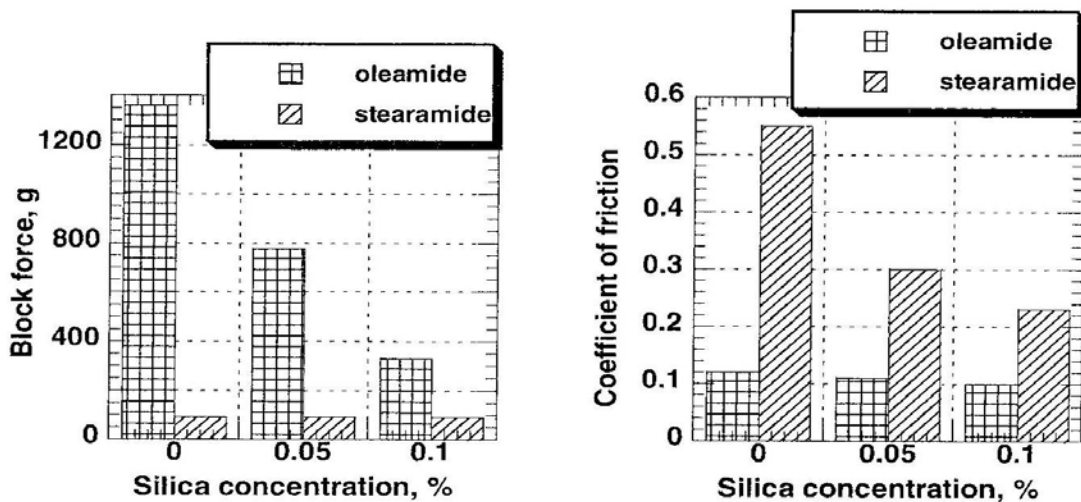


Figure 1.8 Effect of antiblocking silica agent on block force (on the left) and coefficient of friction (on the right) of polyethylene films containing 0.1% Stearamide or Oleamide [52].

### 1.8.6 Effect of slip additives on mechanical properties

The organic antiblocking, release and slip additives are [52]:

- added in small concentrations
- incompatible with the matrix polymer
- insoluble in polymer

- acting on the surface
- filling free spaces in amorphous regions.

If the tensile strength is decreased by the slip additive, it indicates that the additive is soluble in the polymer and interferes with its crystallization or affects crystalline region. If the elongation is increased by some additive, it suggests that it acts as a plasticizer [52].

Solid clear gel particles of ultra high molecular weight polydimethylsiloxane are added to reduce friction coefficient of thermoplastic resins. They differ from other additives in that they are solid particles and are completely inert to the matrix resins. They have no influence on tensile strength, elongation and modulus [52].

### **1.8.7 Fatty acid amides as slip agents**

Fatty acid amides are the most common slip additives used to reduce the coefficient of friction at the surface [51, 53]. Amide slip additives are used in a wide range of polymers and they play a vital role in the performance of many plastic materials [54]. These are the 'classic' lubricants, derived from natural oils and fats which act by migrating to the surface. According to type, they can improve mould release, melt flow, lubricity and scratch/scuff resistance and can reduce the friction coefficient, static build-up and wear [55]. As amides are generally incompatible with the polymers, they migrate or bloom to the surface easily and form a crystalline structure that decreases the friction coefficient. Amide slip agents include primary amides, secondary amides, and bisamides [51]. Primary amides include Stearamide, Oleamide and Erucamide and are used as slip and anti-blocking agents [55]. Generally speaking, Stearamide and Behenamide give the best anti-block performance whereas Oleamide and Erucamides give the best slip properties [51, 55]. Behenamide is used in bi-axially oriented polypropylene (BOPP) film, for example, to provide both slip and antiblocking properties while maintaining clarity [51]. Secondary amides include oleyl palmitamide and stearyl erucamide. These have good thermal stability, showing no appreciable breakdown below about 350°C, and are therefore suitable as lubricants for engineering/technical plastics with processing temperatures above 300°C [55]. However, amides provide only short-term scratch protection [56].

Erucamide(*cis*-13-docosenamide) is the most widely used amide, followed by Oleamide [51, 53]. It is a C-22 fatty acid amide that possesses a double bond at C-13 position. Ozone is extremely effective at selectively cleaving this double bond, creating the C-9 aldehyde nonanal. In industrial practice, Erucamide is used in the range of 0.05 to 0.2%. It is a preferred slip release agent but it may undergo substantial blooming subsequent to molding resulting in an agglomeration of the Erucamide on the surface of the molded polymeric article. This agglomeration can cause gumming. Surprisingly stearyl erucamide (Crodamide 212) has been found to avoid the blooming problem [52]. Erucamide is also considered to impart moderate 'antiblocking' properties [53]. It tends to possess good oxidative stability and low volatility. It also offers good release properties for injection moulding [55]. Figure 1.9 shows that the friction coefficient depends upon the Erucamide added. Increased amounts of the Erucamide are gradually less effective as friction coefficient reaches the equilibrium characteristic of composition [52].



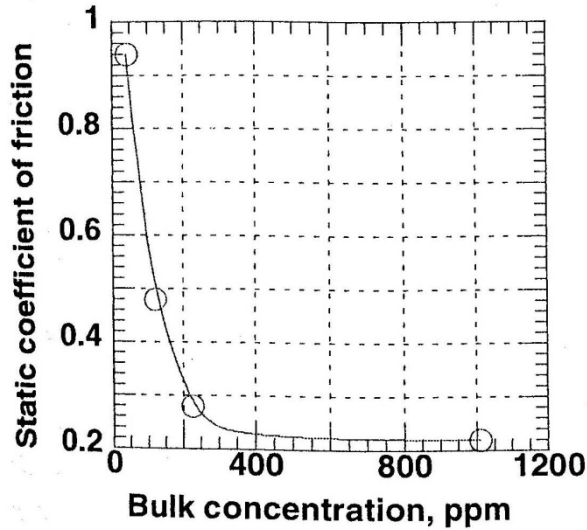


Figure 1.9 Static coefficient of friction of LLDPE film containing different bulk concentrations of Erucamide [52].

When choosing an amide slip, formulators consider migration rate, efficiency in reducing friction coefficient and thermal stability. Amides must have time to migrate to the surface before antiblocking and slip properties take effect [51]. Time of storage facilitates the amides in their migration to the surface ultimately resulting in decreased friction coefficient [52]. Migration rates vary with amide type, polymer type, slip concentration and the temperature. Primary amide like unsaturated Erucamide and Oleamide migrate quickly and are the most efficient slip agents [51]. Duration of allowed migration time and the type of additive are also important. Figure 1.10 shows that it takes a long time for slip agent to reach its highest concentration on the surface in its undisturbed state. The figure also shows that Oleamide migrates more readily to the surface than Stearamide [52].

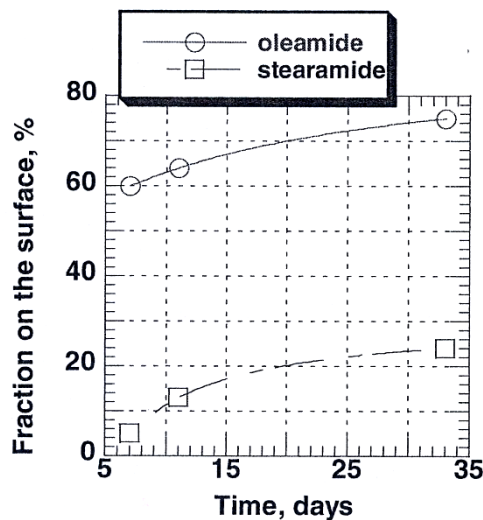


Figure 1.10 The percentage of the total added slip agent found on surface vs. time of storage [52].

Thermal degradation is known to have an adverse effect on the properties of slip agents and can cause various slip additives (particularly those with poor thermal stability) to become ineffective at reducing the coefficient of friction [53]. Thus besides reduction in friction coefficient, thermal oxidative stability is becoming more important as processors increasingly use

polymers with higher processing temperatures [51]. Amide additives residing on the surface may be degraded by oxidation or UV radiation or lost by evaporation [52]. Oxidative degradation of slip can result in slip property loss, increased colour, and odour [51]. The surface concentration of Erucamide does not change with time at room temperature but decreases drastically when temperature increases to 55°C [52]. Amides with higher thermal stability are also less volatile and will remain in the polymer even at higher processing temperatures. Saturated versions of Erucamide and Oleamide offer better thermal stability than their unsaturated counterparts, and, in general, Erucamides are more thermally stable than Oleamides. Secondary amides and bisamides are even more thermally stable. They are used in the higher temperature cast film process and in engineering polymers such as styrenics and are useful for maintaining friction coefficient over a long storage life [51]. A high aging temperature increases degradation rate and volatile losses, resulting in decreased amount of active slip agent on the surface. Influence of contact with solids and liquids may also remove sufficient amount of slip agent from the surface of the material leading to an increase the friction coefficient [52].

Due to concerns about vehicle interior air quality (VIAQ), the people are increasingly cautious about using additives that bloom to the surface and contain volatile organic compounds (VOCs) that contribute to fogging or malodours. Although migratory additives such as Erucamide have traditionally been used to improve the scratch and mar performance; however, in addition to VOC concerns, Erucamides can potentially interact with stabilizers and cause surface stickiness [56]. Erucamide is irritating to eyes, respiratory system and skin. The toxicological properties have not been thoroughly investigated [52].

## 2 Scratching of polymer surfaces

### 2.1 Introduction

The surfaces of most polymeric materials are highly sensitive to scratches, due to which their use is restricted for high performance optical devices. In other circumstances, these materials are used for moving mechanical parts, where friction and wear properties are important. A scratch may be regarded as a tangential indentation. Hence standard indentation laws can be used to analyse the geometry of the scratches left by a moving tip on the surface of a viscoelastic viscoplastic materials such as PMMA [57]. Scratch damage is recognized as one of the key factors limiting the service life of polymer products. It is, therefore, important to investigate the scratch damage on both the surface and the subsurface of the polymeric materials [6].

The two main scratch damage patterns found are to be the plastic flow scratch pattern and the fracture scratch pattern. Shear yielding is the main cause of the plastic flow scratch pattern, while tensile tear on the surface and shear-induced fracture on the subsurface are the main damage mechanisms found in the fracture scratch pattern. Subsurface damage is known to contribute to most of the fracture resistance in polymers. It is believed that material removal and the ability of the scratch damage to scatter light are sometimes related to the nature of subsurface damage [6]. The scratch process is generally regarded as a complicated mechanical process. Scratch performance of polymers is determined by both the material properties and the stress field induced by scratch, which is related to the scratcher geometry [6, 58]. Polymers are peculiar materials, in that they show a wide range of surface deformation characteristics for relatively small variations in the applied strain, normal load, rate of deformation (the sliding velocity), or the bulk temperature of the polymer [3, 59]. Hence, the response of the material depends greatly upon the actual mechanism which occurs during the deformation [59]. The materials deformation characteristic is extracted from the scratch width and surface micro-features such as cracks, crazes and plastic flows [58]. Because of the large elastic recovery of polymers and their complex rheological behaviour, the analysis and the interpretation of this test is far more difficult than that for metals [14].

Important variables that can change the damage response of polymers during scratching are strain (defined by the angle of attack and the friction), scratching velocity, normal load (this determines the depth of scratch), temperature or thermal effects, state of lubrication and the stiffness property of the scratching device [3, 14, 60-62]. In order to rationalize various effects, Briscoe et al. have proposed the idea of using scratching maps while presenting scratching data. Though qualitative in nature, scratching maps give an excellent way of identifying some broad deformation behaviour of polymers such as ductile, brittle or visco-plastic for a wide range of experimental parameters [60].

The use of scratch test on polymers has been increasing in recent years to understand the response of polymers to single point damage [33, 60]. Probably this has been because of the reason that polymers are being used as bearing or decorative surfaces and the performance of these polymeric surfaces can be severely compromised due to scratching or large-scale wear. The asperities on the surface of a hard material, if they come in contact, can easily produce scratches on the polymer surface. The occasional presence of hard debris or third-body can also be a source of scratches on the polymer surfaces. Several researchers have used scratch test to compare resistance to scratching for different polymers [60]. As a simplification of the complex abrasion process, the scratch test has been used effectively for identifying the main parameters in the wear resistance of material surfaces [6]. Scratching of materials is a convenient and now very popular means of characterizing surface hardness and dynamic scratch resistance of materials and coatings [3, 14, 15,

58-60]. Some of the areas where this test has been successfully used in the engineering field, both by research and industry, include the determination of the friction coefficient and hardness of materials, characterizations of coatings, paints and thin-films, modelling of the wear of materials and the estimation of different material deformation characteristics when subjected to hard asperity damage [58]. So understanding of this test is of great interest to both academic and industrial communities [14].

## 2.2 Historical background

The scratch test is a very old experimental method used to study the mechanical and surface properties of materials. As early as 1722 Reaumur developed a scratch scale which was a measure of the position on an end quenched steel bar which could be scratched by the metal specimen [14]. Exactly, a century later (1822) Mohs proposed 10 minerals in increasing order of scratch hardness: each mineral will scratch the one below it on the scale but will not scratch the one above it [14, 33, 58]. Thus the scratch hardness of a material was determined by drawing a mineral from the Mohs' scale on the surface of the given material. The relative scratch hardness was then decided based on whether or not the mineral made a scratch on the surface of the material. If the mineral made a scratch on the material then the material was considered as softer than the mineral. Scratch tests were carried starting from either end of the Mohs' scale (diamond as the hardest and talc as the softest minerals) to determine the exact position of the given material in terms of relative hardness. Finally, the scratch hardness of the material was given as a number [58].

Another century later (1954) Tabor demonstrated that a metal surface of (indentation) hardness  $H_1$  will be scratched by a point of hardness  $H_2$  if  $H_2 \geq 1.2 H_1$  and that each Mohs standard is approximately 60% harder than the preceding one [58, 63]. The Tabor's study demonstrates clearly the connections between the (indentation) hardness  $H$  and the scratch hardness  $H_s$ , a problem related to the models of contact and friction between solids, but the accurate relations are still not well understood even for metals [14, 58]. Tabor's work was the basis for many later works for metals which was also extended to polymers showing the plastic yielding similar to metals [58].

The work by Schallamach has contributed much in understanding the scratching and abrasive wear failure of rubbers. Schallamach performed experiments on rubber surfaces by sliding sharp needles and blunt indenters. The damage created by these indenters, also known as "isolated stress concentrators", depended upon the type of the indenter. The sharper needles produced tearing cracks in the direction of sliding while blunter indenters produced cracks with larger diameter of the elliptical crack perpendicular to the direction of sliding. This behaviour is different in elastomers from what is seen in ductile materials such as metals and thermoplastic polymers; and is somewhat analogous to that seen in ceramics. However, if a polymer shows rubbery behaviour under any particular set of conditions (temperature, plasticization etc), the responses shown by Schallamach do appear to dominate the damage characteristics [58].

The transition between ploughing (or rubbing) and cutting was firstly investigated by Mulhearn and Samuels. A main parameter related to the scratch test is the attack angle. They stated precisely by experiments the existence of a critical attack angle  $\beta_c$  below which ploughing occurs without any material removal and above which cutting occurs with the formation of a chip.

Sue and co-workers focused on the use of the scratch test for evaluating the surface scratch resistance of different polymers. They observed that the scratch process is a function of the basic material properties such as the elastic modulus, the yield strength and the tensile strength as well as material surface characteristics such as the coefficient of friction. Kaneko used AFM to study the

microwear processes for three polymers, PMMA, PC and epoxy. Adams et al., working on PMMA, showed that parallel scratches do not produce wear particle and the material is displaced as “pile-ups” or ridges on the sides of the scratch [58].

Several scratch testers for polymers were introduced in the literature. Of these, the constant load scratch test developed by Ford Motor Company (Ford Lab Test Method, FLTM) is being considered as an industrial standard. Another new scratch tester, which uses an atomic force microscope (AFM) and an acoustic emission device, was developed by CSEM Company. This new progressive load scratch tester can provide the load-displacement information during scratch and the residual scratch profile after scratch [6]. By building a new apparatus to observe the real contact surface under load Gauthier and Schirrer, demonstrated that the contact surface at the rear part decreases as the attack angle  $\beta$  increases [14].

### 2.3 Indentation & scratching hardness/processes

Conventionally, normal indentation methods are used to characterize the hardness of various materials including polymers. The key difference between the normal indentation method and the scratching is that the indenter is uniformly supported over the contact area in normal indentation and the hardness is a near-static response of the material. As the indentation force is supported by the material right beneath the indenter, a high compressive stress is built in the vicinity which causes mostly plastic deformation (probably also involving some volume change in polymers) with limited strain. However, in a scratch hardness test, an indenter tip is made to move across the surface of a material, resulting in a significant amount of elastic/plastic deformation and brittle cracking (due to tangential scratch force acting as tensile force on the rear half of the tip). The consideration of the support of the normal load by the material may be important for a proper definition of scratch hardness. For a perfectly plastic material, there is no recovery after deformation, and hence there is no support for the rear half of the indenter tip as it moves forward. In contrast, for perfectly elastic material, there can be full recovery of the material, and thus the tip will be supported in the rear half as well. For visco-elastic materials, the recovered material will offer only a partial support for the indenter in the trailing zone. This support will depend upon the material's rate of recovery and the imposed scratch velocity [31, 57, 60]. The indentation process involves a strong shear-compression stress field and the sliding process is a shear-stress dominant process. The scratch process is assumed to be the superposition of an indentation process and a sliding process. The maximum tensile stress generated by an indentation process is much less than that due to a scratch process. This indicates that the indentation test alone is not adequate for predicting the scratch behaviour of polymers since the stress fields involved in the two processes are significantly different [6].

There are two forces, as discussed above, acting during the scratching process. The first force is the normal load applied during a scratch test that is supported by the contact area between the indenter and the material. The second is the scratch or friction force which is the material's response against deformation due to indenter dynamics in the tangential direction. These two forces are orthogonal to each other and hence can be used independently for the calculation of scratch hardness/resistance of the material. Based on this concept, two parameters have been defined, scratch hardness (corresponding to the normal load) and the tangential hardness (corresponding to the frictional force). The scratch hardness for an elastic contact [30, 58] can be written as:

$$H_s = \frac{4W}{\pi d^2} \quad 2.1$$

where  $W$  is the normal load and  $d$  is the scratch width after the test. Equation (2.1) assumes that the material at the rear end of the moving indenter recovers elastically within the given time scale and hence fully supports the normal load. This assumption is not applicable when the contact is plastic or viscoplastic in nature. For such contacts the rear half of the indenter will not be completely supported by the scratched material and hence only front part of the indenter will mainly be in contact with the material and thus supporting much of the normal load. For the perfectly plastic case, we can write [58],

$$H_s = 2 \times \frac{4W}{\pi d^2} \quad 2.2$$

Hence, a generalised equation for scratch hardness can be written as [4, 6, 14, 15, 31, 33, 57-60]:

$$H_s = \frac{W}{A} = q \times \frac{4W}{\pi d^2} \quad 2.3$$

where  $A$  is the projected area supporting the normal load and  $q$  is a parameter that varies according to the response of the material.  $q$  is approximately 2 for a rigid-plastic material whereas  $q > 1$  for visco-elastic plastic materials [57, 58, 60] and  $q \approx 1$  for visco-elastic materials [57, 58].

The tangential hardness or the scratch resistance is generally given as [15, 58],

$$H_T = F_s / A_T \quad 2.4$$

where  $F_s$  is the scratch force required to move an indenter on the surface of a material and  $A_T$  is the projected contact surface between the material and the indenter in the direction of scratching (tangential direction). A schematic representation of the contact surfaces for the above-mentioned two cases is shown in Figure 2.1. The value of  $A_T$  will depend upon the material's deformation characteristics, such as the formation of prow in front of the indenter and the frictional condition between the indenter, and material moving past the indenter.

Studying the scratching properties of a material by a pendulum scratch apparatus (the indenter strikes the material at one point and scratches deep into the material making an arc before coming out of the material), the potential energy of the pendulum lost in making the scratch is related to the scratch resistance of the material. This kind of hardness is referred as dynamic hardness and is given by the following relation [58];

$$\text{Dynamic hardness, } H_D = E_D / V \quad 2.5$$

where  $E_D$  is the energy loss in making scratch and  $V$  is the scratch volume. It has been shown that the dynamic hardness is, in essence, similar to the tangential hardness or scratch resistance [58].

The definition of the scratch hardness, originally developed for almost perfectly plastic materials like metals, cannot be applied to polymeric materials when the response is purely elastic, since the hardness then tends to infinity. In this case, the contact pressure is usually taken as the hardness [3, 57]. The contact pressure  $P$  is defined as the ratio of the normal load to the contact area observed through a transparent sample during sliding of the tip. When the mean strain is higher than the yield strain, the tip generates plastic flow and the contact pressure is termed as yielding pressure  $P_{\text{yield}}$  [57].

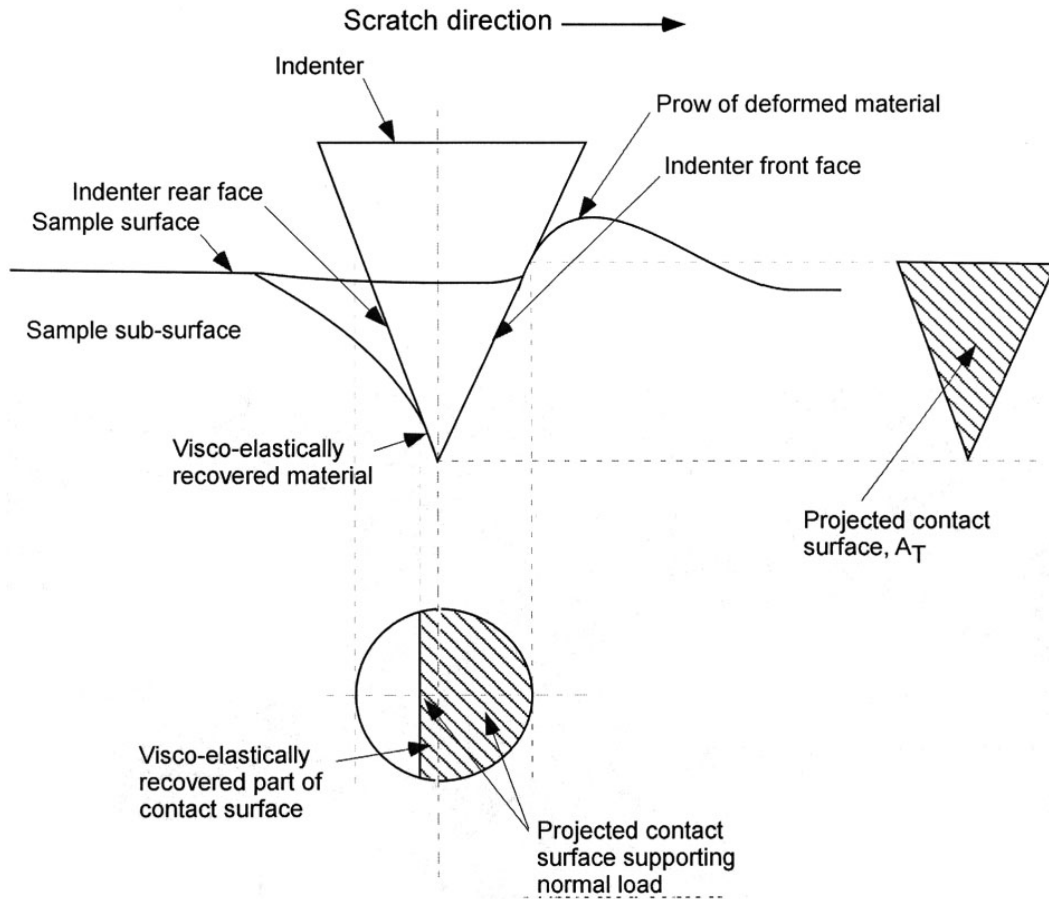


Figure 2.1 Schematic and first order, representation of the normal and tangential contact surfaces during scratching. For the normal projected surface, the visco-elastic part has also been shown [58].

The scratching process senses the material properties in a volume that is between two and three times the maximum depth of penetration and the contact radius of the indenter [59]. The influence of the interface friction is also significant; a lower interface friction will generally turn out an increase in the scratch hardness [59, 60]. When the scratch hardness is plotted as a function of normal load, a decreasing trend of scratch hardness with normal load is observed for low yield strength polymers [58, 60] such as PP, PVC and PC (Figure 2.2). For high yield strength polymers such as PEEK, PET, POM and PMMA, there is some indication that the computed scratch hardness increases initially for intermediate loads and then decreases. It is possible that the reduction in scratch hardness for softer polymers is due to high interfacial friction which induces the tip to go deeper into the material due to which, it experiences a low interfacial friction (due to thermal effects) and the tip may not go deeper into the material in the same proportion as the normal load is increased. Higher load also brings thermal effects in the bulk of the polymer surrounding the indenter which ultimately softens the material leading to higher scratch depth and lower scratch hardness. Thus the higher depth of scratch instituted by high normal load has the tendency to lower the computed scratch hardness due to thermal softening effects. The interfacial friction plays a role initially for some high yield strength polymers when the normal load is not very high. Initial increase in the normal load may reduce the effective coefficient of friction for harder polymers due to thermal effects which is limited only to the interface. Hence, the lower shear stress causes the indenter tip to move slightly up (in relative terms) giving lower depth and width of the scratch and higher hardness values. However, if the normal load is further increased,



the thermal effect extends to a larger volume around the tip causing a general reduction in the yield strength of the material, and hence a decrease in the scratch hardness [60].

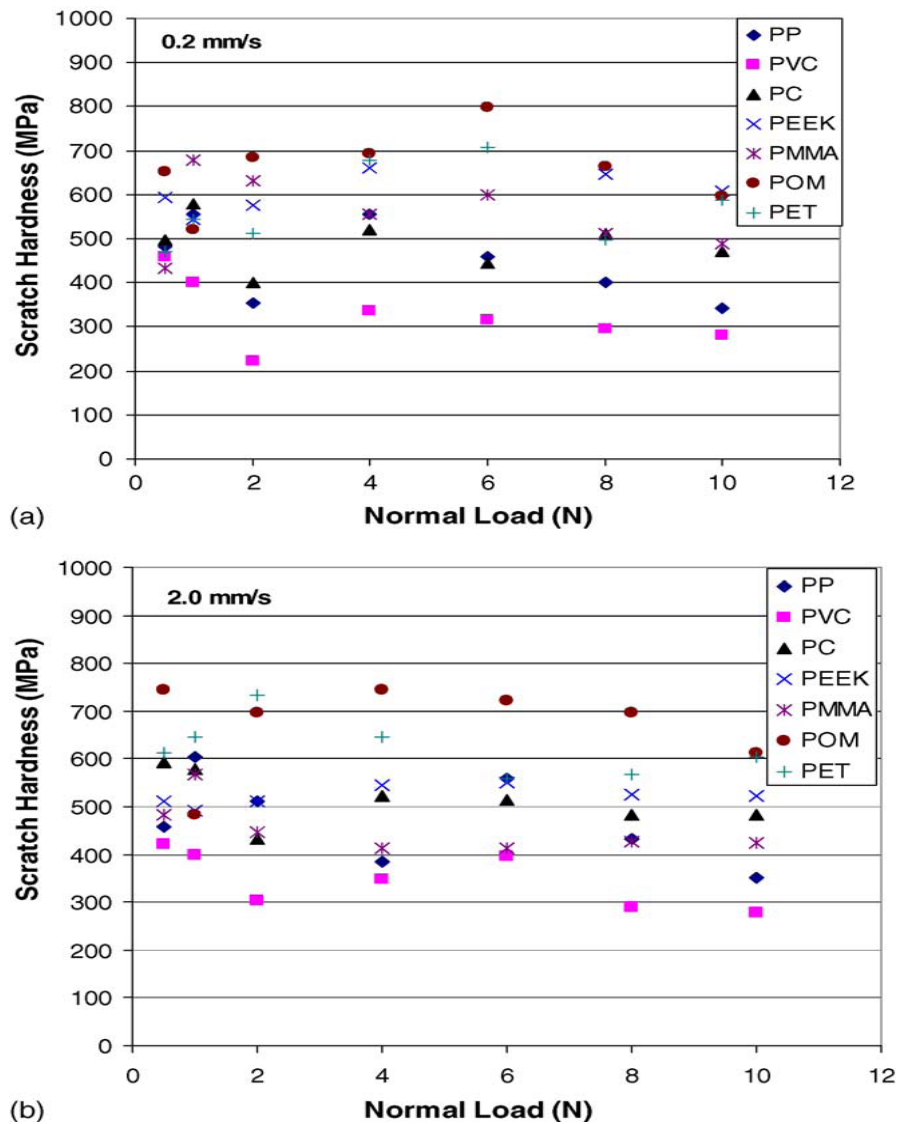


Figure 2.2 Scratch hardness as a function of applied normal load for polymers. The unrecovered scratch depth for the loads varied between 60 and 450  $\mu\text{m}$ . Scratching speed was maintained as (a) 0.2 mm/s and (b) 2.0 mm/s. Scratch hardness tends to be low at very high normal loads or at high scratch depths [60].

There is not much difference in the hardness values for two different scratching speeds which means that the ratio  $W/d^2$  is not affected much with the change in the scratch speed [3, 7, 60]. Figure 2.3 shows that the evolution of the hardness both under indentation and scratch conditions as a function of the temperature is equivalent for PMMA. The difference in hardness in indentation and scratch for each temperature is due to the difference in strain rate applied during both tests [3]. The fact that the scratch hardness values are greater than the normal indentation hardness reflects the strain rate sensitivity of an elasto-viscoplastic material. The expected reduction in the measured normal hardness and increase in the measured scratch hardness (probably due to friction between the indenter and polymer) is likely to be relatively small [7].



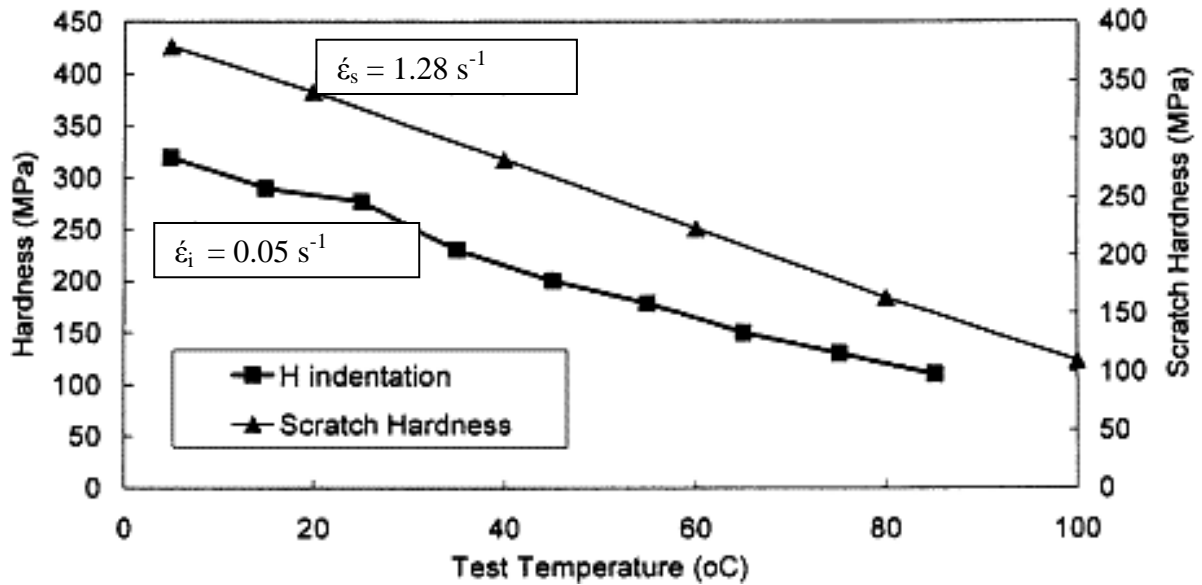


Figure 2.3 Indentation and the scratch hardness of PMMA measured at various temperatures. The strain rates used for the indentation and the scratch experiments were  $0.05 \text{ s}^{-1}$  and  $1.28 \text{ s}^{-1}$  respectively [3].

The scratch hardness has many advantages over normal hardness method [58, 59]. Firstly, the measurement of the scratch hardness is very simple in comparison to that for the normal hardness method and it is in a form which is suitable for organic polymers. Secondly, the scratch hardness method also provides information regarding the surface deformation characteristics of the material [59]. Thirdly, the scratch hardness requires relatively simpler machines and it can be used for both static and dynamic mechanical property characterizations [58].

## 2.4 Experimental studies of scratching process

### 2.4.1 Scratch test apparatus

Experiments are carried out using two basic types of scratch test devices. The first is a generic design where an indenter is passed over the surface of a polymer under a fixed normal load and sliding velocity condition: the Eldredge & Tabor Design. The scratch depth is determined by the scratch hardness of the material and the exact value of the vertical penetration may vary slightly from point to point depending upon material's local surface properties. Figure 2.4(a) illustrates a simple schematic of the design. The other type of scratch data is obtained using a pendulum sclerometer and Figure 2.4(b) demonstrates the schematic outline of this design. For the pendulum sclerometer, the indenter attached to the pendulum is brought to certain height and is released. The pendulum arm makes a free swing upon release whereby the indenter scratches the surface of the material as it approaches the lowest height. The pendulum swings to the other side of the vertical axis reaching a certain height. The difference between the height of release and the height attained on the other side represents the energy lost during scratching [58].

Conventional scratching devices give a relatively fixed depth, since the motion of the indenter is parallel to the surface and thus the imposed depth is nearly constant. In contrast, a pendulum sclerometer provides an arced motion of the indenter so as to impose damage at a range of depths [62].

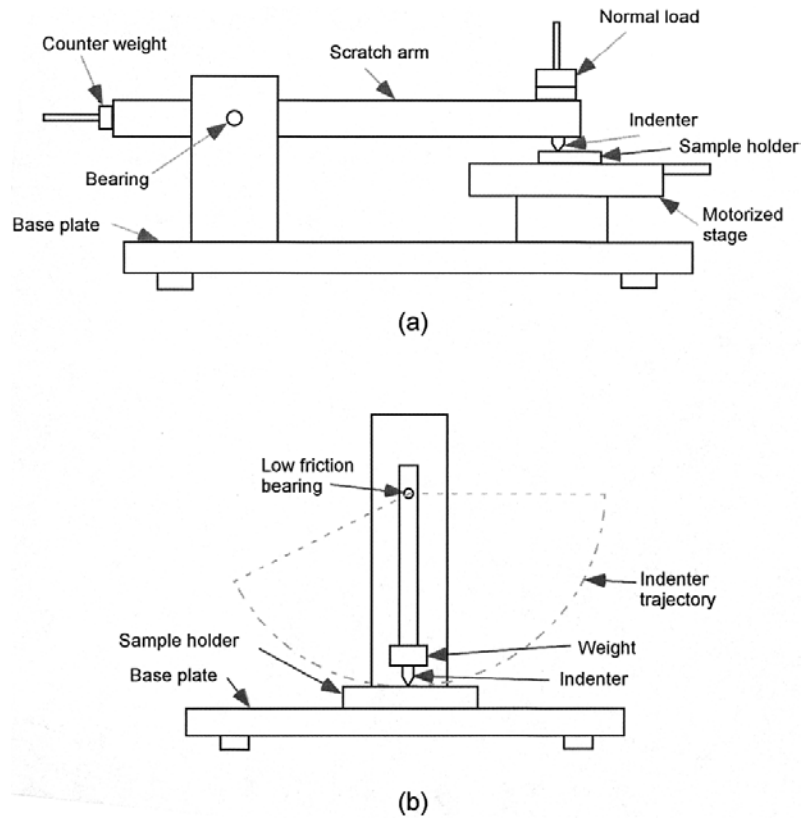


Figure 2.4 (a) Schematic drawing of a linear scratch test machine; (b) Schematic drawing of a pendulum-type sclerometer [58].

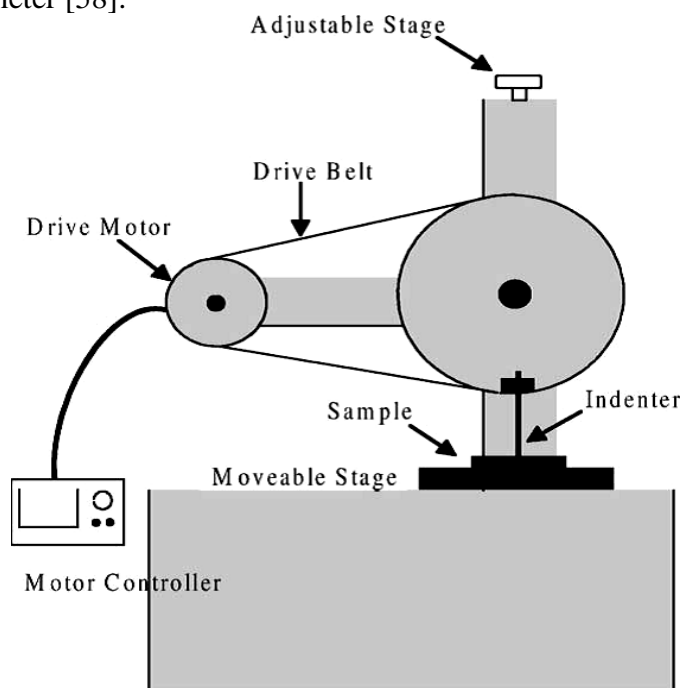


Figure 2.5 Schematic representation of the modified sclerometer apparatus [62].

A schematic representation of the modified sclerometer apparatus can be seen in Figure 2.5. The apparatus consists of a flywheel, a pulley and an adjustable motor holder allowing the control of the belt strain. A stepper motor is chosen to drive the system. At very low velocities (<10 mm/s), the motor is a source of vibrations and at speeds above 500 mm/s, the torque provided

is not high enough to ensure scratching at constant speed. The experiments at higher velocities (500 mm/s–3 m/s) do not employ the motor driven stage and are conducted by simply spinning the flywheel by hand. At a high speed and following the motion using a high-speed camera (enabling the rotational cycle of the motion to be followed with sufficient detail) provides a velocity measurement. The gradual loss of momentum allows a range of velocities to be probed. At velocities below 500 mm/s, however, there is insufficient momentum to complete the cycle and impose a complete scratch profile [62].

## **2.4.2 Micro-visio scratch apparatus**

The scratch apparatus described in detail by Gauthier and Schirrer [13, 17, 18, 57] is based on a commercial servo-mechanism bearing a small transparent environmental chamber that contains the sample and the moving tip. It is described in detail in section 4.1.2. According to the adjustment of the normal load, temperature, strain rate and tip geometry, the contact between the hard tip and the polymer surface may be elastic, or it may generate a visco-elastic groove or a plastic scratch.

## **2.4.3 Experimental variables**

The important experimental variables in any scratch study are the normal load, the sliding speed, the indenter angle (for conical indenters), the penetration depth, and the ambient temperature. The interfacial friction (lubrication) and the thermal conductivity of the indenter may also be relevant [58, 62]. The effect of normal load, or penetration depth, is to change the volume of the deformed material. For conical and pyramidal indenters, the change in the depth of the scratch does not, in principle, change the imposed strain and the tip defect influences apart. However, for a spherical indenter a change in the normal load will also bring a change in the effective strain since the depth of indentation will be changed [58].

Ductile deformation during a scratch test is often evaluated through the contact pressure, the residual depth of the groove, and the height of the pile-up. The contact pressure has been also shown equivalent to the hardness in indentation. The applied load at which the fracture occurs is used as a measure of the fracture toughness [3].

## **2.4.4 Different types of indenters**

As discussed in section 2.2, it is generally accepted that for one material to scratch another, the indenter or scratching particle must be at least 20% harder than the damaged surface: actually this factor depends rather upon the shape of the scratching particle, varying between only just over unity for a nearly spherical particle to about 1.6 for a much more angular indenter [31]. Several types of indenters are being used in various scratch test applications. Mostly pyramidal indenters are preferred, but spheres of various diameters and conical indenters are also used (Figure 2.6) [32, 64]. It is also a common practice to use a Berkovich indenter, made of diamond, which has a three-sided pyramidal shape. The four-sided pyramidal Vickers indenter is less popular since, practically, it is more difficult to fabricate with such a small tip radius [32].

## **2.4.5 Nano-indentation and nano scratch test**

Nano-indentation and nano scratch testing are powerful techniques to determine the mechanical properties of polymers in bulk or in the form of thin films. The attractiveness of these

techniques can be found in the simplicity in the measurement principle in combination with the wealth of information that can be extracted from these measurements. Scratch testing is nevertheless very useful for comparative, qualitative studies and is, therefore, often employed in the analysis of consistency of the properties of polymers in industrial productions [15, 31, 32].

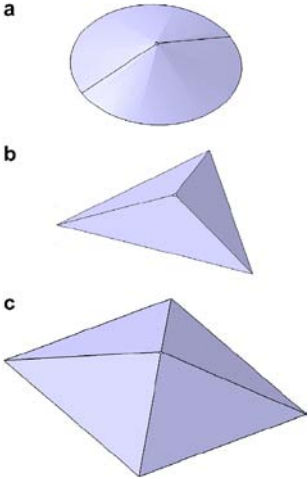


Figure 2.6 Indenters geometry: (a) conical; (b) Berkovich; (c) Vickers [64].

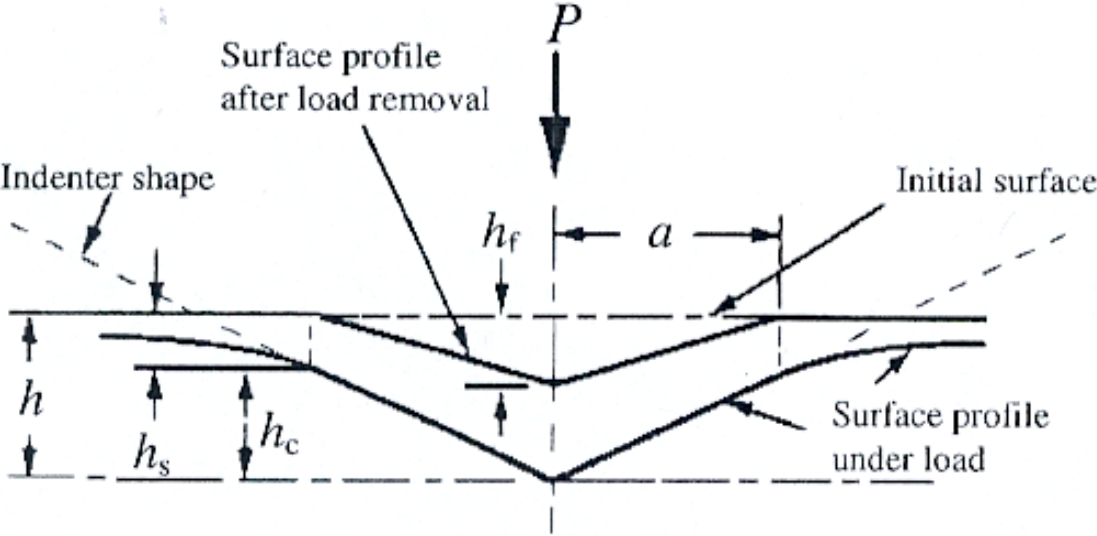


Figure 2.7 Schematic representation of a section through an indentation using a conical indenter [32].

The principle of recording the indentation using a nano indenter is straightforward. As illustrated in Figure 2.7, the material surface is indented with a tip (the indenter) loaded with a force  $P$ , resulting in a penetration depth  $h$  of the indenter into the material. During the indentation, the force  $P$  and the indentation depth  $h$  are recorded as a function of time, and so a load-displacement curve is obtained as shown in Figure 2.8. A recording indentation experiment generally consists of a single loading-unloading cycle. As the specimen is loaded to a maximum force  $P_{max}$ , the indentation depth increases to a maximum  $h_{max}$ . If the plastic deformation occurs, a different curve is followed upon unloading and the final depth is not zero but some finite value  $h_f$ , due to plastic deformation of the material during indentation. The projected contact area is

generally expressed in terms of contact depth  $h_c$ , as defined in Figure 2.8. The slope of the unloading curve  $S$  is used to calculate the elastic modulus of the material [32].

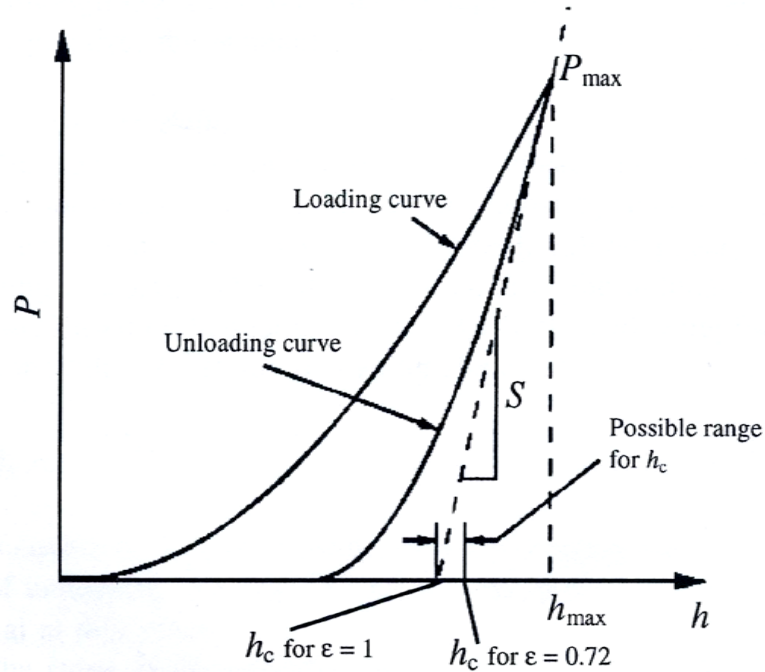


Figure 2.8 Schematic representation of a typical indentation load-displacement curve.  $\epsilon$  is a constant depending upon the geometry of the indenter. It is 1 for a flat punch, 0.72 for a conical indenter, and 0.75 for a paraboloid and for a Birkovich indenter [32].

## 2.5 Different aspects of scratching of polymers

### 2.5.1 Scratch force during scratching

When an indenter is passed over the surface of a polymeric material, the energy supplied through the indenter is used for three actions irrespective of material's intrinsic mechanical behaviour. The first part of energy is consumed in supporting the normal load and the second part overcomes the resistance of the material to tangential deformation in the tangential direction. The resistance to deformation can be further sub-divided into ploughing component and traction component. The ploughing component of energy dissipation is used for material deformation (elastic and plastic) and fracture in the stressed volume of the material whereas the traction component involves the frictional work done due to material sliding against the indenter's front face. Third part of the energy is consumed in overcoming the elastic hysteresis loss in the material (applicable to visco-elastic solids) in the form of mainly thermal energy. The elastic hysteresis loss in some way is related to the frictional energy dissipation and its magnitude will depend upon the type of the material and the type of contact [58, 60]. Thus we can write;

$$E_{\text{total}} = E_N + (E_P + E_F) + E_H \quad 2.6$$

where  $E_{\text{total}}$  = total energy spent during scratching,  $E_N$  = energy spent in supporting the normal load,  $E_P$  = ploughing component of energy dissipation,  $E_F$  = frictional energy dissipation and  $E_H$  is the hysteresis loss [58].

In terms of volumetric energy deployment during a scratch process, the energy is consumed mainly in two zones: the interface (a very thin layer subjected to a very high shear strain, a high strain rate and adhesive slipping) and a larger and deeper volume beneath the tip where visco-plastic visco-elastic yielding occurs [65-67]. The deeper volume is roughly spherical and is further divided into two zones: the nearest close to the tip is under pure hydrostatic pressure, while the more distant is plastically deformed when full plasticity appears around the tip [57].

As discussed above, the scratch force is the resistance force imposed by the material on the tip movement. The scratch forces for different polymers are found to be very close to each other for lower loads (smaller depths), but the difference between forces increases as the normal load (or scratch depth) is increased. It is important to note that the differences in the scratch forces across various polymers do not reflect their yield strengths as can be seen in Figure 2.9(a). That is, polymers which have low yield strengths, such as PP and PVC, do not necessarily show low scratch force. This explains that the scratch force is a very strong function of the interfacial friction. The effect of interfacial friction is larger for softer polymer as the depth of scratch and hence the area of real contact will be greater for softer polymer than that for harder polymer. Thus, one may say that the scratch force is adjusted by the indenter tip based on the interfacial friction and yielding properties of the polymer. The above is applicable to all polymers which deform in ductile manner. For polymers which show brittle fracture behaviour, such as PMMA and PC, the above observation may not be strictly applicable as the crack initiation and propagation are additional modes of energy dissipation [60].

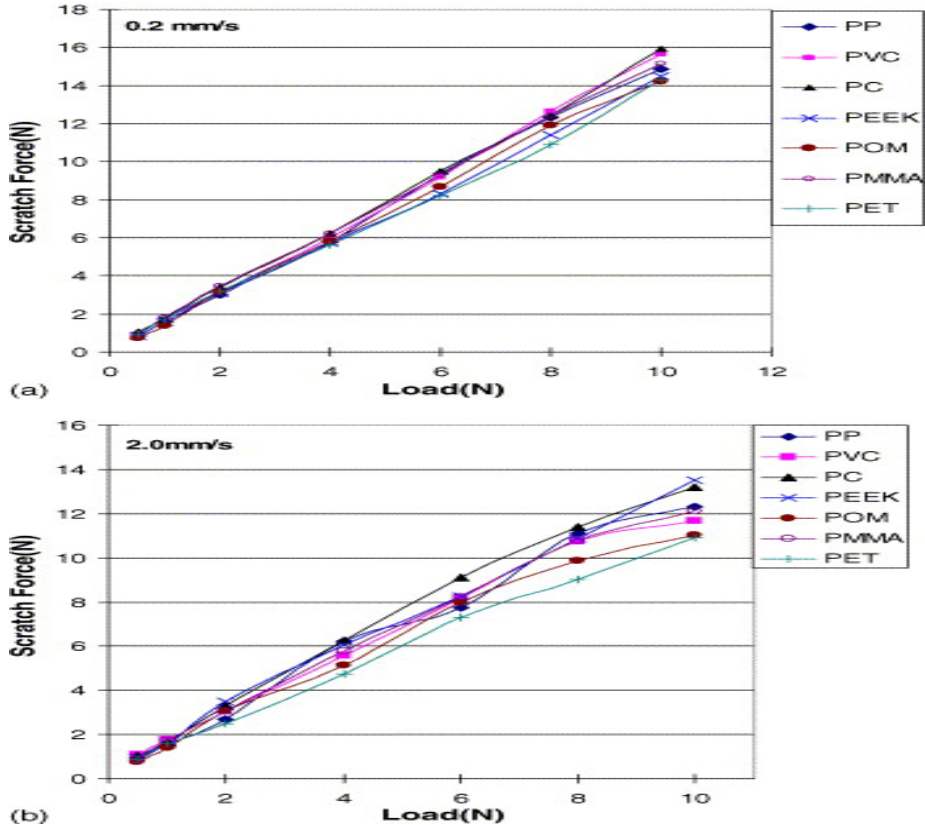


Figure 2.9 Measured scratch force as a function of normal load for two scratching speeds used. The coefficient of friction, which is the ratio of scratch force to the normal load, is constant for low scratching speed, however, the coefficient of friction decreases with increasing normal load at higher scratching speed [60].

For higher scratch speed, there is a significant decrease in the coefficient of friction at higher normal load and the difference in scratch force between different polymers appears at relatively lower loads (Figure 2.9(b)). This difference increases as the normal load is increased. The magnitude of the scratch force at high scratching speed is lower than that for the low scratching speed for each normal load. This difference in scratch force for a polymer is more obvious for higher normal load and the difference can be as high as 25% for 10 N normal load. The lower magnitude of scratch force at higher scratching speed may be because of two effects. The first effect may be the reduction in the effect of interfacial friction due to higher scratching speeds. In a sliding test, many polymers exhibit lower coefficient of friction as the sliding speed is increased. This means that if the coefficient of friction decreases then the interfacial component of scratch force is reduced and therefore the ploughing component will be the only contributor to the total scratch force. Moreover the size of the contacts area for a given normal load decreases with increasing sliding velocity. As the conical tip is never perfect, the ratio between its cross section and the normal projected contact area decreases. Due to decrease in mean contact strain, the elastic unloading increases resulting in decrease in ploughing friction. The second effect during high scratching speed is the generation of heat energy in the deformed zone due to both plastic deformation and elastic hysteresis in the material leading to a reduction in the ploughing force. Actually the self heating during scratch test may be as high as making the polymer temperature close to its glass-transition temperature. This makes the material softer resulting in the reduction of ploughing force required for a given depth. The other observation at high scratch speed and higher load is a reduction in the coefficient of friction. It can be concluded that when the scratch speed is high, there is strong thermal effect leading to a reduction in the interfacial friction [60, 62].

## 2.5.2 Scratch width and scratch depth

Polymers undergo a large amount of recovery due to the visco-elastic visco-plastic nature and in some cases; there is also the possibility of change in volume under compressive stress and due to the crazing phenomenon. During scratching, the material is pushed sideways (in the width direction of the scratch) and a large hydrostatic/compressive stress is generated beneath the tip (in the depth direction of the scratch) and in front where the material prow is created supporting the tangential scratch force. Because of the presence of the free surface on the side way (this means that the material can simultaneously relax while being deformed) and the fact that the magnitude of stresses are much smaller at the sides, the percentage of post-scratching recovery in the width direction after scratching is generally small. This is in contrast to the depth where extremely high hydrostatic/compressive stress during scratching can lead to high post-scratching recovery, and thus considerable reduction in the scratch depth measured after scratching (Figure 2.10). The polymers can show approximately between 50 and 85% reduction in the depth after scratching due to elastic recovery [6, 60]. PMMA, in particular, shows very high recovery; 56.8% when scratched by a conical tip and close to 75% when scratched by a Berkovich indenter. Very low load scratching clearly indicates that the depth of the scratch decreases after scratching, whereas there is a possibility of some enlargement of the width of the scratch as a result of scratch depth recovery [60].

For a spherical blunt scratcher with radius R, the relationship between the scratch depth h during scratch and the contact zone size a can be shown to be [6]

$$h = R - \sqrt{R^2 - a^2} \quad 2.7$$

and for a conical tip, scratch depth, h, is given as [60]:

$$h = \frac{d}{2 \tan \theta}$$

2.8

where  $d$  is the width of the scratch and  $2\theta$  is included cone angle of the tip. However, this calculation is based on the assumption that the recovery of the material in the width direction is much less compared to that in the depth. The scratch depth and scratch force show some relation with the yielding property of the materials. Rigid polymers with high moduli have low scratch depths [6, 60]. For example, PVC and PP having low yield strengths, show higher scratch depth in comparison to other polymers for the same scratch force. The scratch force required for any scratch depth is less when the scratch speed is higher for polymers (Figure 2.11). Thus, it may be said that higher scratch speed makes scratching easier producing deeper scratches for the same scratch force when compared to that at slower speed. This is an important point to note as higher speed is normally related to higher strain rate, and hence, the material should behave as stronger giving lower scratch width and depth when compared to the data at lower scratching speed [60].

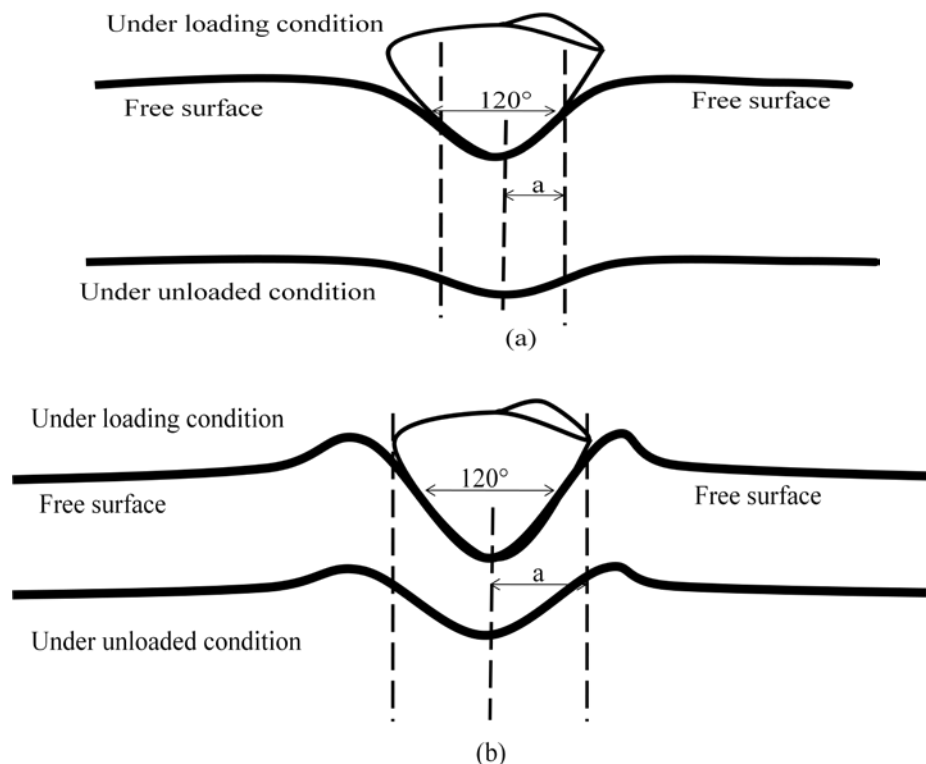


Figure 2.10 The difference in post-scratching recovery of polymers in horizontal and vertical directions for low (a) and for high (b) contact strains. The contact radius remains almost unaffected even in case of high strain and lateral pads.

In a scratch test for polymers, it is important to note that very large recovery in the scratch depth is, in fact a kind of self-healing process that can reduce the damaging effects of scratches such as the loss of gloss. A scratch with less depth and visco-plastically recovered surface would reflect more light (glossy) than a deeper and unrecovered scratch. POM recovers about 33%, whereas the recovery for PMMA is as high as 62% [60].

The life time of a micro-scratch  $t$  is the ratio of the scratch length  $l$  to the sliding speed  $V_{tip}$  [2, 17] and is typically about 10 s [17].

$$t = l/V_{tip}$$

2.9



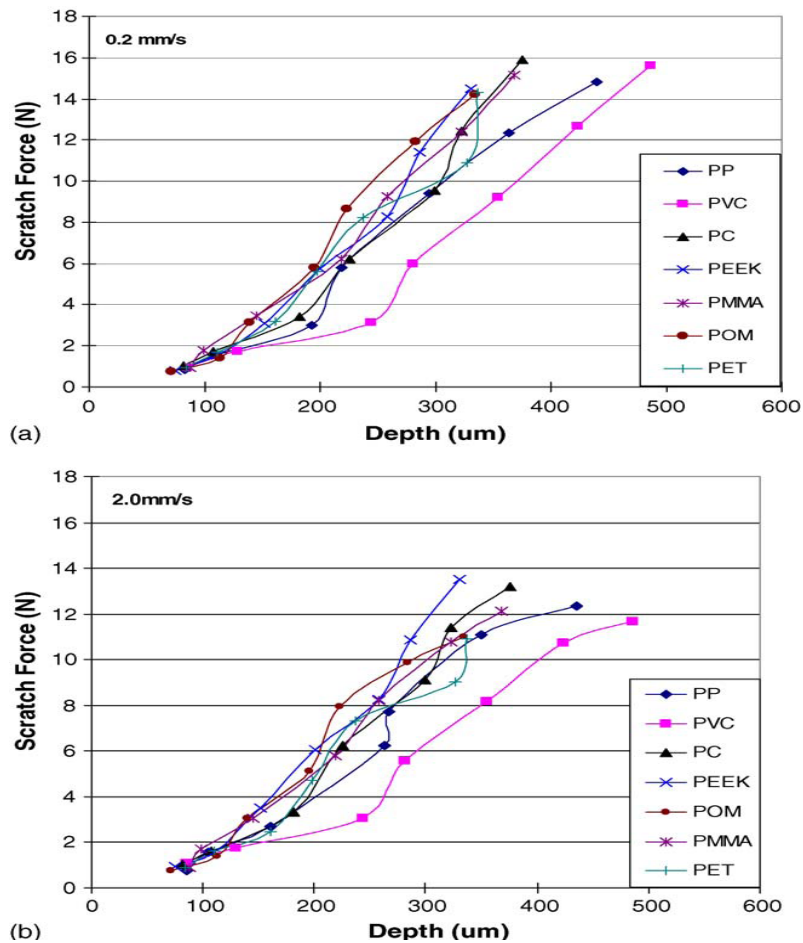


Figure 2.11 Scratch force as a function of unrecovered scratch depth. The scratch speeds were (a) 0.2 mm /s and (b) 2.0 mm /s. The data show ‘S’ form of the curves [60].

### 2.5.3 Deformation mechanisms

Depending upon certain mechanical properties, polymers deform in a variety of ways which are indicative of their bulk mechanical properties. On one extreme is the purely ductile behaviour and on the other extreme is the behaviour shown by PMMA where the material removal takes the form of cutting, probably owing to poor elongation-before-failure property for PMMA. The material is easily sheared off without much plastic deformation around the indenter. It is very easy to observe some detached debris particle along the scratch for PMMA [60].

When an indenter is passed over the surface of a material, the damage instituted in the material is a direct result of stresses (primarily compressive or tensile) generated in the affected part. Material in the front part of the indenter experiences compressive stress whereas tensile stresses are generated at the rear end of the moving indenter. The elastic modulus of a polymer plays an important role in determining the scratch depth and the type of damage produced during scratching. A certain amount of rigidity (high modulus) would be helpful in reducing the scratch depth if the polymer is prone to ductile failure. However, for brittle polymers, high rigidity may induce high stress concentration leading to failure by cracking and crazing. The interfacial friction also affects the surface stresses that are generated in the material. High friction coefficients lead to high tensile stresses at the rear end of the indenter leading to failure of the material by cracking; quite typical behaviour of brittle solids [58].

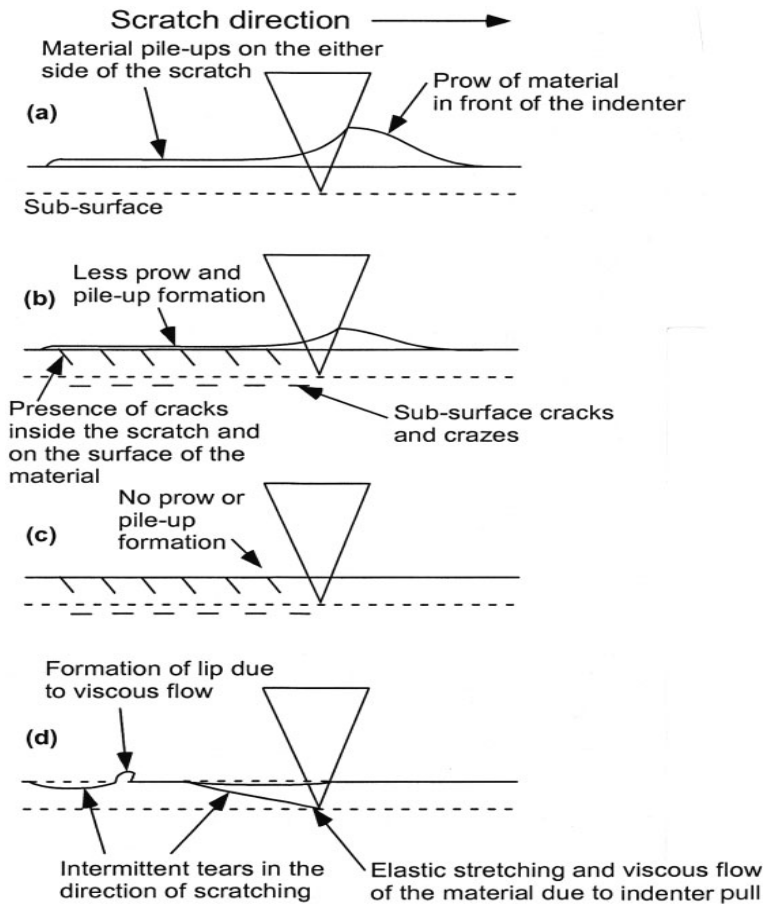


Figure 2.12 Schematic representations of the main polymeric material responses to scratching. (a) ductile, (b) ductile and brittle, (c) brittle, and, (d) elastomeric responses [58].

Figure 2.12 shows, schematically, the various types of material damage during scratching for (a) ductile, (b) ductile and brittle, (c) brittle, and, (d) elastomeric responses. In a ductile response, the material deforms visco-plastically and forms “pile-ups” on the either sides of the scratch. A “prow” is also formed near the front part of the indenter. For a ductile and brittle response, the material shows both ductile ploughing and brittle fracture. The extent of the ductile plastic deformation is less. The cracks may appear on the surface or subsurface of the material. The direction and shape of the crack will depend upon the nature of the material and the location of the maximum applied tensile stress. The brittle response is exclusively shown by ceramics and glasses. There is no evidence of the formation of pile-up or prow; however, the plastic deformation is possible in the high compressive stress region just in front of the indenter. In an elastomeric response as shown by the sharp indenter, the material shows intermittent tears in the direction of the traverse of the indenter. The indenter punctures the material, due to an isolated stress concentration, and pulls the molecules in the direction of motion until fracture. A considerable amount of viscous flow of the material is possible showing the formation of “lips” or even loosely attached debris particles [58].

### 2.5.3.1 Brittle response to indentation and scratching

Surface and sub-surface cracks and crazes are found for brittle materials such as a glassy polymer like PMMA. Many of the commonly used polymers are essentially rather brittle at normal temperatures and under various strain rate situations. Therefore, during normal indentation or scratching experiments, the presence of cracks is a common feature along with the ductile

deformation or ploughing. For normal indentation, the cracks are nucleated at the edges of the contact or in the sub-surface of the material immediately below the indenter where the tensile stresses are found to be the maximum. Also, the presence of a plastically deformed region around the indenter tip produces a strain mismatch between the plastically and elastically deformed regions (usually during unloading) leading to the generation of a residual tensile stress. This residual tensile stress can also lead to brittle fracture [58]. Figure 2.13 shows that the fractures are all occurring behind the actual contact between the indenter and the sample surface. This type of fracture is due to tensile stresses developed behind the contact as is illustrated in Figure 2.14. The size of the contact is controlled by the compressive strength of the surface, resisting the motion of the indenter. The compression zone is located in front of the contact. This suggests the presence of tensile stresses behind the contact causes the fracture to initiate and propagate. The geometry of the indenter affects the orientation of the compressive stresses, therefore influences significantly the amplitude of the tensile stresses generated in the back of the contact. When these tensile stresses reach the ultimate tensile strength, the material starts fracturing at the bottom of the groove [3].

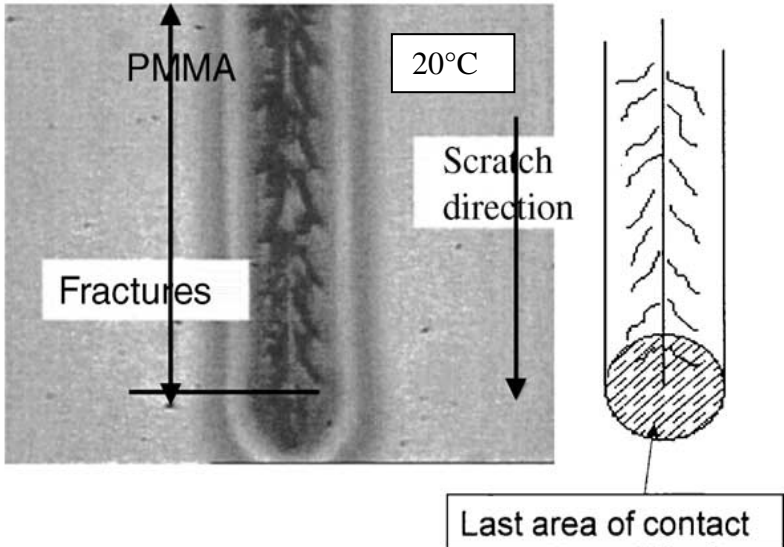


Figure 2.13 Observation of the end of the scratch corresponding to the last position of the indenter. It shows that the fractures occur behind the contact [3].

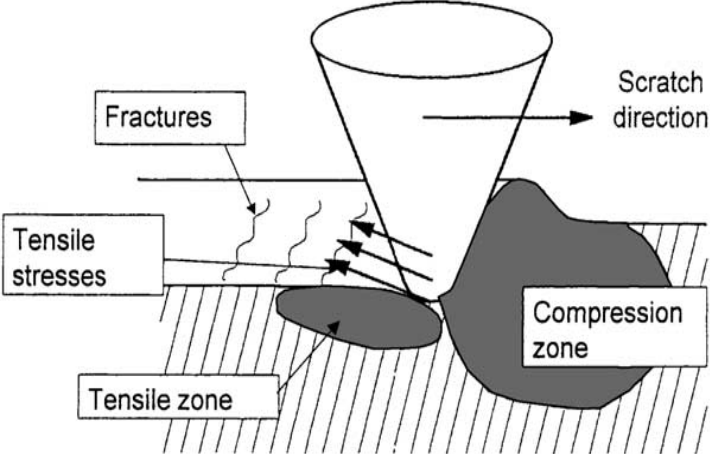


Figure 2.14 Illustration of the distribution of the various stresses present around the contact during a scratch experiment [3].

Response (Pictorial)	Generic	$\alpha$
	Elastic	180°
	ironing	150°
	Ductile Ploughing	120°
	Ductile Machining + Cracking	90°
	Brittle Machining	60°
		30°
		0°

Figure 2.15 A qualitative representation of the influence of semi-included cone angle  $\alpha$  upon the type of damage produced. The figure only shows the effects and is not drawn to any scale. For clarity, the pictorial view does not show the change in the cone angle [58].

### 2.5.3.2 Scratch deformation maps

Figure 2.15 gives the guidelines on how one may identify the prevailing different deformation mechanisms in a scratch test. Lower values of the cone angles give a brittle type of damage feature involving cracks and significant chip formation. Increasing the load, which also causes an increase in the depth of scratch, has similar effect as reducing the cone angle; that is, the material behaves more in brittle manner. Thus moving towards the higher cone angles and lower loads gives ductile ploughing to fully elastic deformations. A surface is considered to be scratch resistant if the nature of the deformation is fully elastic or visco-elastic visco-plastic. These kinds of damages are either recoverable over a period of time or they do not spoil the surface in any engineering sense (surface appearances or reduction in the strength due to the presence of cracks). In contrast, brittle fracture can be most damaging to a surface. Deformation maps can provide a convenient tool to assist in the engineering and design of a surface [58].

## 2.5.4 Elastic recovery of a scratch on a polymeric surface

### 2.5.4.1 True contact area and true contact strain

Various types of the contact between two surfaces may be illustrated depending upon the nature of the deformation involved. A contact area which is entirely plastically deformed is known as a 'viscoplastic contact'. If the contact area is not entirely plastically deformed, it is called a 'viscoelastic-plastic contact' [17]. Elastic-plastic contact behavior also plays a key role in damage modes involving wear and friction often occurring in these processes and systems [34]. Figure 2.16 shows four in-situ photographs of the contact area between a spherical tip and a PMMA surface taken by an experimental apparatus. Figure 2.16a corresponds to a quasi-elastic contact with a relaxation time equal to the contact time, where incipient interference fringes reveal a slight dissymmetry. Figure 2.16b depicts a visco-elastic contact where the groove relaxes after a time interval longer than the contact time. In the elastic-plastic contact as shown in Figure 2.16c, the

strain under the contact is not completely plastic, there is no frontal push pad and the lateral pad of the groove appears only after elastic unloading of the contact strain. Finally, Figure 2.16d shows a plastic contact where the frontal push pad and lateral pads form a continuous cord [13, 16, 66].

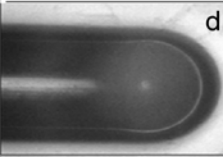
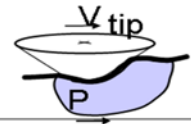
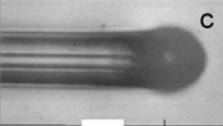
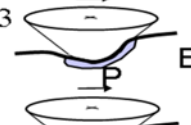
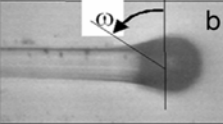
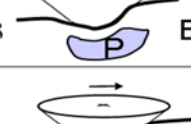
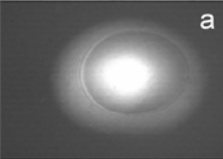
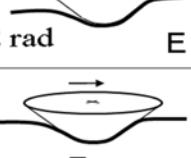

	<i>Contact</i>	$\rho/\sigma_{yield}$	<i>Groove recovery</i>
	<i>Plastic</i> 	1.5 - 2	Sometime if appropriate temperature
	$\mu_{loc} > 0.3$ <i>Elasto plastic</i> 	1.1 - 1.5	Possible
	$\mu_{loc} < 0.3$ <i>Viscoelastic</i> 	0.7 - 1.1	Recovering time > contact time
	$\omega < \pi/2$ rad <i>Elastic</i> 	< 0.7	During the contact time
	$\omega = \pi/2$ rad <i>Elastic</i> 		

Figure 2.16 Typical photographs of the true contact area during scratching of a PMMA surface with a spherical tip [13, 66].

The contact area between a moving tip and a polymer surface is divided into a front part and a rear part. The latter may be defined by an angle  $\omega$  ( $\tan \omega = a_r/l$ , where  $l$  is the half width of the groove left behind the tip) as defined in Figure 2.17 [16], obtained for a 240  $\mu\text{m}$  radius sphere moving over a PMMA surface. The shape of the contact area changes with temperature, tip speed and the normal load on the tip [16, 17]. The rear and the front areas may be predicted in the case of plastic and elastic-plastic contacts on a polymer surface. The rear contact area is due to the elastic recovery of the polymer and depends on the plastic deformation around the contact. Even for a moving tip, the rear area can be almost identical to the front area if the contact is almost elastic and the mechanical loss factor is low. The length  $a_r$  of the rear contact may be estimated from the length  $a_f$  of the front contact and the bulk mechanical properties [16, 17]. In the case of a perfectly elastic contact, the ratio  $a_r/a_f$  is 1, while for an elastic-plastic contact, this ratio is [16]:

$$\frac{A_r}{a_f} = 1 - \left[ 1 - \sqrt{\frac{2c\sigma_y}{E^*} \tan \theta} \right] \frac{\varepsilon - \varepsilon_e}{\varepsilon - \varepsilon_p} \quad 2.10$$

and for a plastic contact:

$$\frac{A_r}{a_f} = \sqrt{\frac{2c\sigma_y}{E^*} \tan \theta} \quad 2.11$$

where  $\sigma_y$  is the yield stress,  $E^*$  is the normalised elastic modulus at the contact  $\left[ \frac{1}{E^*} = \frac{1-\nu_1^2}{E_1} + \frac{1-\nu_2^2}{E_2} \right]$ ,  $\theta$  is the apex angle of the conical scratching tip and  $c$  the coefficient connecting the yield stresses measured in a hardness test and under compression ( $c \approx 2$  for polymer).  $\varepsilon_e$  and  $\varepsilon_p$  denote the

contact strains at the end of the elastic contact area and at the beginning of the plastic contact area respectively.

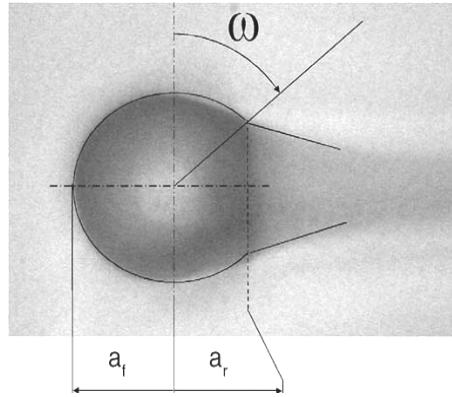


Figure 2.17 Photograph of the contact area during scratching. This area has a front part defined by the length  $a_f$  and a rear part defined by the angle  $\omega$  or by the length  $a_r$  [16].

Another important parameter is the strain rate near and far from the tip [57]. The mean effective strain rate  $d\varepsilon/dt$ , can be given as the ratio of the sliding speed ( $V$ ) to the scratch width ( $l$ ) observed post-mortem [7, 13, 17, 57, 59, 66]. i.e.

$$d\varepsilon/dt = V/l \quad 2.12$$

The strain rate may be several decades higher in the interfacial zone than in zones far from the tip. In the case of normal indentation, Tabor has shown that the constant ratio of hardness to yield stress for a perfectly plastic solid may be applied to a solid strain hardening, provided that the yield stress is replaced by the flow stress measured under simple compression at a representative strain  $\varepsilon_r$  [7, 33, 57-59, 62, 65, 67] defined as for a conical tip:

$$\varepsilon_r = 0.2 \tan \beta \quad 2.13$$

where  $\beta$  is the angle between the tip and the surface. For a spherical tip, it may be written as [33, 34, 57-59, 65, 68],

$$\varepsilon_r = 0.2 a/R \quad 2.14$$

where  $R$  is the radius of the tip and  $a$  is the radius of the surface contact area. Briscoe et al. observed that in a visco-elastic material, the proportionality can be lower than 0.2 [34, 57, 58]. For them, a value of 0.16  $a/R$  will give a better result. It may be realized that for a conical indenter, if the included cone angle is fixed, the strain remains the same regardless of the depth of penetration. In this case, the depth change is said to provide “geometrically similar” indentation conditions. However, for a spherical indenter, the amount of strain imposed to the material will increase as the depth of penetration is progressively increased [58].

The strain is proportional to the ratio of the contact radius to the tip radius for a spherical tip, or to the angle of the cone for a conical tip. In the case of a visco-elastic contact, the ratio  $a_r/a_f$  is lower than that in the elastic case, as is illustrated in the Figure 2.18. If the material displays strain hardening, the contact strain decreases and  $a_r$  increases. The apparent friction coefficient can likewise vary strongly under these circumstances [16].



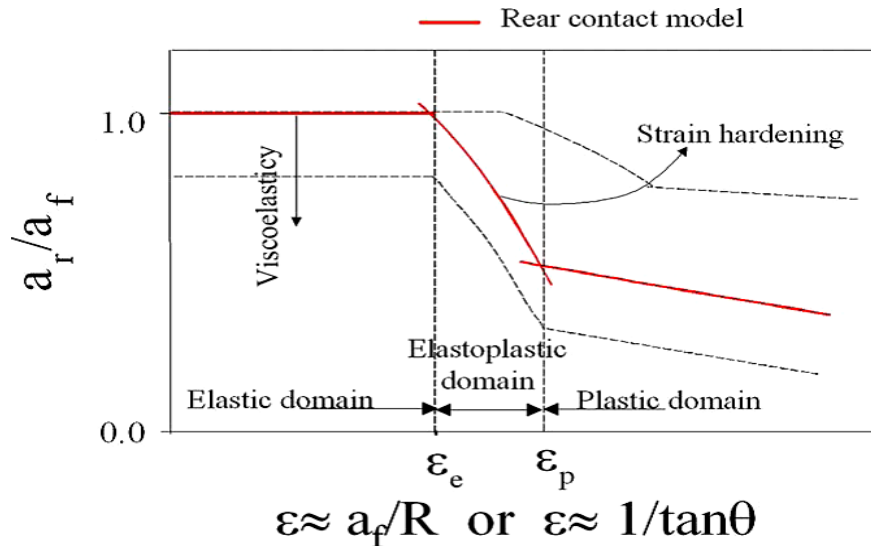


Figure 2.18 The ratio of the rear part to the front part of the contact area as a function of the mean strain during contact. This ratio decreases in the case of a visco-elastic body and increases if the material shows strain hardening [16].

#### 2.5.4.2 Viscoplastic scratch

For the viscoelastic and viscoplastic materials like PMMA, the cross section of a groove is not identical to the profile of the grooving tip [57]. The partially elastic deformation of the surface recovers partly instantaneously and partly after a very short delay [57, 58], so that the depth of a groove is less than the penetration of the tip during its motion as discussed earlier. Relaxation measurements at room temperature further indicates that the relaxation of grooves in PMMA is negligible after a few tenths of a second and thus these grooves are called viscoplastic scratches [57]. Figure 2.19 shows the relaxation during viscoplastic scratching. On the left, there is in situ photograph and on the right, the geometrical parameters are drawn on the photograph. The groove left by a rear contact is narrower than the contact area due to elastic relaxation and the edges of the plastic flow left on the surface lay parallel [57].

#### 2.5.4.3 Viscoelastic grooves

The geometry of the true contact area is modified as the sliding speed of the tip increases. For a viscoelastic and viscoplastic material like PMMA and at the constant normal load, an increase in tip speed decreases the true contact radius and hence the ratio between the true contact radius and the radius of the tip is also reduced (and also the mean strain). On the other hand, an increase in tip speed increases the strain rate and provided that the initial mean strain is no more than a few percent, a transition from viscoplastic scratching to viscoelastic grooving took place (Figure 2.20) [57]. At intermediate sliding speeds, the material compressed in front of the tip does not generate a pad and the edges of the groove left on the surface do not lie parallel. The groove relaxes within a time lapse comparable to the contact time of the tip. At higher sliding speeds, the deformation of the surface recovers almost instantaneously and the contact area becomes quasi-symmetric. The recovery of the groove and the symmetry of the contact area can be estimated by means of an angle  $\omega$  varying from 0 to  $\pi/2$ . As  $\omega$  increases, the true contact radius decreases whereas the contact area remains almost constant. Hence the transition from viscoplastic scratch to viscoelastic groove appears at almost constant contact pressure [57].

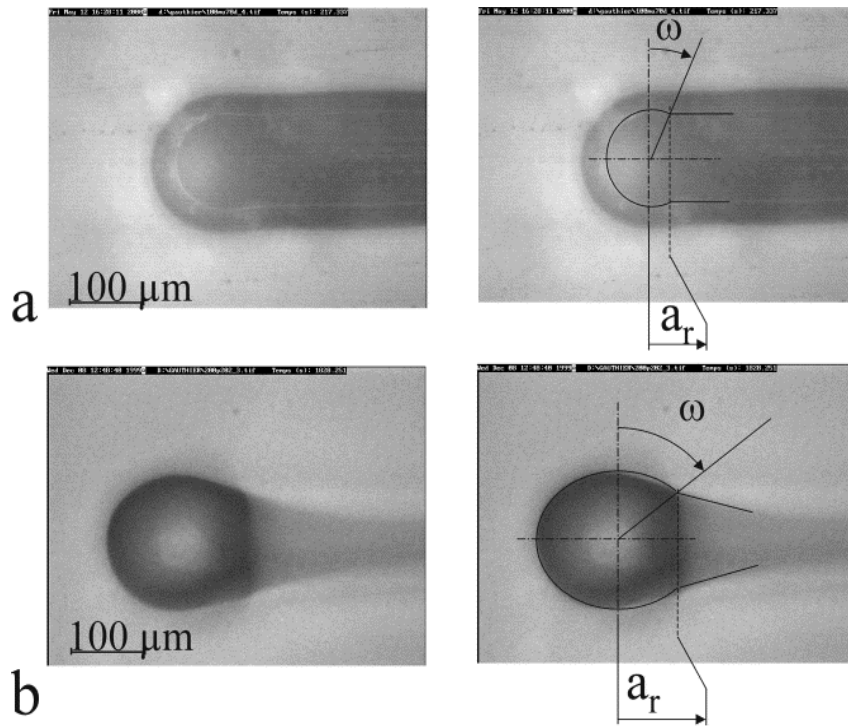


Figure 2.19(a) Photograph of the moving tip during plastic scratching at 70°C with a spherical tip of radius 100  $\mu\text{m}$ . The edges of the groove stay parallel for a very short interval after contact, since the mean strain is sufficient to generate plastic flow around the tip. (b) Photograph of the moving tip during visco-elastic grooving. The length  $a_r$  and angle  $\omega$  drawn on the two right-hand pictures characterise the recovery of the scratch [57].

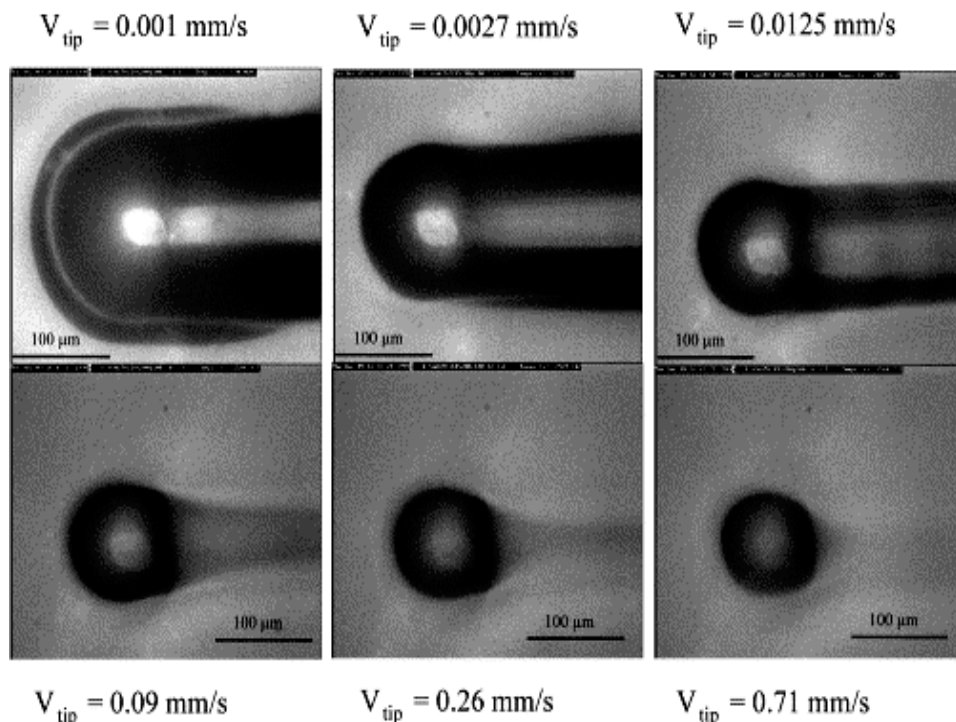


Figure 2.20 Photograph of a typical transition from viscoplastic scratching to viscoelastic grooving and at further higher tip speed, to quasi-elastic sliding. At low tip speed, the edges of the plastic flow lie parallel, while at intermediate speed the sides of the groove relax within a time comparable to the contact time [57].



Figure 2.21 gives a schematic representation of the evolution of the rear contact angle  $\omega$  as a function of the mean contact strain  $\varepsilon$ .  $\varepsilon_e$  and  $\varepsilon_p$  denote the contact strains at the end of the elastic contact area and the beginning of the plastic contact area, respectively. In a viscoelastic contact, the rear contact angle  $\omega$  is equal to  $\pi/2$ . If the material displays strain hardening, the contact strain decreases and  $\omega$  increases. Elastic and elasto-plastic domains are increased in case of lower friction (Figure 2.21) [17]. As the strain rate and temperature vary, even under constant loading, the contact area may also vary considerably and the strain near the contact may change from viscoelastic to viscoplastic [16, 17].

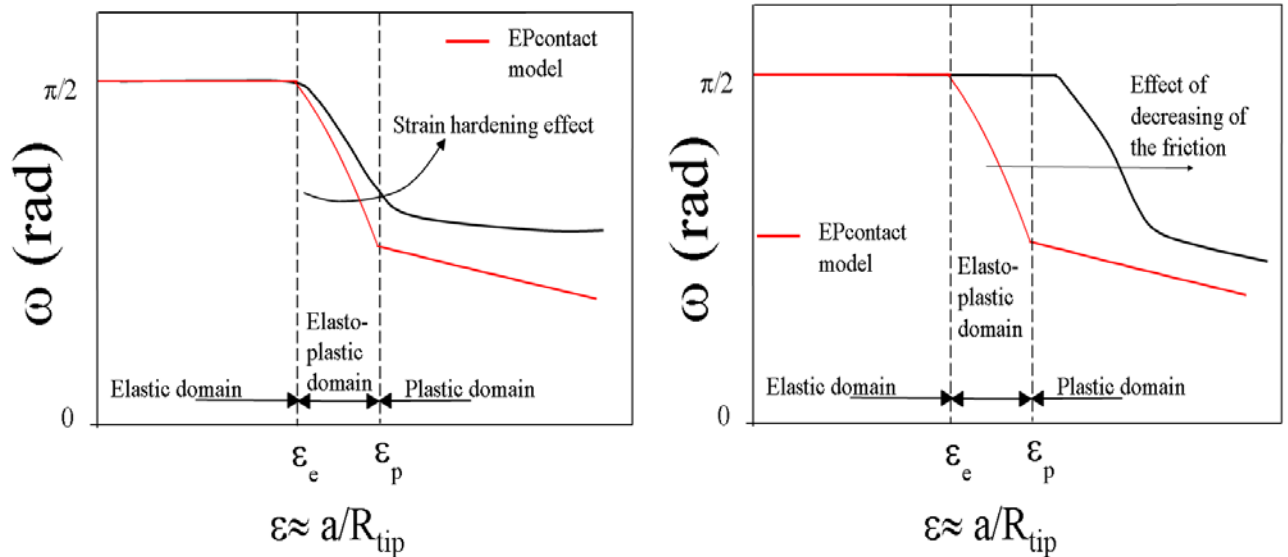


Figure 2.21 Rear contact angle  $\omega$  as a function of the mean contact strain. This angle decreases in the case of a visco-elastic-plastic or visco-plastic contact and increases if the material shows strain hardening [16, 17]. Elastic and elasto-plastic domains are increased in case of lower friction.

#### 2.5.4.4 Analysis of the total deformation

Figure 2.22(a) depicts a schematic yield volume around the tip during scratching, where the elastic recovery closes up the plastic groove left behind the contact. The total elastic plastic groove depth  $h_{ep}$  may be split into its plastic/ploughing part  $h_p$  and its elastic part  $h_e$  [7, 57] as mentioned in Figure 2.22(b). The elastically recovered part  $h_e$  is proportional to the contact width under load and depends upon the temperature and the tip shape and speed. Such modelling in two parts is used to describe the total penetration depth of indentation curves and the same method may be transposed to scratch grooves to estimate the rear contact area during scratching [57].

#### 2.5.5 Stick-slip behaviour

When two solids in contact slide relative to each other at a constant velocity, two sliding processes can occur. The motion can be continuous, or it can proceed in jerks. In the second case, the sliding surfaces "stick" together until, as a result of the gradually increasing pull or push, there is a sudden break with a consequent rapid "slip". This blinking behaviour is termed as stick-slip. Stick-slip occurs in many systems and has been claimed to be a basic component of earthquakes [69].

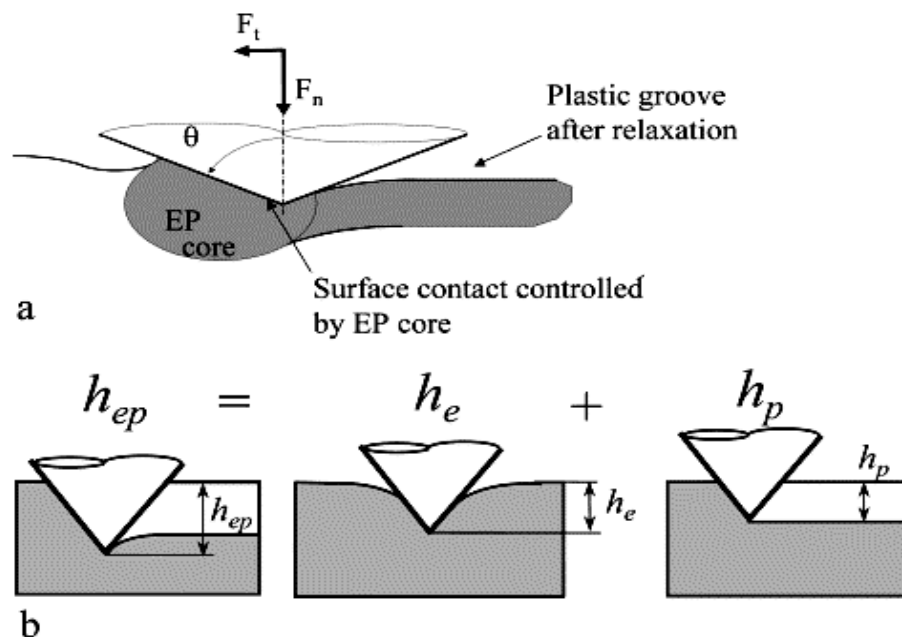


Figure 2.22(a) Schematic yield volume around the tip during scratching. After passage of the tip, the elastic recovery closes up the plastic groove. (b) The splitting up of the penetration depth of the tip into two terms: the elastic and plastic/ploughing terms [57].

With most of the polymers, a large variation in the width is found along a single scratch which is also due to the stick-slip behaviour that causes pockets of deep and shallow scratch depths as the tip moves in a kind of “hopping” motion. As the indenter moves during scratching, a prow is built in front of it. A lower interfacial friction makes the indenter to move up in a way similar to the effect due to the presence of a lubricant. If the interfacial friction is high, there is a tendency for the indenter to move deep inward due to the combined actions of the normal (acting vertically downward) and tangential forces. Thus, under certain conditions of the interfacial friction, the indenter goes deeper into the material, building even higher prow. This process comes to a halt when the tangential force increases to a level when the prow finally yields giving way to the indenter's forward movement. The “slip” (a sign of the breaking or yielding of the prow) happens at a very fast rate due to the stored elastic energy in the scratching arm, and thus the arm basically snaps back to the original position as soon as the “slip” initiates. This process gives rise to the periodic fluctuation in the scratch force (high scratch force during stick and low scratch force during slip) and a changing scratch width and depth as observed for many polymers.

The scratch force fluctuates drastically during any scratching event and this fluctuation depends upon the polymer type, the normal load and the sliding speed used. Almost all polymers may show stick-slip behaviour (that can be said either due to the stiffness of the scratching apparatus or due to the difference in static and dynamic friction). Increasing normal load increases the amplitude of the scratch force fluctuation with some complex changes in the frequency of stick-slip over the scratch distance. The tendency for stick-slip is less noticeable for PMMA which shows a continuous removal of the material during scratching. However, this behaviour of PMMA can be changed to stick-slip motion at very high speeds. This type of stick-slip is a characteristic of elastomers and rubbers before yielding generally showing large elastic and visco-elastic deformation. For polymers, the stick-slip during scratching (or sliding) depends upon their bulk mechanical properties. As a general rule, one may say that the more rubbery (visco-elastic) the polymer is, the more stick-slip (in terms of amplitude) it is likely to show [60].

Increasing normal load and scratch depth has tendency to increase the occurrence of stick-slip motion because the resistance to motion imposed by the material in the bulk is higher. However, stick-slip also depends upon the crystalline nature of the material, the interfacial friction between the material and the tip surface, the roughness, the slip rate and the stiffness of the cantilever arm used for measuring the scratch force [60, 69]. Crystallinity determines the process of energy dissipation in the deformation zone. Ductile (as shown by semi-crystalline polymers) and elastomeric (high stretchability as shown by rubbers) behaviour will raise the scratch force during stick event due to high volume of the material being deformed. In contrast, for highly brittle behaviour (as shown by amorphous polymers), the material failure takes place by micro-crack initiation and its growth leading to fine chip formation and hence the scratch force build-up is less. For highly brittle polymer, the occurrence of stick-slip is reduced due to the more efficient material removal process. It is possible that we may observe stick-slip for a brittle type of polymer if the length of the crack tends to be larger before failure. Thus, during each stick event, the cracks will grow until a big chunk of wear debris is removed. The high interfacial friction has the tendency to bring the tip deeper into the material and hence the volume of the deforming material increases leading to stick event. Thus, a reduction in the coefficient of friction can reduce the occurrence of stick-slip event [60].

## **2.5.6 Material removal and wear debris formation**

Depending upon the type of the material and the nature/severity of the contact, the material deformation can take place around the scratch tip with or without wear debris formation. The material deformation is strongly dependent upon the nature of the polymer at the test temperature [60]. Microscopic examination of the scratches revealed that, at relatively light load, there is no debris produced. As the normal load is increased beyond a critical value,  $F_c$ , wear debris caused by micro-fracture appears on the scratch sides on ceramic materials and on some metallic materials. However there is no correspondence found between the initiation of the micro-fracture and increase in friction coefficient with increasing loads [68]. Increasing load does not change the deformation mechanism in terms of ductile or brittle nature of the polymer. However, for brittle polymers such as PMMA and PC, some onset of plastic deformation can be seen. The amount of material, which is fully or partially removed from the bulk, increases with increasing depth. This is true for all polymers indicating that the failure of the material is not only dependent upon the amount of strain (which is fixed for conical tip) but also upon the normal load and the depth of penetration [60].

The process of wear particle formation follows two routes. The first route involves the brittle failure and crack formation. The formation of cracks and crazes can lead to wear debris as “chips”. The second route is through the ductile ploughing where the material may experience very local areas of extremely high strain. The material present in these highly strained areas will undergo massive plastic deformation and eventually detach from the bulk as a debris particle. Subsurface crazing and change in the volume also occurs during scratching. These sub-surface events will further lead to the formation of cracks if the load is higher or if the scratching process is repeated on the same track [58].

## **2.6 Material properties that affect the scratch damage**

### **2.6.1 Elastic modulus**

Elastic modulus plays an important role in the scratch process, especially during the indentation stage [6, 58]. The Young's modulus, scratcher geometry, and Poisson's ratio directly

determine the size of the contact zone during scratch. By assuming Poisson's ratio to be from 0.35 to 0.4 for most polymers, typical elastic moduli of polymers range from 1~10 MPa for rubbery elastomers and to 3 GPa for engineering plastics. For lower modulus polymers, the size of the contact zone increases significantly with decreasing modulus. It is interesting to note that for polymers with high Young's modulus, the effect of a small change in the Young's modulus on the contact zone size becomes insignificant. The penetration depth is more sensitive to the modulus when the modulus is lower than 1 GPa. As the maximum tensile stress is on the surface just behind the scratcher during scratch, polymers with higher moduli exhibit a higher maximum tensile stress on the surface. This may lead to the formation of surface cracks, crazes, cavitations, and debonding between phases of multiphase polymers. Thus the Young's modulus plays an imperative role in generating scratch damage. A certain level of rigidity in polymers can help to maintain a small scratch depth if the polymer is prone to plastic flow scratch damage. On the other hand, polymers with high rigidity induce high stress concentration during scratch, which could promote the formation of surface cracks, crazes, cavitations, and debonding. In this case, it is preferable to lower the modulus or increase the ductility of the polymer [6] (especially for the thermosetting polymers below  $T_g$ ).

### **2.6.2 Yield stress and tensile strength**

The yield stress determines the plastic zone size. Polymers with a higher yield stress are subjected to smaller plastic flow scratch damage. On the other hand, if the maximum tensile stress on the surface exceeds the tensile strength and if the tensile strength is lower than the yield stress of the polymer, cracks are formed on the scratch surface. Consequently, the tensile strength of the polymer plays an important role in determining the formation of either the plastic flow scratch pattern or the brittle fracture scratch pattern on the scratch surface. The plastic flow scratch pattern is preferable to the brittle fracture scratch pattern, since the brittle fracture scratch pattern can scatter light more easily resulting in enhanced scratch visibility [6].

### **2.6.3 Coefficient of friction**

The maximum tensile stress at the contact surface is dramatically increased when the coefficient of friction is high. This suggests that the polymers with high coefficients of friction tend to exhibit crazing, cracking, debonding, and cavitation types of brittle scratch damage. An increase in the coefficient of friction causes the location of the plastic zone to shift toward the surface. This means that if the polymer is prone to plastic flow scratch damage, an increase in yield zone size on the surface will occur. A larger plastic flow scratch damage may appear on the surface. Thus a low coefficient of friction is desirable for polymers to be scratch resistant [6].

### **2.6.4 Thermal effects**

Compared to metals and ceramics, organic polymers are greatly affected by the introduction of thermal changes. Even a slight increase, say a few degrees Celsius, in the temperature above room temperature may not only soften the material but also change its brittle-ductile deformation characteristics. The major brittle-ductile transition occurs at the glass transition temperature  $T_g$  and in comparison to metals, for polymers,  $T_g$  is often rather close to the ambient temperature. Hence a mild increase or decrease in temperature will change greatly the material's deformation and damage characteristics. For polymers, the scratch velocity with its associated adiabatic heating is a major source of thermal energy. This thermal energy is generated due to the energy losses at higher rates of the deformation and the associated frictional loss. It is reported that the temperature inside a scratch can go as high as 100°C for PMMA scratched at speed of  $> 1.5$  m/s by 90° and 120°

conical indenters making the polymer temperature close to its glass transition temperature [58] ( $T_g$  for PMMA is ca. 119 °C).

As significant thermal effects arise at higher scratching velocities, the influence of the thermal characteristics, such as the thermal conductivity and heat capacity of the indenter should be considered as a system variable. A modified model may be employed to approximate this increase in the overall contact temperature  $\Delta T$  as,

$$\Delta T = \frac{\frac{2}{\pi} \tan \beta \left(\frac{W}{2L}\right) v}{\sqrt{\lambda \rho c v L}} \quad 2.15$$

where  $L$  is the half width of the scratch,  $W$  the load given by  $W = H\pi L^2$ ,  $H$  the hardness of the polymer,  $v$  the velocity,  $\beta$  the attack angle of the indenter (30° for a 120° indenter, for example),  $\lambda$  the thermal conductivity of the indenter material,  $c$  its specific heat and  $\rho$  is the density of the material [62].

## 2.7 Improvement in scratch resistance

Most polymeric glasses are sensitive to scratching and resistance to marring and scratching is desirable due to the growing use of plastics in industrial applications [8, 17, 56]. Increasing the scratch resistance is equivalent to introducing an elastic contribution into a fully plastic behaviour or to increasing the elastic component in elastic–plastic behaviour. The major difference between polymeric and other classes of materials is the capacity to recover the groove left on the surface and this capacity is one way to improve the scratch resistance of polymeric surfaces. The recovery has a time and temperature dependency and may be accelerated if the glass temperature has been crossed during the life time of the groove [17]. Recently, the use of various slip additives is enhanced to improve the scratch resistance of polymeric surfaces.

There are four ways to improve the scratch resistance [17, 56].

1. By decreasing the ratio  $E/\sigma_{\text{yield}}$ , where  $E$  is the Young's modulus and  $\sigma_{\text{yield}}$  the yield stress, although this carries the major risk of decreasing the Young's modulus with subsequent loss of the macroscopic mechanical properties. One may note that an elastomeric material having a low  $E/\sigma_{\text{yield}}$  ratio is not sensitive to scratching but only to cutting, cracking and wear.
2. By introducing a strain-hardening effect into the stress–strain relationship of the bulk material, which is a means of increasing the elastic unloading in an elastic–plastic strain.
3. By coating the material. Deposition of a scratch-resistant coating, ranging from a few nanometres to a few microns, is an effective way to improve the scratch behaviour of polymeric surface. Appropriately chosen coatings can reduce the coefficient of friction and wear rate without changing the bulk properties of the material [17, 70]. However, a thin scratch-resistant coating cannot prevent yielding on the macroscopic scale of the contact. A coating decreases the yielding in the elastic–plastic behaviour of the contact if the local friction coefficient between the surface and the tip is low. The major benefit is the reduction of the ‘scratching contact strain’ [17]. This technique, however, is criticised due to the large difference between the elastic strain domains of the substrate and that of the coating.
4. Use of slip additives. Migratory slip additives such as Erucamide have traditionally been used to improve scratch and mar performance [56]. These slip and antiblock may be added directly by the

resin producer [51]. According to type, they can improve mould release, melt flow, lubricity and scratch/scuff resistance and reduce static build-up and wear [55]. However, due to concerns about vehicle interior air quality (VIAQ), the people are increasingly cautious about using additives that bloom to the surface and contain volatile organic compounds (VOCs) that contribute to fogging or malodors. Amides provide only short-term scratch protection [56].

## 2.8 Conclusions

The greatest advantage of the scratch test is in its ability to provide a large number of surface property characteristics that are very useful for tribological applications. Similar to the normal hardness, the scratch hardness data can also be related to the bulk mechanical properties of the material such as the yield stress and the elastic modulus. The scratch test has potential for use with ultra-thin and composite-layered surfaces [58]. Following conclusions can be made:

1. Scratch force is a strong function of the interfacial frictional conditions between the indenter tip and the polymer material. High interfacial friction leads to severe stick-slip motion of the scratching tip if the polymer is behaving as ductile or rubbery material. Brittle polymers can also show stick-slip at higher scratch depths.
2. Scratch hardness has decreasing trend with increasing normal load (0.5–10 N) and scratch depth (in the range of 60–400  $\mu\text{m}$ ) for low yield strength polymers. For high yield strength polymers, there is an increase in the scratch hardness with increasing normal load; however, finally, the hardness shows decreasing a trend for higher loads.
3. Stick-slip motion in scratching of polymers is a strong function of whether the polymer is semi-crystalline (generally ductile) or amorphous (generally brittle), interfacial friction, scratch depth and the stiffness property of the scratching arm.
4. Debris formation in single-pass scratching for ductile and elastomeric polymers is strongly related to the stick-slip events. During every stick event, the high stress generated in the polymer coupled with temperature rise causes extrusion type of flow for a thin layer of polymer which is in contact with the tip surface. This extruded material is removed from the bulk which can be found at equal distance along the length of the scratch. For brittle polymers, the debris formation takes place by the crack nucleation and crack propagation processes [60].
5. Material properties, such as modulus and yield stress/tensile strength both on the surface and subsurface, along with other factors, such as the friction coefficient and elastic recovery, are expected to influence the scratch process [6].
6. A certain rigidity in polymers is beneficial to giving good scratch resistance. Shear yielding, tensile tear on the surface, and shear-induced fracture on the subsurface are the main damage mechanisms during scratch [6].
7. With brittle solids, the high hydrostatic pressure developed around the deformed region may be sufficient to inhibit brittle fracture and so mean that under these conditions both indentation and scratch hardness are measures of the plastic rather than the brittle properties of the solid. When fracture does occur, it may often driven by the stresses associated with the mismatch between conditions in the plastically deforming zone and the surrounding material within which the conditions are elastic. Cracks may often propagate as the material is unloaded, that is effectively behind the indenter in a scratch test [31].

## 3 Friction analysis of polymers

### 3.1 Introduction

The industrial use of polymers as friction materials in both homogeneous and heterogeneous forms is widely increased. As a result, wear and friction properties of polymers are under extensive analysis. These processes are dependent upon many factors including the type and physical state of the polymer, the temperature, the sliding velocity, the roughness, the normal load and the contact geometry [61]. The increase of surface roughness leads to a decrease of real area of contact, which is beneficial to minimize the friction and stiction. However, an increase of surface roughness causes larger maximum contact pressure, accordingly large surface and subsurface stresses, which are not desirable to improve wear. Also, the increase of surface roughness makes local plastic contact occur at low load which is not desirable for wear, since wear is more likely to occur when asperities touch plastically [70].

Elastic deformation and adhesion are among the many different processes that contribute to resistance to relative motion during sliding contact. The resistive forces on rough surfaces are developed at the true contact areas between asperities. As surfaces slide against each other, different pairs of asperities come into contact. Location, size and orientation of the contact areas, and the contact forces that are developed at each surface, depend on asperity distributions, mechanical properties of the surfaces, external loads, and their relative motion [71].

The apparent friction coefficient is the ratio between the tangential and the normal load applied to a moving body in contact with the surface of a material [13-18]. It includes a “true local” friction coefficient, which is the scission at the interface between the tip and the surface being scratched, and a “geometrical” friction coefficient, which is the ploughing effect due to the wave front created ahead of the moving tip and depends upon the shape of the tip [13, 16]. Like in any other mechanical test, three basic types of behavior of the material at the interface are observed: purely elastic, elastic-plastic and fully plastic [16, 66]. A surface flow line model was developed by Gauthier et al. to deduce the geometrical and true friction coefficient at the interface between a moving scratching tip and the surface from the apparent friction coefficient [13, 16]. Using this model, several situations may be simulated to predict the influence of the geometry of the tip on the scratch resistance of the material [13]. The polymer true friction coefficient displays temperature and sliding speed dependency which may be attributed to the surface thermodynamics. It is shown that the local friction depends upon the level of strain in the polymer at the contact interface [13, 66].

Experiments show that shear stress at points of true contact (or local friction) depends on the contact pressure and in most cases, such a dependence is linear. Interfacial shear stresses may result from a combination of shear resistance of adhesion and contaminants in the interface. However studies also show that for rough surfaces, adhesion usually has negligible effect on the contact area and pressure [71].

### 3.2 Different scales in friction mechanism

There are three relevant scales of friction as given below [13]:

1. The macroscopic friction scale
2. The apparent local friction scale
3. The molecular friction or interfacial scission true friction scale



### 3.2.1 The macroscopic friction scale

The macroscopic scale is that of the relevant motion between two macroscopic bodies. The contact area is composed of a large number of elementary discontinuous areas having various geometries [13, 66, 70]. The macroscopic friction coefficient is the contribution of the interactions between a large number of microscopic elementary contacts, but the friction of each of these elementary contacts is only an apparent value. This apparent value is itself the sum of a true local friction (the ratio between the interfacial shear stress at the interface and the local pressure) and the viscous and/or elastic-plastic and/or plastic flow of the material around the local contact area [16]. At this macroscopic level, the friction coefficient is one of the various physical parameters contributing to the dissipated energy, which is the origin of wear phenomenon between moving surfaces [13].

Measurements of the macroscopic friction reveal a dependency on temperature and sliding speed and attempts have been made to give a physical sense to this dependency [13, 66]. The first macroscopic contact analysis concerned the static contact of metallic materials, for which adhesion at the interface of the contact could be neglected. These initial studies allowed confirmation of Bowden and Tabor's relation linking the normal load to the real contact area and definition of the transition condition from elastic to elastic-plastic contact. The three relevant scales of friction are shown in Figure 3.1.

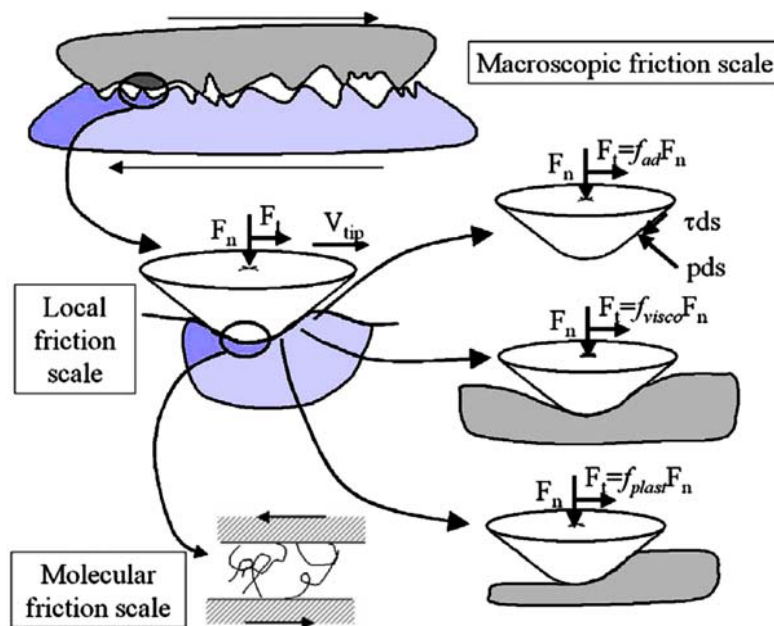


Figure 3.1 The three relevant scales of friction named as macroscopic, local and molecular friction scales [13].

### 3.2.2 The local friction scale

At the local scale, the contact area is a smooth planar surface with perfect continuous contact between the bodies [13, 66]. The most complicated situation arises in the local interfacial level whether either mechanics or thermodynamics control the friction [16]. In polymers, the local friction presents a peak when the glass transition temperature is reached and the evolution of the friction is comparable to that of mechanical loss factor  $\tan\delta$ . Although these two peaks are displayed at almost same temperature but they cannot be said to occur due to same phenomenon.



The origin of this friction peak is attributed to adhesion hysteresis corresponding to the energy dissipation of a loading-unloading cycle [13, 66]. As soon as the friction concerns representative elementary volumes of the material, the notion of contact pressure and contact strain should be taken into account. At this scale, the test apparatus is a micro-scratch or more recently a nano-scratch apparatus. As discussed in chapter 2, the energy consumption during scratching is located mainly in two zones. The first zone is the interface; a very thin layer subjected to extremely high shear strain, a high strain rate and adhesive slipping. The second zone is spherical and its size is comparable to that of the groove left on the surface. The strain rate of this volume will be lower than that in the interfacial layer [13, 61, 65, 66]. The apparent friction is the ratio between the tangential force and the normal load [13-18, 66] and there is competition in this friction between an adhesive term and a ploughing term. The latter term may be decomposed further into two parts: one part due to the visco-elasticity and the other due to the plasticity [13, 16, 18]. Hence the friction may be written as:

$$\mu_{app} = \mu_{ad} + \mu_{visco} + \mu_{plast} \quad 3.1$$

### 3.2.3 The molecular friction scale:

Friction tests performed under an AFM allowed study of the friction at the level of the polymer chains. The AFM is also employed to measure the friction force, to study nano and micro scratches and to determine the surface topography of a sample. However, the results obtained at this scale are sometime unpredictable [13]. The friction may be independent of the sliding speed, while the depth of the groove can vary with the scratching speed. It has been observed that the friction is stable only after a sliding length approximately equal to the contact width [13, 66]. At the molecular level and using a spherical tip having a large radius (typically a surface force apparatus or a pin on disc apparatus), sliding studies show that the friction depends upon the sliding speed in relation to the interpenetration of the macromolecular chains, while the adhesion hysteresis is linked to the dissipated work when the chains remains in their original state. This penetration decreases with the sliding speed and disappears when the network begins to slide on a solid-like brush. The brush is solid-like if the friction decreases to tend to an asymptotic value, or liquid-like if the friction increases with the sliding speed [13].

## 3.3 Different types of friction

The relevant types of friction are given below [13]:

1. Adhesive friction
2. Ploughing friction
3. Visco-elastic friction
4. Plastic friction
5. Static and dynamic friction

### 3.3.1 Adhesive friction

The Bowden and Tabor mono-contact analysis permits the association of the adhesive friction to the adhesive shear for a plastic contact [13, 18]. If the angle between the front face of the moving tip and the surface is small, then the adhesive force is [13]

$$F_{ad} = \tau S_n \quad 3.2$$

and the normal load is

$$F_n = pS_n \quad 3.3$$

where  $\tau$  is the shear stress at the moving contact area;  $p$  is the local contact pressure which is equal to the hardness of the softer material [3, 7, 13, 17, 18];  $S_n$  is the real contact area.

Therefore, the adhesive term  $\mu_{ad}$  of the friction in equation (3.1) becomes

$$\mu_{ad} = F_{ad} / F_n = \tau / p \quad 3.4$$

For temperatures below the glass transition temperature, Brisco and co-workers has shown that the interfacial shear stress may be written as [13, 16, 66]

$$\tau = \tau_o + \alpha p \quad 3.5$$

Thus the adhesive term of the friction can be written as

$$\mu_{ad} = \frac{\tau_o}{p} + \alpha \quad 3.6$$

where  $\tau_o$  and  $\alpha$  are constants for a polymer when all other parameters are fixed.  $\tau_o$  is usually equal to one MPa and  $\alpha$  lies in the range 0.08~0.6 for a large variety of solid polymers [13, 16, 18] : for example, for PMMA ,  $\alpha = 0.36$  and  $\tau_o = 10$  MPa, when scratch hardness is typically equal to 250 MPa at room temperature [16].

### 3.3.2 Ploughing friction

The ploughing friction coefficient is estimated as the ratio between the cross section of the groove (grey in Figure 3.3) and the normal section of the contact area. The visco-elastic origin of the ploughing component of the friction is given by Moore. Bucaille et al. have generalised Tabor's approach to take into account the rear contact defined by the rear contact angle  $\omega$  (Figure 3.2a) and thus the ploughing friction is defined as:

$$\mu_{plough} = \frac{2}{\pi} \cot\theta \left[ \frac{\pi \sin\left(\omega + \frac{\pi}{2}\right)}{\pi + 2\omega} \right] \quad 3.7$$

However, a simple rear contact angle does not separate the different mechanical components (viscoelasticity, or elastic unloading after an elastic-plastic or fully plastic contact), that contribute to the rear contact and decrease the friction. This model of the ploughing friction allows one to obtain the limiting cases for  $\omega = 0$  and  $\pi/2$ , but it neglects the triangular sector inside the dorsal angle (Figure 3.2a). The ploughing friction depends on the apex angle  $\theta$  and the rear contact angle  $\omega$ . An approximate calculation allows the estimation of the cross section as a triangular section having a width at the base equal to the rear width of the contact and a height equal to that of the hyperbola, as indicated in Figure 3.3. The ploughing part of the friction including the rear contact angle is

$$\mu_{plough} = \frac{2}{\pi} \cot\theta \left[ \frac{\pi \cos\omega(1 - \sin\omega)}{\pi + 2\omega + 2\sin\omega} \right] \quad 3.8$$

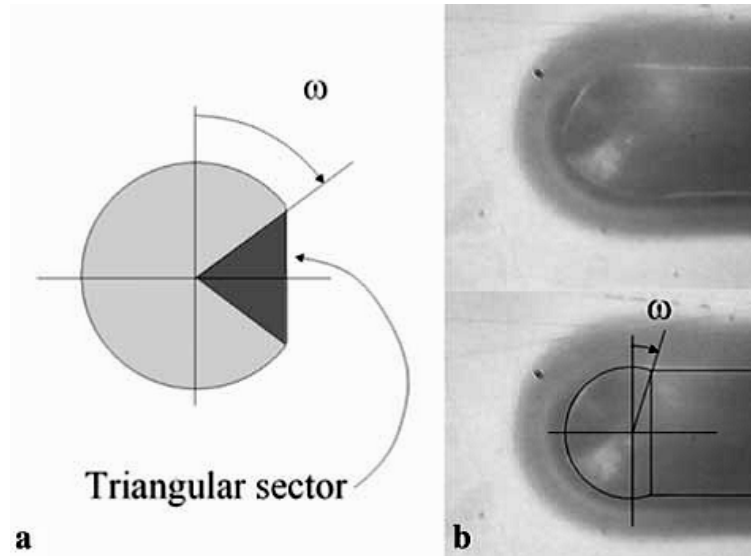


Figure 3.2 (a) Model of the contact area showing the triangular sector; (b) Photograph of the true contact area during scratching of a PMMA surface with a  $120^\circ$  apex angle tip and estimation of the shape of the contact area. The triangular sector has to be taken into account to determine the contact area [13].

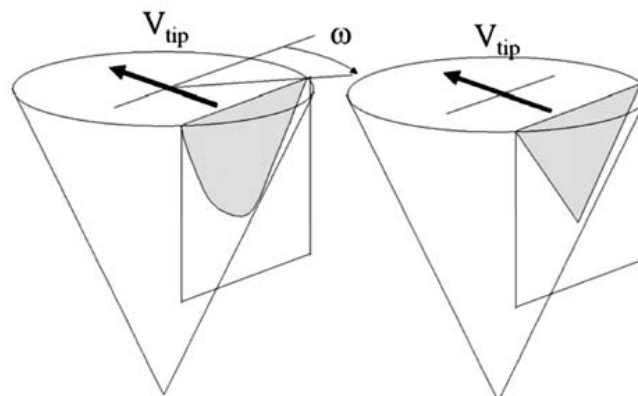


Figure 3.3 Geometrical definition of the rear contact and the cross section used to estimate the ploughing friction. Exact solution on the left and triangular solution on the right [13].

For  $\omega = 0$ , above equation is equal to Tabor's friction coefficient. The true friction will be zero and the apparent friction becomes equal to the geometrical friction and the contact will be purely plastic. For  $\omega = \pi/2$ , the apparent and true frictions should be the same i.e. the ploughing friction is null and the contact is purely elastic in this case. Small discrepancy in estimation of the true contact area for conical tip geometry can lead to important shifts in the ploughing friction coefficient [13, 16].

### 3.3.3 Visco-elastic friction

Bulgin et al. and Moore considered that during continuous sliding contact on a polymeric surface, there is alternately adhesion between the polymer and the moving tip for a short time and then relaxation after a certain displacement distance. The Voigt model provides a relation between the friction coefficient and the loss factor for such cases as [13]:

$$\mu_{\text{visco}} = \frac{K}{H} \tan\delta \quad 3.9$$

where  $K$  is a constant and  $H$  is the hardness. In rolling tests on an elastomeric material, Moore reported a friction peak in phase with the loss factor peak  $\tan\delta$ . Bueche and Flom and many other authors have observed similar behaviours for various polymeric surfaces [13, 72, 73].

### 3.3.4 Plastic friction

The term  $\mu_{\text{plast}}$  due to plasticity in equation 3.1 is usually evaluated for a perfectly dissymmetric contact from the plastic model given by Bowden and Tabor. Figure 3.4 shows that this model is applied to a perfectly conical tip and considers the ratio between the frontal projected and horizontal contact areas. If the half apex of the conical tip is  $\theta$ , the plastic friction is [13, 16]

$$\mu_{\text{plast}} = \frac{2}{\pi} \cot\theta \quad 3.10$$

This relationship suggests that the plastic term of the friction coefficient depends only on the tip geometry and does not take into account the elastic-plastic behaviour of the material or the contact shape, which depends on partial elastic unloading. Tabor's model cannot be applied to visco-elastic-plastic materials having a low ratio of the elastic modulus to the yield stress, as in the case for polymers [13]. The scratching of polymers shows elastic unloading that partially recovers the rear contact [13, 57]. Furthermore, for a visco-elastic-plastic contact where elastic and plastic strains exist in the material surrounding the contact tip, this elastic unloading can be very important. In the case of visco-elastic contact, the contact area becomes quasi symmetric [13].

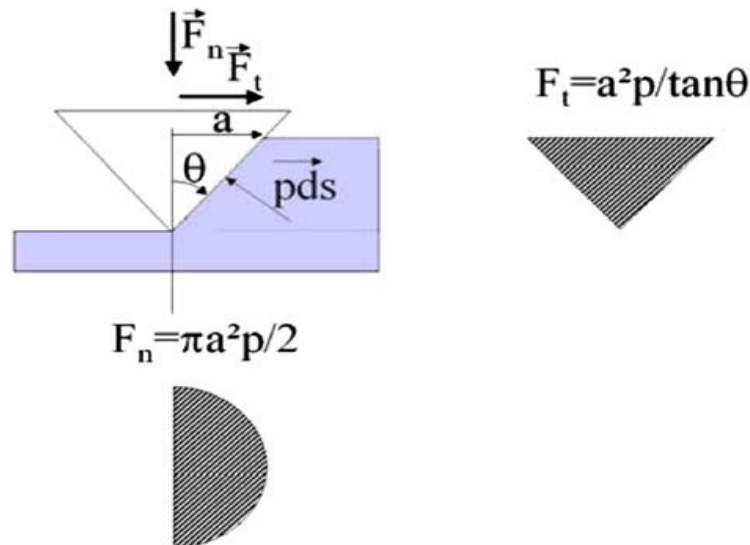


Figure 3.4 Plastic friction model applied to a perfectly conical tip and a rigid perfectly plastic behaviour [13].

### 3.3.5 Static and dynamic coefficients of friction

In case of the stable sliding, the measured friction is the dynamic coefficient of friction  $\mu_d$ , defined as the shear stress required to maintain slip motion divided by the corresponding normal stress. For stick-slip, the measured friction is the static coefficient of friction  $\mu_s$ , defined as the maximum shear stress reached before sudden slip divided by the corresponding normal stress [69].

### 3.4 Parameters controlling the friction coefficient

Even for a given tip geometry, strain rate and the mean contact strain the coefficient of friction is influenced by a number of factors like physical properties of the surface, measuring conditions and the material characteristics. These can be listed as [52]:

- Temperature
- Time after processing
- Material thickness
- Quality of mixing
- Surface free energy
- Surface adhesion force
- Surface in contact
- Surface roughness
- Concentration of friction reducing additive
- Pore volume in inorganic additive
- Interaction between additives
- Transfer of surface components to another material in contact

Temperature influences Brownian motion and diffusion and affects hardness of materials, which in combination influences the adhesive properties of surface and ultimately their friction coefficient. Temperature affects materials friction coefficient during storage, transportation, processing and use. In majority of cases, a well compounded material regains its initial friction coefficient when temperature of material is lowered [52].

Diffusion of additives is time and temperature controlled process. Erucamide migrates to the surface very rapidly during the first hour after the material manufacture (due to its lower surface energy as discussed in section 1.3). Even faster changes occur during processing. For example, when material is cooled down, amide migrates rapidly to the surface and reduces the friction coefficient. The first phase of rapid migration is followed by regular arrangements of amides molecules on the surface. In this phase, friction coefficient is further reduced. Later changes in friction coefficient are much slower. Eventually equilibrium value is established, determined by the temperature, polymer, type and concentration of additives (Figure 3.5) [52]. Figure 3.5 shows the effect of Erucamide concentration and the aging on the friction coefficient of low density polyethylene film. Two different trends are observed. Friction coefficient decreases linearly with the increasing concentration of Erucamide when friction coefficient is measured as soon as the film is made. But for the measurements carried out after one hour, the friction coefficient decreases initially with increasing concentration but then approaches constant value at 400 ppm and then remains constant, independent of the concentration. This shows that different properties may be expected during the process and during storage [52].

Material thickness is very important during migration of additive to the surface. Quality of mixing is also important especially in case of inorganic additives as their efficiency depends upon the dispersion. Friction coefficient of the material also depends upon the surface properties of other material in contact. Surface roughness is also important but is not the decisive parameter influencing the friction coefficient [52].

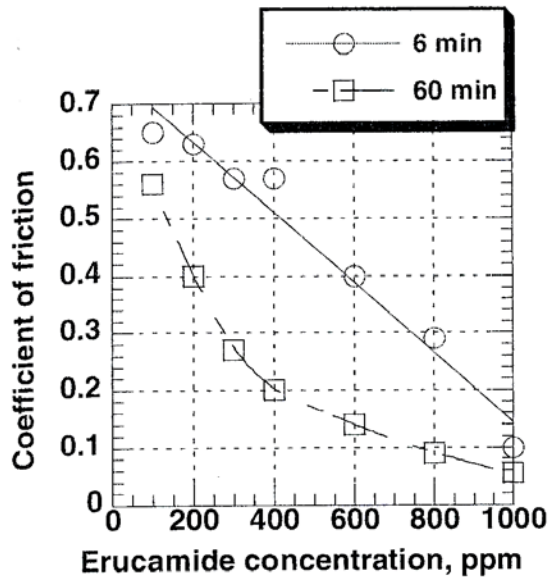


Figure 3.5 Coefficient of friction of LLDPE film measured after 6 and 60 minutes from the extrusion vs. erucamide concentration [52].

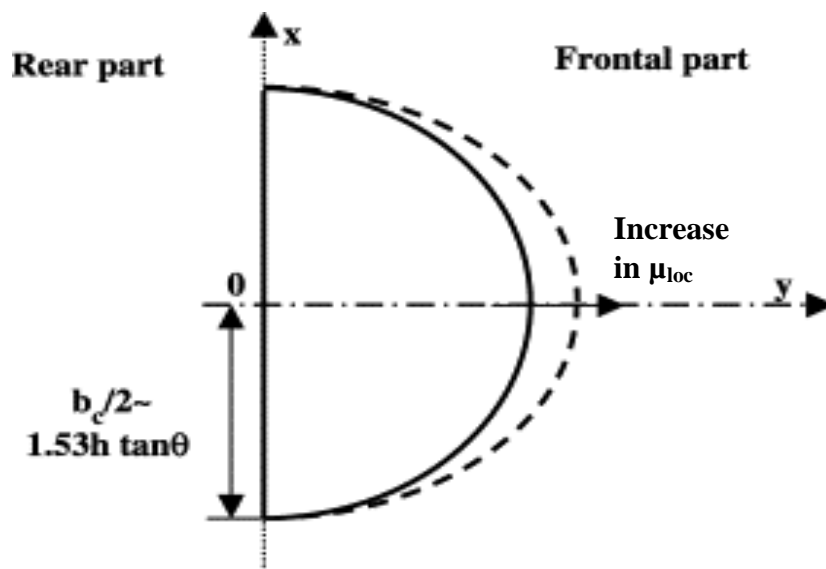


Figure 3.6 Influence of the local friction coefficient  $\mu_{loc}$  on the contact surface (top view) in scratching an elastic perfectly plastic material ( $\epsilon_e \approx 0.35\%$ ) with a conical indenter ( $\theta = 70.3^\circ \rightarrow X \approx 100$ )-h constant, where  $X$  is the indentation index, defined as  $X = E \cot \theta / \sigma_y$  [14].

### 3.5 Effect of friction on different parameters

#### 3.5.1 Geometry of contact and volume average plastic strain

As the local friction coefficient  $\mu_{loc}$  increases, the flow remains of or is converted to the ploughing type and Figure 3.6 describes schematically the evolution of the contact geometry with friction for a given penetration depth. As a first approximation the contact width  $b_c$  and the contact height  $h_c$  remain constant, an unexpected feature. On the contrary, the frontal height  $h_{fc}$  increases significantly. So the top view of the contact is about half of an elliptic disk whose eccentricity increases with the friction [14]. So the friction produces an accumulation of the material on the frontal surface of the indenter. As a first approximation, the frontal height to the penetration depth

ratio  $h_{fc}/h$  is a linear function of the local friction coefficient  $\mu_{loc}$  (Figure 3.7). The volume average plastic strain  $\varepsilon_v$  increases markedly from 0.95 to 1.61 as  $\mu_{loc}$  increases from 0 to 0.2 as shown in Figure 3.7 and this increase is very similar to that of the frontal edge height  $h_{fc}$  [14]. The effect of friction coefficient on contact geometry is also evident from Figure 2.21 indicating that rear contact angle  $\omega$  is increased by decreasing friction; ultimately resulting in increased elastic-plastic domains of polymers.

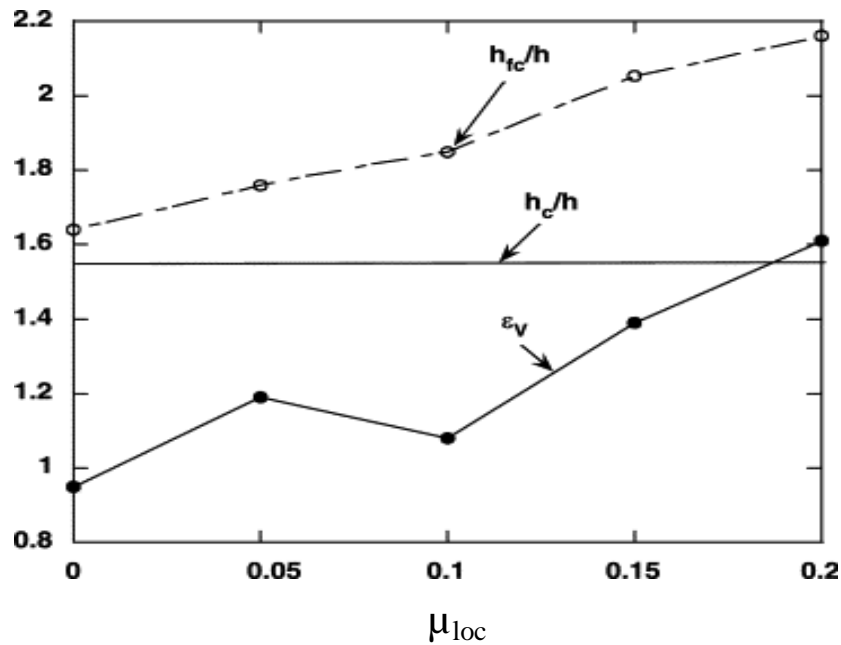


Figure 3.7 Influence of the local friction coefficient  $\mu_{loc}$  on the volume average plastic strain  $\varepsilon_v$  and on the frontal and lateral edge height  $h_{fc}$  and  $h_c$  in scratching an elastic perfectly plastic material ( $\varepsilon_e \approx 0.35\%$ ) with a conical indenter ( $\theta = 70.3^\circ \rightarrow X \approx 100$ ) [14].

### 3.5.2 True friction coefficient as a function of the normalized contact pressure

The normalised contact pressure ( $p_m/\sigma_y$ ) is the ratio of the contact pressure to the yield stress determined at the same strain rate and temperature. Figure 3.8 depicts the true friction coefficient as a function of the normalized contact pressure that indicates that 3 months ageing of PMMA at 30°C does not affect the friction properties significantly.

Three domains may be distinguished: Firstly, at a very low normalized contact pressure (below 0.1), the true local friction is highly scattered as the pressure is close to zero and the ratio of scission to pressure diverges. Hence points below a normalized pressure of 0.1 are not shown. Secondly, at an intermediate normalized contact pressure (between 0.1 and 1), the high friction of a rejuvenated surface decreases continuously with pressure, whereas the low friction of an aged surface remains more or less constant while increasing slowly. Thirdly, at a high normalized contact pressure (above 1, fully yielded contact), the true friction coefficient tends to a unique value of about 0.45, whatever the ageing. This corresponds to the true friction coefficient estimated from scratching.

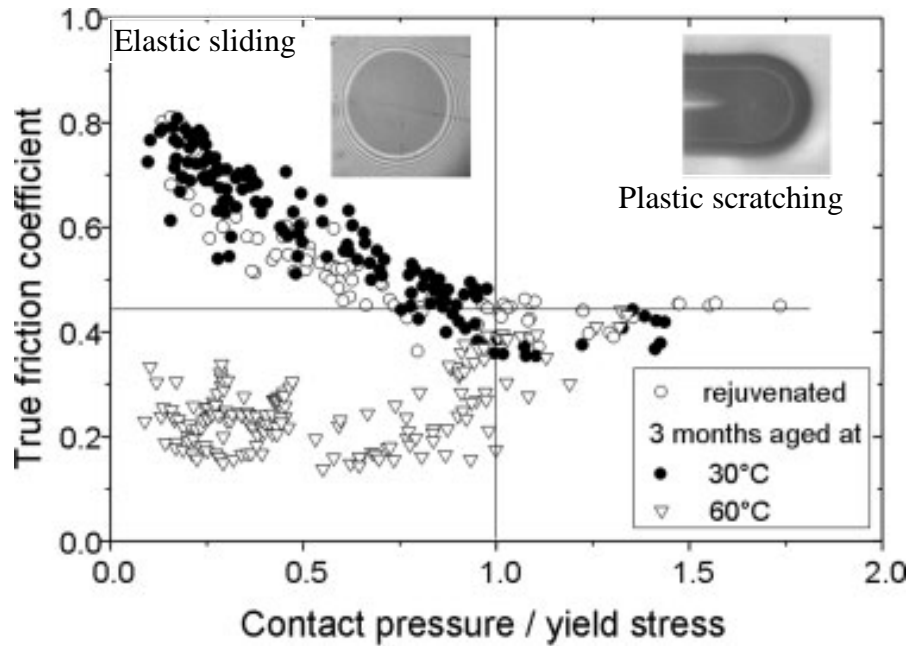


Figure 3.8 True friction coefficient versus normalized contact pressure for variable ageing of the PMMA sample [66].

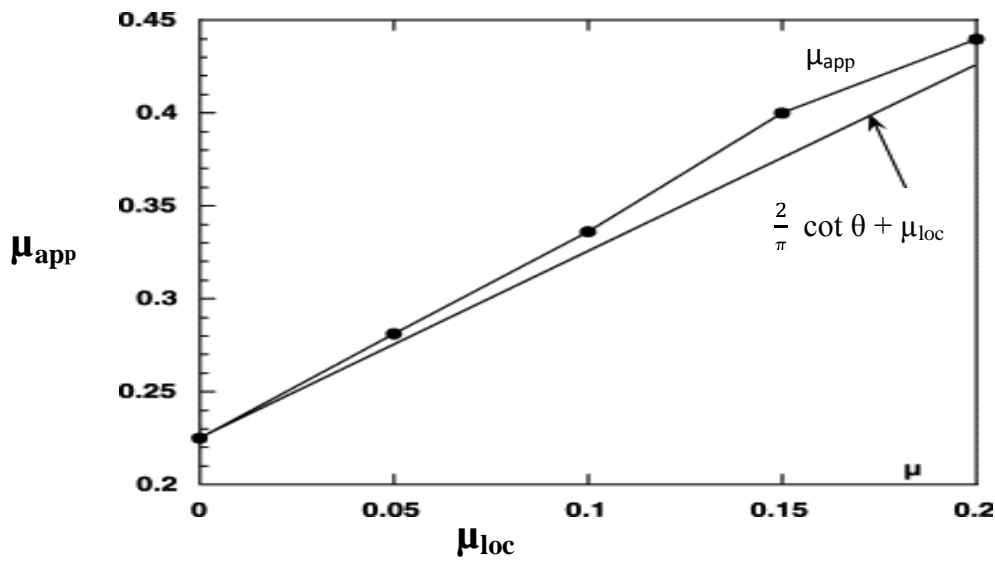


Figure 3.9 Influence of the local friction coefficient  $\mu_{loc}$  on the apparent friction coefficient  $\mu_{app}$  in scratching an elastic perfectly plastic material ( $\epsilon_e \approx 0.35\%$ ). with a conical indenter ( $\theta = 70.3^\circ \rightarrow X \approx 100$ ) [14].

### 3.5.3 Apparent friction coefficient and scratch hardness

As expected, the apparent friction coefficient  $\mu_{app}$  increases with the (real or local) friction coefficient  $\mu_{loc}$  (Figure 3.9). This increase is linear and is well described in first approximation by the classical relation of Bowden and Tabor for modelling the friction between solids, that is defined as [14]:

$$\mu_{app} = \frac{2}{\pi} \cot \theta + \mu_{loc} \quad 3.11$$



However, this is true only for moderate local friction as for very low and higher local friction,

$$\mu_{\text{app}} \neq \mu_{\text{plough}} + \mu_{\text{loc}} \quad 3.12$$

An unexpected result is that for a given penetration depth, the normal force  $F_n$  does not vary significantly with the friction (for  $\mu_{\text{loc}} < 0.2$ ); as the contact width is also constant. It implies that the apparent scratch hardness and the residual groove profile is quasi-independent on the friction coefficient for a given value of the normal force. The apparent scratch hardness of metals does not depend on the conditions of lubrication and the residual groove profile does not vary significantly with the apparent friction coefficient [14]. However, for polymers as discussed in chapter 2, a lower interface friction coefficient will generally turn out an increase in the scratch hardness.

For the case of normal hardness for metals, Tabor has suggested a relation between the hardness values with and without friction as;

$$H_N = H_{N,\mu=0} (1 + \mu \cot 2\alpha) \quad 3.13$$

where  $H_N$  is the normal hardness at a value of the interfacial coefficient of friction  $\mu$ ,  $H_{N,\mu=0}$  is the corresponding “frictionless” normal hardness and  $\alpha$  is the semi-included angle of the conical indenter [58].

### 3.5.4 Surface free energy and the friction coefficient

The knowledge of the surface free energy of a solid is of interest in the fields such as adhesion and adsorption where the forces at and across an interface operate [74]. It was earlier believed that friction is only controlled by the geometry of the asperities of the surfaces involved. However, it was observed later that if two surfaces adhere to each other at rest, there is a finite value of friction even at zero externally applied load. That means the friction is decided not only by the geometry of the asperities and the mechanical behavior of the material but also by the surface free energy or adhesion force of the surfaces. Both theoretical and experimental results proved that the role of surface energy on friction is not negligible especially when the applied load is very small. However, the friction between two solid bodies depends not only on the surface energies but also on the surface roughness [21].

It is known that when two surfaces (e.g. ball and a flat surface) come into contact, there is finite force acting between them, known as attractive or pull-off force,  $F_o$ . This force, which depends upon the surface free energies of the solids, was first derived by Bradley in 1932 and is given as,

$$F_o = 2\pi R (\gamma_1 + \gamma_2 - \gamma_{12}) \quad 3.14$$

where  $\gamma_1$  and  $\gamma_2$  are surface free energies of the two surfaces,  $\gamma_{12} = (\sqrt{\gamma_1} - \sqrt{\gamma_2})^2$  and  $R$  is the contact radius [21].

Shear stress  $\tau$  increases linearly with increasing  $P$  although the magnitude of  $\tau$  is strongly influenced by the attractive force,  $F_o$  (that is the adhesive interactions between the surfaces). It is well noted that higher  $F_o$  provides higher  $\tau$ . The linear relation  $\tau = \tau_o + \alpha P$  as proposed by Bowden

and Tabor is also confirmed where the pressure coefficient ( $\alpha = 0.0013$ ) is same for all  $F_o$ . However, the normal pressure-independent initial shear stress,  $\tau_o$  increases as  $F_o$  is increased. Robbins et al. have also confirmed it by molecular dynamic simulation.  $\tau_o$  is the initial shear stress when the contact pressure,  $P = 0$ . It is an important parameter controlling initial friction which changes with the pull-off force,  $F_o$  [21].

The relationship between  $F_o$  and  $\tau_o$  can be modeled by an exponential curve of the following form,

$$\tau_o = c_1 \exp(nF_o) \quad 3.15$$

where  $c_1$  and  $n$  are constants that depend upon the nature of the surface of the materials [21].

Since  $\tau = \tau_o + \alpha P$  and the initial friction force,  $F_i = \tau A$ , we can write as

$$F_i = \tau_o A + \alpha P A \quad 3.16$$

By dividing above equation with applied load,  $W$ , we obtain the initial coefficient of friction,  $\mu_i$  as [21]

$$\mu_i = [(\tau_o/W) \times A] + \alpha \quad 3.17$$

where  $P = W/A$ . Finally, we can correlate  $\mu_i$  as a function of attractive or pull-off force,  $F_o$  using equation 3.14 and equation 3.16 as

$$\mu_i = [c_1 \exp(nF_o) \times A / W] + \alpha \quad 3.18$$

For the visco-elastic materials, Bowden and Tabor suggested that the contact area,  $A$  is nearly proportional to  $W^{0.75}$ . Since  $A = c_2 W^{0.75}$  where  $c_2$  is a constant equal to  $0.74 \pm 0.18 \text{ m}^2 \text{ N}^{-0.75}$ , above equation then becomes [21],

$$\mu_i = [c_1 c_2 \exp(nF_o) / W^{0.25}] + \alpha \quad 3.19$$

Erhard and Lavielle studied friction between different polymers with different surface energies ( $55\text{--}90 \text{ mJ/m}^2$ ) and found that the coefficient of friction was exponential to the surface energies of the sliding polymers. Surface energy is also directly responsible for the removal of the polymer material as wear debris [21].

The surface free energy of the final polymer may be influenced also by the nature of material of the mould. For example, the surface free energy of nitrile butadiene copolymers NBR depends upon the surface free energy of the mould in which the product is molded. Lower the surface free energy of the mould, lower is the surface energy of the molded product, lower is the adhesion force to mold and lower is the friction coefficient of the final product [52].

### 3.6 Conclusions

The overall friction coefficient in a scratching test is influenced by many factors such as material type, sliding speed, temperature, lubricated condition, normal load, and the indenter geometry. The origin of this dependency is often attributed to surface thermodynamics while neglecting the influence of the contact mechanism. The ratio of adhesive interfacial force to the

total scratch force tended to unity when the cone angle of the indenter is increased in single-pass scratch tests. This may also mean that the ploughing effect decreases with the increasing cone angle of the indenter. The overall friction coefficient is found to increase with the increasing attack angle (equivalent to decreasing included angle of the tool) in scratching experiments by a wedge and is seemed to yield a value greater than unity for large attack angles. The ploughing term is more dominant in scratch experiments and the friction (tangential) force will also increase with the increasing interfacial or local friction coefficient  $\mu_{loc}$  between the indenter and the specimen, and thus, the overall or apparent friction coefficient  $\mu_{app}$  should increase with  $\mu_{loc}$ . Thus the  $\mu_{app}$  is a strong function of the included angle of the indenter and the interfacial frictional properties of the contacting materials. Polymer friction also shows a large dependence on temperature and sliding speed [15].

The apparent friction and the local true friction shows peaks correlated with the loss factor while the ploughing friction is linked with the contact symmetry, which has a visco-elastic or plastic origin. The physical origin of the ploughing friction peak resides in the variation of the contact shape, itself related to the evolution of the loss factor. Adhesion hysteresis appears to be one of the parameters responsible for the true local friction. Other parameters acting on the true local friction are the contact time and the temperature [13].

Surface roughness has a significant effect on friction/stiction and wear. An increase of surface roughness leads to a decrease of the real area of contact, which is beneficial to minimize friction and stiction. However, the increase of surface roughness results in larger maximum contact pressure, which is not desirable to decrease wear. Also the increase of surface roughness leads to local plastic contacts at low loads which is not desirable regarding wear, since wear is more likely to occur for plastic, rather than for pure elastic contacts [70].



## **Section two**

# **Experimental and simulation results**



## 4 Experimental work and discussion

### 4.1 Materials and methodology

#### 4.1.1 Materials

The comparative effect of Crodamide and PEG on surface and bulk properties of PMMA was studied using a standard grade PMMA (V825), having molecular weight about 100K. It was provided by Arkema in the form of 3 mm thick sheets having the dimension 8 cm \* 10 cm. The effect of these plasticizers was studied by testing the samples containing 0, 1, 3, and 5 % of either of the both; i.e. PEG and Crodamide. PEG is generally recognised as an internal lubricant and is preferred due to its low cost and antiblock properties [52]. Due to compatibility with most of polymers, fatty acid amides are very useful to surmount many of the slip, blocking and mould-release problems faced by the polymers [52, 75, 76]. Crodamide, similar to other fatty acid amides, has superior thermal stability which permits its use at relatively higher process temperatures where use of other conventional additives is not recommended [76, 77]. PEG [(C<sub>2</sub>H<sub>4</sub>O) nH<sub>2</sub>O] employed had Mol. Wt. 3350 and was purchased from Sigma-Aldrich. The Crodamide used was Crodamide-212 (stearyl erucamide, C<sub>40</sub>H<sub>79</sub>NO) having Mol. Wt. 590 and was purchased from Croda Chemicals.

The comparative effect of three fatty acid amides namely Erucamide, Behenamide and Stearamide was studied using a standard grade PMMA, polymerized within the laboratory in the form of 3 mm thick sheets having the dimension 12 cm \* 18 cm. Erucamide is favoured over Oleamide owing to its higher melting point and higher heat resistance, desirable at higher operating temperatures of polymers. It also dominates Oleamide due to its lower volatility and colour stability. At low concentration levels, the Erucamide is useful without disturbing much other physical characteristics of the polymer [78]. The effect of Erucamide [CH<sub>3</sub>(CH<sub>2</sub>)<sub>7</sub>CH=CH(CH<sub>2</sub>)<sub>11</sub>CONH<sub>2</sub>, Mol. Wt. 337.59 g/mol] was studied by testing the samples containing 0, 0.05, 0.1, 0.15 and 0.2 wt% of Erucamide. Analogous to other fatty acid amides, Behenamide is normally used to decrease the friction and abrasion of the polymer surfaces [52]. It gives an improved scratch resistance maintaining high transparency when used for anti-blocking properties [79]. The consequence of Behenamide [CH<sub>3</sub>(CH<sub>2</sub>)<sub>20</sub>CONH<sub>2</sub>, Mol. Wt. 339.6 g/mol] was studied by testing the samples containing 0, 0.05 and 0.1 wt% of Behenamide. Stearamide is also used to improve processability, to diminish friction and abrasion of the polymer surface [52]. The effect of Stearamide [CH<sub>3</sub>(CH<sub>2</sub>)<sub>16</sub>CONH<sub>2</sub>, Mol. Wt. 283.5 g/mol] was studied by testing the samples containing 0, 0.1, and 0.3 wt% of Stearamide. A sample containing 0.1% Behenamide and 0.2% of Erucamide was also tested in order to examine the synergy in action between the two as discussed in section 1.8.5. The higher limits of the plasticizers were restricted to above percentages due to their solubility problem in MMA monomer solution at room temperature. Moreover, these limits are also proposed in literature as discussed in section 1.8.6. All the three plasticizers and MMA monomers [C<sub>5</sub>H<sub>8</sub>O<sub>2</sub>, Mol. Wt. 100.12 g/mol] were purchased from Sigma-Aldrich.

The effect of an additive (Crodamide-212 and Crodamide-Er or refined Erucamide) on surface and bulk properties of two different grades of PMMA was studied by using its two standard grades V825 and HT121. They were provided by Arkema in the form of 3 mm thick sheets having the dimension 8 cm \* 10 cm. HT121 has greater thermal stability than V825. Its T<sub>g</sub> is 15°C higher than that of V825. Moreover, HT121 has acidic functional group located at the main polymer chain.

The effect of reticulation or cross linking on surface and bulk properties of PMMA was also studied by using a non-reticulated standard grade PMMA (496), and a reticulated PMMA (495) having 0.6 wt % of butanediol dimethacrylate (BDMA) as a reticulating agent. They were also provided by Arkema in the form of 3 mm thick sheets having the dimension 8 cm \* 10 cm. Both were nano-structured containing 10% of poly (n-butyl acrylate) (PBA) as soft elastomeric rubbery phase. PBA is generally used to enhance toughness of the PMMA and is employed in its nano structured form in order to get an improved transparency of the end product.

### **Preparation of PMMA samples:**

The preparation procedure of PMMA (whether used in the laboratory or used at Arkema) is given below.

325 ppm of AIBN (Azobisisobutyronitrile) [ $C_8H_{12}N_4$ , Mol. Wt. 164.21 g/mol] were used as initiator in the polymerization of MMA monomers. 35 ppm of Terpinolene [ $C_{10}H_{16}$ , Mol. Wt. 136.24 g/mol] were also used as a polymerization reaction regulator/ stabilizer because it acts as chain transfer agent. The preparation procedure can be summed up as follows:

- Preparation of the solution: by weighing the appropriate amounts required for a given number of PMMA sheets, the reagents are introduced into a flask and are shaken and agitated well. Then the solution is degassed by putting it under vacuum for about 20 minutes.
- Preparation of the mould: the mould consists of two plates of glass laid out in parallel and separated by a flexible PVC gasket which ensures the sealing of the mould along with the uniform spacing of the plates. The snap rings are tightened against glass plates to grip them externally.
- Pouring of the solution: this is carried out at the side where the gasket is open. Then the gasket is positioned back using a knife. To eliminate the bubbles from air, the solution is poured with the help of a cutter and clipper.
- Polymerizing conditions: the moulds containing the monomer solution are placed in the drying oven regulated at 63°C. After 16 hours, the temperature is raised to 125°C and is maintained for 30 minutes. Then it is allowed to be cooled down to room temperature.
- To recover the PMMA sheet, it is enough to lose the external grips of the mould and remove the glass plates.

#### **4.1.2 Scratching apparatus and the indenter**

The scratch apparatus, known as the micro-visio-scratch apparatus, is based on a commercial servomechanism having a small translucent environmental box that contains the sample and the moving tip (Figure 4.1). It is fitted with a built-in microscope allowing in situ examination of the contact area and the groove left on the surface (that is practicable because of the transparency of the tested polymers). Scratch test may be performed over a large range of speeds ( $10^{-3}$  to 15 mm/s) and in a temperature range ( $-60^{\circ}C$  to  $+120^{\circ}C$ ) covering both  $\alpha$  and  $\beta$  transitions of broad-spectrum polymers. The normal load applied to the tip can be varied from 0.05 to 35 N. The control of the moving tip, the recording of the load, the speed of the sliding tip and the temperature are computer driven. The tip starts to move at the lowest value of the velocity (or at the lowest value of normal load in the alternate mode) and accelerates stepwise up to the highest value. At each step, it moves over a distance of at least 1 mm so as to get a groove that can be easily measured and photographed in situ. The input parameters are the normal load, tip geometry, temperature and the sliding speed whereas the output parameters are the tangential force, groove geometry and the true contact area. Sliding and scratching tests are characteristically carried out at mounting normal load at a constant speed for a given temperature. At every loading step, the true



contact area is photographed in situ. This image helps one to find out the shape and width of the contact area and gives information on the width of the groove for a lifetime varying from four times the contact time for a large contact width (plastic contact) to 10 times the contact time for an elastic or visco-elastic contact during sliding phase [18].

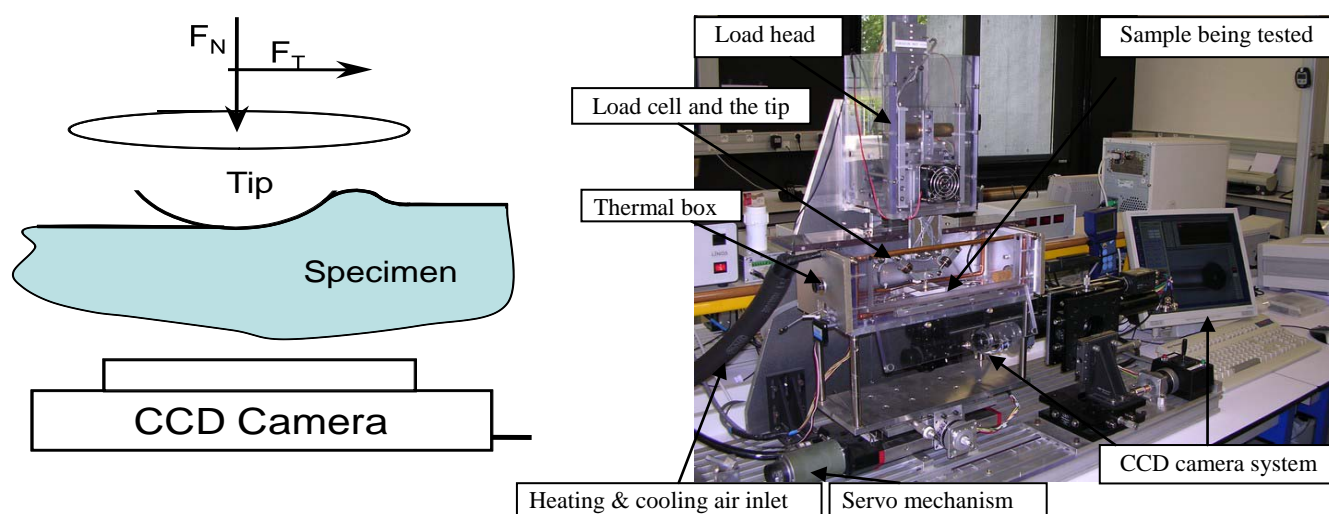


Figure 4.1 A schematic diagram (on the left) and the photograph (on the right) of the scratch apparatus.

All samples were scratched by means of a conical scratcher (tip radius = 116  $\mu\text{m}$  and apex angle =  $60^\circ$ ) with a varying load from 0.05N to about 5N depending upon the test temperature (ranging from  $-40^\circ\text{C}$  to  $85^\circ\text{C}$ ). The scratcher was made of diamond, and the sliding speed was maintained at 0.03 mm/s. A typical procedure as described in detail by S. Lafaye [13] was used to perform the friction tests.

### 4.1.3 Measurement of the surface free energy

There are no direct reliable methods for the measurement of surface free energy of solids [9, 19, 20, 23, 24, 74, 80]. So the indirect method based on contact angle measurements in properly chosen liquid systems has been used. As the indirect method is based on several hypotheses concerning the relationship between the contact angle and the surface energy, the values reported are often different from one to another. The nature of wetting liquid influences the results as well [19, 24]. The measurement of contact angles with different liquids and the calculation of surface energy were carried out at room temperature by using the contact angle measuring apparatus “Digidrop” from GBX, equipped with “Windrop” software for the drop-shape analysis. Three typical liquids (ultra pure water, diiodomethane from Aldrich and pure ethylene glycol from Prolabo) were applied. The liquid drop ( $\sim 2\text{--}3 \mu\text{l}$ ) was placed onto the polymer surface with a precise microsyringe supplied with a steel needle. The drop image was recorded by video camera, and the contact angle on both sides of the drop was read immediately. The drop shape was solved numerically by means of mathematical functions. The measurements were repeated several times by settling other drops on the same plate. Each contact angle is the average value of 10 measurements. The surface free energy ( $\gamma_s$ ) as well its dispersive ( $\gamma_s^d$ ) and polar ( $\gamma_s^p$ ) parts were calculated using the appropriate computer program installed in the same contact angle equipment.

To calculate the surface energy, three well-known equations, i.e. the Owens-Wendt equation, the Wu equation and the van Oss (acid-bas) equation, were used among various equations applicable to the polymers [25]. These three equations along with some others are based

on the Young's equation that describes the contact angle as a result of the force equilibrium between the surface tension in the solid and the liquid surface tension [23, 25]. The basis of the Young's equation is based on expressing the solid-liquid interfacial free energy as a function of the surface free energies of a solid and a liquid. The interfacial free energy is always lower than the sum of the surface free energies of the contacting phases, which are caused by the existence of various kinds of intermolecular interactions across an interface [23, 80]. The Young's equation is given as [21, 23, 24, 74, 80-82]:

$$\gamma_s - \gamma_{SL} = \gamma_L \cos \theta \quad 4.1$$

where  $\gamma_s$  is the solid surface free energy,  $\gamma_L$  is the liquid surface free energy,  $\theta$  is the contact angle and  $\gamma_{SL}$  is the interfacial free energy of solid-liquid system. The value of surface energy calculated from three equations for pure PMMA is almost the same and is in well agreement with the value quoted in the literature [9, 20, 22-26, 74, 80].

#### 4.1.4 Measurement of the bulk properties

The specimens with different levels of plasticizer content were tested using Instron Uniaxial Tensile Testing Machine, model 4500 (Figure 4.2) with capacity of 10 KN and ram velocity ranging from  $10^{-3}$  mm/s to 10.0 mm/s. The samples may be tested from  $-70^\circ\text{C}$  to  $150^\circ\text{C}$  and the machine is provided with two load cells of 10 KN and 200 N. The samples may be experimented for traction, compression, shear, bending/flexion, relaxation, mechanical spectrometry and dynamic mechanical analysis (DMA) from 0.002 Hz to 5 Hz. The main objectives of the tests are to obtain the values of Young's modulus, loss modulus, loss factor, Poisson ratio, compression yield stress and strain, nominal and shear stress and strain at break and the relation of these values versus different plasticizer contents in PMMA.



Figure 4.2 The photograph of the Instron Universal Testing Machine model 4500.

#### 4.1.5 Nano-indentation apparatus

The different specimens were also tested using Ultra Nano Hardness Tester (UNHT), manufactured by CSM Instruments (Switzerland), with capacity of 30  $\mu\text{N}$  to 100 mN having a load resolution of 5  $\mu\text{N}$  (Figure 4.3). The nano scratch test may be performed at sliding/scratching velocity ranging from  $10^{-3}$  mm/s to 3 mm/s. It has maximum depth limit of 50  $\mu\text{m}$  with a depth resolution of 1 nm. Berkovich and spherical indenter of radius 2 or 22  $\mu\text{m}$  may be used. It is provided with three loading capacities of 1N, 10 mN and 100 mN for nano scratching whereas with one loading capacity of 100 mN for nano indentation. It is also facilitated with AFM and in situ video system. The samples can be tested at a wide range of temperature varying from  $-50^\circ\text{C}$  to

120°C and from 0.01 mbar to atmospheric pressure. The humidity may be varied from 0 to 80%. The main objectives of the tests are to obtain the values of Young's modulus, hardness and elastic recovery at different levels of depth, and the relation of these values versus different plasticizer contents in PMMA.

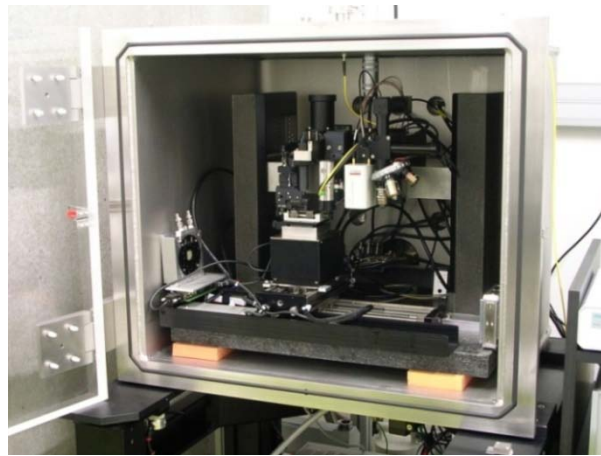


Figure 4.3 The photograph of the Nano indentation/scratch apparatus.

## 4.2 Experimental results and discussion

### 4.2.1 Comparative study of the effect of Crodamide and PEG

#### 4.2.1.1 Effect on surface properties

##### 4.2.1.1.1 Friction coefficient

The experimental results indicate that the Crodamide is more effective than PEG in reducing the friction coefficient of PMMA (Figure 4.4 and Figure 4.5). The friction coefficient decreases with increasing Crodamide content. On the other hand, in case of PEG, the coefficient of friction decreases initially on introduction of PEG (up to 1%) but no additional reduction in the friction coefficient is observed on further addition of PEG. Moreover, at higher temperature, no any significant effect of addition of PEG on the reduction of the friction coefficient of PMMA is noticed. Due to higher molecular weight of PEG, it is difficult to be migrated to the surface and form a film lowering the friction coefficient (as is done by Crodamide). The values of bulk properties like Young's modulus of the two cases (as shown in section 4.2.2.2) also support this consideration.

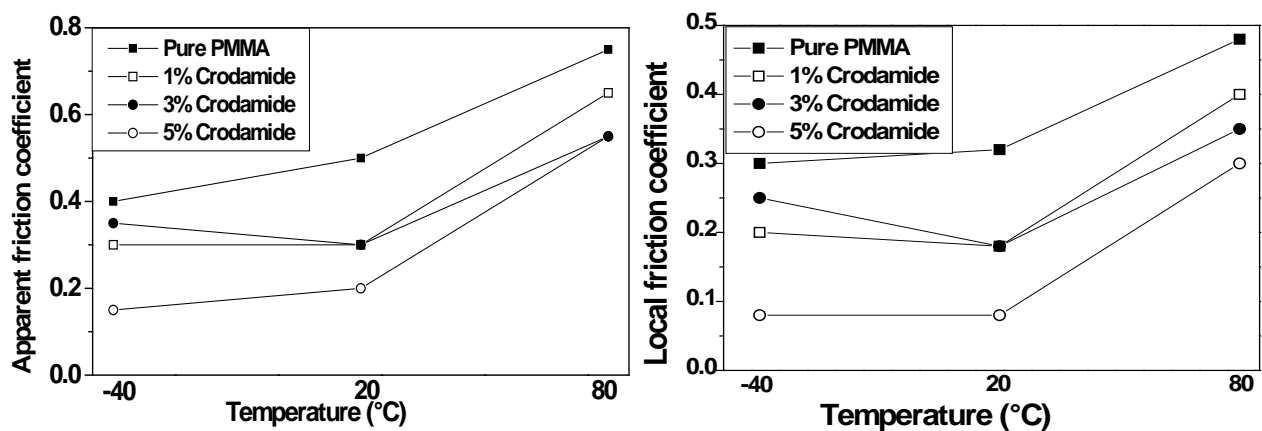


Figure 4.4 Effect of Crodamide on apparent (on the left) and on local friction coefficient (on the right) of PMMA at -40°C, 20°C and 80°C (sliding speed = 0.03 mm/s, tip radius = 116  $\mu$ m, normal load = 1N).

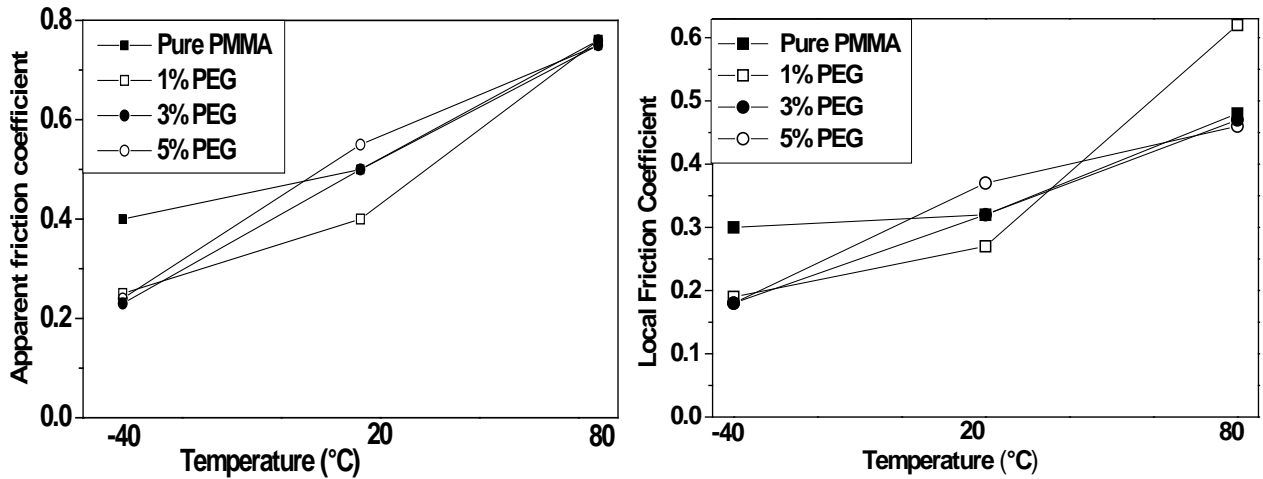


Figure 4.5 Effect of PEG on apparent (on the left) and on local friction coefficient (on the right) of PMMA at -40°C, 20°C and 80°C (sliding speed = 0.03 mm/s, tip radius = 116 μm, normal load = 1N).

#### 4.2.1.1.2 Effect of physical ageing on friction coefficient of Crodamide-plasticized PMMA samples

No any considerable effect of physical ageing at room temperature was observed on the friction coefficient of pure PMMA (Figure 4.6 and Figure 4.7 ). This is in good agreement with the work of E. Charrault et al., [66] who showed that the ageing merely at higher temperature affects the friction coefficient of pure PMMA. However, it is interesting to note that ageing of Crodamide plasticized PMMA even at room temperature affects the friction coefficient a lot. The advantage of reduced friction coefficient by the introduction of Crodamide is disappeared by the physical ageing even at room temperature. This is probably due to the vaporization of fatty acid amides with time.

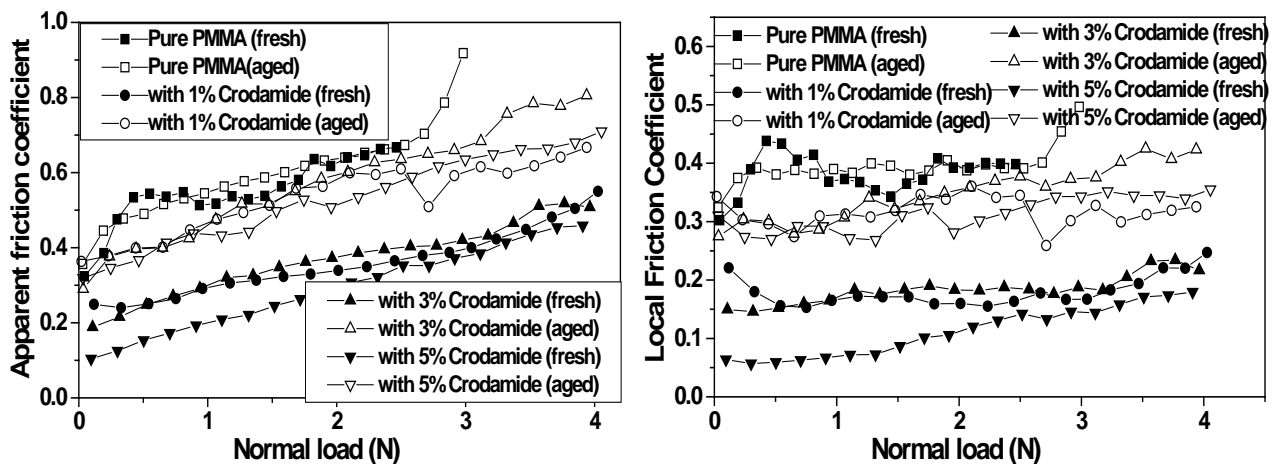


Figure 4.6 Effect of physical ageing for 2 years at room temperature on apparent (on the left) and on local friction coefficients (on the right) of Crodamide-plasticized PMMA samples measured at room temperature. (sliding speed = 0.03 mm/s, tip radius = 116 μm)

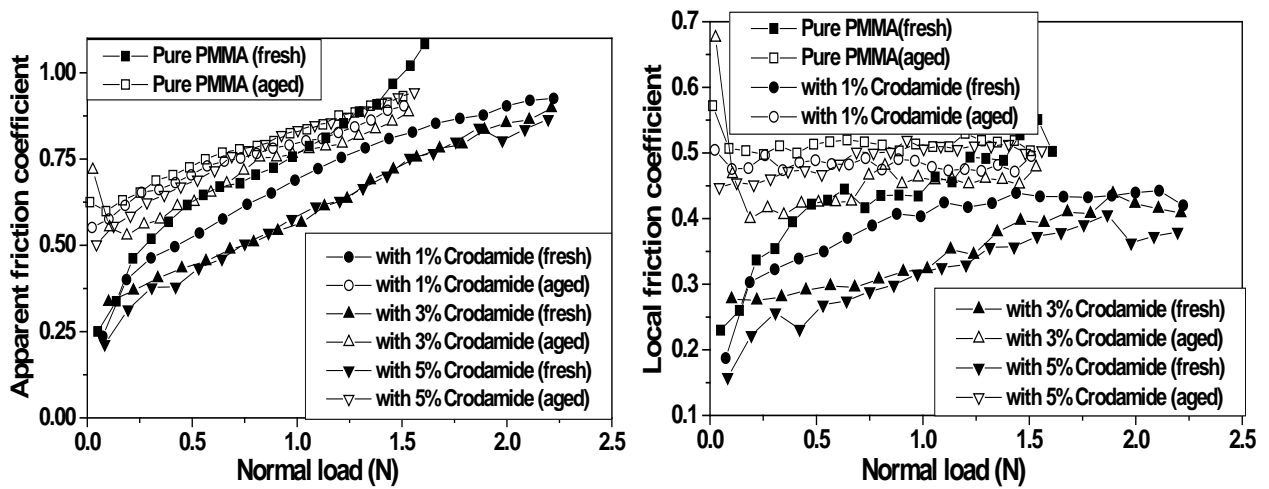


Figure 4.7 Effect of physical ageing for 2 years at room temperature on apparent (on the left) and on the local friction coefficient (on the right) of Crodamide-plasticized PMMA samples measured at 85°C. (sliding speed = 0.03 mm/s, tip radius = 116  $\mu\text{m}$ )

#### 4.2.1.1.3 Effect of a heating cycle on friction coefficient

The effect of a heating cycle at 80°C for half an hour on surface behavior was also studied. It is interesting to note that Crodamide and PEG plasticized PMMA displayed entirely two different behaviors after having a heating cycle. Heating treatment affects the friction coefficient of Crodamide plasticized samples adversely i.e. the friction coefficient of PMMA containing Crodamide has been increased by the heating cycle (Figure 4.8). It may be due to the evaporation of small fatty acid molecules. This is in contrast to the PEG plasticized PMMA where heating treatment reduced the friction coefficient.

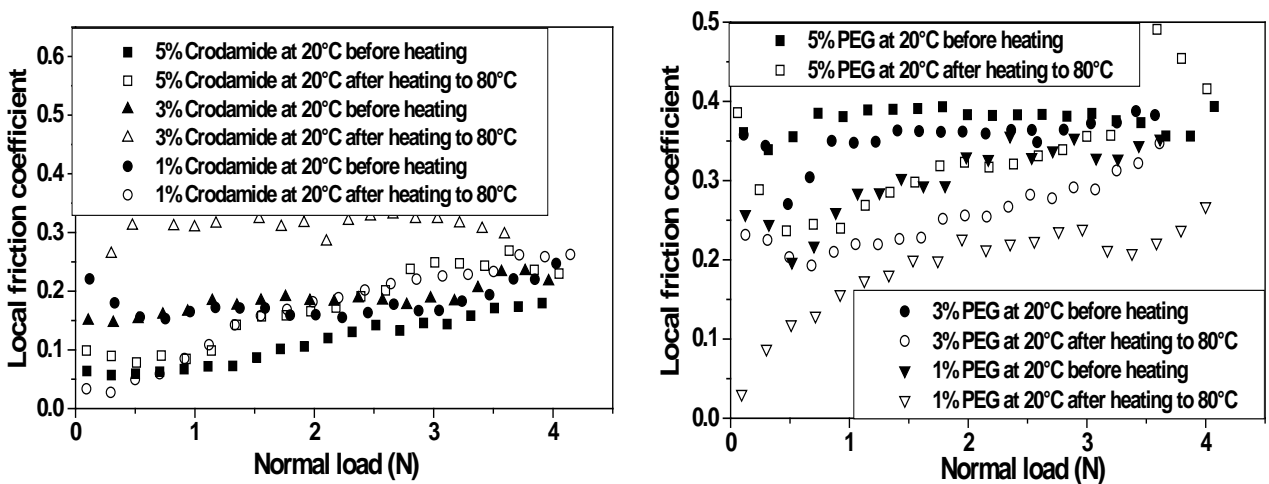


Figure 4.8 Effect of heating cycle at 80°C for 30 minutes on local friction coefficient of Crodamide (on the left) and of PEG (on the right) plasticized samples of PMMA measured at room temperature. (sliding speed = 0.03 mm/s, tip radius = 116  $\mu\text{m}$ )

#### 4.2.1.1.4 Rear contact angle ( $\Omega$ ) during scratching

As discussed in chapter 2, the rear contact angle ( $\Omega$ ) is the indicator of the nature of the contact between the sliding tip and the polymer surface. It is evident from the experimental results that the introduction of Crodamide in PMMA modifies the nature of the contact and enhances the

visco-elasticity in the contact. This is reflected well in the value of rear contact angle and in the in situ photograph of the contact. If we see, for example, the values of rear contact angle for the samples containing different percentages of Crodamide at room temperature (Figure 4.9), it can be seen that at same value of contact strain (0.22), the value of omega is changed significantly by the introduction of Crodamide. It is about 0.4 radian for pure PMMA (having higher value of friction coefficient) that increases to about 0.9 radian for Crodamide –plasticized PMMA (having a lower friction coefficient). So it can be concluded that the decrease in friction coefficient is associated with the increased value of the rear contact angle and ultimately with the nature of the contact. In situ photographs of the contact demonstrate that the contact nature is plastic for pure PMMA at contact strain about 0.22. On the other hand, it is viscoelastic for Crodamide-plasticized samples at the same value of contact strain (Figure 4.9). Similar behaviour was observed at low and high temperatures (Figure 4.10).

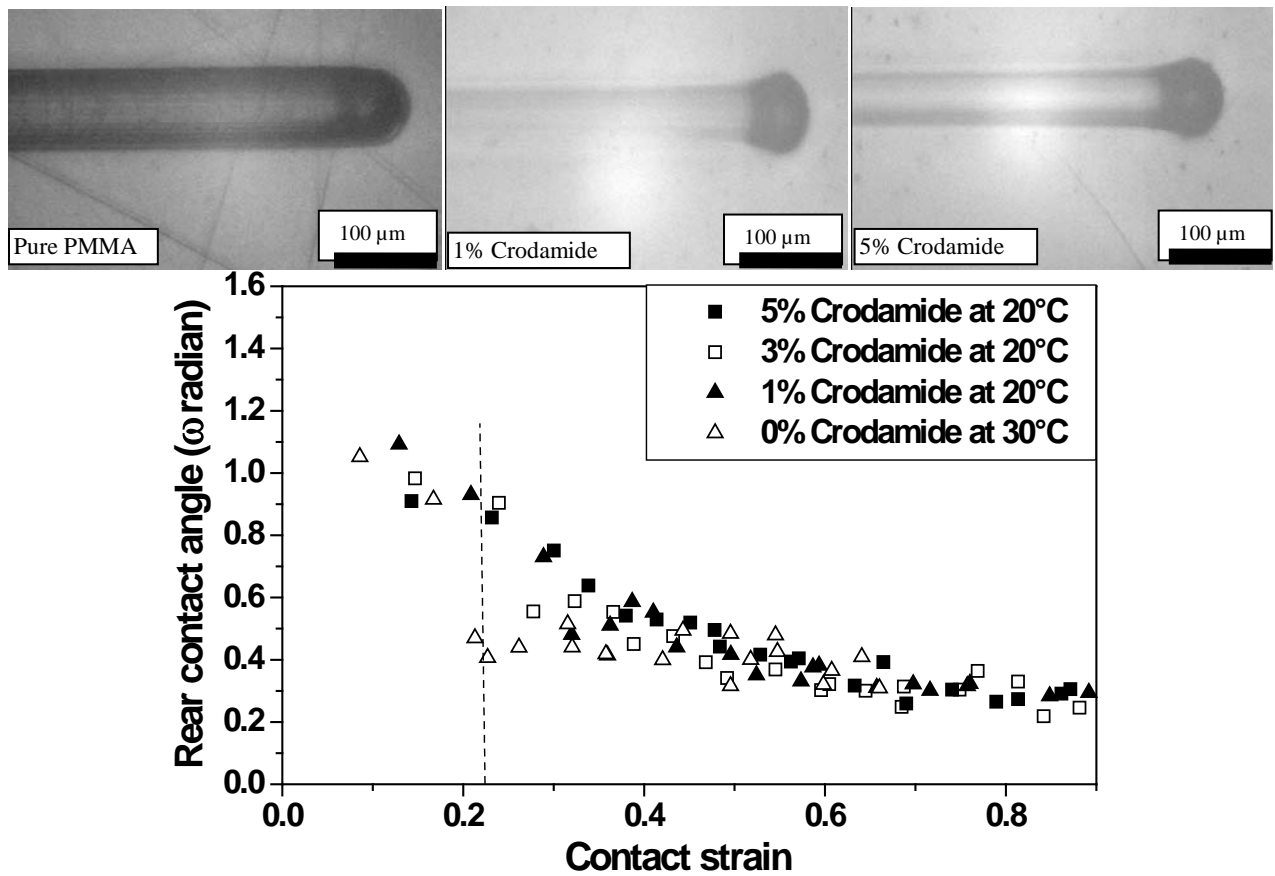


Figure 4.9 Variation of Omega (radian) with contact strain (defined by the ratio  $\frac{a}{\sqrt{R^2 - a^2}}$ , where a is the mean contact radius and R is the tip radius) for various percentages of Crodamide in PMMA at room temperature (sliding/scratching speed = 0.03 mm/s, tip radius = 116 μm). (Only some selected images concerning to the contact strain = 0.22 are shown).

It is interesting to note that at the same conditions of temperature and contact strain (0.22), the nature of contact for PEG plasticized samples of PMMA is similar to that of pure PMMA, i.e. almost plastic (Figure 4.11). The values of the rear contact angle for PEG plasticized samples also remain almost same as that of pure PMMA for a given value of contact strain. The little decrease in friction coefficient for the sample containing 1% PEG is also reflected well in the nature of contact as is clear from the in situ photograph. The value of rear contact angle is also increased a little bit correspondingly for the sample containing 1% PEG. The variation of rear contact angle by PEG at

low and high temperatures is shown in Figure 4.12. It is important to note that at low and moderate temperatures, the contact is purely elastic for all samples at very low contact strains (up to the mean contact strain  $\leq 0.1$ ) and is purely plastic at very high values of contact strain ( $\geq 0.7$ ) as is clear from Figure 4.9 to Figure 4.12. It is clear that at moderate contact strains (about 0.1 to 0.7); the nature of the contact is elastic plastic at low and moderate temperatures.

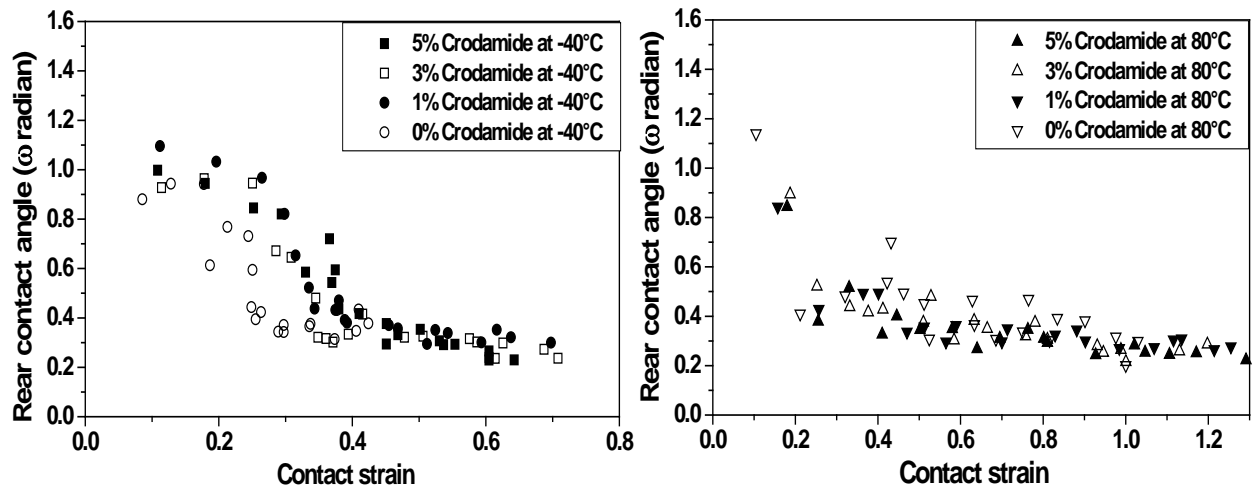


Figure 4.10 Variation of Omega (radian) with contact strain for various percentages of Crodamide in PMMA at low (on the left) and at high (on the right) temperatures (sliding/scratching speed = 0.03 mm/s, tip radius = 116  $\mu\text{m}$ ).

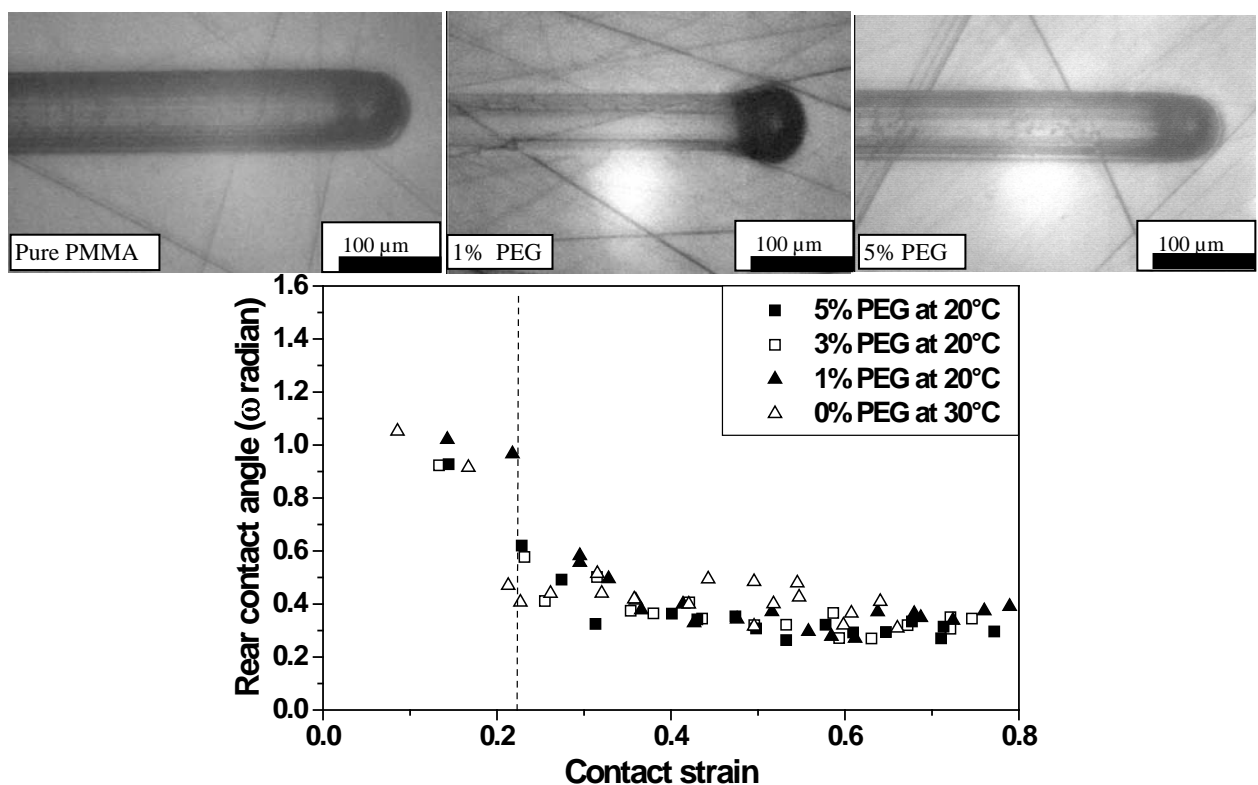


Figure 4.11 Variation of Omega (radian) with contact strain for various percentages of PEG in PMMA at room temperature (sliding/scratching speed = 0.03 mm/s, tip radius = 116  $\mu\text{m}$ ). (Only some selected images concerning to the contact strain = 0.22 are shown).



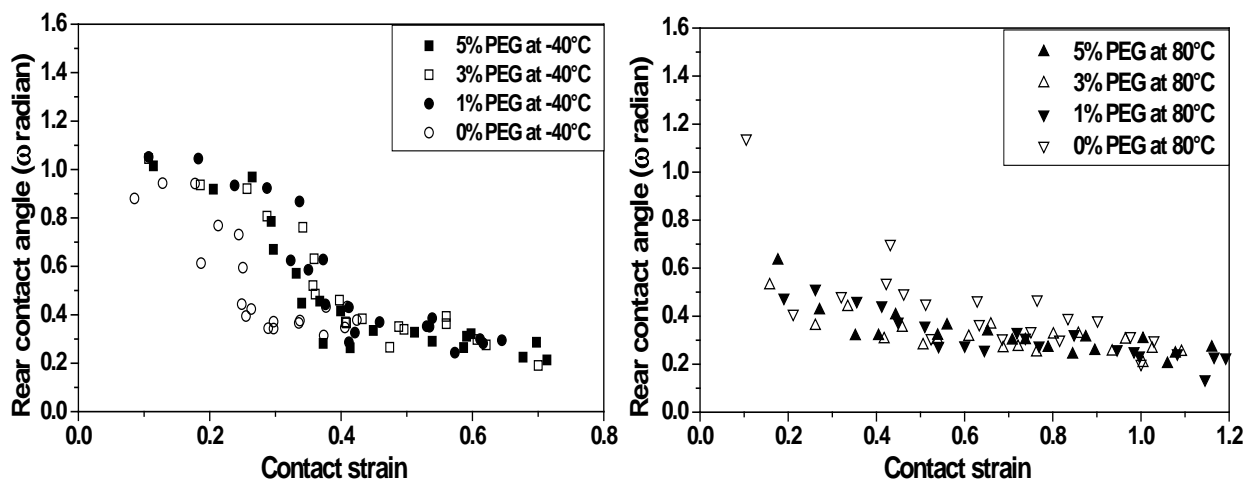


Figure 4.12 Variation of Omega (radian) with contact strain for various percentages of PEG in PMMA at low (on the left) and at high (on the right) temperatures (sliding/scratching speed = 0.03 mm/s, tip radius = 116  $\mu$ m).

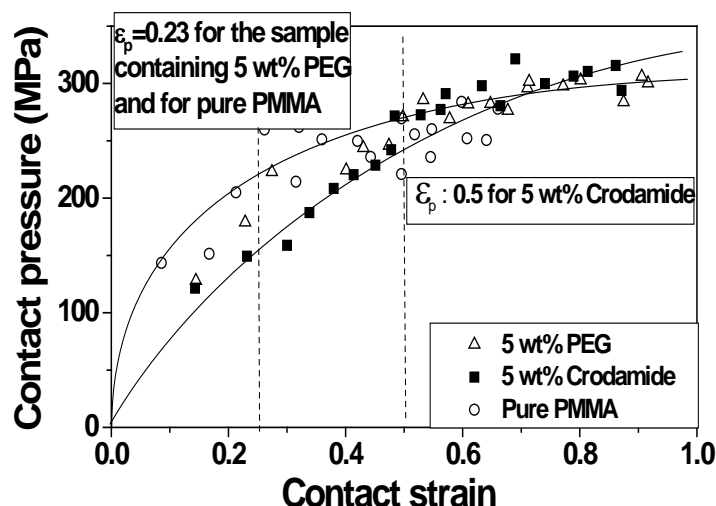


Figure 4.13 Variation of the contact pressure with contact strain for three different samples of PMMA at room temperature displaying also the scratch behavior (sliding/scratching speed = 0.03 mm/s, tip radius = 116  $\mu$ m).

We know that the slope of contact pressure-strain curve during elastic and visco-elastic region of polymers is a function of both the Young's modulus and the friction coefficient [17]. Experimental results indicate that this slope is almost same for the samples showing higher friction coefficient like pure PMMA and the sample containing 5wt % PEG; whereas it is changed significantly for the samples showing lower friction coefficient like the sample containing 5 wt% Crodamide (Figure 4.13). As the friction coefficient is almost same for the pure PMMA as well as for the sample containing 5 wt% PEG, one may expect that the bulk properties like Young's modulus also do not change significantly by the introduction of PEG. However, one cannot conclude it clearly for the Young's modulus of the samples containing Crodamide. Figure 4.13 also indicates evidently that the yielding stress remains almost same for all the samples (as the contact pressure at higher contact strains becomes almost constant for all samples and we know that the contact pressure is identical to twice the yield stress during scratching) whereas the yielding strain (at which elastic sliding changes to plastic scratch) is changed significantly for the sample showing



lower friction coefficient. It is about 0.23 for the pure PMMA as well as for the sample containing 5 wt% PEG (both showing higher friction coefficient) whereas it is increased to about 0.5 for the sample containing 5 wt% Crodamide (displaying a lower friction coefficient). These findings are also confirmed by measuring the bulk properties like Young's modulus and yield stress and strain and are discussed in section 4.2.1.2.

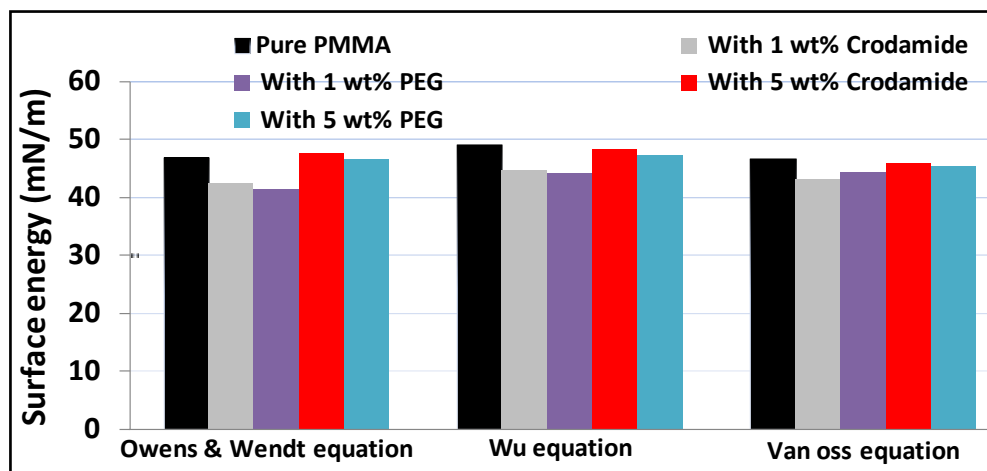


Figure 4.14 The effect of Crodamide and PEG on surface free energy of PMMA at 20°C.

#### 4.2.1.1.5 Surface free energy

The surface free energy was calculated only for pure PMMA, the samples containing 1 wt% and 5 wt% of Crodamide as well as the samples having 1 wt% and 5 wt% of PEG. The values of surface energy calculated from three equations for pure PMMA are almost the same and are in well agreement with the literature values [20, 23, 25, 26, 74, 80, 83]. The experimental results show almost the same surface energy for the plasticized samples showing a reduced friction coefficient as well as for the pure PMMA (Figure 4.14). This is in well agreement with the findings of B. Podgornik et al. [84] showing also that the surface energy data may not be related with tribology performance of the lubricated surfaces although the changes in surface morphology certainly changes the surface energy. Moreover, the investigations regarding nano-scale lubricated contacts made by H. Berro et al. [85] also showed that the friction coefficient increases initially with increasing surface energy for low values ( $\mu \leq 0.09$ ) but for higher friction values, the effect of increasing surface energy on friction becomes negligible. On the other hand, it is in contrast to the work of M. Minn et al. [21] which shows that the friction coefficient and surface energy are directly proportional to each other. However, they concluded it by studying the changes in surface energy in conjunction with the corresponding changes in friction coefficient brought about by using coatings and by air plasma treatment. So, it can be said that the friction between two solid bodies depends upon a number of factors like their surface energies, their surface roughness as stated by Tabor [86] and on the mechanical behavior of the contact. It is well established that the local friction coefficient is equal to the adhesive friction for a completely smooth and elastic contact. But for a rough surface, the local friction will not be equal to the actual adhesive friction. In this case, local friction will be higher than real adhesive friction resulting in an increased yielding rate. However, an appropriate plasticizer can decrease the friction coefficient by decreasing the roughness of a rough material resulting in a more smooth and elastic surface. In this case, local friction will become equal to the adhesive friction resulting in a decreased yielding rate. It can be believed that fatty acid amides reduce the friction coefficient either by decreasing the roughness or by changing the mechanical behavior of the surface/contact, resulting in change of

nature of the contact and the mechanical behavior of the contact cannot be said to be modified by altering the surface energy of PMMA.

#### 4.2.1.2 Effect on bulk mechanical properties

##### 4.2.1.2.1 Elastic modulus

Elastic modulus displays a principal part in the scratch process, particularly during the indentation stage. It is well known that the Young's modulus, scratching tip geometry, and Poisson's ratio directly decide the range of the contact zone during scratch at a given temperature. For polymers with lower modulus, the dimension of the contact zone increases a lot with decreasing modulus. However, for polymers with higher Young's modulus, the effect of a small change in the Young's modulus on the size of the contact zone becomes immaterial.

The penetration depth is more responsive to the modulus when it is inferior to 1 GPa. A certain level of stiffness in polymers can assist to maintain a low scratch depth if the polymer is inclined to plastic flow scratch damage. The maximum tensile stress is on the surface immediately at the rear of the scratcher during scratch. It is clear that polymers with higher moduli demonstrate a higher maximum tensile stress on the surface, resulting in the development of surface cracks, crazes, cavitations, and debonding between phases of multiphase polymers. In this case, it is preferable to lower the modulus or enhance the ductility of the polymer [6].

As the percentage content of plasticizer in all cases is not so high, their consequence on the mechanical properties is not up to significant value (Figure 4.15 to Figure 4.18). The results shown correspond to experiments at 0.05 Hz and the experiments at 0.5 Hz and at 5 Hz showed similar trend. Both Crodamide and PEG have no remarkable effect on major bulk properties like Young's modulus. However, PEG disturbs these properties a little bit more than that by Crodamide. This difference of bulk behaviour can be attributed to the enhanced tendency of migration of Crodamide from bulk to the surface of the material as is discussed in section 4.2.1.1.1. Due to higher molecular weight of PEG, it migrates a little to the surface and mainly remains inside the bulk of material and hence disturbs the bulk behaviour more pronouncedly as compared to the Crodamide.

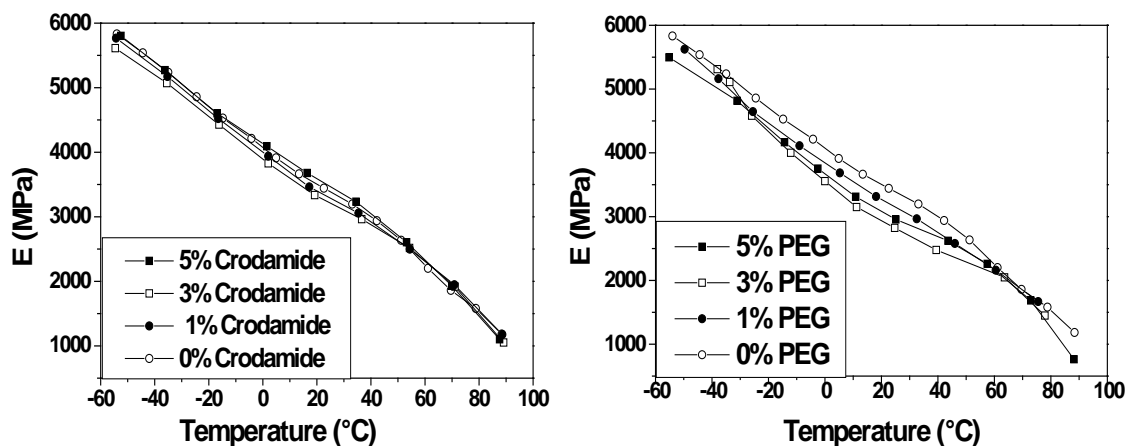


Figure 4.15 Effect of Crodamide (on the left) and of PEG (on the right) on Young's modulus (E) of PMMA.

It is significant to note that the loss modulus, loss factor and Poisson ration have been increased to some extent by the introduction of both plasticisers and this effect is more pronounced in case of Crodamide (Figure 4.16 to Figure 4.18).

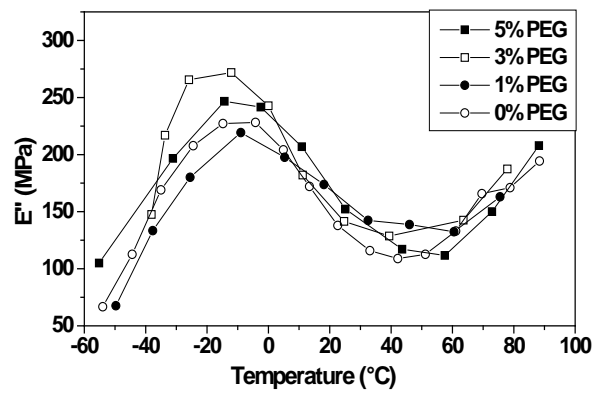
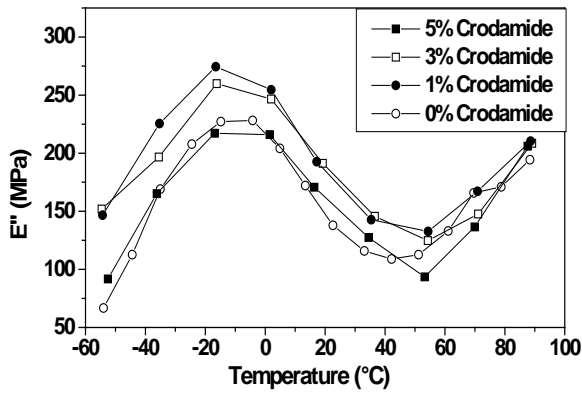


Figure 4.16 Effect of Crodamide (on the left) and of PEG (on the right) on loss modulus ( $E''$ ) of PMMA.

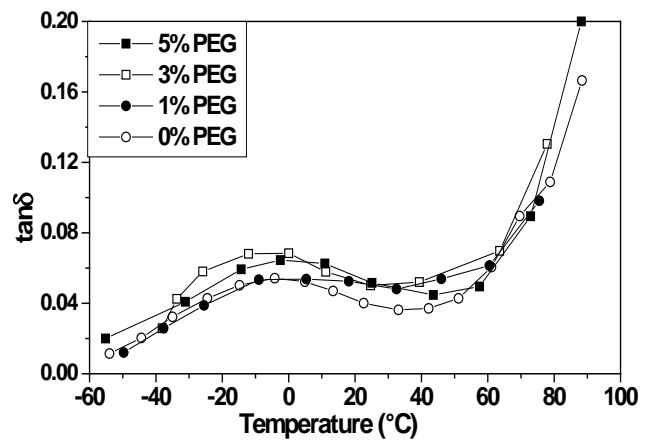
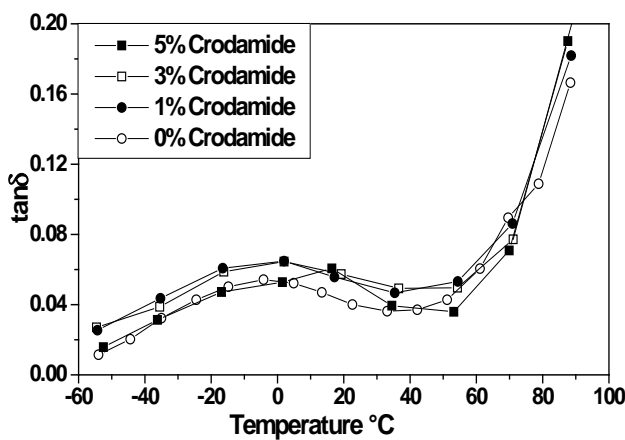


Figure 4.17 Effect of Crodamide (on the left) and of PEG (on the right) on loss factor ( $\tan \delta$ ) of PMMA.

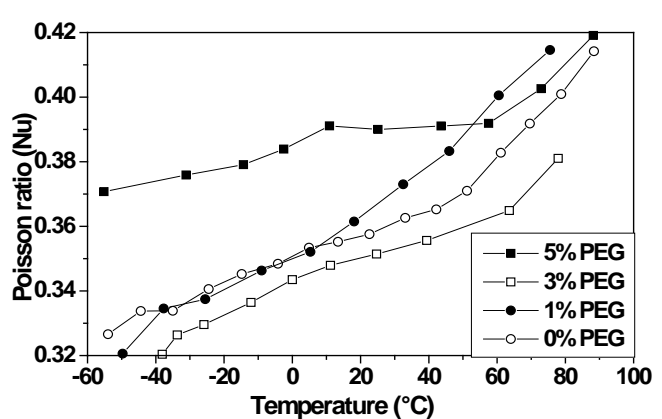
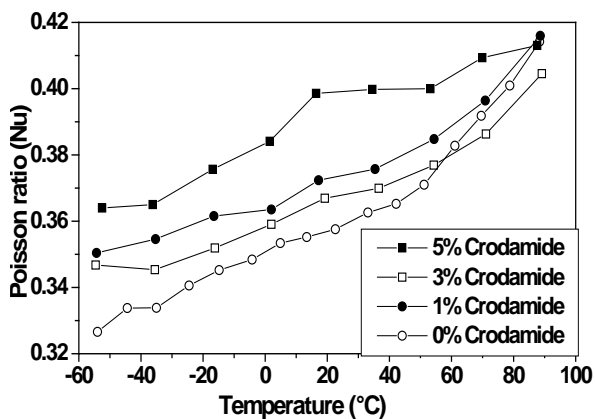


Figure 4.18 Effect of Crodamide (on the left) and of PEG (on the right) on Poisson ratio (Nu) of PMMA.

The effect of reversing the heating order during the measurement of bulk properties was also studied. An expected small decrease in bulk properties was observed in case of going from high to low temperature during test as is clear from Figure 4.19 to Figure 4.22 and that was more pronounced in case of Young's modulus as well as in case of the Poisson ratio (Figure 4.19 and Figure 4.22). The results shown correspond to experiments at 0.5 Hz and the experiments at 0.05 Hz and at 5 Hz showed similar trend.

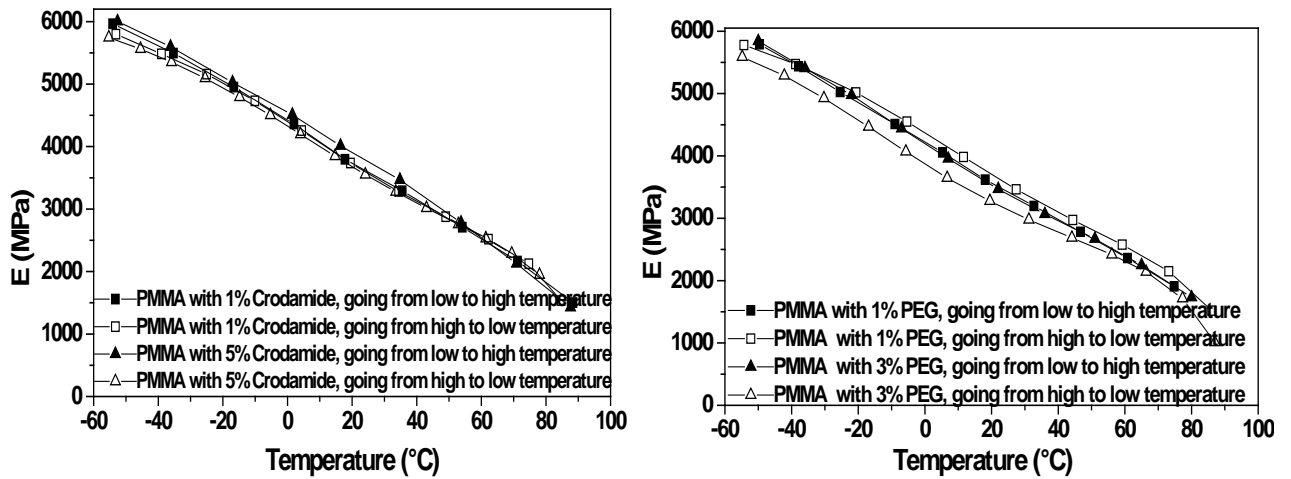


Figure 4.19 Effect of changing the heating order on Young's modulus ( $E$ ) of PMMA containing Crodamide (on the left) and PEG (on the right).

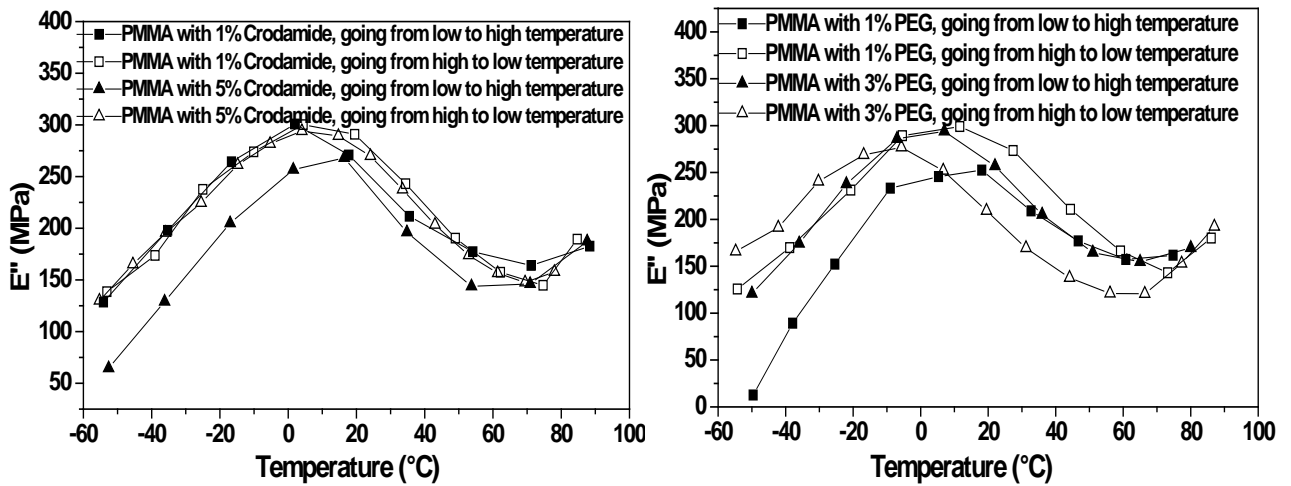


Figure 4.20 Effect of changing the heating order on loss modulus ( $E''$ ) of PMMA containing Crodamide (on the left) and PEG (on the right).

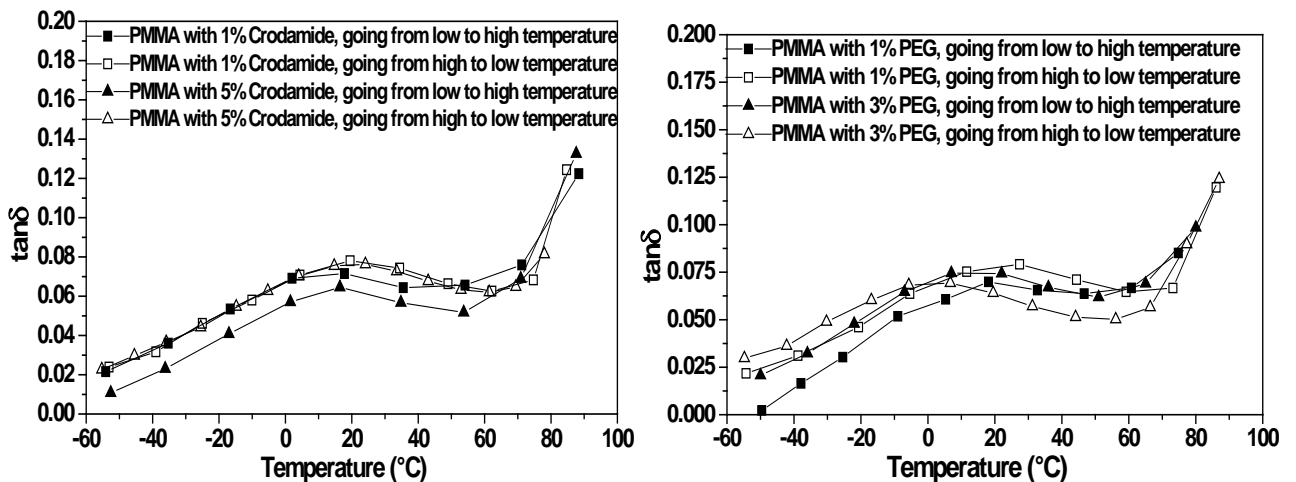


Figure 4.21 Effect of changing the heating order on loss factor ( $\tan \delta$ ) of PMMA containing Crodamide (on the left) and PEG (on the right).

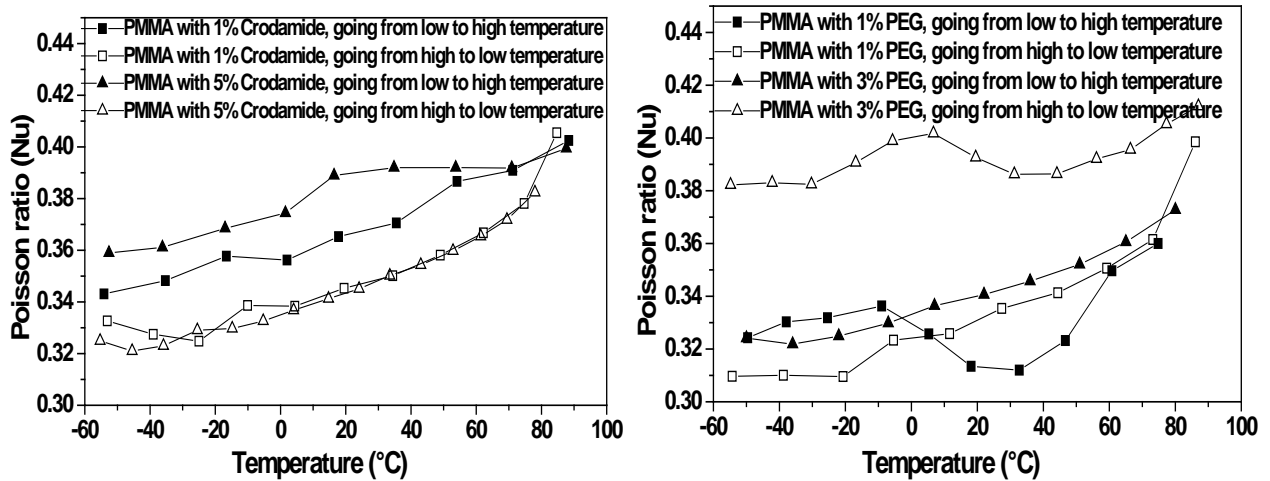


Figure 4.22 Effect of changing the heating order on Poisson ratio (Nu) of PMMA containing Crodamide (on the left) and PEG (on the right).

#### 4.2.1.2.2 Yield stress and yield strain

The yield stress plays a prime role to determine the upper boundary of the mean contact pressure and the size of the plastic zone. Polymers having an elevated yield stress are subjected to smaller plastic flow scratch damage. On the other hand, cracks are generally generated on the scratch surface if the utmost tensile stress on the surface exceeds the tensile strength and if the tensile strength is lesser than the yield stress of the polymer. Therefore, the tensile strength and the yield stress of the polymer play a key role in determining the growth of either the plastic flow scratch pattern or the brittle fracture scratch pattern on the scratch surface [6].

The effect of Crodamide and PEG on the yield stress and yield strain is not very clear. Generally speaking, there is no any considerable change observed in the yield stress and yield strain of PMMA as a consequence of both plasticizers (Figure 4.23 and Figure 4.24). This confirms the prediction that was based on the data obtained from the micro visio scratch apparatus as discussed in section 4.2.1.1.4. The results shown correspond to experiments at compression strain rate =  $10^{-3} \text{ s}^{-1}$ . The experiments at compression strain rate =  $10^{-1} \text{ s}^{-1}$  and at compression strain rate =  $10^{-2} \text{ s}^{-1}$  showed similar trend.

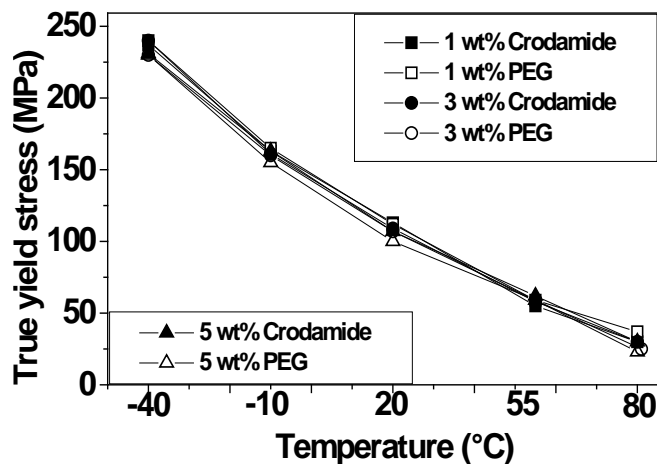


Figure 4.23 Effect of Crodamide and PEG on yield stress of PMMA at different temperatures.

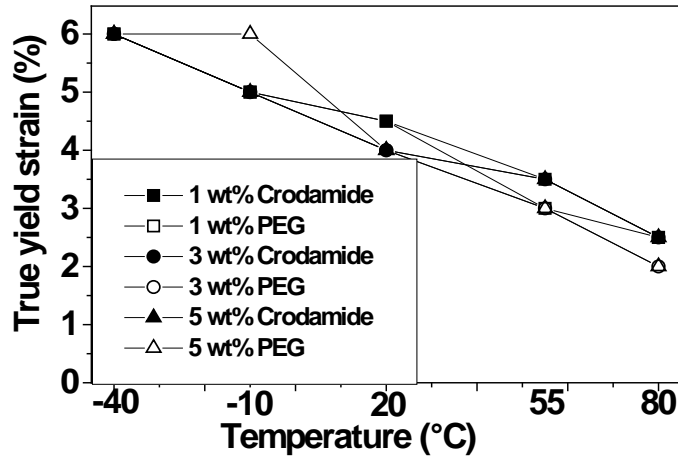


Figure 4.24 Effect of Crodamide and PEG on yield strain of PMMA at different temperatures.

It is remarkable to note that if we see the scratch limiting contact strain (at which the elastic sliding converts to plastic scratching) calculated from the rear contact angle values (the value of contact strain at which the value of rear contact angle becomes almost constant), there is a significant increase in scratch limiting contact strain (at low and moderate temperatures) for the cases showing decreased friction coefficient (samples containing Crodamide and the sample containing 1wt% PEG) as shown in Figure 4.25. So it can be confirmed that the decrease in friction coefficient is associated with the modification of the nature of the contact and that the elastic sliding is promoted by increasing the value of yielding strain at the contact.

As is seen in section 4.2.1.2, there is no any considerable change found in the bulk properties like Young modulus, yield stress and yield strain caused by Crodamide whereas a considerable reduction in friction coefficient is observed. At the same time, we notice that the yielding strain at the contact for the Crodamide-plasticized samples is increased notably (Figure 4.14 to Figure 4.25). So, it can be said that the decrease the friction coefficient is brought about by modifying the nature of the contact and this is achieved by renovating the mechanical behavior of the PMMA over a very small area close to the surface (the area in which contact lies) ensuing in a more elastic contact. This modification of mechanical behavior over a small area close to the surface may not be attributed due to change in surface free energy as discussed in section 4.2.1.1.5.

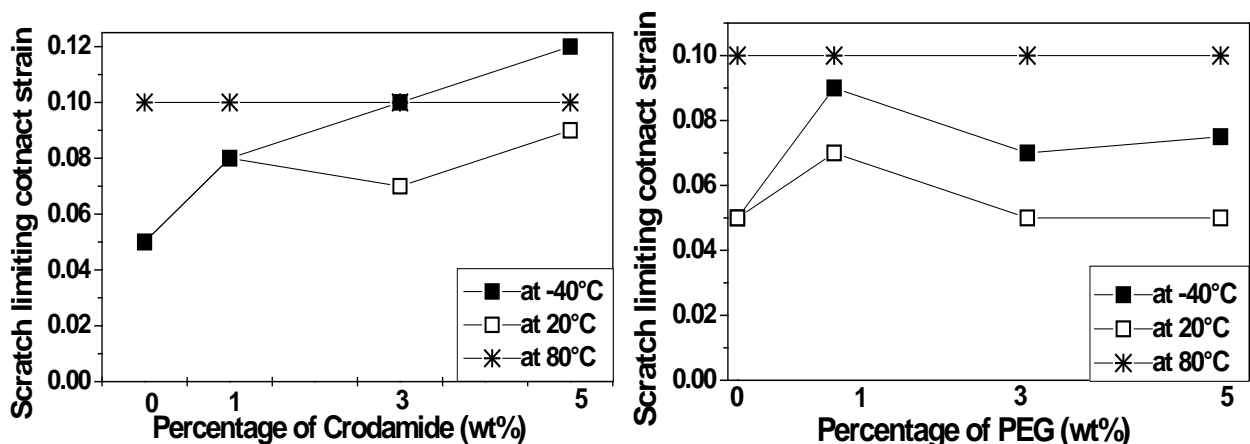


Figure 4.25 Effect of Crodamide (on the left) and of PEG (on the right) on scratch limiting contact strain of PMMA at different temperatures (tip radius = 116  $\mu\text{m}$ , sliding speed = 0.03 mm/s).

### 4.2.1.2.3 Nominal and shear stress and strain at break

The effect of both Crodamide and PEG on nominal stress and nominal strain at break for PMMA is also not very clear. Generally speaking, both increase these values a little bit and this is more pronounced in case of PEG (Figure 4.26 to Figure 4.28). However, at low temperature, Crodamide first decreases the nominal stress and strain at break of PMMA but further increase in its content again increases the nominal stress and strain values of PMMA. Similarly the effect of both Crodamide and PEG on shear stress and shear strain at breakage for PMMA is not very clear (Figure 4.29 to Figure 4.31). Generally speaking, shear stress and strain at breakage are affected a little by both the Crodamide and PEG. The results shown correspond to experiments at traction strain rate =  $10^{-3} \text{ s}^{-1}$ . The experiments at traction strain rate =  $10^{-1} \text{ s}^{-1}$  and at traction strain rate =  $10^{-2} \text{ s}^{-1}$  showed similar trend. Moreover, the values at  $80^\circ\text{C}$  correspond to the point at which nominal/shear stress becomes constant as the sample was not broken for given set of parameters.

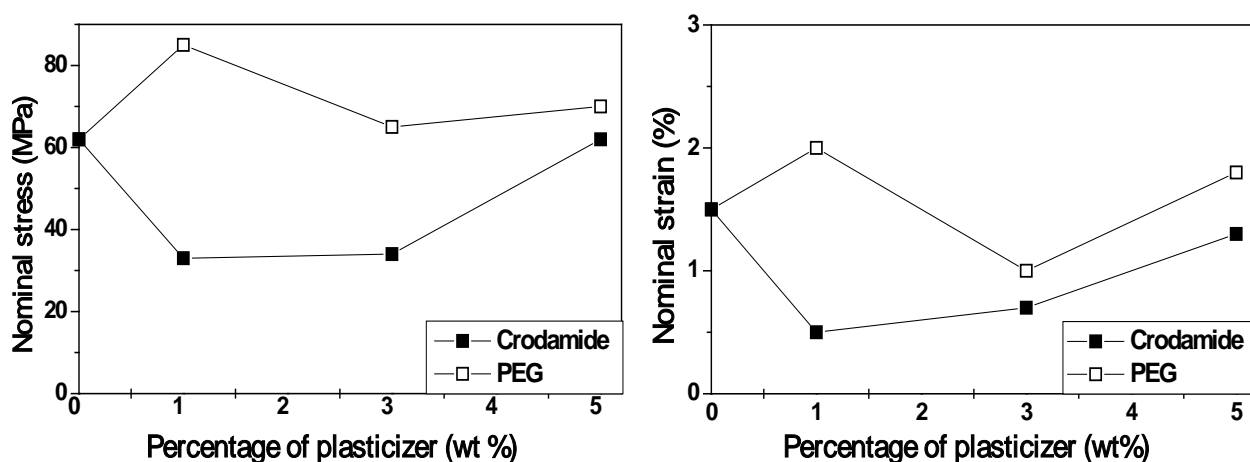


Figure 4.26 Effect of Crodamide and PEG on nominal stress (on the left) and on nominal strain at break (on the right) of PMMA at  $-40^\circ\text{C}$ .

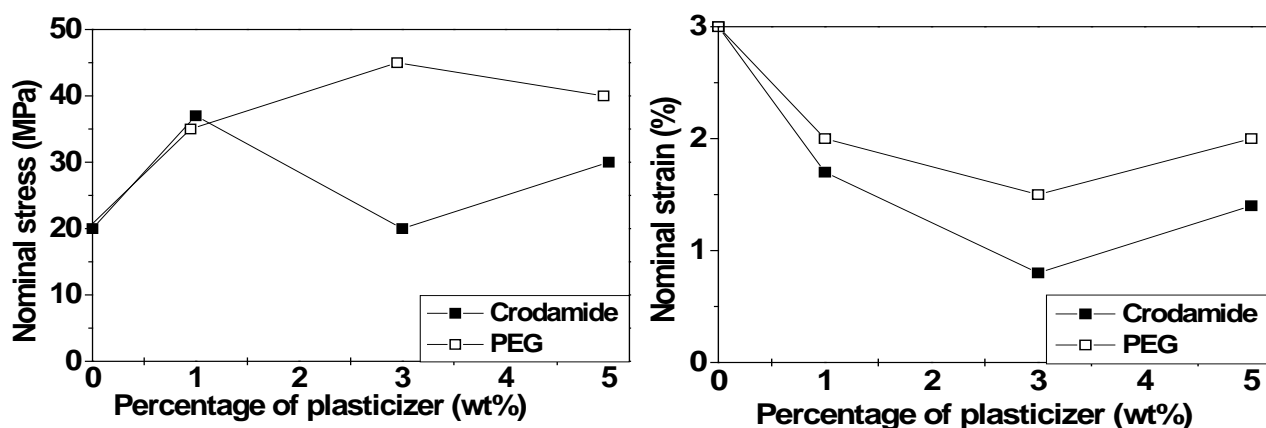


Figure 4.27 Effect of Crodamide and PEG on nominal stress (on the left) and on nominal strain at break (on the right) of PMMA at  $40^\circ\text{C}$ .

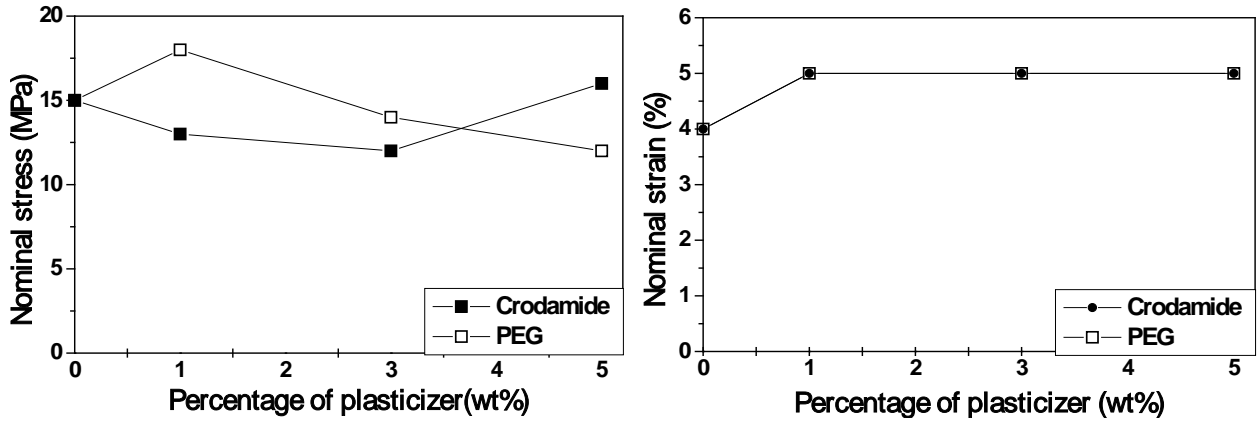


Figure 4.28 Effect of Crodamide and PEG on nominal stress (on the left) and on nominal strain at break (on the right) of PMMA at 80°C.

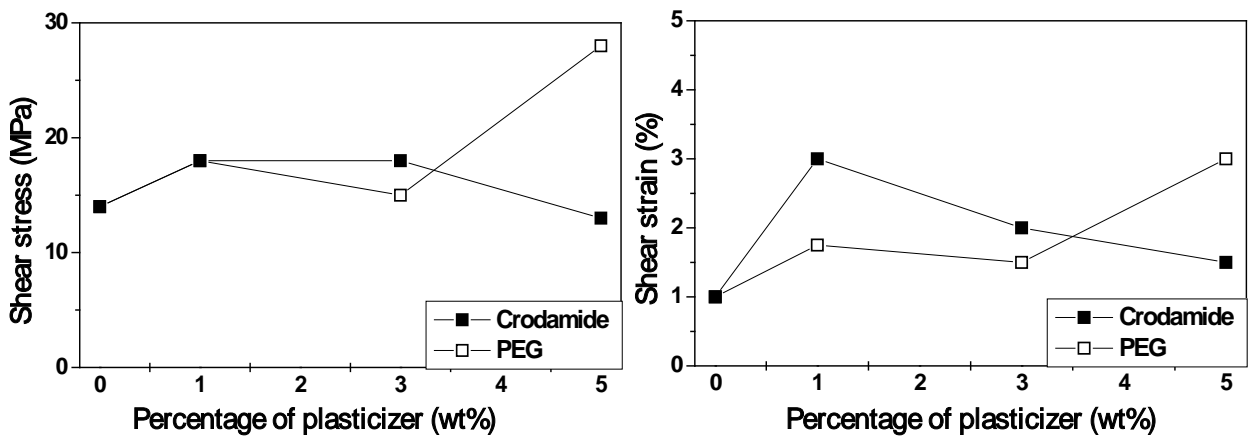


Figure 4.29 Effect of Crodamide and PEG on shear stress (on the left) and on shear strain at break (on the right) of PMMA at -40°C.

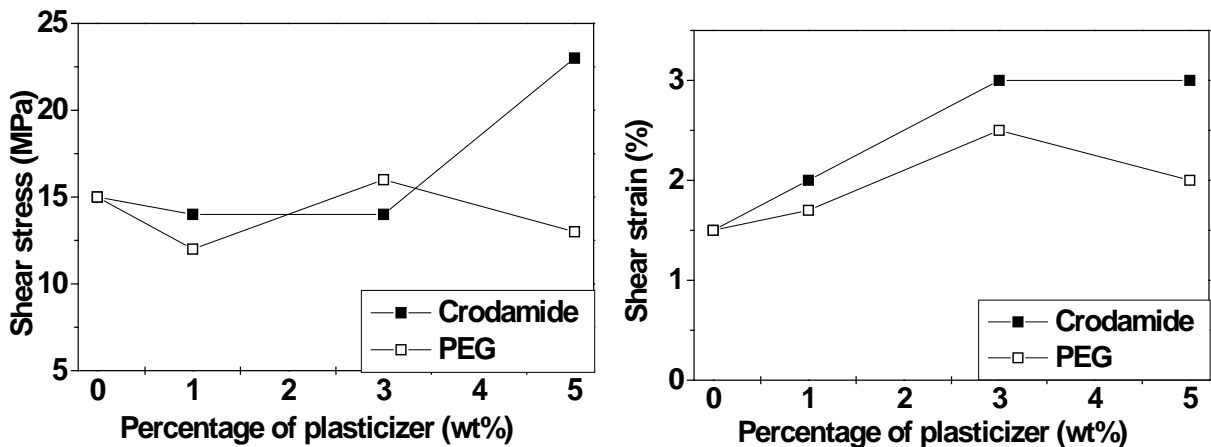


Figure 4.30 Effect of Crodamide and PEG on shear stress (on the left) and on shear strain at break (on the right) of PMMA at 40°C.



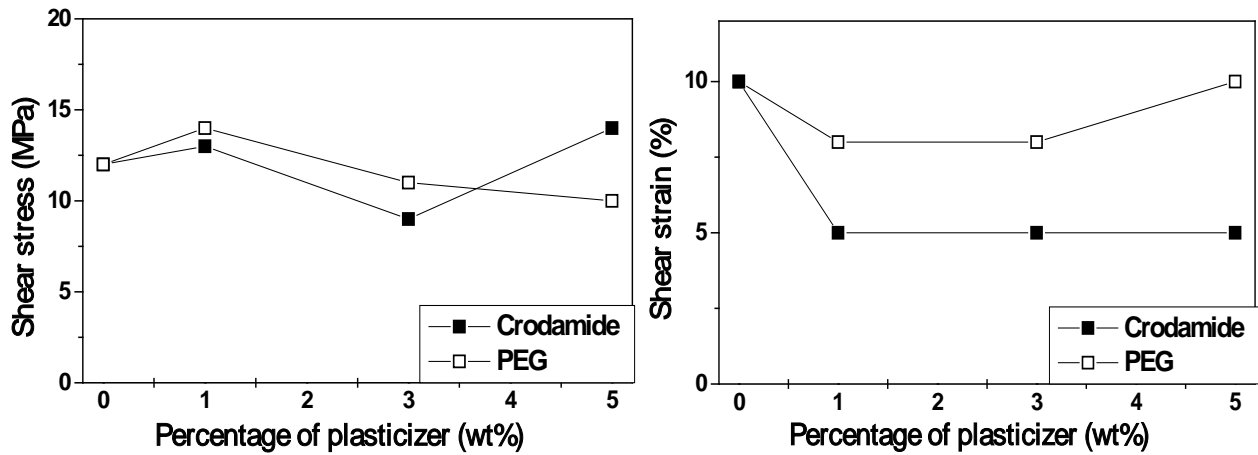


Figure 4.31 Effect of Crodamide and PEG on shear stress (on the left) and on shear strain at break (on the right) of PMMA at 80°C.

#### 4.2.1.3 Bulk mechanical properties on nano scale

As mentioned in previous section that no any significant effect of both plasticizers is found on the bulk mechanical properties of PMMA even for the samples showing a lower coefficients of friction. On the other hand, we have seen that the yielding strain at contact has been increased for the samples showing lower friction coefficient. As the slip additives migrate to the surface in order to reduce the friction coefficient, therefore, it might be considered that bulk behavior may be modified over a very small volume close to the surface (due to presence of excessive amount of slip additive close to the surface). To verify this consideration, some samples were tested over nano scale using a spherical indenter to avoid/reduce the yielding at the contact. Unexpectedly, no any significant difference between the samples showing lower and higher friction coefficients was found for the bulk behavior over nano scale (Figure 4.32 to Figure 4.34). For example, the Young's modulus and hardness detected by nano indenter for the pure PMMA and the sample containing 5 % Crodamide change almost in the same manner with respect to depth, although they have significant difference in friction coefficient. Similarly the sample containing 5 % PEG showing almost same friction coefficient as the pure PMMA shows a lower value of Young's modulus and hardness detected by the nano indenter. On the other hand, we may observe some increase in elastic recovery and yielding strain close to the surface for the samples displaying a lower friction coefficient. So it cannot be concluded surely that the reduction in friction coefficient by the Crodamide is due to the variation of bulk mechanical properties over a small volume very close to the surface.

It is necessary to mention that the yielding strain  $\epsilon_y$  was calculated as  $H/2E$  since  $\epsilon_y = \sigma_y/E$  and normally  $\sigma_y = H/2$ , where  $H$  is the indentation hardness and  $E$  is Young's modulus. Further as  $H \propto F/A$  and  $E \propto F/\sqrt{A}$  (as  $S \propto F/h_e$  and also  $S \propto E * a \propto E * \sqrt{A}$  where  $S$ ,  $F$ ,  $h_e$ ,  $a$  and  $A$  are the stiffness, force, elastic deflection, contact radius and contact area respectively), so the term  $H/2E$  is very much dependent of area involved. As the effects of foreign matters and surface roughness in calculating area on nano scale cannot be avoided/ neglected, so a small error in value of the surface area can affect the value of  $H/2E$  a lot. To be independent of such consequences, an area-independent term  $H/E^2$  is introduced as also indicated by K. Demmou et al. [87]. It is interesting to note that term is independent of the depth and remains almost constant throughout the indentation depth tested (Figure 4.34). This is in contrast to other parameters detected by nano indentation experiments that change with depth. This fact highlights the importance of area consideration in nano indentation experiments. Moreover, the plasticized samples have a little bit higher value of

$H/E^2$  than that of pure PMMA. However it is difficult to explain the reason of this difference between pure and plasticized PMMA.

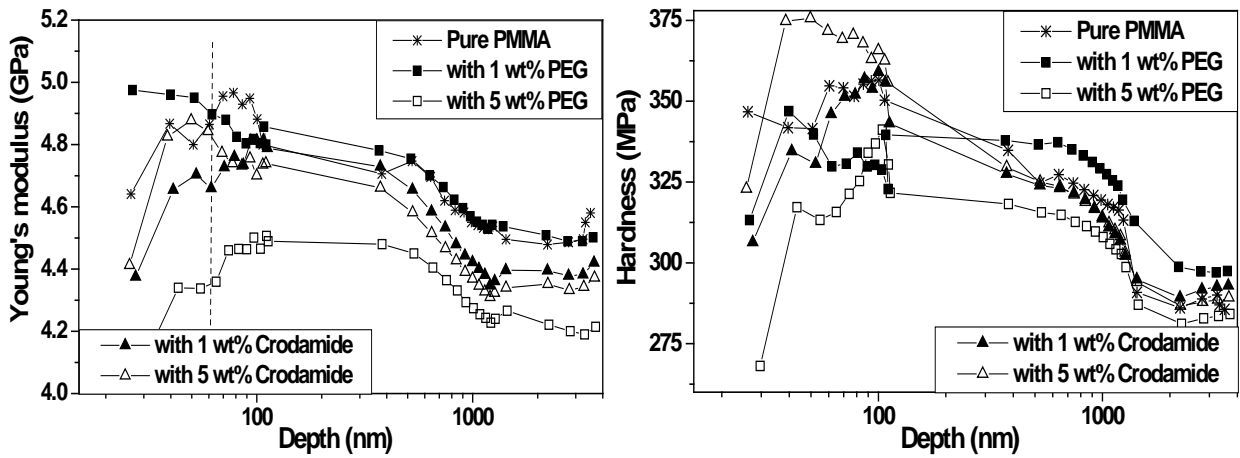


Figure 4.32 Variation of Young's modulus (on the left) and of hardness (on the right) with depth for PMMA at room temperature measured by nano indentation.

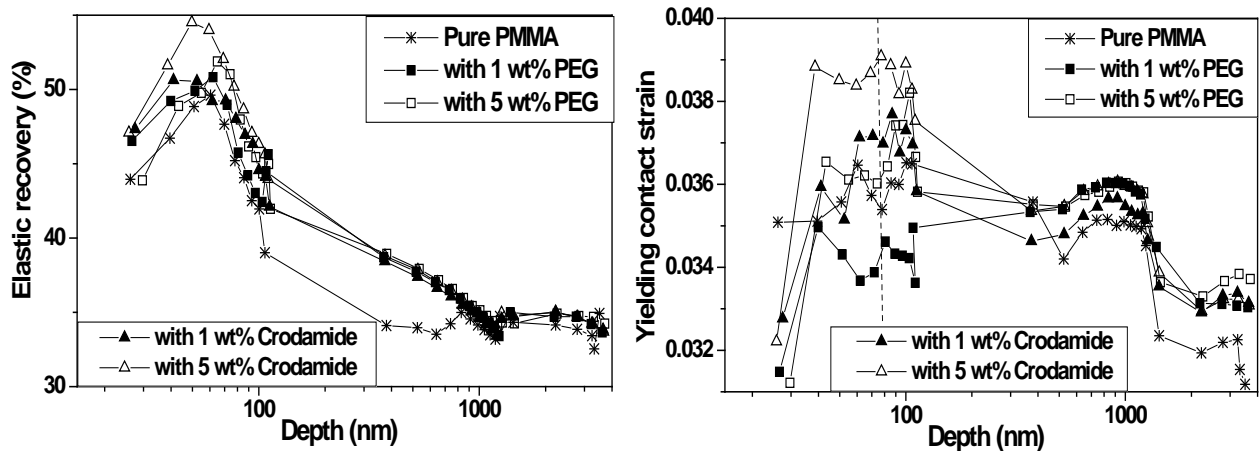


Figure 4.33 Variation of elastic recovery (on the left) and of yielding contact strain defined by  $H/2E$  (on the right) with depth for PMMA at room temperature measured by nano indentation.

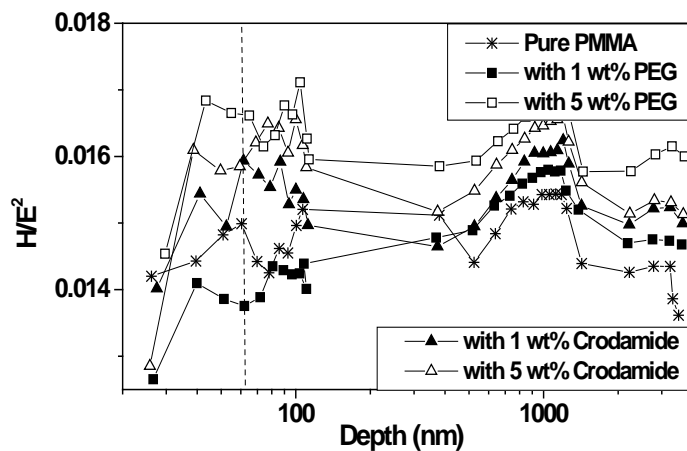


Figure 4.34 Variation of  $H/E^2$  with depth for PMMA at room temperature measured by nano indentation.

It is important to indicate that these nano indentation experiments were performed using three different maximum load capacities to get appropriate accuracy at different levels of depth. The first one was of 0.1 mN that gave indentation up to 100 nm, the second was of 10 mN that is used for the indentation depth up to 1000 nm and finally the third one was of 100 mN for an indentation depth beyond 1200 nm. The effect of change in loading capacity can also be seen in the trend shown in experimental results. Moreover, the abnormal values at indentation depth less than about 50 nm can be attributed due to surface roughness and pollution problems and may be ignored. It is necessary to mention that these nano indentation experiments were carried out several months after the scratch tests.

#### **4.2.1.4 Conclusions**

Following conclusions can be made:

1. The coefficient of friction of PMMA can be decreased by the use of an appropriate plasticizer.
2. The Crodamide is more effective than PEG for reducing the friction coefficient of PMMA and the decrease in friction coefficient is proportional to the Crodamide content.
3. The decrease in friction coefficient of PMMA by Crodamide is not at the cost of bulk properties like Young's modulus. They remain almost unaffected.
4. The decrease in friction coefficient is associated with the modification of the nature of the contact between the tip and the polymer surface.
5. Physical ageing at room temperature does not affect the friction coefficient of pure PMMA. This is in contrast to the Crodamide-plasticized PMMA whose friction coefficient is increased by the physical ageing at room temperature.
6. The heat treatment (at 80°C) increases the friction coefficient of Crodamide-plasticized PMMA whereas it reduces the friction coefficient of PEG-plasticized PMMA.
7. The use of Crodamide is also favourable as it also improves slightly the bulk mechanical properties along with improving the surface properties in contrast to PEG that trims down the bulk properties a little bit.
8. Generally speaking, nominal stress and nominal strain at break of PMMA are increased a little bit by both Crodamide and PEG but at low temperatures, it is decreased a little by Crodamide.
9. Similarly, shear stress and shear strain at break of PMMA are affected a little bit by both Crodamide and PEG.
10. Generally speaking, the bulk yield stress and yield strain of PMMA are not changed considerably by both Crodamide and PEG.
11. The decrease in friction coefficient by Crodamide is not reflected in the significant change in surface free energy. The surface energy remains almost same for the pure PMMA as well as for the plasticized samples by PEG and Crodamide.
12. No any clear relation is found between the decrease in friction coefficient and the bulk properties measured at nano scale.

### **4.2.2 Comparative study of the effect of different fatty acid amides**

#### **4.2.2.1 Effect on surface properties**

##### **4.2.2.1.1 Friction coefficient**

The experimental results indicate that the Erucamide is the most effective fatty acid amide in reducing friction coefficient of PMMA among the three amides tested (Figure 4.35 and Figure 4.36). In all cases, fatty acid amides are proved to be good slip agents only when they are present in very small quantities. They reduce the friction coefficient significantly at lower percentage contents. But further increase in their content gives an adverse effect, which may be attributed due

to anti-plasticization phenomenon probably caused by gumming of excessive amount at the surface as discussed in section 1.8.6. At higher percentage contents of fatty acid amides, no any significant effect on friction coefficient is observed. The optimum content of Erucamide is found to be 0.05 wt%, whereas it is 0.1 wt% in case of Behenamide and Stearamide. It is also observed that the combination of 0.1 wt% Behenamide (showing a considerable decrease in friction coefficient when present alone) and 0.2 wt% Erucamide has no any considerable effect on friction coefficient of PMMA.

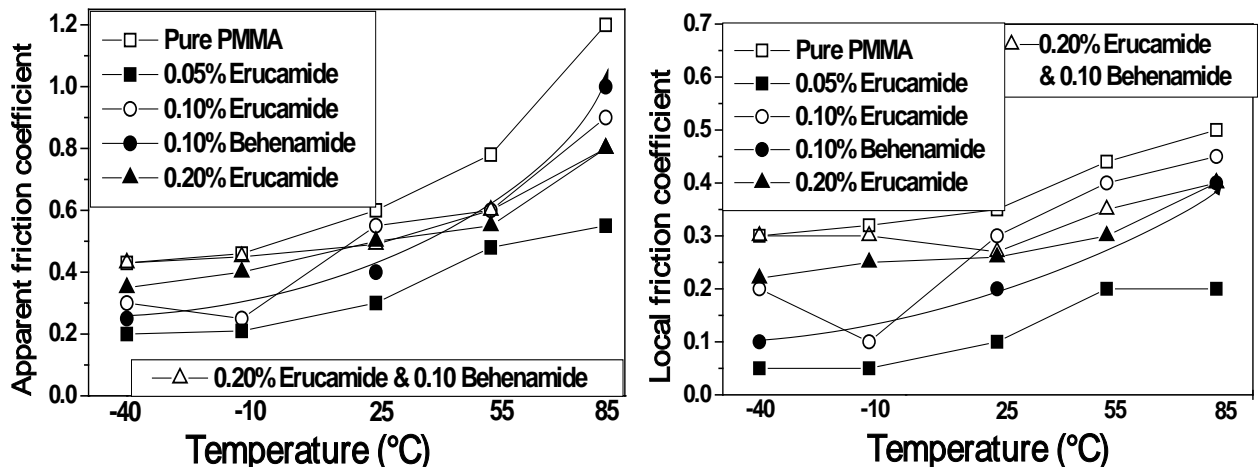


Figure 4.35 Effect of Erucamide and Behenamide on apparent (on the left) and on local friction coefficient (on the right) of PMMA at different temperatures (tip radius = 116  $\mu\text{m}$ , normal load = 2N, sliding/scratching speed = 0.03 mm/s).

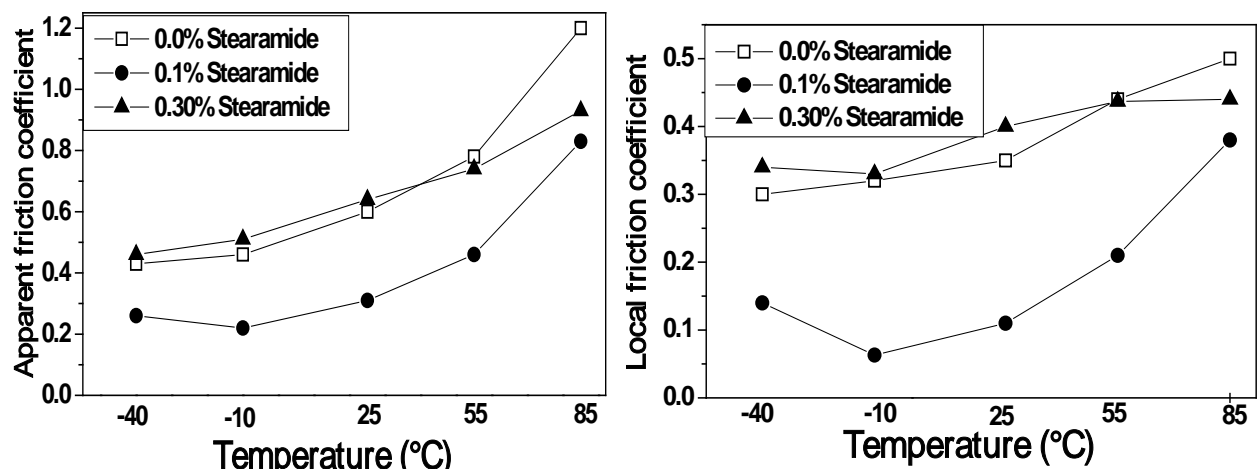


Figure 4.36 Effect of Stearamide on apparent (on the left) and on local friction coefficient (on the right) of PMMA at different temperatures (tip radius = 116  $\mu\text{m}$ , normal load = 2N, sliding/scratching speed = 0.03 mm/s).

#### 4.2.2.1.2 Rear contact angle ( $\Omega$ ) during scratching

We know that the value of the rear contact angle ( $\Omega$ ) is an indicator of the nature of the contact between the sliding tip and the polymer surface. The experimental results indicate that the introduction of fatty acid amides in PMMA modifies the nature of the contact. Their presence in very small amounts (Erucamide (0.05 wt %), Behenamide (0.1 wt %) and Stearamide (0.1 wt %)) enhances the visco-elasticity in the contact. However, a further increase in their content makes the

contact again as plastic as a consequence of gumming effect as discussed in section 1.8.6. The enhancement of the visco-elasticity in the contact is well pictured in the values of the rear contact angle and also in the in situ photographs of the contact. If we see, for example, the values of rear contact angle at room temperature for the samples containing different percentages of Erucamide (Figure 4.37), we observe that at the same value of contact strain (to illustrate for example, 0.3), the value of omega is changed significantly by the introduction of Erucamide. It is about 0.3 radian for pure PMMA and for the samples containing more than 0.05 wt% of Erucamide (all showing higher friction coefficient) that increases to about 0.7 radian for the samples containing 0.05 wt% Erucamide and that containing 0.1 wt% Behenamamide (both having lower value friction coefficient).

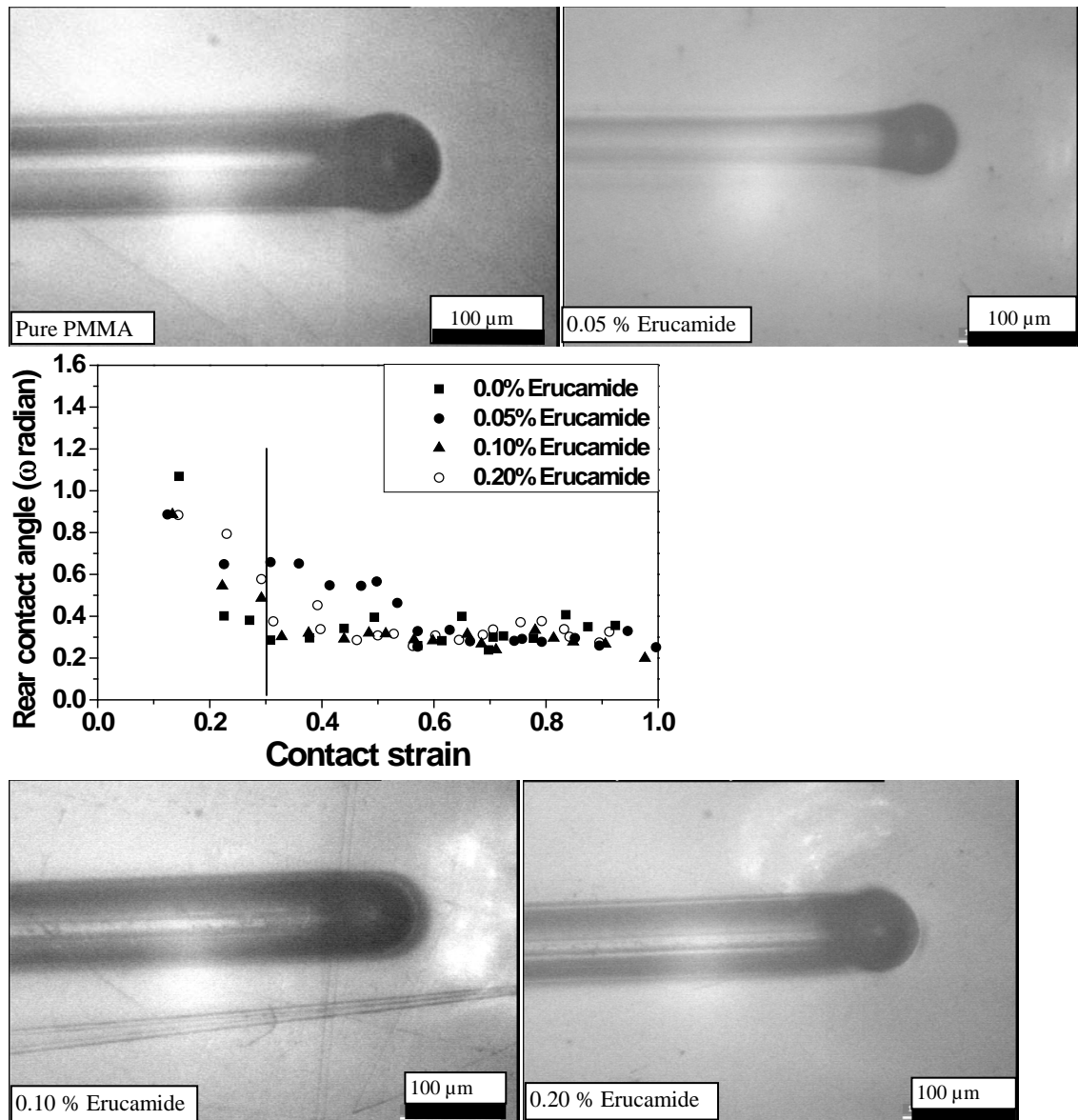


Figure 4.37 Variation of Omega (radian) with contact strain for various percentages of Erucamide in PMMA at room temperature (sliding/scratching speed = 0.03 mm/s, tip radius = 116 μm). Only some selected images concerning to the contact strain = 0.3 are shown.

So it can be concluded that the decrease in friction coefficient is associated with the increase in the value of the rear contact angle and ultimately with the nature of the contact. In situ photographs of the contact demonstrate that the nature of the contact is plastic for pure PMMA and

for samples containing more than 0.05 wt% of Erucamide at contact strain about 0.3 at room temperature. The appearance of lateral and frontal push pads can be seen in this plastic contact. On the other hand, it is visco-elastic for samples containing 0.05 wt% Erucamide and 0.1 wt% Behenamide at the same value of contact strain. Identical results were obtained at lower and higher temperatures (Figure 4.38).

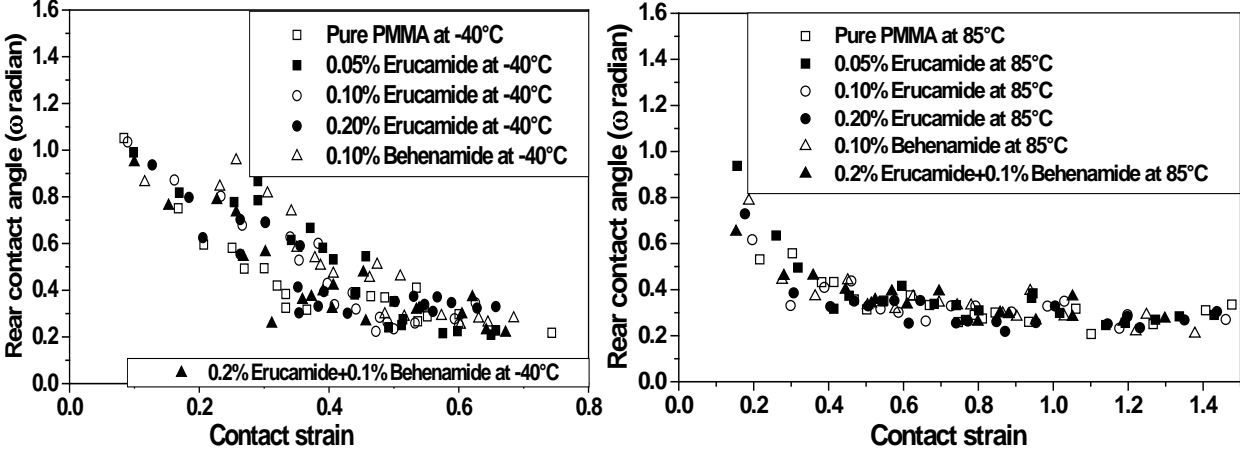


Figure 4.38 Variation of Omega (radian) with contact strain for various percentages of Erucamide and Behenamide in PMMA at low (on the left) and at high temperatures (on the right) (sliding/scratching speed = 0.03 mm/s, tip radius = 116 μm)

Analogous results were observed in case of Stearamide where the sample containing 0.1 wt% Stearamide (displaying lower friction coefficient) showed elevated value of rear contact angle and this increased value is reflected well by in situ photograph that shows a visco-elastic contact for this content of Stearamide (Figure 4.39 and Figure 4.40). However, at a given temperature, the contact is purely elastic at very low contact strains ( $\leq 0.1$ ) and is purely plastic at very high contact strains ( $\geq 0.7$ ) for all cases irrespective of the content or type of the plasticizer (Figure 4.37 to Figure 4.39).

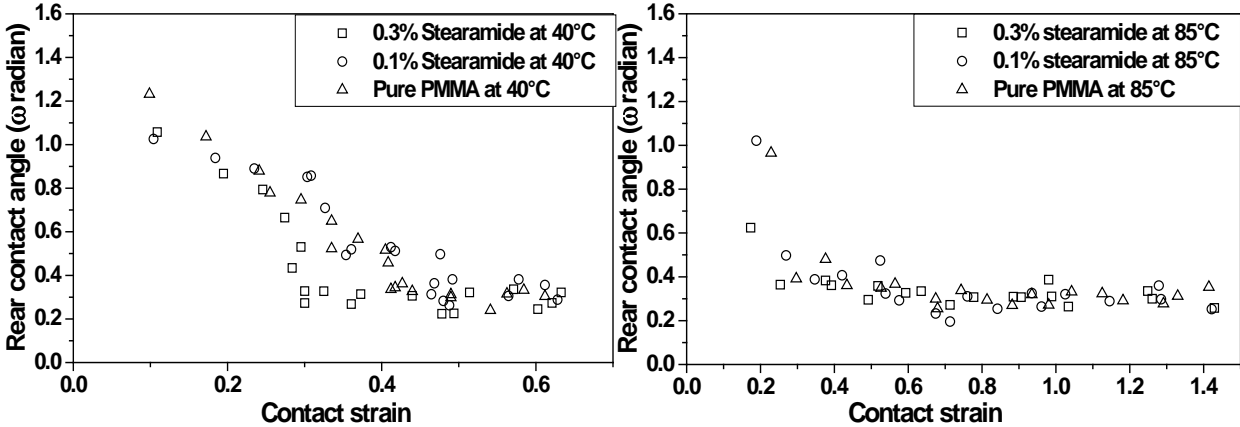


Figure 4.39 Variation of Omega (radian) with contact strain for various percentages of Stearamide in PMMA at low (on the left) and at high temperatures (on the right) (sliding/scratching speed = 0.03 mm/s, tip radius = 116 μm).

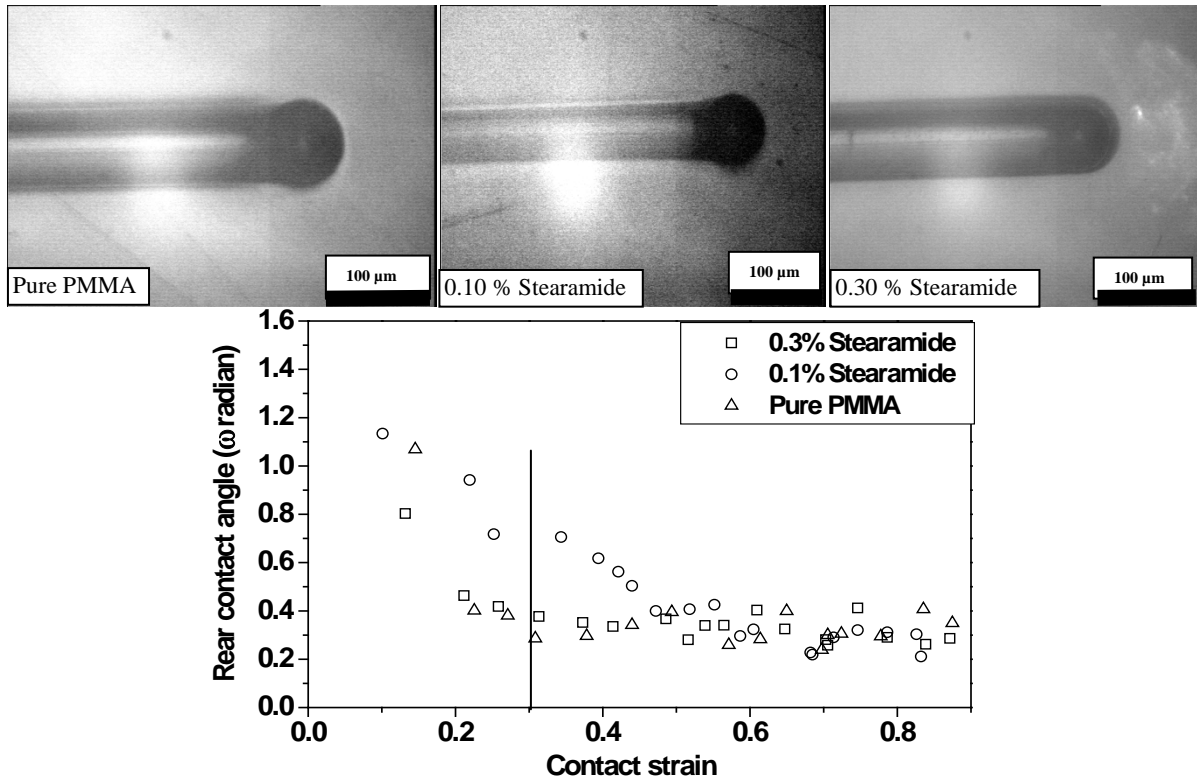


Figure 4.40 Variation of Omega (radian) with contact strain and the percentage of Stearamide for PMMA at room temperature (sliding/scratching speed = 0.03 mm/s, tip radius = 116  $\mu\text{m}$ ). All images concern to the contact strain = 0.3.

We know that the slope of contact pressure-strain curve during elastic and visco-elastic region of polymers is a function of both the Young's modulus and the friction coefficient [17]. This slope is almost same for the samples showing higher friction coefficient like pure PMMA and the samples containing higher contents of fatty acid amides (for example, 0.10 wt% Erucamide) whereas it is changed a lot for the case showing lower friction coefficient (the sample containing 0.05 wt% Erucamide, for example) as shown in Figure 4.41. As the friction coefficient is almost same for the pure PMMA as well as for the sample containing 0.10 wt% Erucamide, one may expect that the bulk properties like Young's modulus also does not change by the introduction of fatty acid amides. However, it cannot be concluded clearly for the Young's modulus of lower content of fatty acid amides. Figure 4.41 also clearly indicates that the yielding stress at contact remains almost same for all the cases (as the yield stress is equal to the half of the contact pressure during scratching) and the contact pressure at higher contact strains becomes almost constant for all samples. However, the yielding strain at the contact (at which elastic sliding changes to the plastic scratch and is indicated by the contact strain after which the contact pressure becomes almost constant) is changed significantly for the samples showing lower friction coefficient. It is about 0.27 for the pure PMMA as well as for the plasticized samples showing higher friction coefficient whereas it increases to about 0.6 for the sample containing 0.05 wt% Erucamide (displaying a lower friction coefficient). It can also be alleged that the fatty acid amides when present in lower amounts, keep the contact as elastic one even at higher contact strains.

#### 4.2.2.1.3 Surface free energy

The surface free energy was calculated only for pure PMMA and the samples containing 0.05% Erucamide and 0.1% Behenamide. The values of surface energy calculated from three

different equations for pure PMMA are almost the same and in well agreement with the literature value [20, 23, 25, 26, 74, 80]. The experimental results show that the surface free energy for the plasticized samples showing a significant reduction in the friction coefficient remains almost same as that of pure PMMA (Figure 4.42). This can be said again to be in agreement with the work done by B. Podgornik et al. [84] and that by H. Berro et al. [85] but is in contrast to the work of M. Minn et al. [21] as discussed in section 4.2.1.1.5. It can be summarized that fatty acid amides reduce the friction coefficient by forming a very thin elastic layer, resulting in modification of nature of the contact.

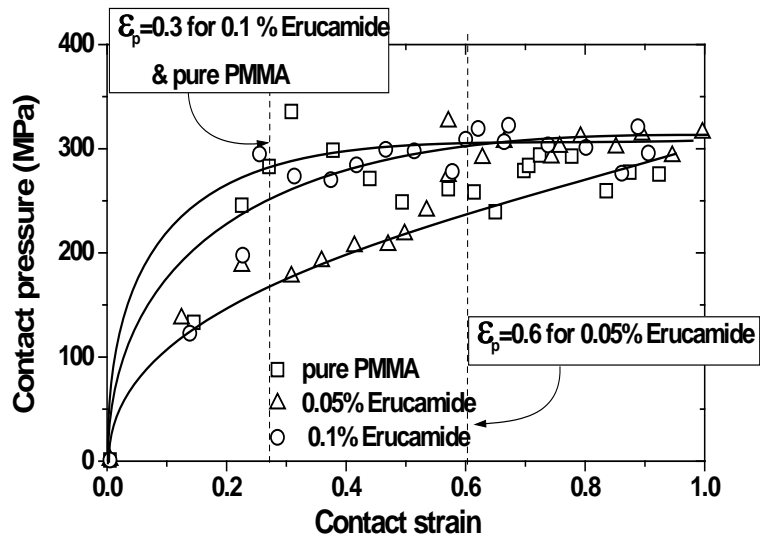


Figure 4.41 Variation of the contact pressure with contact strain at room temperature for three different samples of PMMA (sliding/scratching speed = 0.03 mm/s, tip radius = 116 μm).

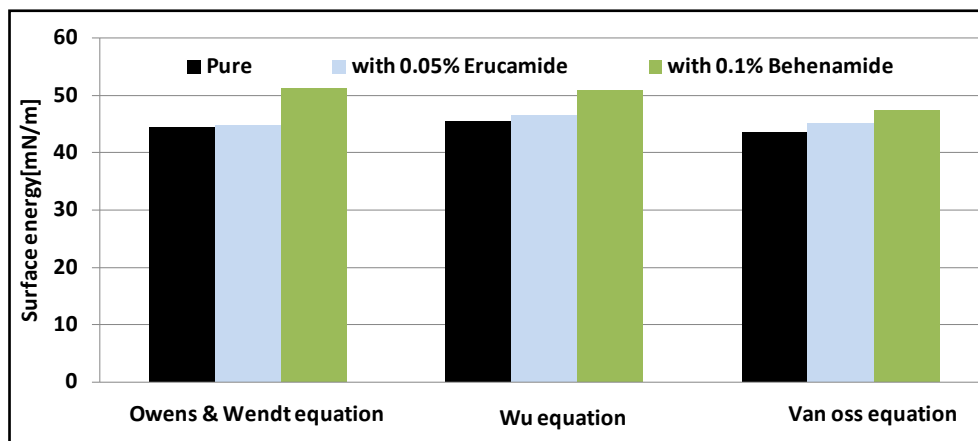


Figure 4.42 The effect of Erucamide and Behenamide on surface free energy of PMMA at 20°C.

#### 4.2.2.2 Effect on bulk mechanical properties

##### 4.2.2.2.1 Elastic modulus

Elastic modulus displays a principal part in the scratch process as mentioned in section 4.2.1.2.1. As the percentage contents of plasticizers in all cases are not so high, their consequence on the bulk mechanical properties is not up to a significant value which is conformity of the prediction from the results obtained from micro visio scratch apparatus as discussed in section 4.2.2.1.2 (Figure 4.43 to Figure 4.46). The results shown correspond to experiments at 0.05 Hz and





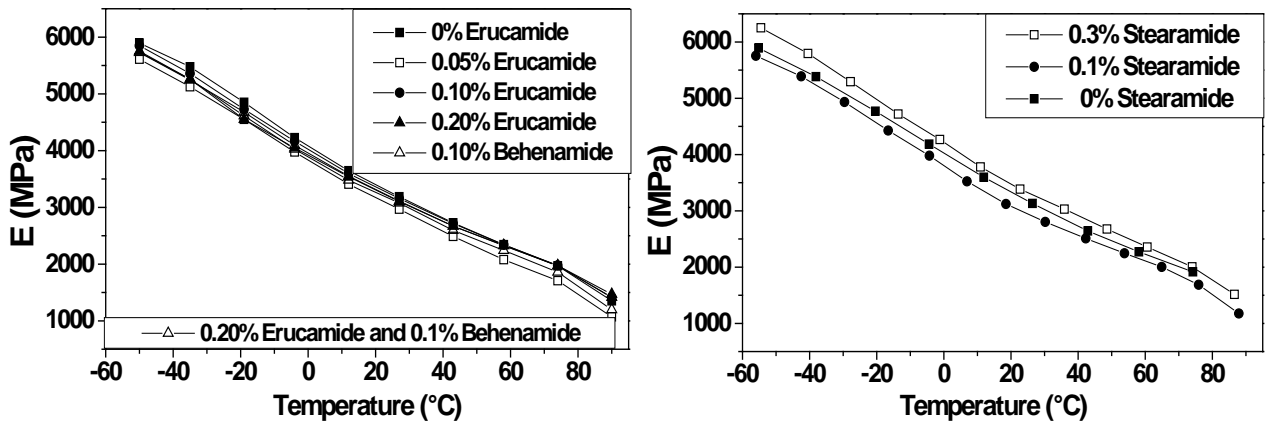


Figure 4.43 Effect of Erucamide, Behenamide (on the left) and of Stearamide (on the right) on Young's modulus (E) of PMMA at different temperatures.

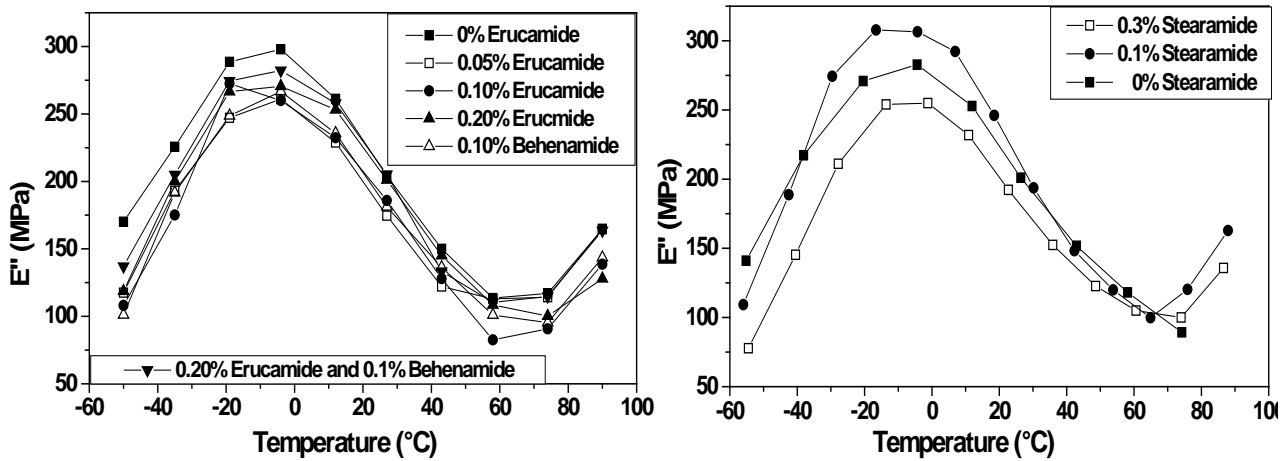


Figure 4.44 Effect of Erucamide, Behenamide (on the left) and of Stearamide (on the right) on loss modulus (E'') of PMMA at different temperatures.

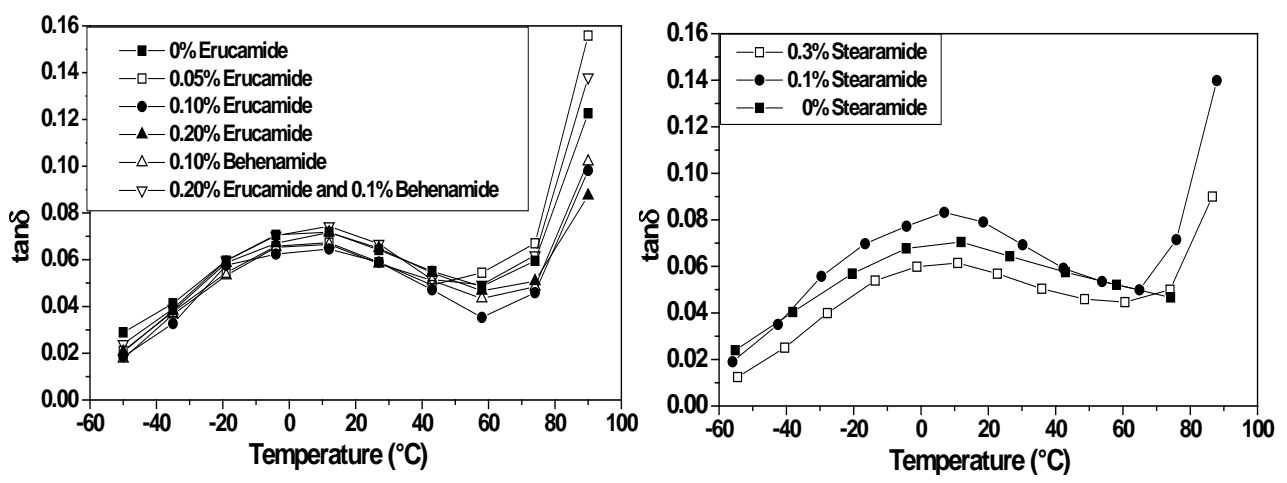


Figure 4.45 Effect of Erucamide, Behenamide (on the left) and of Stearamide (on the right) on loss factor (tan δ) of PMMA at different temperatures.

the experiments at 0.5 Hz and at 5 Hz displayed similar trend. All fatty acid amides have no remarkable effect on major bulk properties like Young's modulus. However, Stearamide disturbs these properties comparatively more than do both Erucamide and Behenamide. It is also interesting to note that the samples showing lower friction coefficient (0.05 wt% Erucamide, 0.1 wt% Behenamide and 0.1 wt% Stearamide) have a little bit decreased value of Young's modulus. This is in good agreement with the results mentioned by Xiang C. et al. [6].

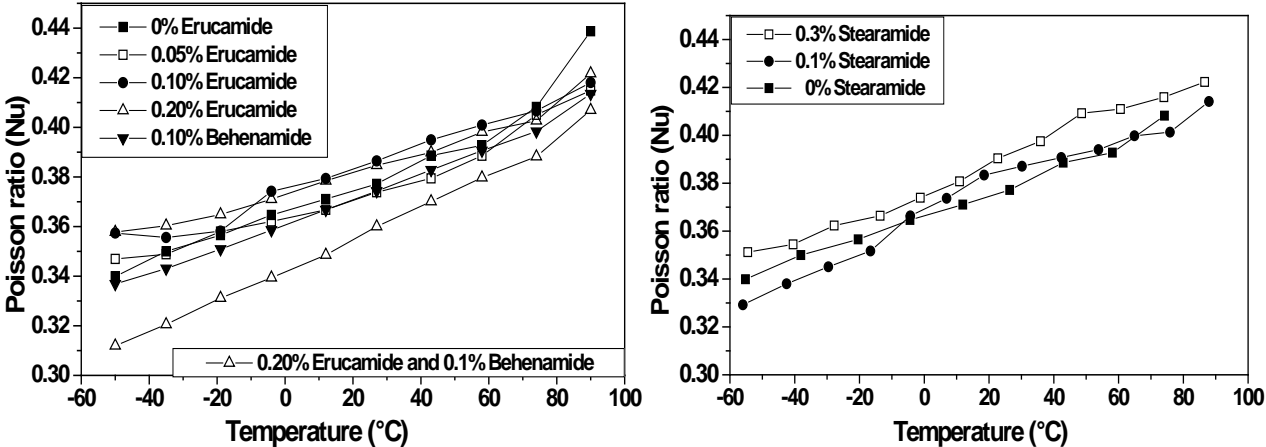


Figure 4.46 Effect of Erucamide, Behenamide (on the left) and of Stearamide (on the right) on Poisson ratio (Nu) of PMMA at different temperatures.

4.2.2.2.2 Yield stress and yield strain

The effect of fatty acid amides on yield stress and yield strain of PMMA is not very clear. Generally speaking, they do not affect these values to a significant worth for PMMA. However, it is interesting to note that Erucamide first decreases the yield stress and yield strain of PMMA but further increase in its content again increases the yield stress and strain values for PMMA (Figure 4.47 and Figure 4.48). The results shown correspond to experiments at compression strain rate =  $10^{-2} \text{ s}^{-1}$ . The experiments at compression strain rate =  $10^{-1} \text{ s}^{-1}$  and at compression strain rate =  $10^{-3} \text{ s}^{-1}$  showed similar trend.

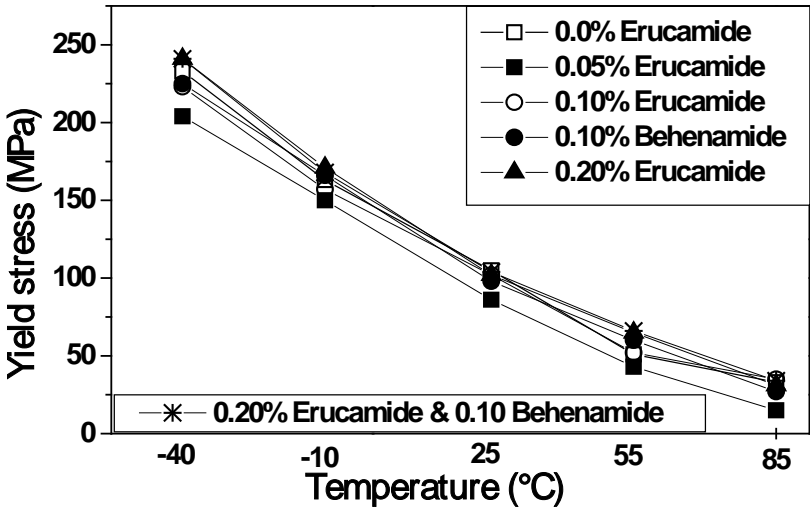


Figure 4.47 Effect of Erucamide and Behenamide on yield stress of PMMA at different temperatures.

It is remarkable to note that if we see that scratch limiting (or yielding) contact strain (at which the elastic sliding is converted to plastic scratching), we observe that there is a significant increase in scratch limiting contact strain (the value of contact strain at which the value of rear contact angle becomes almost constant) for all the three cases showing decreased friction coefficient (sample containing 0.05 wt% Erucamide, sample containing 0.1 wt% Behenamide and the sample containing 0.1 wt% Stearamide). So it may be believed that the decrease in friction coefficient is associated with the modification of the nature of the contact and that the fatty acid amides when present in lower amounts promote elastic sliding by increasing the yielding strain at the contact (Figure 4.49 and Figure 4.50).

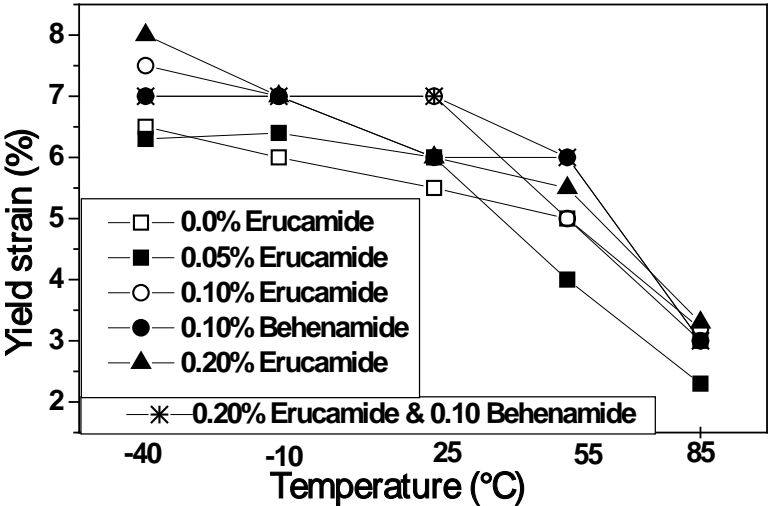


Figure 4.48 Effect of Erucamide and Behenamide on yield strain of PMMA at different temperatures.

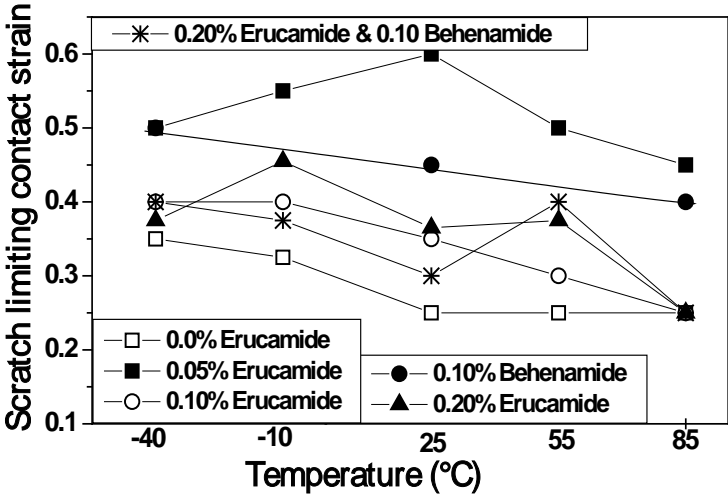


Figure 4.49 Effect of Erucamide and Behenamide on scratch limiting contact strain of PMMA at different temperatures (tip radius = 116  $\mu\text{m}$ , sliding speed = 0.03 mm/s).

There is no any clear relation found between the decrease in friction coefficient brought about by the fatty acid amides and the change in the bulk yield stress and strain of PMMA; but the yielding strain at the contact is increased significantly for the samples showing low friction coefficients. So, it can be concluded that the fatty acid amides, when present in appropriate

amounts, decrease the friction coefficient by modifying the nature of the contact and this is achieved by modifying the mechanical behavior of the PMMA over a very minute volume close to the surface by switching it to more elastic.

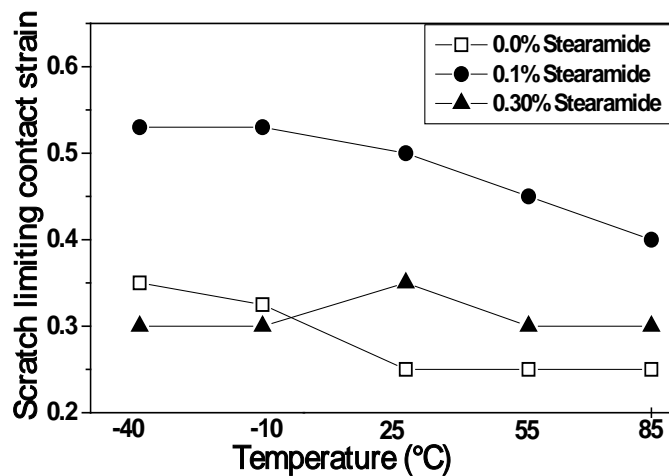


Figure 4.50 Effect of Stearamide on scratch limiting contact strain of PMMA at different temperatures (tip radius = 116  $\mu\text{m}$ , sliding speed = 0.03 mm/s).

#### 4.2.2.3 Bulk mechanical properties on nano scale

As discussed in previous section, there is no any significant effect of three plasticizers found on the bulk mechanical properties of PMMA even for the samples showing a lower coefficient of friction. On the other hand, we have seen that the yielding contact strain has been increased for the samples showing lower friction coefficient. It has been also well established that the slip additives migrate to the surface and form a very thin film in order to reduce the friction coefficient. Therefore, it might be considered that bulk behavior may be modified over a very small volume close to the surface (due to presence of excessive amount of slip additive close to the surface). To verify this consideration, some samples were tested over nano scale using a spherical indenter to avoid/minimize yielding at the contact. Unexpectedly, no any significant difference was found between the samples showing lower and higher friction coefficients (Figure 4.51 to Figure 4.53). For example, the Young's modulus and hardness detected by nano indenter for pure PMMA, the sample containing 0.1 % Behenamide and the sample containing 0.05 % Erucamide change almost in the same manner with respect to depth, although they have significant difference in their friction coefficients. Similarly the sample containing 0.2 % Erucamide having almost same friction coefficient as the pure PMMA show almost same value of Young's modulus and hardness as detected by the nano indenter. So one may conclude that the change in friction coefficient made by very small amount of fatty acid amides is not due to the variation of bulk properties over a small volume very close to the surface. Moreover, the term  $H/E^2$  as discussed in section 4.2.1.3 is independent of depth in contrast to other parameters detected by the nano indentation. However, here the trend is opposite to that discussed in section 4.2.1.2.3. Surprisingly, here we find that the value of the term  $H/E^2$  for pure PMMA is higher than that of plasticized samples. It is hard to find a reasonable justification for this difference in behavior of the two cases.

It is important to indicate that these nano indentation experiments were performed using three maximum load capacities to get appropriate accuracy as discussed in section 4.2.1.3. The effect of change in loading capacity can also be seen in the trend shown in experimental results.

Moreover, the abnormal values at indentation depth less than about 70 nm can be attributed due to surface roughness and pollution problems and may be ignored.

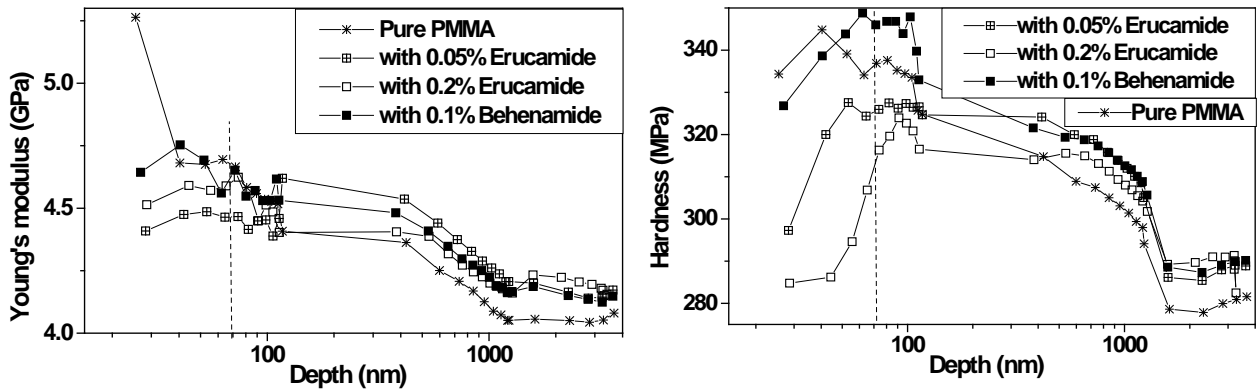


Figure 4.51 Variation of Young's modulus (on the left) and of hardness (on the right) with depth for various percentages of fatty acid amides in PMMA at room temperature as measured by nano indentation.

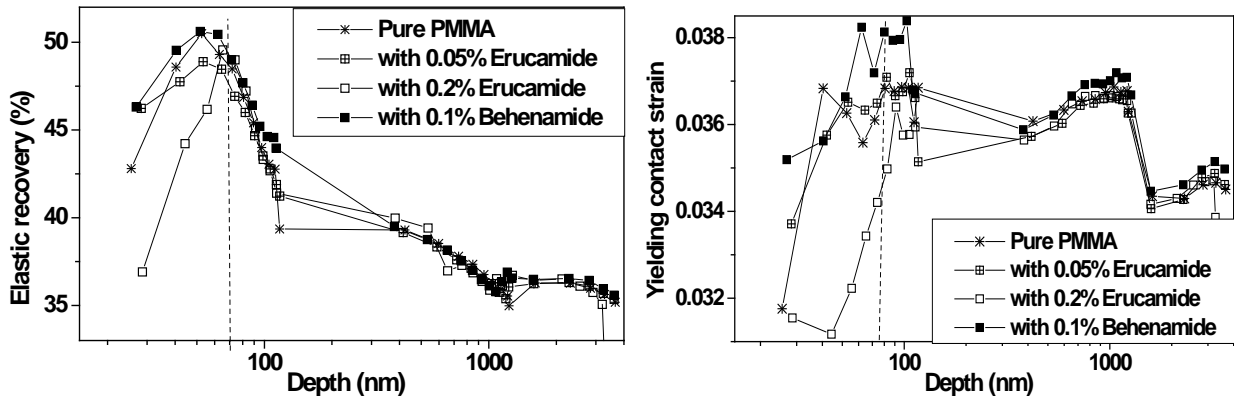


Figure 4.52 Variation of elastic recovery (on the left) and of yielding contact strain defined by  $H/2E$  (on the right) with depth for various percentages of fatty acid amides in PMMA at room temperature as measured by nano indentation.

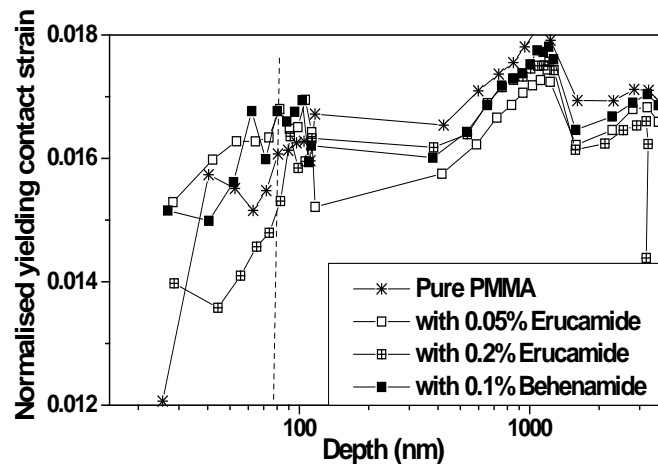


Figure 4.53 Variation of  $H/E^2$  with depth for various percentages of fatty acid amides in PMMA at room temperature as measured by nano indentation.

#### 4.2.2.4 Conclusions

The following conclusions can be drawn:

1. The coefficient of friction of PMMA can be decreased by the use of an appropriate plasticizer.
2. The fatty acid amides are more effective in lower amounts than being in higher amounts for reducing the friction coefficient of PMMA.
3. The use of Erucamide up to 0.05 wt%, Behenamide up to 0.1 wt% and Stearamide up to 0.1 wt% gives maximum reduction in friction coefficient. Further increase in their content has adverse effect on reduction of friction coefficient.
4. The decrease in friction is associated with the nature of the contact between the tip and the polymer surface.
5. The decrease in friction coefficient by lower amounts of fatty acid amides is brought about by increasing the yielding strain at the contact.
6. The decrease in friction coefficient of PMMA by fatty acid amides is not at the cost of bulk mechanical properties like Young's modulus. They remain almost unaffected
7. Generally speaking, the bulk yield stress and yield strain are not changed significantly by fatty acid amides. However, at lower contents, they are decreased a little bit.
8. The decrease in friction coefficient is not reflected in the change in surface free energy. The surface energy for the plasticized samples showing lower friction coefficient and for pure PMMA remains almost same.
9. No any clear relation found between decrease in friction coefficient and the change in bulk properties measured at nano scale.

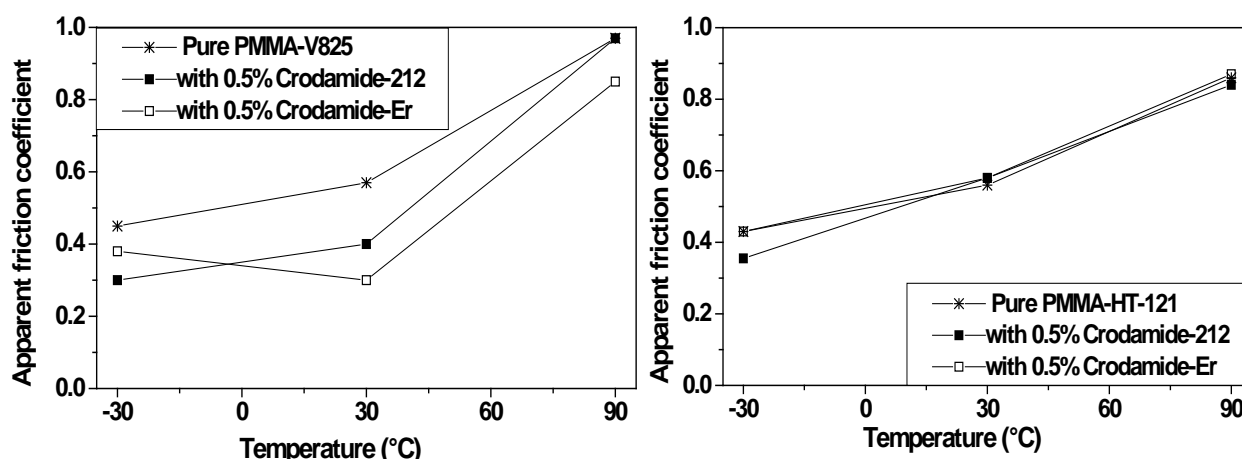


Figure 4.54 Effect of Crodamide-212 and Crodamide-Er on apparent friction coefficient of two types of PMMA, V825 (on the left) and HT-121 (on the right) at different temperatures (tip radius = 116  $\mu\text{m}$ , normal load = 1.5 N, sliding/scratching speed = 0.03 mm/s).

### 4.2.3 Comparative study of the effect of a plasticizer on two different grades of PMMA

#### 4.2.3.1 Effect on surface properties

##### 4.2.3.1.1 Friction coefficient

The effect of two fatty acid amides i.e. Crodamdie-212 and Crodamide-Er on the friction coefficients of two different commercial grades of PMMA was studied. The experimental results indicate that a specific slip additive, effective for a specific polymer grade may be useless for the other grades of the same polymer (Figure 4.54 and Figure 4.55). Both Crodamide-212 and Crodamide-Er decrease the friction coefficient of PMMA-V825. However, the extent of decrease is

different at different temperatures. On the other hand, in case of PMMA-HT121, the coefficient of friction remains almost unaffected by both fatty acid amides.

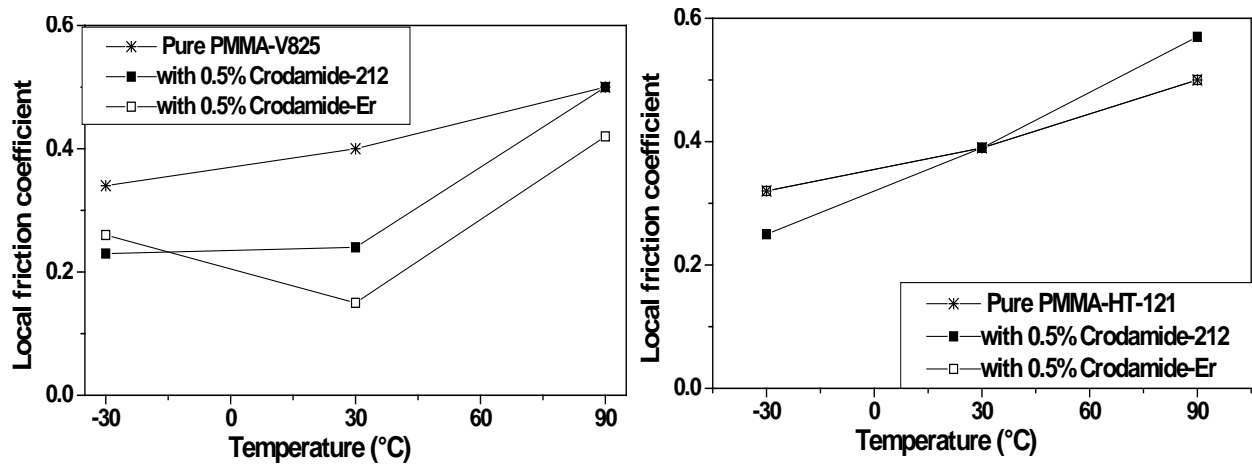


Figure 4.55 Effect of Crodamide-212 and Crodamide-Er on local friction coefficient of two types of PMMA, V825 (on the left) and HT-121 (on the right) at different temperatures (tip radius = 116  $\mu\text{m}$ , normal load = 1.5 N, sliding/scratching speed = 0.03 mm/s).

#### 4.2.3.2 Effect on bulk mechanical properties

##### 4.2.3.2.1 Elastic modulus

As the percentage contents of plasticizers in both cases are not so high, their consequence on the bulk mechanical properties is not up to a significant value (Figure 4.56 to Figure 4.59). The results shown correspond to experiments at 0.5 Hz and the experiments at 0.05 Hz and at 5 Hz showed similar trend. Both amides have no any remarkable effect on major bulk properties. However, the Young's modulus and the Poisson ratio have been increased a little bit by both additives for PMMA-HT121 (showing no any change in surface properties).

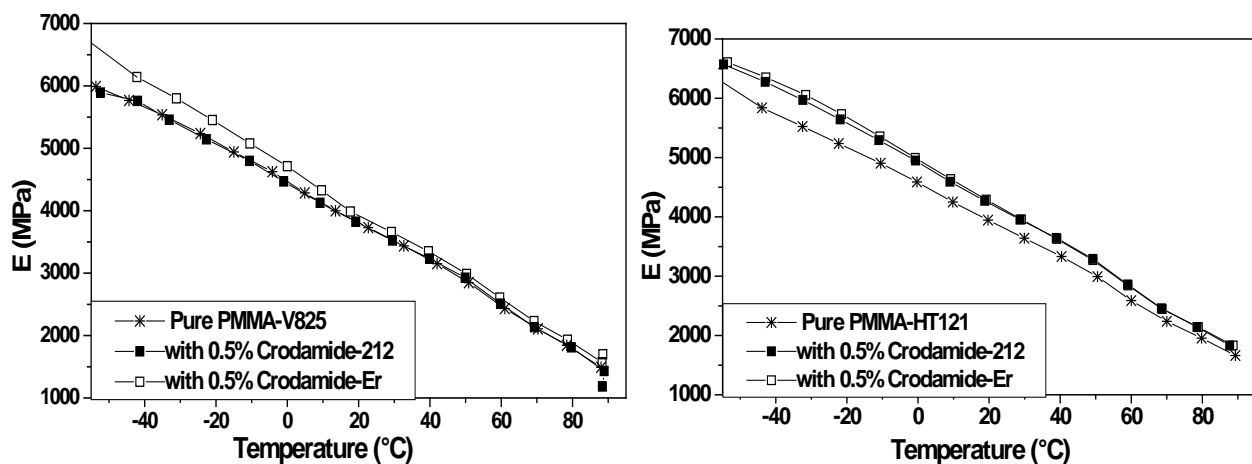


Figure 4.56 Effect of Crodamide-212 and Crodamide-Er on Young's modulus ( $E$ ) of two types of PMMA, V825 (on the left) and HT-121 (on the right) at different temperatures.

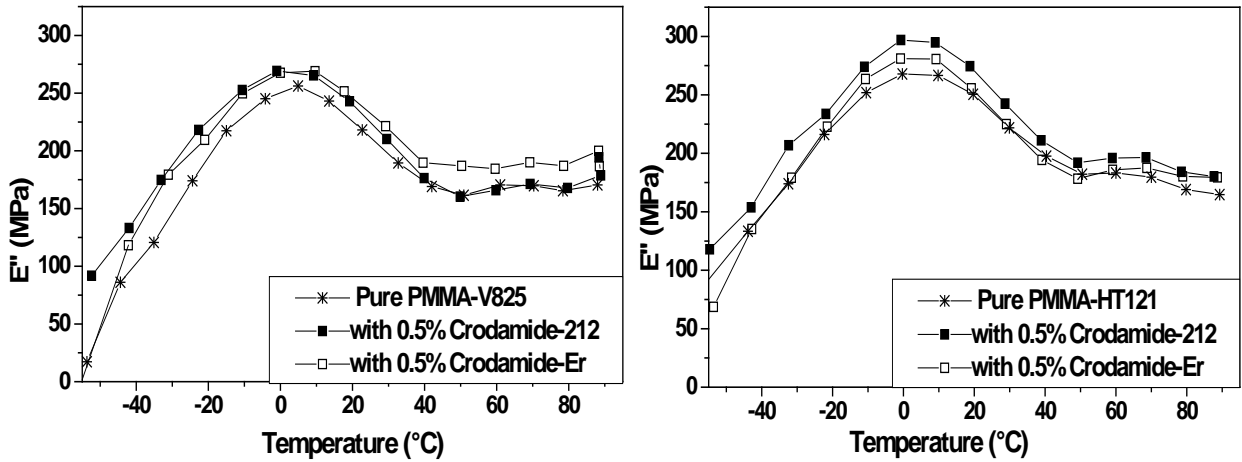


Figure 4.57 Effect of Crodamide-212 and Crodamide-Er on loss modulus ( $E''$ ) of two types of PMMA, V825 (on the left) and HT-121 (on the right) at different temperatures.

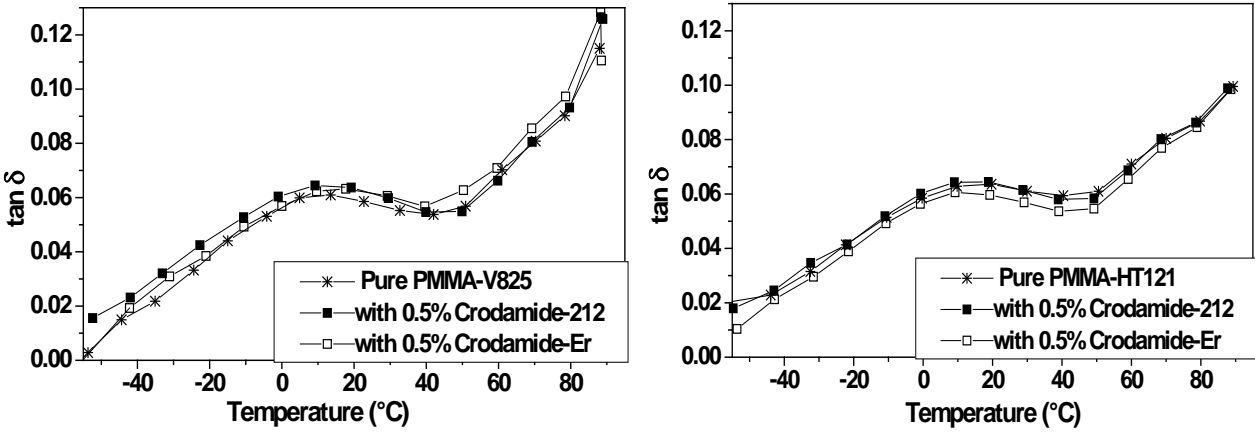


Figure 4.58 Effect of Crodamide-212 and Crodamide-Er on loss factor ( $\tan \delta$ ) of two types of PMMA, V825 (on the left) and HT-121 (on the right) at different temperatures.

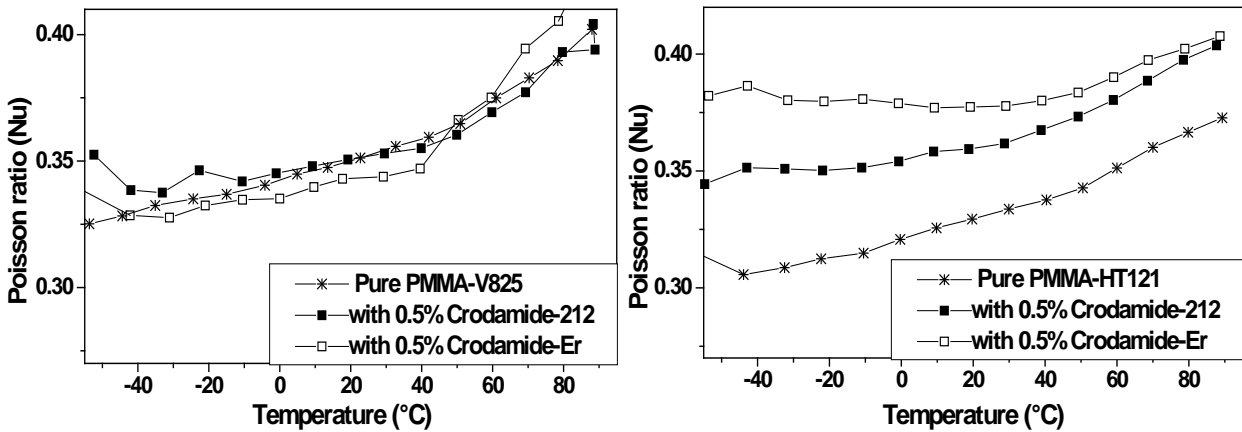


Figure 4.59 Effect of Crodamide-212 and Crodamide-Er on Poisson ratio ( $\nu$ ) of two types of PMMA, V825 (on the left) and HT-121 (on the right) at different temperatures.



### 4.2.3.3 Conclusions

The following conclusions can be drawn:

1. The coefficient of friction of PMMA can be decreased by the use of an appropriate plasticizer.
2. The fatty acid amides effective for reducing the friction coefficient of a specific grade of PMMA may not be effective for another grade.
3. The fatty acid amides are more effective for PMMA having lower  $T_g$ .
4. The decrease in friction coefficient of PMMA by both additives is not at the cost of bulk mechanical properties. They remain almost unaffected.

## 4.2.4 The effect of reticulation on surface and bulk behaviour of PMMA

### 4.2.4.1 Effect on surface properties

#### 4.2.4.1.1 Friction coefficient

The experimental results indicate that the reticulation is not favourable for reducing the friction coefficient of PMMA (Figure 4.60). Reticulated PMMA showed higher friction coefficient than the non-reticulated one (and it is more clear in local friction coefficient). It is important to mention that although PBA was used in the form of nano particles to avoid/ minimise its effect on the transparency, but even then, it disturbs the transparency of PMMA. The in situ images of non-reticulated PMMA were not so much clear to be analyzed correctly for the evolution of the local friction coefficient, the mean contact strain, the rear contact angle and so on. It is also important to note that both non-reticulated and reticulated PMMA displayed lower friction coefficient at higher temperature that is an unexpected phenomenon. The standard grade PMMA like V825 shows an increase in friction coefficient with increasing temperature. This abnormal behaviour of reticulated and non-reticulated PMMA may be attributed due to the presence of nano-structured PBA (poly (n-butyl acrylate)). Similarly the heat treatment at 90°C for half an hour reduced the friction coefficient of both reticulated and non-reticulated PMMA and the effect is more significant in case of reticulated PMMA (Figure 4.61). This is again in contrast to the common commercial grade of PMMA that generally shows an increase in friction coefficient after being heated at higher temperature. This abnormal behaviour of reticulated and non-reticulated PMMA may be again considered due to the presence of PBA. It may be supposed that the soft elastomeric nano particles of PBA migrate to the surface at higher temperature resulting in a decrease in friction coefficient.

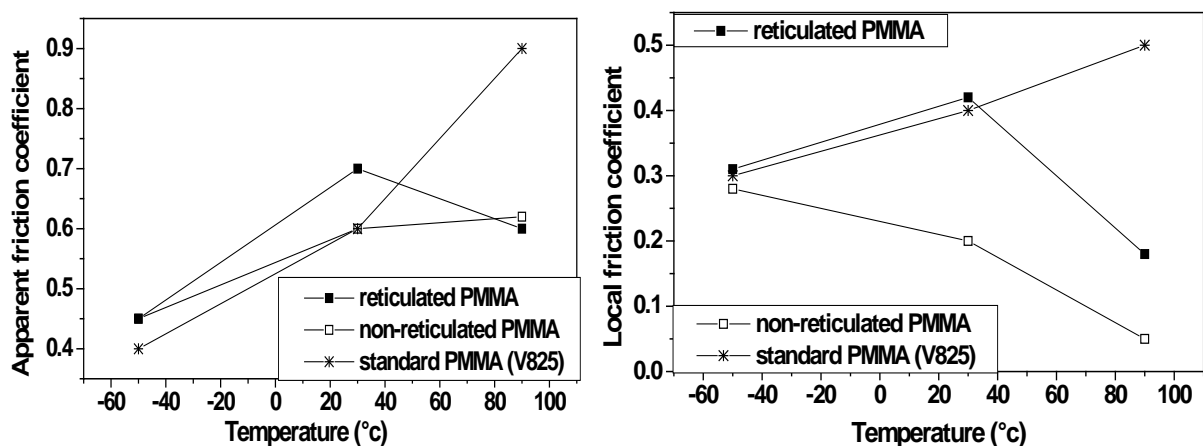


Figure 4.60 Effect of reticulation on apparent (on the left) and on local friction coefficient (on the right) of PMMA at different temperatures (tip radius = 116  $\mu\text{m}$ , normal load = 1.5 N, sliding/scratching speed = 0.03 mm/s).

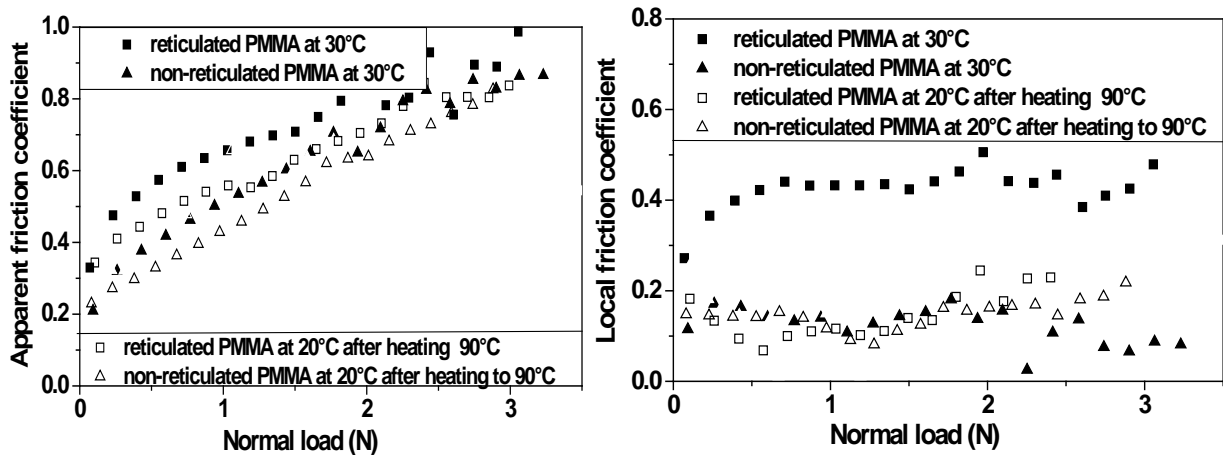


Figure 4.61 Effect of a heating cycle at 90°C for 30 minutes on apparent (on the left) and on local friction coefficient (on the right) of reticulated and non-reticulated PMMA measured at room temperature (tip radius = 116  $\mu\text{m}$ , sliding/scratching speed = 0.03 mm/s).

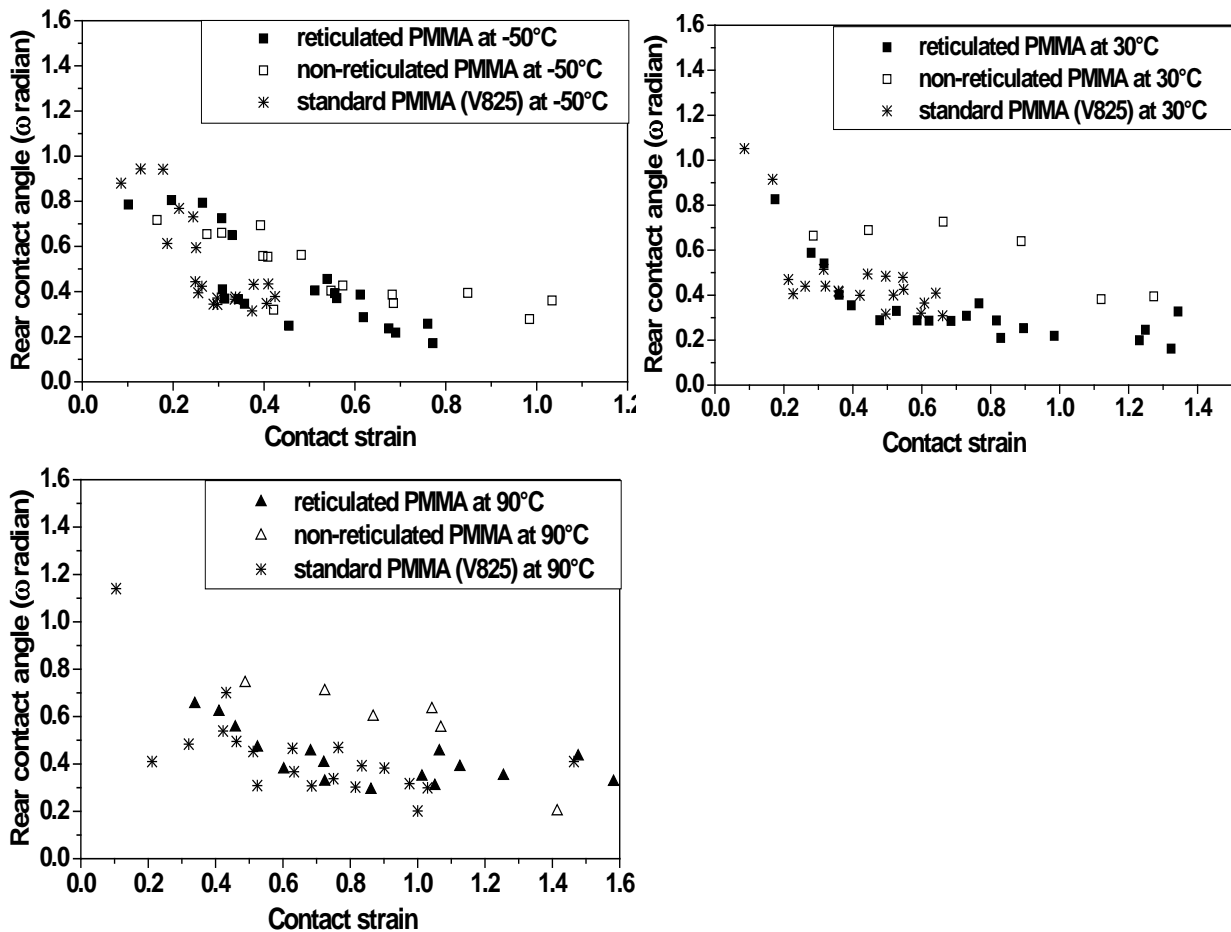


Figure 4.62 Variation of Omega (radian) with contact strain for reticulated and non-reticulated PMMA at different temperatures (sliding/scratching speed = 0.03 mm/s, tip radius = 116  $\mu\text{m}$ ).

#### 4.2.4.1.2 Rear contact angle (Omega) during scratching

As mentioned earlier, the value of the rear contact angle (Omega) is an indicator of the nature of the contact between the sliding tip and the polymer surface. The experimental results

indicate that the reticulation of PMMA modifies the nature of the contact. This modification of the nature of the contact is well reflected in the values of rear contact angle. If we see, for example, the values of rear contact angle at different temperatures (Figure 4.62), we observe that the value of omega is decreased significantly by the reticulation. So it can be concluded that the increase in friction coefficient is associated with the decrease in the value of the rear contact angle and ultimately with the nature of the contact. Reticulation introduces plasticity in the PMMA due to which the friction coefficient is increased. The deviation in the rear contact angle values for non-reticulated PMMA as compared to those of reticulated and standard PMMA may again be attributed to frustrating in situ images that give error to estimate the rear contact angle.

#### 4.2.4.2 Effect on bulk mechanical properties

##### 4.2.4.2.1 Elastic modulus

The experimental results demonstrate that the presence of nano structured and elastomeric PBA decreased the elastic modulus significantly as compared to that standard grade PMMA. However, the reticulation has improved the Young's modulus and decreased the loss factor. The decrease in Young's modulus with rising temperature is more uniform in case of reticulated samples as compared to non-reticulated samples (Figure 4.63 and Figure 4.64). In case of non-reticulation, the Young's modulus decreases initially very rapidly with increasing temperature till the temperature approaches zero and then a slight decrease in Young's modulus is observed with further increase in temperature. On the other hand, in cases of reticulated samples, the Young's modulus decreases with almost same rate throughout the temperature range. This trend is similar to a standard type of PMMA. It is also interesting to note that the non-reticulated PMMA showing lower friction coefficient has a decreased value of Young's modulus. This is in good agreement with the results mentioned by Xiang C. et al. [6]. A slight increase in loss modulus is also observed in reticulated samples at high temperatures. Moreover, a very significant increase in the loss factor ( $\tan \delta$ ) values is observed in case of non-reticulated samples. It can be assumed that the presence of PBA does not give a homogeneous composition resulting in decreased Young's modulus and transparency but resulting in an increased loss factor. However, reticulation of such a composition results in an enhanced homogeneity furnishing superior transparency and improved modulus.

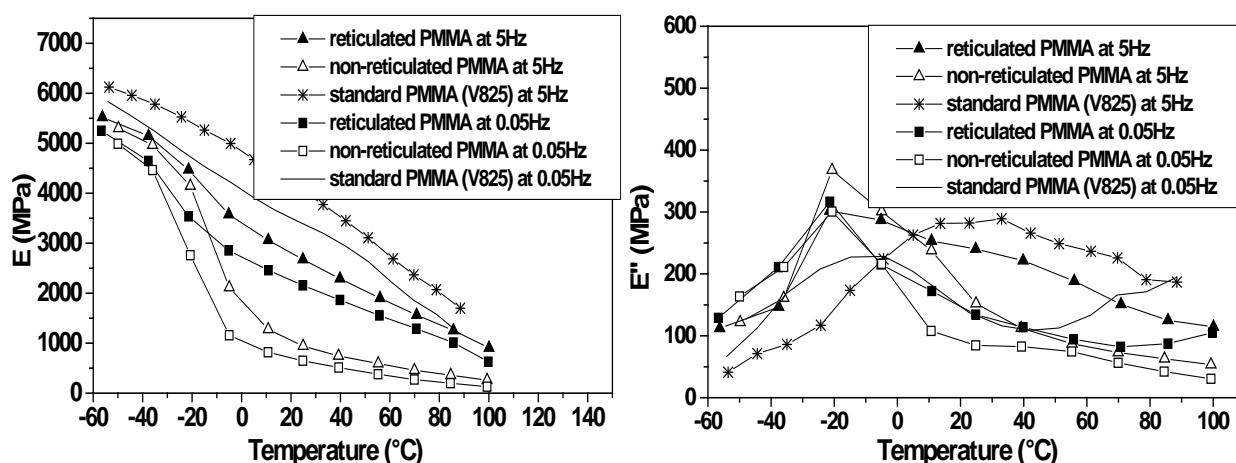


Figure 4.63 Effect of reticulation on Young's modulus E (on the left) and on loss modulus E'' (on the right) of PMMA at different temperatures. (The results of experiments at 0.5 Hz showed similar trend).

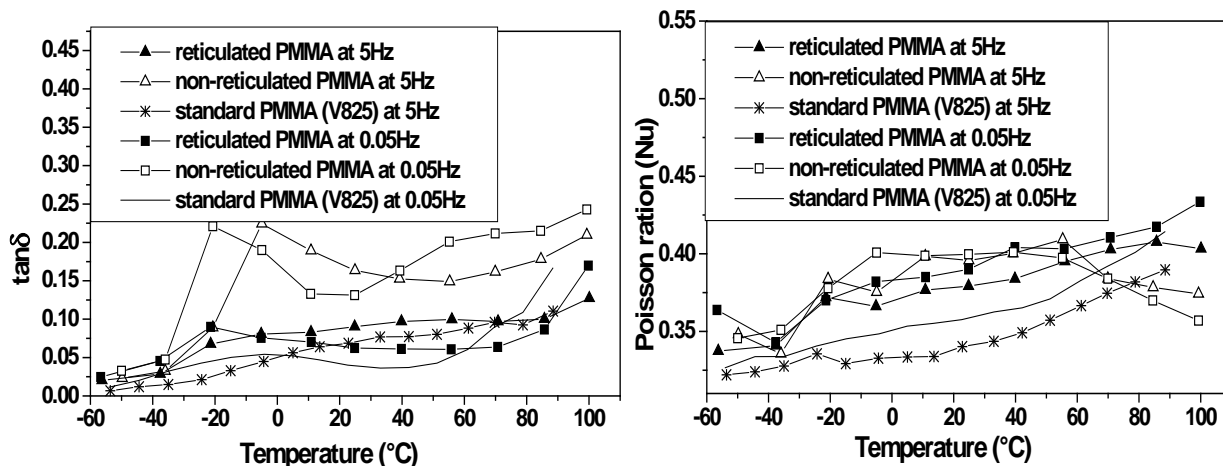


Figure 4.64 Effect of reticulation on loss factor  $\tan \delta$  (on the left) and on Poisson ratio Nu (on the right) of PMMA at different temperatures. (The results of experiments at 0.5 Hz showed similar trend).

#### 4.2.4.2.2 Nominal and shear stress and strain at break

Like Young's modulus, the nominal stress and nominal strain at break has been decreased by the introduction of PBA in PMMA but the reticulation of such a PMMA containing PBA increases again the nominal stress and nominal strain at break (Figure 4.65). However, the shear stress and the shear strain at breakage of PMMA is generally increased at lower temperature but is decreased at higher temperature by the presence of PBA. The reticulation of such a PMMA further increases the shear stress but decreases the shear strain at break a little bit (Figure 4.66). It is interesting to note that the effect of increasing temperature on shear stress at break is almost negligible for standard PMMA but the shear stress at break for reticulated and non-reticulated PMMA is decreased significantly with increasing temperature. The results shown correspond to experiments at traction strain rate =  $10^{-3} \text{ s}^{-1}$ . The experiments at traction strain rate =  $10^{-1} \text{ s}^{-1}$  showed similar trend. Moreover, the values at  $80^{\circ}\text{C}$  correspond to the point at which nominal/shear stress becomes constant as the sample was not broken for given set of parameters.

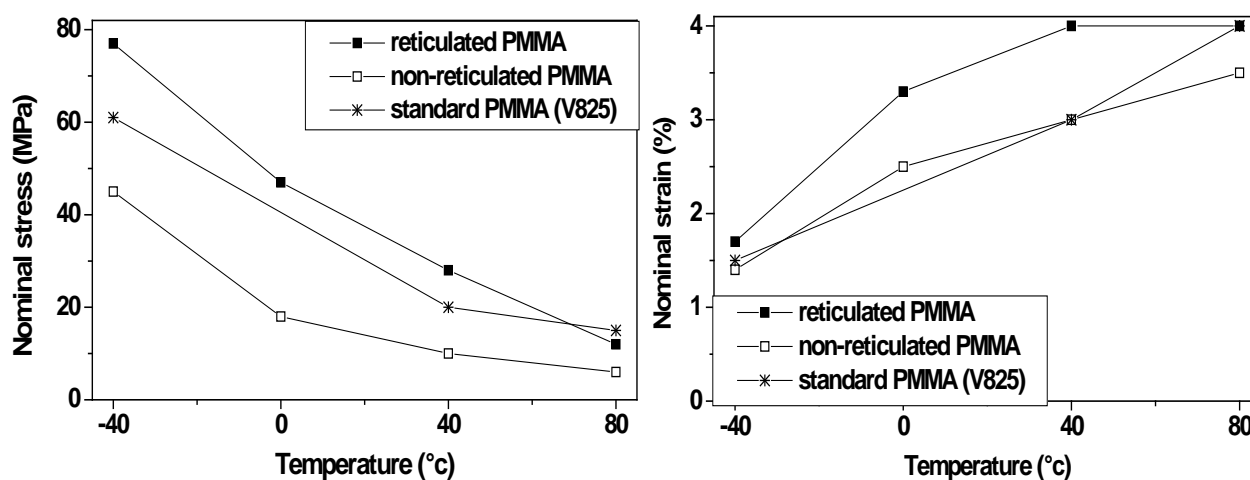


Figure 4.65 Effect of reticulation on nominal stress (on the left) and on nominal strain at break (on the right) of PMMA at different temperatures.

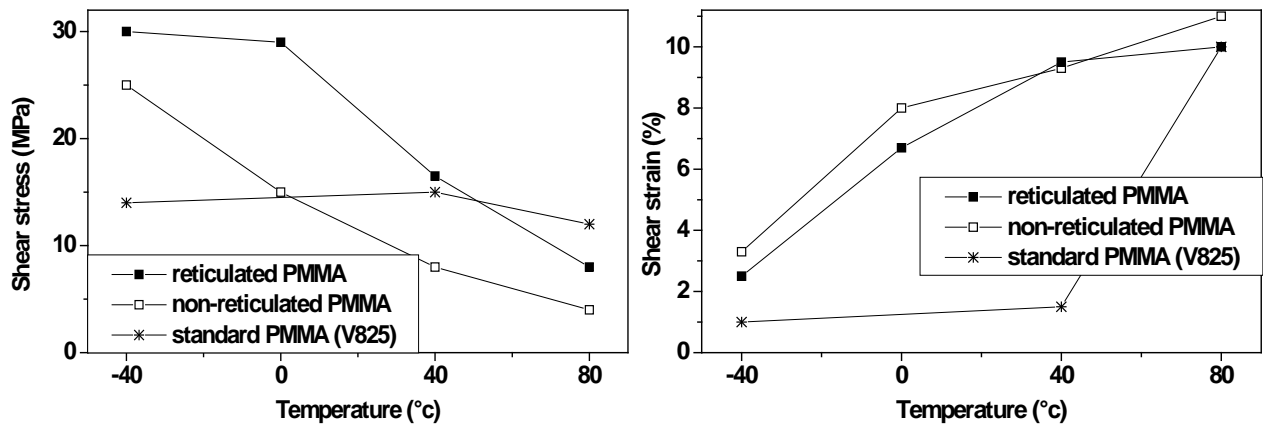


Figure 4.66 Effect of reticulation on shear stress (on the left) and on shear strain at break (on the right) of PMMA at different temperatures.

#### 4.2.4.3 Conclusions

Following conclusions can be drawn:

1. The coefficient of friction of PMMA is increased by the reticulation.
2. The change in friction coefficient by reticulation is associated with the nature of the contact between the tip and the polymer surface.
3. PMMA containing PBA whether reticulated or not, display a lower friction coefficient at higher temperature as compared to that at moderate or lower temperature.
4. The heat treatment at higher temperature reduces the friction coefficient of both reticulated and non-reticulated PMMA and this reduction is more significant in case of reticulated PMMA. This behaviour may be attributed due to the presence of nano structured PBA.
5. The poor transparency of the non-reticulated PMMA indicates that presence of PBA furnishes a comparatively heterogeneous composition. However, reticulation improves the homogeneity and gives an enhanced transparency.
6. Bulk mechanical properties of PMMA like Young's modulus and loss modulus are decreased by the presence of PBA. But these values are improved by the reticulation whereas loss factor and Poisson ratio are increased by the presence of PBA and reticulation decreases these values a little bit.
7. Generally speaking, nominal stress and nominal strain at break are decreased by the presence of PBA. However, these values are again increased by the reticulation.
8. Shear stress at break are increased by the reticulation and by the presence of PBA but shear strain at break is increased by the PBA but is decreased a little bit by the reticulation.

### 4.3 Gratifying findings

- The friction coefficients of polymers like PMMA can be decreased significantly by using an appropriate plasticizer like Erucamide and Stearyl erucamide or Crodamide-212. It is found that the fatty acid amides are effective slip agents only when present in lower amount with the exception of Stearyl erucamide. This is probably due to their gumming effect in case of their excessive amounts as discussed by Wypych [52]. The use of Erucamide up to 0.05 wt%, Behenamide up to 0.1 wt% and Stearamide up to 0.1 wt% gives maximum reduction in friction coefficient. Further increase in their contents has adverse effect on reduction of friction coefficient. The use of Crodamide-212 is beneficial in that the friction coefficient decreased directly with its increasing content and so one can reduce the friction excessively by increasing

its content. On the other hand, in case of Erucamide or other fatty acid amides, it is useful only in lower amount and so the drop off in the friction coefficient is limited. The plasticizer like PEG, Behenamide and Stearamide are not found as effective as Erucamide or Stearyl erucamide (Crodamide-212) in decreasing the friction coefficient of PMMA.

- The decrease in friction coefficient is associated with the nature of the contact as is clear from the values of rear contact angle. The friction is decreased by modifying the nature of the contact between the two surfaces and the plasticizer introduces the visco elasticity in a plastic contact and enhances the elasticity in an elastic plastic contact.
- The friction coefficient is decreased by the appropriate plasticizer without changing much the bulk mechanical behaviour of PMMA like Young's modulus, yielding stress and strain, nominal and shear stress and strain at break and so on. However, it is interesting to note that yielding strain at the contact is increased significantly for the samples showing decreased friction coefficient. It is surprising that the decreased friction coefficient is not reflected in a significant change in surface free energy. The surface energy of the pure PMMA and that of low friction plasticized samples is found to be almost same. It can be said to be in agreement with the work of H. Berro [85] and that by Podgornik [84] but is in contrast to the work of M. Minn [21]. Similarly no any clear relation could not be found between decrease in friction coefficient and the subsequent change in the bulk mechanical properties close to the surface as determined by the nano indentation for the low friction plasticized PMMA. The change in bulk behaviour with respect to the depth as measured by nano indentation is found to be almost similar for the pure PMMA as well as for the plasticized samples.
- The friction coefficient of pure PMMA is neither changed significantly by physical ageing at room temperature nor by heating treatment at higher temperature. However, the advantage of decreased friction coefficient obtained from an appropriate plasticizer is not permanent. The friction coefficient of plasticized PMMA is increased slowly by the physical ageing even at room temperature or by a heating treatment at higher temperature. This is due to evaporation of the plasticizer molecules to the atmosphere.
- Any slip additive like fatty acid amides effective for reducing the friction coefficient of a specific grade of a polymer may not be effective for another grade of the same polymer. It is found that the fatty acid amides are more effective for PMMA having lower  $T_g$ .
- The coefficient of friction of PMMA is increased by the reticulation. PMMA containing PBA whether reticulated or not, display a lower friction coefficient at higher temperature as compared to that at moderate or lower temperature. Similarly the heat treatment at higher temperature reduces the friction coefficient of both reticulated and non-reticulated PMMA. This anomalous behaviour may be attributed due to the presence of nano structured PBA. It may be assumed that at higher temperature the soft elastomeric PBA migrates to the surface resulting in a decreased friction coefficient. The poor transparency of the non-reticulated PMMA indicates that the presence of PBA furnishes comparatively a heterogeneous composition. However, reticulation improves the homogeneity and gives an enhanced transparency. Bulk mechanical properties of PMMA like Young's modulus and loss modulus are decreased by the presence of PBA. But they are improved to some extent by the reticulation. On the other hand, the loss factor and the Poisson ratio are increased by the presence of PBA and the reticulation decreases these values a little bit. Generally speaking, nominal stress and nominal strain at break are decreased by the presence of PBA. However, they are again increased by the reticulation. Shear stress at break are increased by the reticulation and by the presence of PBA but shear strain at break is increased by the PBA but is decreased a little bit by the reticulation.

## 5 Simulations by finite element method

### 5.1 Introduction

Any form of scratch tests is a form of controlled abrasive wear and thus it seems reasonable to use such academic tests, not only as a simple means of ranking the materials for their likely resistance to abrasion in service, but also as a reproductive means of assessing the mechanical properties of surfaces. These experiments allow the normal and tangential loads to be applied in a controlled way, and then to evaluate the mechanical response of given surfaces as a function of different experimental parameters, in order to reproduce the nature of the contact in service. As described analytically for elastic contact, scratch testing leads to (i) compressive stresses in front of the indenter, (ii) tensile stresses behind the indenter, and (iii) shearing strain caused by friction between the indenter and the tested surface [67].

As compared to static normal indentation, during the last decades a few studies have been done using finite element approach investigating the mechanics for scratching with conical indenter geometry and often for frictionless contact, in the case of elastic–plastic materials. Recently, similar studies coupling the experimental results and finite element analysis have described the mechanical behaviour of amorphous polymeric surfaces, especially the transition between quasi elastic and ductile ploughing regimes during scratch with spherical indenter, accounted for the influence of the mean contact strain  $a/R$  and the local friction coefficient  $\mu_{loc}$  [67].

All transitions between (i) elastic sliding and elastic–plastic contact or (ii) elastic–plastic contact and plastic scratching can be described using the finite element approach. The main objective of numerical analysis is to study the effect of friction coefficient and of the contact strain on various parameters during sliding and to define the boundary conditions for the transitions from fully elastic to elastic plastic contact and from elastic plastic to fully plastic scratching process as a function of the mean contact strain  $a/R$  and the local friction coefficient  $\mu_{loc}$ . The material is modelled as an elastic linear hardening plastic material, whose rheological parameters correspond to mechanical properties of an amorphous thermoplastic polymer (PMMA).

### 5.2 Finite element modelling

The scratch tests using the spherical indenters having different radii  $R$  and different penetration depths  $h_t$  were modelled with a three-dimensional finite element code. All calculations were carried out with the implicit FEM package MSC Marc<sup>®</sup>; already successfully used and reported by various researchers [2, 67, 88]. The schematic illustrations of the FEM model for  $a/R$  ratio of 0.5 are presented in Figure 5.1. The domain was modelled as a quarter of a cylinder and to limit the number of elements, it is reduced to half by means of a symmetrical plane (AA'BB' plane  $x = 0$ ). A specific finite element mesh was developed defined by 3 zones, with different sizes of bilinear isoparametric 8-noded brick elements, allowing linear interpolation. The simulations required 24,045 elements and 21,240 nodes. The mesh was refined under the contact area, so that about 95 elements are in contact with the indenter during scratch, for all studied scratching conditions (Figure 5.2). During indentation and scratching phases, the thickness of the smallest element in the contact area was at least 0.3 times the imposed penetration depth. The domain size (the total length  $L_m = 27.2 \mu\text{m}$  and the radius  $r_m = 10.3 \mu\text{m}$ ) was chosen to be sufficiently large so that the boundary effects did not affected the results. The tip radius  $R$  and the penetration depth  $h_t$  were selected to obtain different  $a/R$  ratios (varying between 0.025 and 0.6) and to give a constant

contact radius of about  $1.5 \mu\text{m}$  that affected the same number of elements during indentation and scratch phases for each value of  $a/R$  (Table 5.1). The distance of the indentation from the edge of the sample (along the  $z$ -axis) was more than 5 times the contact radius of the indentation, while the thickness of the sample (along the  $y$ -axis) was at least 23 times the depth of penetration. As boundary conditions, the  $x$ ,  $y$  and  $z$  displacements of the nodes on the cylindrical surface ( $C'CBB'$ ) were defined to be null.

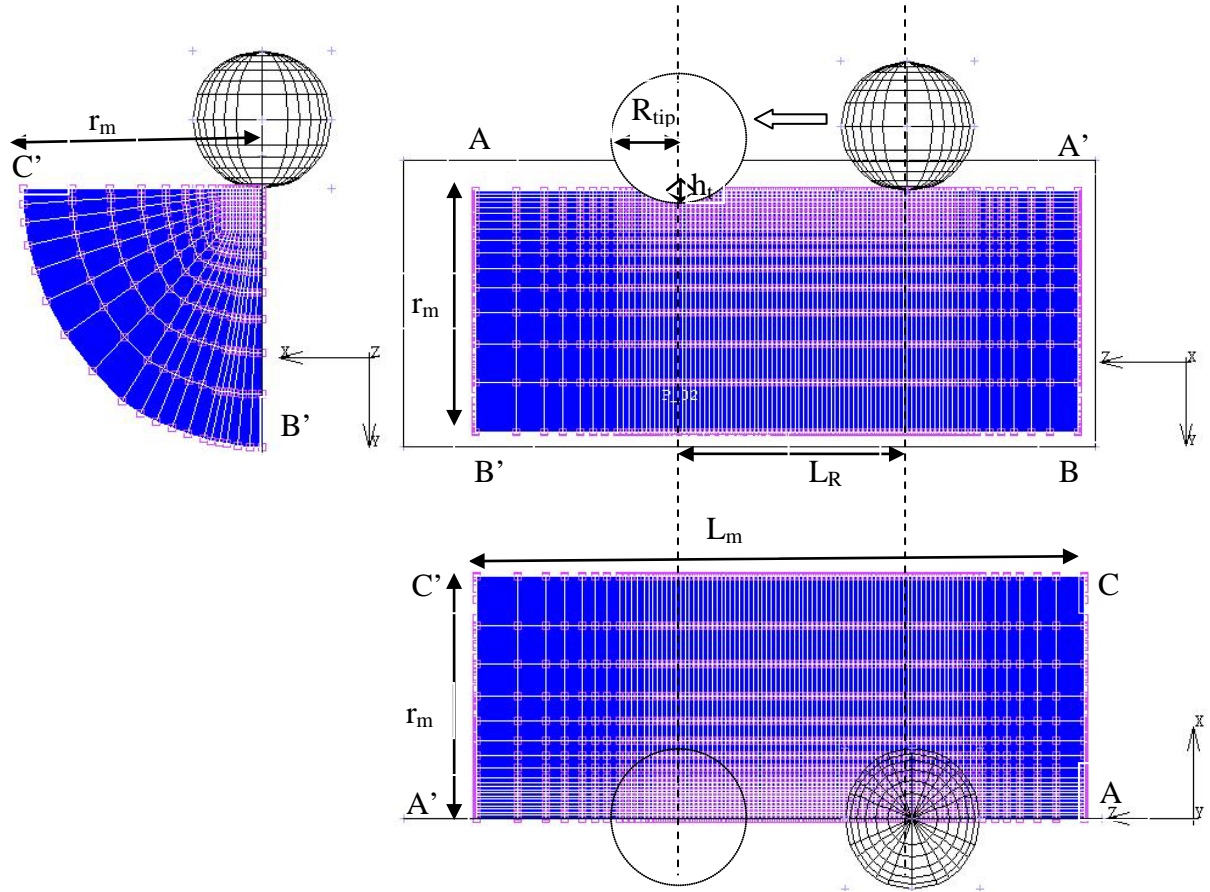


Figure 5.1 Views of the spherical indenter and the mesh used for the finite element simulations of scratch test ( $a/R = 0.5$ ).

Assuming that the experimental results are obtained at a given temperature and constant sliding speed, the analysis may be performed for simple elastic–plastic behaviour. The situation is modelled as being quasi-static and as time-independent, with no influence of the strain rate. In order to reproduce experimental tests, the kinematics may be divided into two distinct phases: (i) a first step, corresponding to the indentation process (along the  $y$ -axis) at a given penetration depth and (ii) a second step, corresponding to the scratching process (along the  $z$ -axis) at constant relative velocity and fixed indentation depth for a given value of  $a/R$  ratio. The analysis of the frontal and lateral path plots obtained from FEM allows the determination of the true contact depth and then the true contact radius during both indentation and scratch phases. The length of the scratch  $L_R$  is chosen so that the normal and tangential loads applied to the indenter reach a steady state. The length  $L_R$  (about  $10 \mu\text{m}$ ) is fixed and corresponds to a ratio  $L_R/a_0$  of more than 6, depending on the simulated ratio  $a/R$  (see Table 5.1).



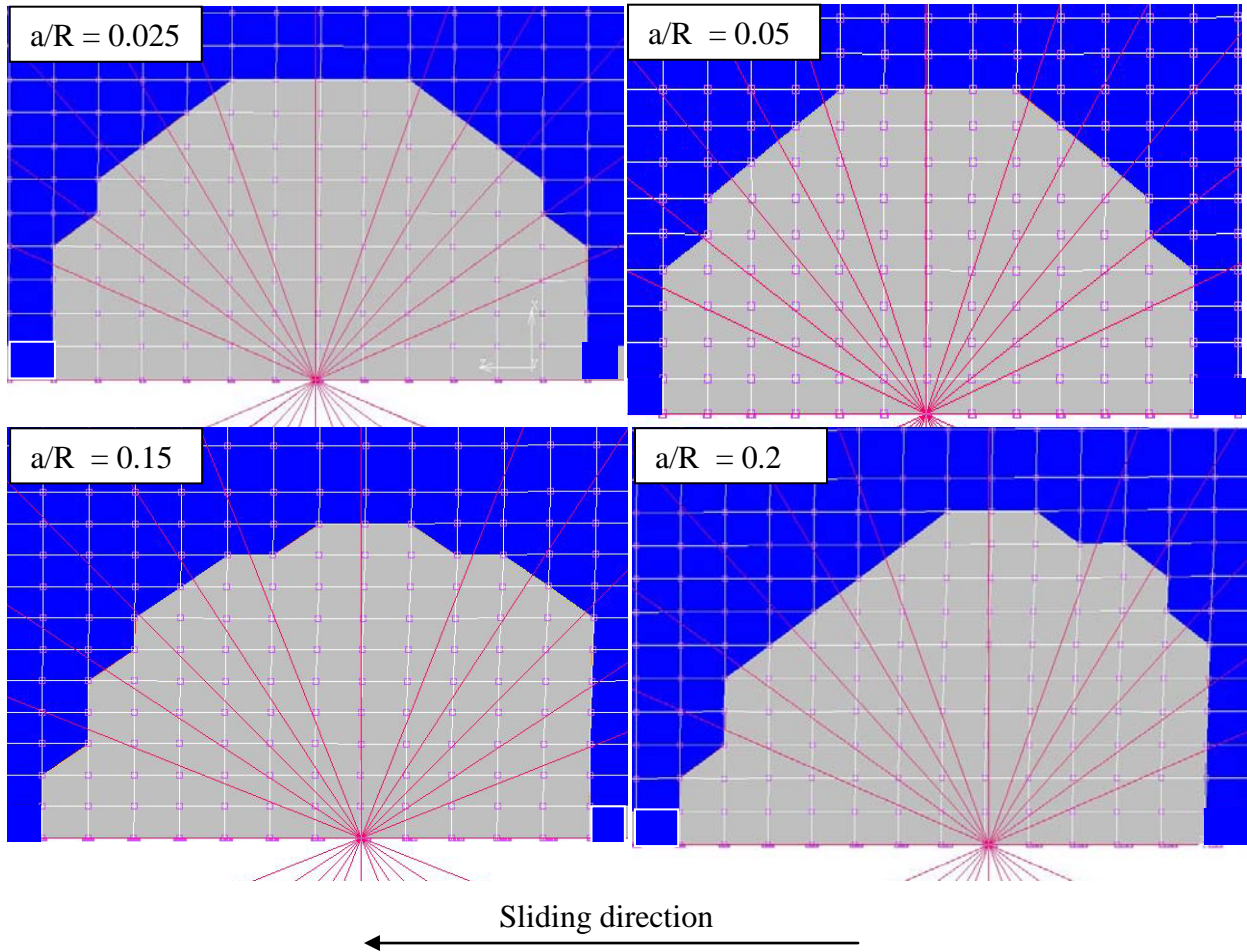


Figure 5.2 The contact status at  $\mu_{loc} = 0$  for different  $a/R$  ratios displaying the almost same number of elements of the material in contact with the indenter during sliding/scratching.

Imposed a/R ratio	Tip radius $R(\mu\text{m})$	Penetration depth, $h_t(\mu\text{m})$	Estimated contact radius, $a_0(\mu\text{m})$	Calculated contact radius, $a_f(\mu\text{m})$	$a_f/a_r$	Calculated ( $a_f/R$ )	Calculated $[a_f/(R^2 - a_f^2)^{0.5}]$	$L_m/a_0$	$r_m/h_t$	$r_m/a_0$	$L_R/a_0$
0.025	60	0.02	1.55	1.27	1.16	0.0212	0.0212	17.6	515	6.6	6.4
0.05	30	0.04	1.55	1.20	1.10	0.0401	0.0402	17.6	258	6.6	6.4
0.075	20	0.05	1.48	1.20	1.09	0.0598	0.0599	18.4	189	6.9	6.9
0.1	16.07	0.07	1.55	1.30	1.16	0.0793	0.0795	17.5	137	6.6	6.4
0.15	10.71	0.11	1.56	1.31	1.06	0.1225	0.1234	17.5	90	6.6	6.4
0.2	7.5	0.15	1.50	1.30	1.04	0.173	0.176	18.1	67	6.9	6.6
0.3	5.0	0.23	1.50	1.47	1.01	0.294	0.307	18.2	45	6.9	6.6
0.4	3.5	0.29	1.40	1.40	0.95	0.40	0.44	19.4	35	7.3	7.0
0.5	3.0	0.4	1.50	1.66	1.06	0.55	0.66	18.2	26	6.9	6.6
0.6	2.25	0.45	1.35	1.47	0.96	0.65	0.86	20	23	7.6	7.3

Table 5.1 Main geometrical characteristics of the finite element model for  $\mu_{loc} = 0$ .  $a_0$  is the imposed contact radius, assuming no elastic deflection and no plastic yielding around the moving indenter [ $a_0 = (2Rh_t - h_t^2)^{0.5}$ ], where  $h_t$  is the imposed penetration depth.

In all simulations performed in this study, the spherical indenter was assumed to be rigid and the rheology of the material to be elastic–plastic. The yield condition is given by von Mises’ yield criterion whereas the stress–strain curve was specified according to modified G’Sell-Jones law [17, 88, 89]:

$$\sigma = K \dot{\epsilon}_{vp}^m \exp(h_g \epsilon_{vp}^2) \quad 5.1$$

where  $\sigma$ ,  $\dot{\epsilon}_{vp}$  and  $\epsilon_{vp}$  are true stress, true strain rate and true strain respectively whereas  $K$ ,  $m$  and  $h_g$  are the rheological parameters. The G’Sell-Jones law can be written in its simplified form as [17, 88]:

$$\sigma = \sigma_y \exp(h_g \epsilon_{vp}^2) \quad 5.2$$

where  $\sigma_y$  is the yield stress obtained from the compression test. Despite the fact that the elasticity of polymers is often non-linear at a given temperature and strain rate, the elastic behaviour is modelled by a linear incremental law defined by Young's modulus  $E$  and Poisson's ratio  $\nu$ , both taken to be constant as previously used by H. Pelletier et al. [88]. The elastic modulus, the yield stress and Poisson's ratio are assumed to be constant and are fixed as  $E = 3.2$  GPa,  $\sigma_y = 100$  MPa,  $\nu = 0.39$ . The rheological parameter  $h_g$  was taken as 0.5 as already used successively by H. Pelletier et al. [17, 88]. This simplified model is close to the true rheology of PMMA as shown in Figure 5.3. The interface between the rigid indenter and the deformable surface is not assumed to be frictionless and frictional effects are included in the analysis by means of an isotropic Coulomb model. Thus, the maximum local shear stress  $\tau_c$  acting at the interface is given by

$$\tau_c = \mu_{loc} p \quad 5.3$$

where  $p$  denotes the local normal pressure and  $\mu_{loc}$  is the coefficient of the local friction between the surfaces in contact [2, 67]. The contact model was implemented in the context of a finite sliding formulation, where arbitrary sliding and rotation between the surfaces could occur. At each ratio  $a/R$ , simulations were performed for different values of the local friction coefficient in the range 0–1.3 in order to identify the boundary conditions for the transitions between different natures of contact.

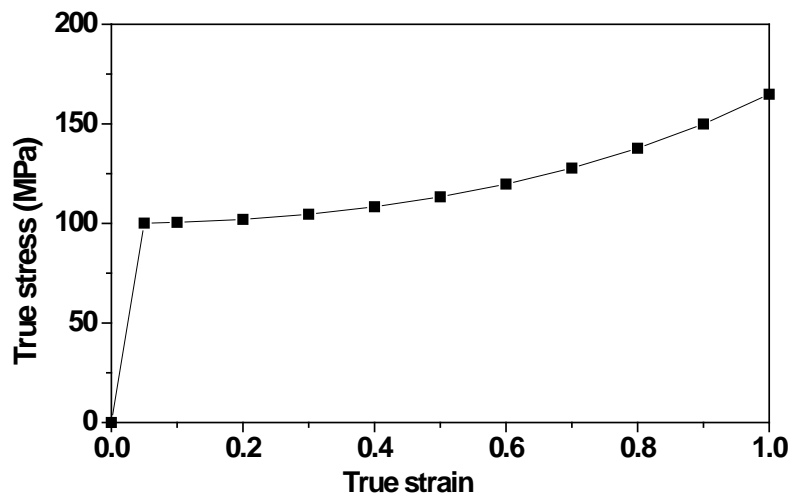


Figure 5.3 The rheological behaviour of PMMA used for the three dimensional simulation of scratch test calculated from equation 5.2.

For each ratio  $a/R$ , the accuracy of the simulation runs is quite similar because the number of elements and nodes in the contact area is almost constant. This limitation is necessary when automatic remeshing box is not used during indentation and scratch phases. All developed FE models for different  $a/R$  ratio used in the present study have validated for purely elastic contacts (elastic sliding contact). Using finite element modelling of indentation and here of scratch experiments, many important data can be extracted, for example the apparent and ploughing friction coefficients, the rear contact angle, the average contact pressure, the maximum contact pressure, the horizontal and shear stresses, the elastic recovery, the elastic and/or plastic strain fields, the frontal and lateral nodal profiles and so on in order to compare easily the results about the contact geometry deduced from the specific experimental setup with those deduced from FEM.

The average contact strain imposed during scratch experiment can be determined (assuming a ratio  $a_f/a_r$  close to 1, where  $a_f$  and  $a_r$  being contact radius at frontal and lateral side) by the relation:

$$a/R = a_c / (R^2 - a_c^2)^{0.5} \quad 5.4$$

with  $a_c = a_f$  in first approximation. This assumption has been verified numerically for all scratch conditions, with a ratio  $a_f/a_r$  varying between 0.95 and 1.16 whatever are the imposed mean strain  $a/R$  and the friction coefficient.

## 5.3 Simulation results and discussion

### 5.3.1 Effect of local friction coefficient and contact strain on various parameters during sliding/scratching

#### 5.3.1.1 Apparent and ploughing friction coefficient

The apparent friction coefficient was taken as the ratio of normal load to the tangential load applied to the indenter whereas the ploughing friction coefficient was calculated simply as the difference between the apparent friction and the imposed local friction coefficient. However, the ploughing friction coefficient is not always equal to the difference between apparent and local friction coefficient as discussed in chapter 3. It is also clear from the results given by simulation since it is observed that the ploughing friction for very low contact strains is less than zero which is not logical. The effect of local friction and  $a/R$  ratio on apparent and ploughing friction is insignificant at lower values but becomes significant for higher values. At a constant local friction coefficient, the apparent and the ploughing friction coefficient remain almost constant with increasing  $a/R$  ratio till the contact strain reaches 0.1. On further increase in contact strain, apparent and ploughing friction coefficient increase significantly and the effect increases with increasing local friction coefficient as shown in Figure 5.4. Similarly for a given lower contact strain, ploughing friction coefficient is very small and both apparent friction coefficient and the local friction coefficient are almost equal (till local friction coefficient = 0.4).

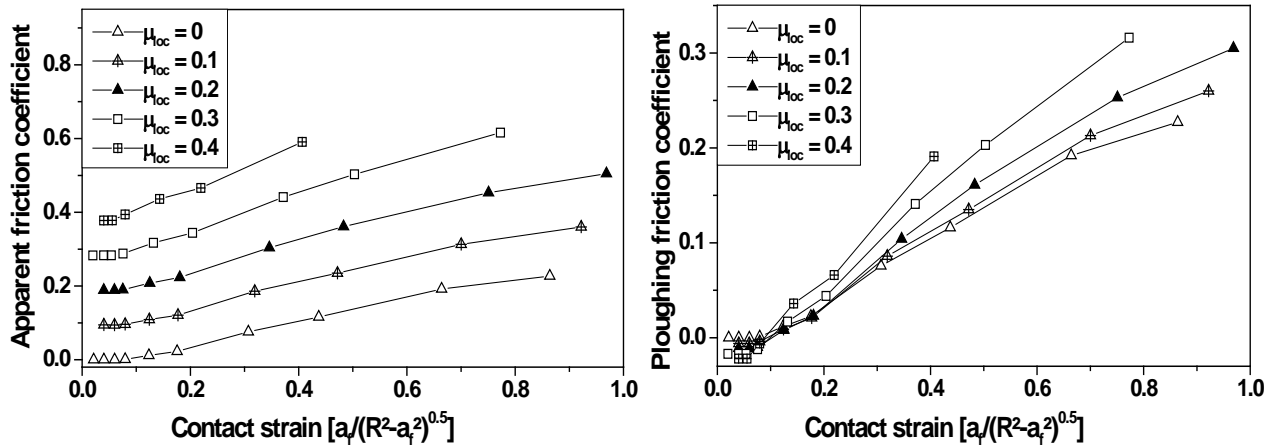


Figure 5.4 Variation of the apparent friction (on the left) and of the ploughing friction coefficient (on the right) with contact strain at room temperature.

### 5.3.1.2 The rear contact angle (omega)

For very low and very high values of  $a/R$  ratio, there is no any significant effect of either local friction coefficient or  $a/R$  ratio on the rear contact angle, as the nature of the contact is fully elastic at very low  $a/R$  value (up to 0.1) for all friction coefficients and is fully plastic for high values of  $a/R$  ratio (Figure 5.5). However, at intermediate contact strains or during the elastic plastic domain of contact, the value of rear contact angle decreases significantly with increasing contact strain. Moreover, the elastic plastic domain is increased by decreasing the friction coefficient. These findings are in well agreement with that stated by Gauthier et al. [57] and as discussed in section 2.5.4.3. For a given lower  $a/R$  ratio (up to 0.1), the effect of friction coefficient on omega is not significant for its lower values (up to 0.4) but it becomes significant for higher values of contact strain and the omega is decreased rapidly with increasing friction coefficient. It is evident that the scratch limiting contact strain (after which the value of omega becomes almost constant for increasing contact strain) decreases with increasing friction coefficient. For example, it is about 0.7 for  $\mu_{loc} \leq 0.1$  that is decreased to about 0.2 for  $\mu_{loc} = 0.4$ . These findings are in agreement with experimental data obtained by the micro-visio-scratch apparatus. It is clear that the values of rear contact angle estimated from the contact status are more realistic and interesting and therefore, these values will be used in the following sections.

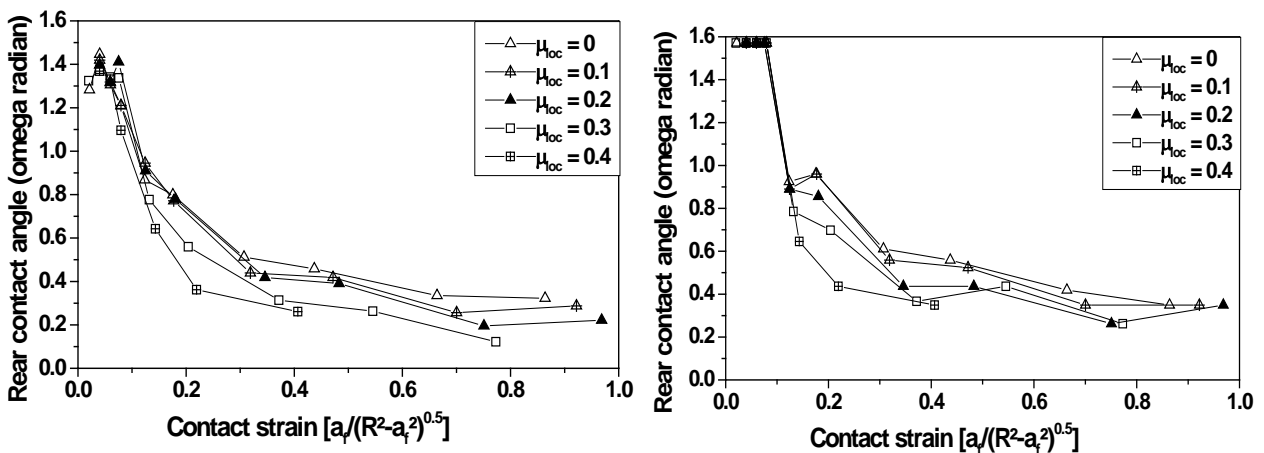


Figure 5.5 Variation of rear contact angle (calculated from contact radius on the left and estimated from the contact status on the right) with contact strain at room temperature.

### 5.3.1.3 Elastic recovery and pile up height

Similar effects of increasing  $a/R$  ratio and of increasing friction coefficient are observed on the geometrical shape of the residual flame, with a diminution of the elastic recovery at the bottom of the groove. These results are conformity of the work reported by H. Pelletier et al. [2]. The elastic recovery and pile up height depend mainly upon  $a/R$  ratio. Elastic recovery remains almost equal to 1 till contact strain 0.1 (independent of the local friction coefficient) as the contact is purely elastic at this contact strain for all friction coefficients. Then it decreases rapidly with increasing contact strain till the contact becomes fully plastic (at contact strain about 0.7) as shown in Figure 5.6. It is important to note that the variation of elastic recovery with increasing contact strain follow the almost same trend as that followed by the rear contact angle. So it is verified that the elastic recovery of the groove left may be estimated by the value of rear contact angle as discussed in section 2.5.4.3 and stated by Gauthier et al. [57]. For a given  $a/R$  ratio, the elastic recovery remains almost same for low & high friction conditions. Similar trend is observed as regards the effect of  $a/R$  ratio and the friction coefficient on the pile up height during sliding/scratching. However, it is in opposite direction to that of elastic recovery i.e. the pile up height increases with increasing  $a/R$  ratio for a given friction coefficient and there is no any significant effect of increasing friction coefficient on pile up height for a given  $a/R$  ratio. Moreover, it is almost same and close to zero for low contact strains (up to  $a/R \leq 0.1$ ) for all friction coefficients as the nature of the contact is purely elastic during these sliding conditions. Similarly, the pile up height becomes again almost constant during fully plastic contact for higher contact strains (at  $a/R \geq 0.7$ ).

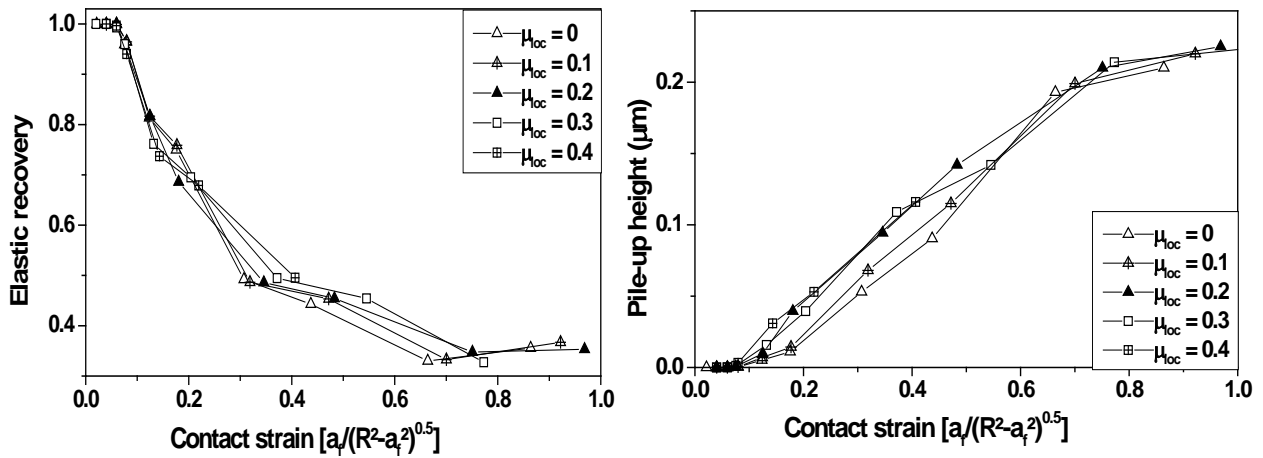


Figure 5.6 Variation of the elastic recovery (on the left) and of the pile up height (on the right) with contact strain at room temperature.

### 5.3.1.4 Average contact pressure

The maximum normal contact pressure was obtained directly from the Mark software whereas the average contact pressure  $P_{av}$  was calculated by dividing the normal force  $F_N$  by the effective contact area  $A_c$  supporting the normal load. The effective contact area  $A_c$  can be written as:

$$A_c = A_T - A_r$$

5.5

where  $A_T$  is the total contact area defined as  $\pi a_f^2$ , assuming  $a_f \approx a_r$ ;  $a_f$  and  $a_r$  being the frontal and the rear contact radius respectively as are defined in Figure 5.7.  $A_r$  is rear side contact area due to elastic recovery of the polymer and is defined as:

$$A_r = \frac{a_f - a_r}{12\sqrt{a_f^2 - a_r^2}} [19 a_f^2 - 6a_f a_r - 13 a_r^2] \quad 5.6$$

The rear contact angle  $\omega$  may be calculated as :

$$\tan \omega = \frac{a_r}{l_r/2} = \frac{a_r}{\sqrt{a_f^2 - a_r^2}} \quad 5.7$$

where

$$l_r = 2\sqrt{a_f^2 - a_r^2} \quad 5.8$$

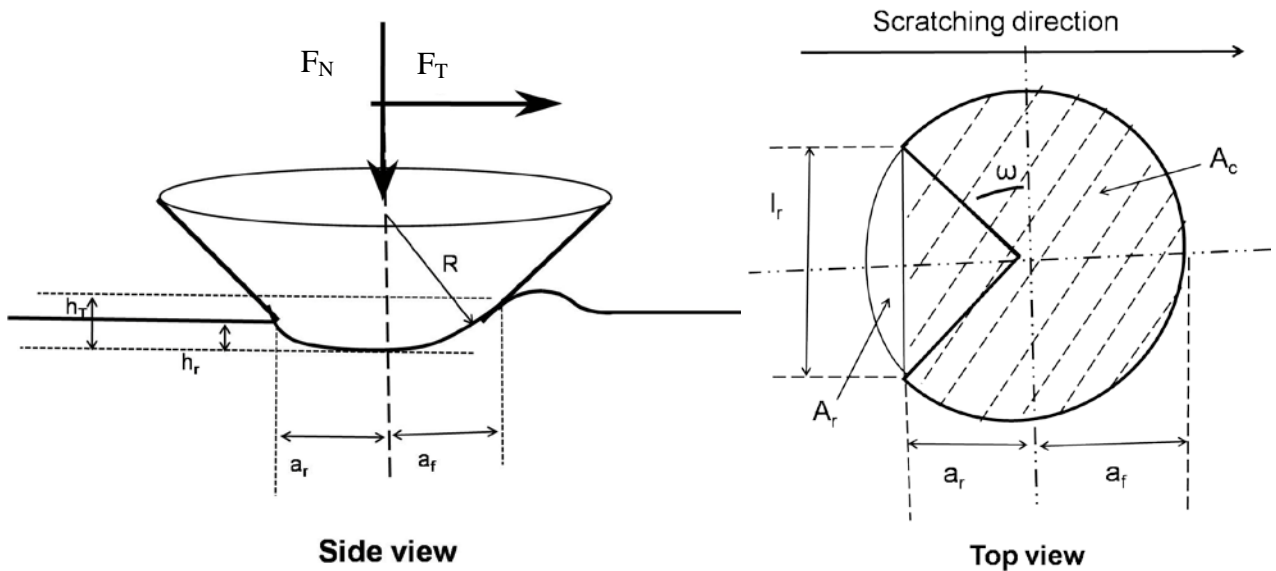


Figure 5.7 The definition of main geometrical parameters used to characterize the geometry of the contact during a scratch test with a spherical indenter.

Simulation results reveal that the average contact pressure also depends mainly upon  $a/R$  ratio like elastic recovery and pile up height. It increases with increasing contact strain at constant friction coefficient but for a given  $a/R$  ratio, it remains almost constant with increasing local friction coefficient. However, for very high contact strain, one may note a small effect of local friction on average contact pressure (Figure 5.8). It is very important to note that if we observe the variation of elastic recovery with increasing contact strain or that of the rear contact angle (Figure 5.5 and Figure 5.6), there is an abrupt change in their values at the contact strain of about 0.1 indicating the transition of the contact behavior from fully elastic to visco-elastic plastic contact. On the other hand, we don't see any remarkable change in average contact pressure at this contact strain (Figure 5.8). So it is confirmed that the transition between fully elastic contact and the elastic plastic contact appears at almost constant contact pressure as discussed in section 2.5.4.3 and stated by Gauthier et al. [57]. However, the small effect of increasing local friction on the mean contact pressure appears at contact strain = 0.1 i.e. in the beginning of the elastic plastic contact domain.

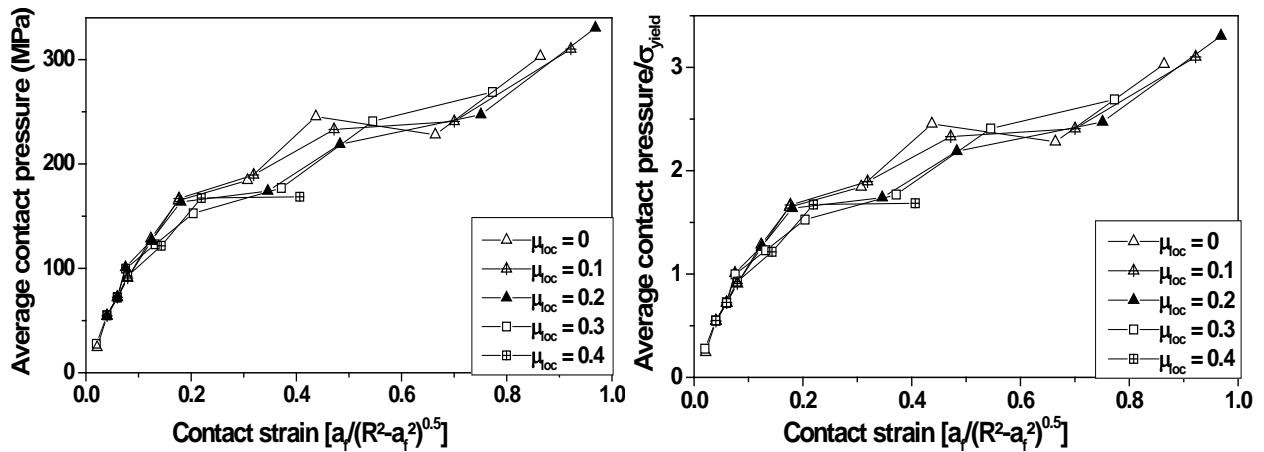


Figure 5.8 Variation of the average contact pressure (on the left) with contact strain and its normalised value (on the right) at room temperature.

### 5.3.1.5 Maximum contact pressure

Like average contact pressure and elastic recovery, the maximum contact pressure depends also mainly upon the contact strain i.e. it increases mainly with increasing contact strain. For a given  $a/R$  ratio, it remains almost constant with increasing local friction coefficient during elastic region i.e. for lower values of contact strain (at  $a/R \leq 0.1$ ) as shown in Figure 5.9. It may depend also on friction coefficient for higher contact strains. Moreover, at higher contact strains, not only the values of maximum contact pressure but also the slope of the curve changes significantly with increasing friction coefficient. It is in good accord with the literature as we know that for the visco elastic region, the slope of the maximum contact pressure vs contact strain curve depends upon friction coefficient [17]. It is interesting to note that the value of maximum contact pressure normalised by the average contact pressure is almost constant and unique (about 1.6) for lower and moderate values of both contact strain and the local friction coefficient (Figure 5.10). However, it increases for increasing local friction coefficient and increasing contact strain for very high values of local friction coefficient and contact strain. It is in good accord with the literature as the curve of the evolution of the normalized pressure ( $p_m/\sigma_y$ ) for the transition from elastic plastic to fully plastic contact as a function of the local friction showed that the contact yielding depended on the geometrical contact, i.e. the ratio  $a/R$  as proposed initially by Tabor [30], and on the true friction coefficient [2].

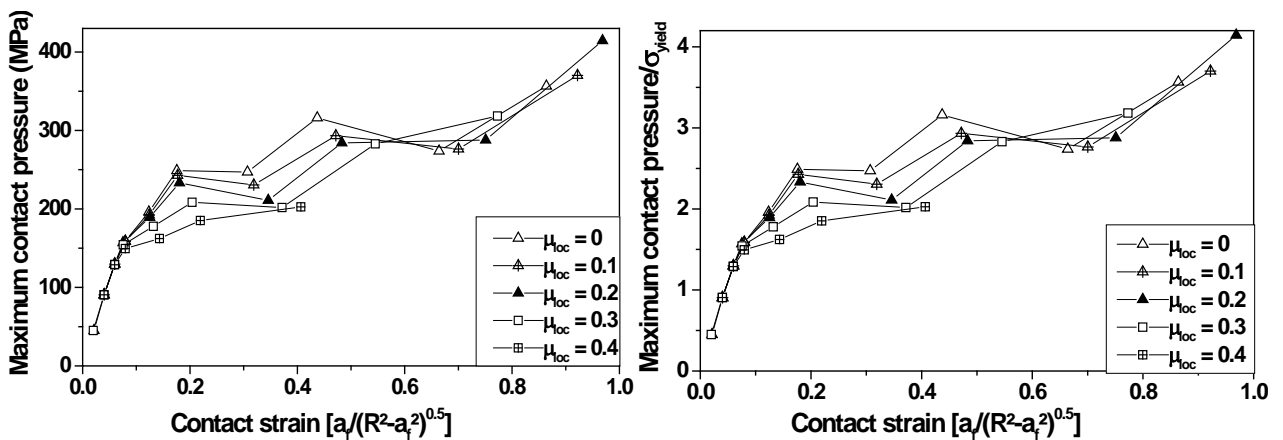


Figure 5.9 Variation of the maximum contact pressure (on the left) with contact strain and its normalised value (on the right) at room temperature.

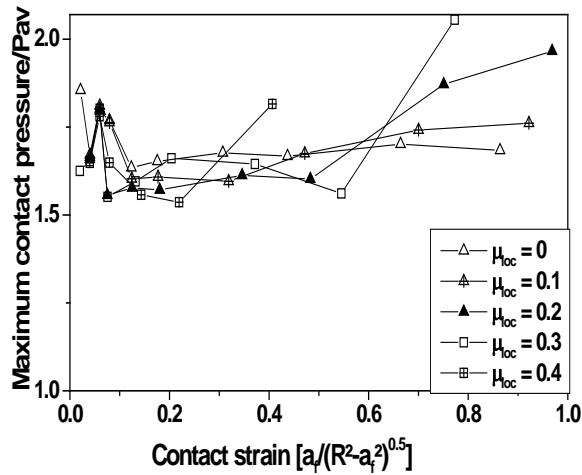


Figure 5.10 Variation of the maximum contact pressure normalised by average contact pressure with contact strain at room temperature.

### 5.3.1.6 Shear stress at maximum contact pressure and the maximum shear stress

The shear stress at maximum contact pressure as well as the maximum shear stress depends upon both contact strain and local friction coefficient (Figure 5.11 and Figure 5.12). However, this dependency is more significant at higher values. Furthermore, the local friction coefficient affects the shear stress much more than the contact strain. It is also interesting to note that the effect of increasing contact strain on normalised shear stress (by average contact pressures) is less significant as compared to simple shear stress especially for low and moderate friction coefficient.

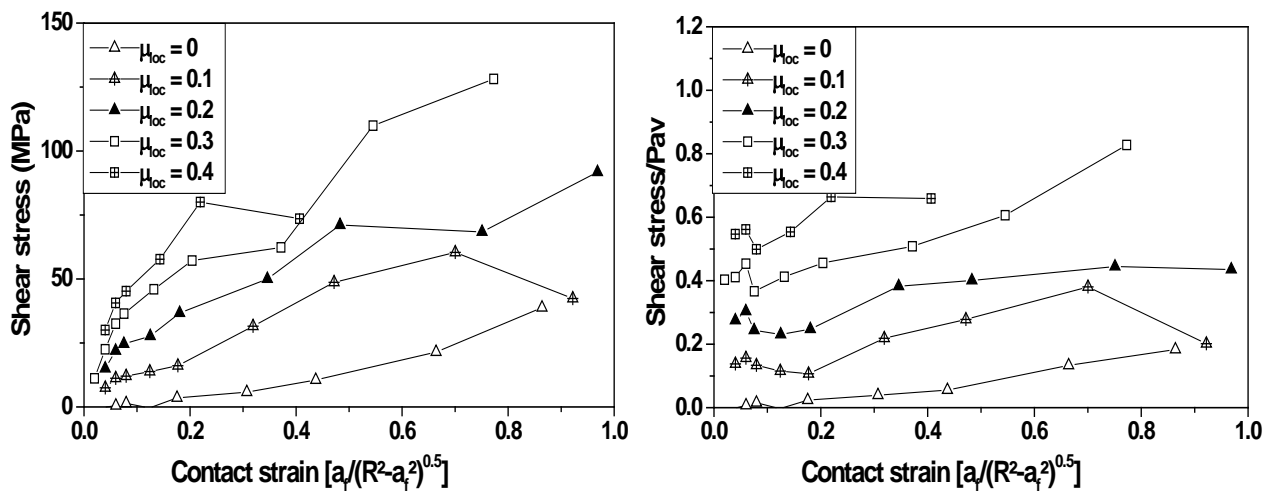


Figure 5.11 Variation of the shear stress at maximum normal pressure with contact strain (on the left) and its normalised value (on the right) at room temperature.



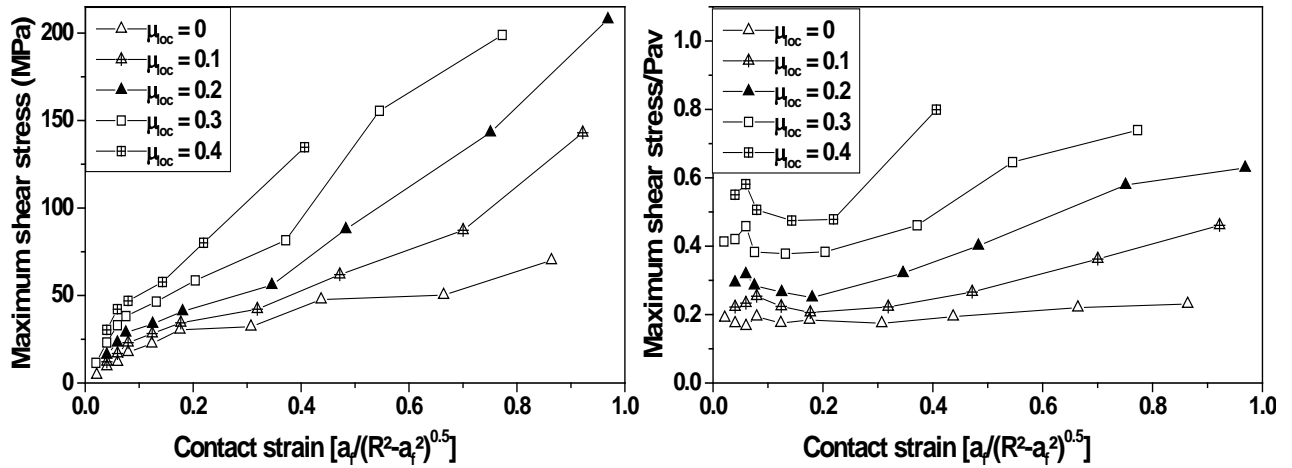


Figure 5.12 Variation of the maximum shear stress with contact strain (on the left) and its normalised value (on the right) at room temperature.

### 5.3.1.7 Horizontal stress at maximum contact pressure and the maximum horizontal stress

In elastic region, i.e. for low local friction coefficient and low contact strain, the horizontal stress (compressive in front of the tip and tensile behind the tip) at maximum contact pressure is almost constant for increasing local friction and depends upon contact strain. However, in elastic plastic and fully plastic regions, it depends both on local friction coefficient and contact strain (Figure 5.13). Moreover, it first increases with increasing contact strain (during elastic region) and then decreases on further increase in contact strain. This is in contrast to its normalised value (by average contact pressure) that remains almost constant (at about 1.2) during elastic region displaying no any significant effect of either increasing friction coefficient or increasing contact strain. However, during elastic plastic and fully plastic region, it decreases with increasing contact strain as well as with increasing friction coefficient.

It is remarkable to note that the maximum horizontal stress in front of the contact remains almost same for all sliding conditions during elastic contact. However, for an elastic plastic and fully plastic contact, it depends upon both the contact strain and the friction coefficient, i.e. it increases with both increasing contact strain and increasing friction coefficient (Figure 5.14). This dependency of horizontal stress on contact strain and on friction coefficient is more reactive at higher values during elastic plastic and fully plastic region. It is valuable to mention that the normalised maximum horizontal stress (by average contact pressure) depends mainly upon friction coefficient during elastic region and for a given friction coefficient, it remains almost constant with increasing contact strain (only in elastic region). However, during elastic plastic and fully plastic region, it depends upon both contact strain and local friction. It decreases with increasing contact strain and increasing friction coefficient.

It is also valuable to note that the maximum horizontal stresses in the contact does not depend upon the friction coefficient and that it changes abruptly with increasing contact strain only during fully elastic region as shown in Figure 5.15. For elastic plastic and fully plastic contacts, the effect of increasing the contact strain also becomes insignificant. Interestingly the normalised value of the maximum horizontal stresses in the contact remains almost same during fully elastic and fully plastic contact but it changes with increasing contact strain during elastic plastic contact domain. So the trend of horizontal stresses at the contact and in front of the contact is found to be entirely different.

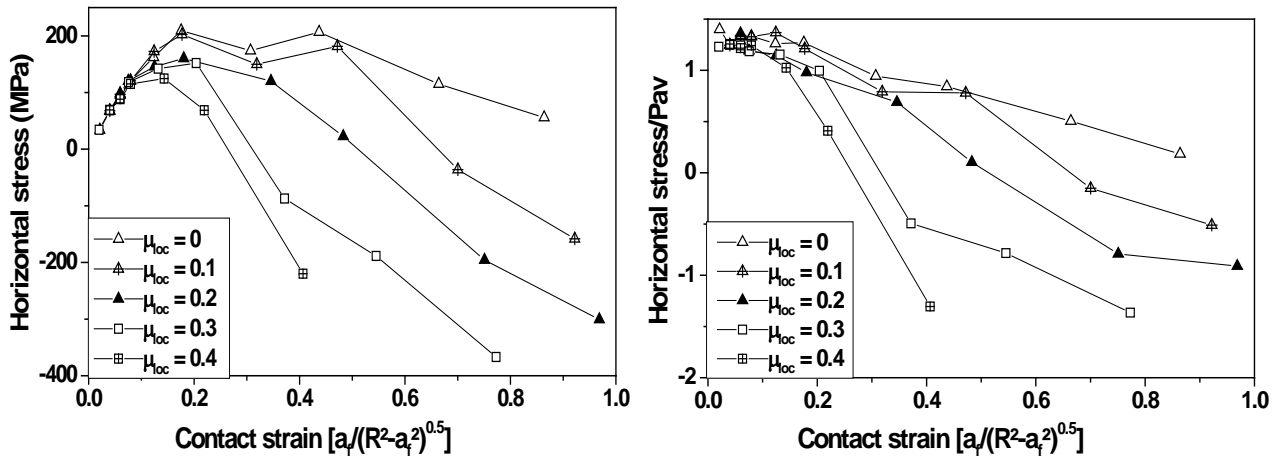


Figure 5.13 Variation of the horizontal stress at maximum normal pressure with contact strain (on the left) and its normalised value (on the right) at room temperature.

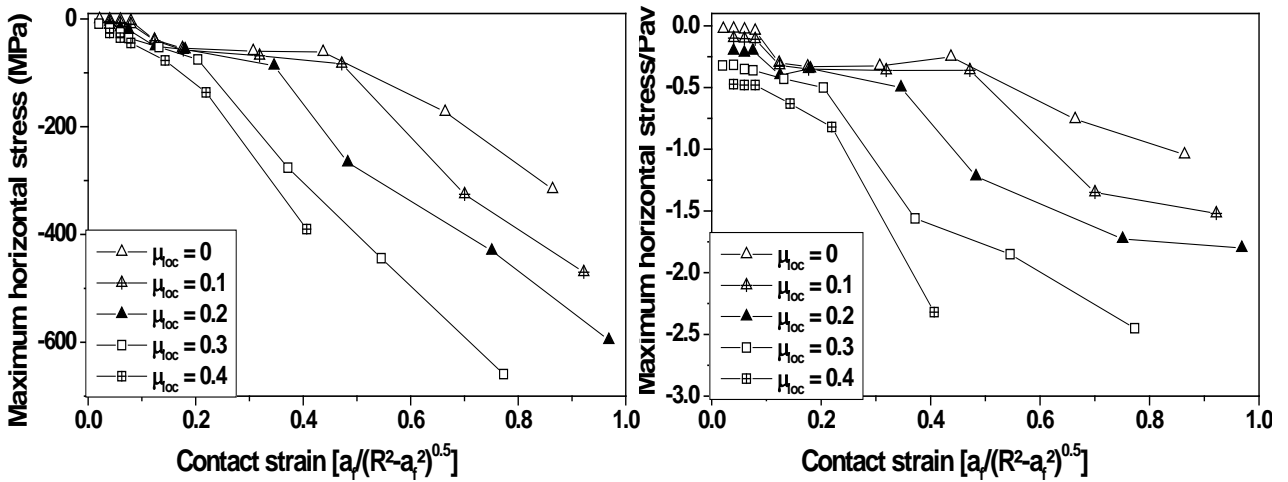


Figure 5.14 Variation of the maximum horizontal stress ahead of contact with contact strain (on the left) and its normalised value (on the right) at room temperature.

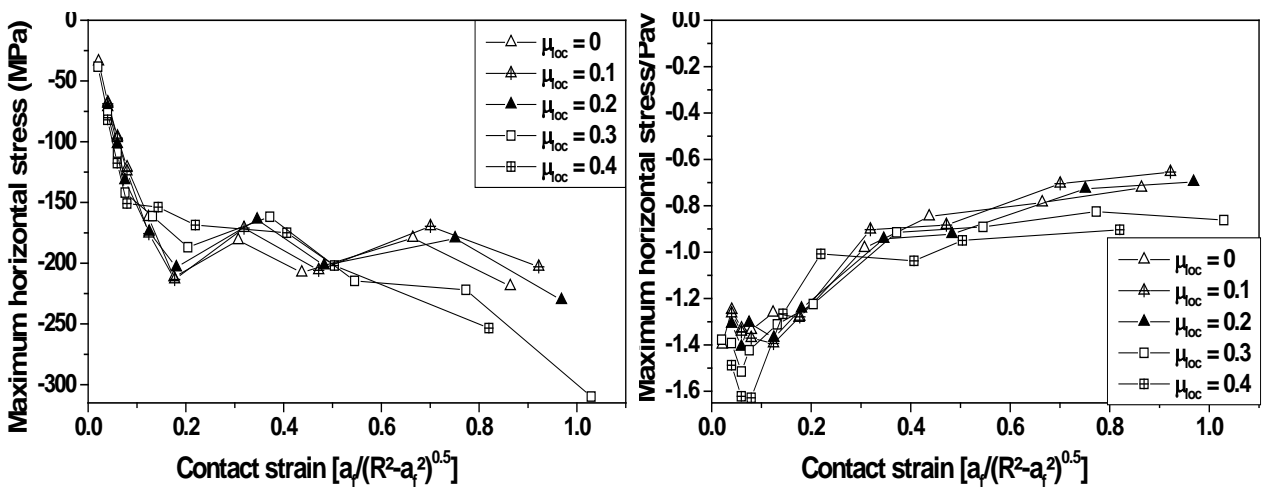


Figure 5.15 Variation of the maximum horizontal stress at the contact with contact strain (on the left) and its normalised value (on the right) at room temperature.

### 5.3.1.8 Equivalent plastic strain

In case of an elastic sliding of an indenter with a spherical tip, the distributions of the stress component and the corresponding strain on the surface of a semi-infinite solid are known and the influence of the true friction coefficient has been clearly demonstrated. The plastic strain field during scratching with a spherical tip is in fact very complex to describe, as it depends not only on the ratio  $a/R$ , but also on the strain hardening of the material [2]. Recently, modelling the contact between a spherical tip and a polymer surface using elliptical contact pressure and shear stress distributions, Gauthier et al. [17] performed numerical simulations to locate the boundaries between (i) fully elastic and elastic–plastic contact and (ii) elastic–plastic and fully plastic contact. The results of numerical simulations reveal the influence of the local friction coefficient on the plastic deformation in scratch experiments with a spherical indenter. Figure 5.16 and Figure 5.17 indicate that the local friction coefficient plays a similar role to the geometrical ratio  $a/R$  in the evolution of the plastic strain during a scratch test with a rigid spherical indenter. At low values of the friction coefficient (or for low values of  $a/R$  ratio), yielding may start well below the surface (and not at the surface), whereas for higher values of the friction coefficient yielding starts at the interface between the moving tip and the surface. The same level of maximal plastic strain can be obtained for various scratching conditions (for different values of  $a/R$  and  $\mu$ ). The FE simulation results reveal that with increasing local friction at constant  $a/R$  ratio or/and with increasing  $a/R$  ratio at constant local friction coefficient, there is

- (i) an increase in the level of plastic strain imposed beneath the moving tip and in the residual groove;
- (ii) a displacement of the location of the maximum plastic strain towards the sub-surface region just beneath the indenter;
- (iii) an important modification of the shape and size of the plastically deformed volume and hence of the corresponding plastic strain gradient.

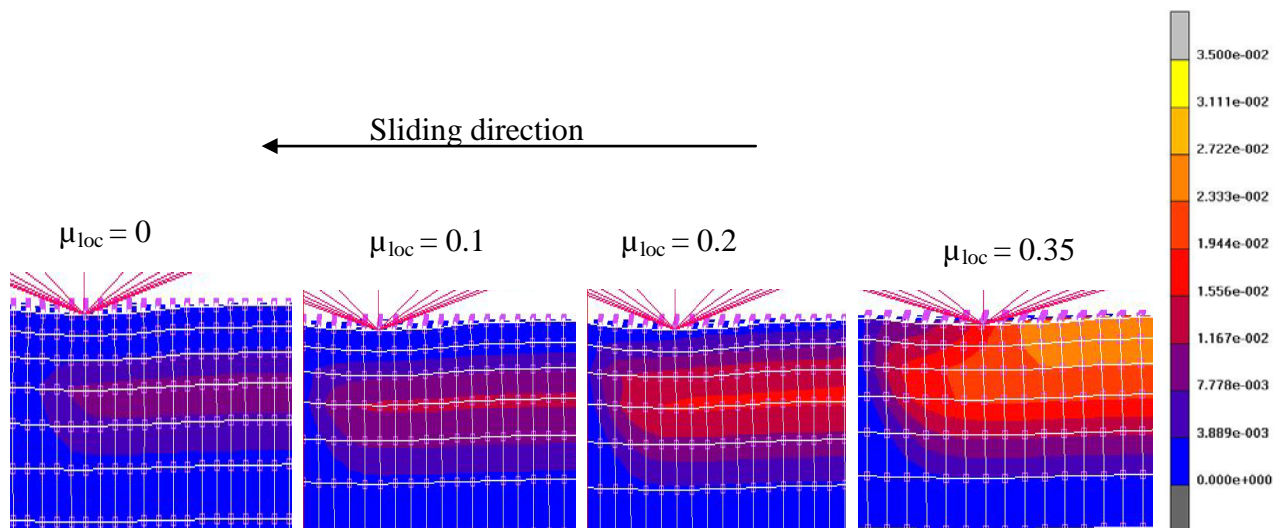


Figure 5.16 Variation of equivalent plastic strain with increasing friction coefficient for imposed  $a/R = 0.1$

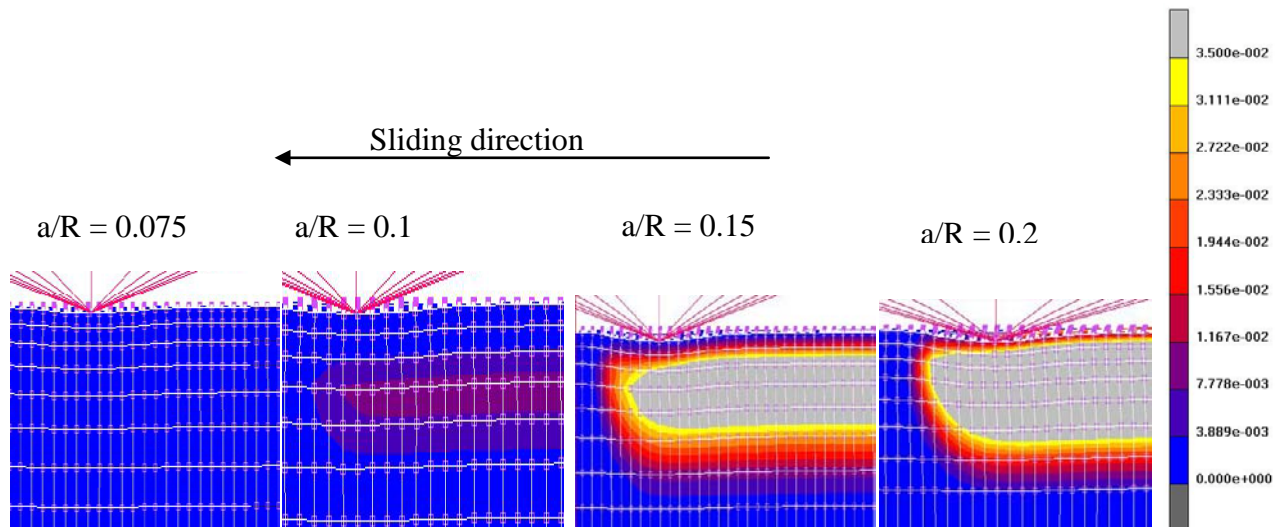


Figure 5.17 Variation of equivalent plastic strain with increasing imposed  $a/R$  for  $\mu_{loc} = 0$

As the plastic strain beneath the indenter is rapidly affected by the local friction as well as by the  $a/R$  ratio, the plastic scratching contact strain must be defined as a function of two variables: (i) the geometrical strain which is related to the ratio  $a/R$  and (ii) the local friction coefficient  $\mu_{loc}$ . These findings agree with those reported by Johnson [90], by E. Charrault [66], by Xiang et al. [6] and by H. Pelletier et al. [2, 67, 88].

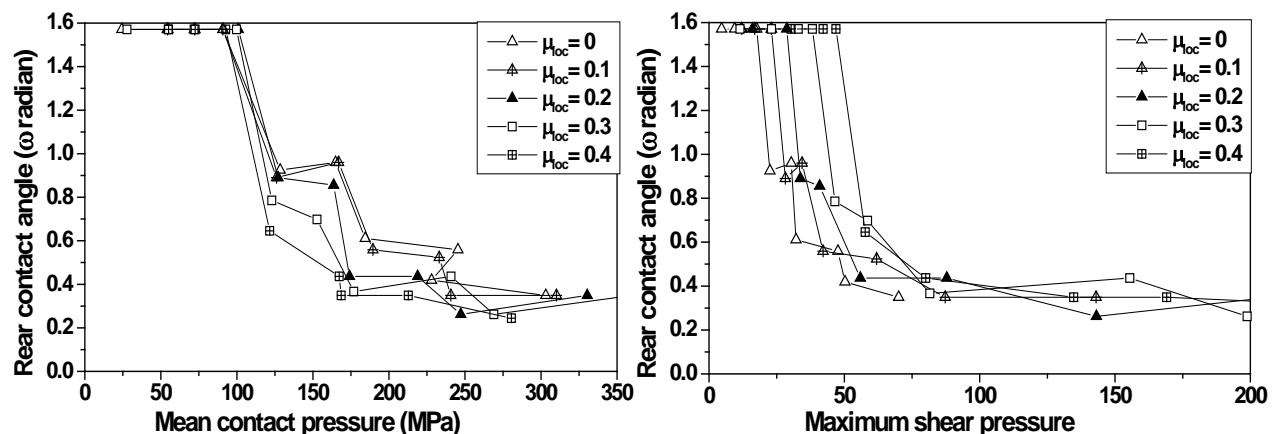


Figure 5.18 Variation of the rear contact angle with mean contact pressure (on the left) and with maximum shear stress (on the right) at room temperature.

It is interesting to note that transition between fully elastic and elastic plastic contact mainly depends upon a critical value of mean contact pressure or a critical value of maximum contact pressure (the value of the contact pressure after which the value of rear contact angle decreases abruptly) and this critical value does not depend on the friction coefficient (Figure 5.18 and Figure 5.19). The mean contact pressure at this transition is almost same (about 100 MPa) for low and high friction sliding conditions. On the other hand, the maximum shear stress at this transition depends a lot on the friction coefficient. There is a significant difference in these values for low and high friction coefficient sliding condition. It increases with increasing local friction coefficients. It is about 25 MPa for  $\mu_{loc} \leq 0.1$  that increases to about 65 MPa for  $\mu_{loc} = 0.4$ . Interestingly, the transition between elastic plastic and fully plastic contacts depends mainly upon a critical value of shear stress and this value of shear stress is almost same for all friction

coefficients. The value of the mean contact pressure at this transition (the value of the mean contact pressure after which the value of rear contact angle becomes almost constant) depends upon local friction coefficient and it increases with decreasing local friction coefficients. It is about 165 MPa for  $\mu_{loc} = 0.4$  that increases to about 250 MPa for  $\mu_{loc} \leq 0.1$ .

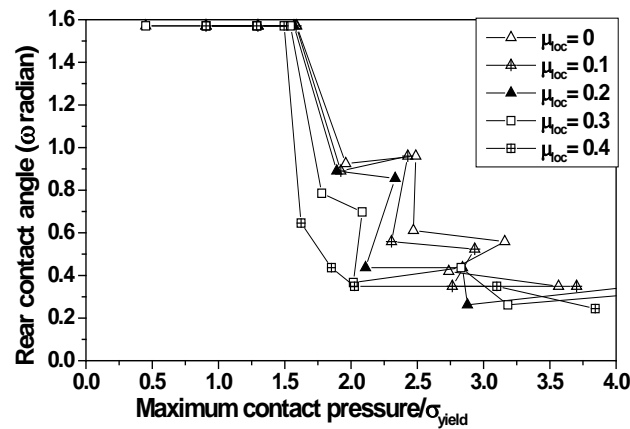


Figure 5.19 Relation between normalised maximum contact pressure and rear contact angle at room temperature.

### 5.3.2 Nature of the contact during different sliding/scratching conditions

Three different criteria are being proposed to differentiate the different types of contact under different sliding/scratching conditions. These three criteria may be listed as follow:

- 1 Criterion 1 based on appearance of equivalent plastic stain required for full yielding in the bulk and at the surface.
- 2 Criterion 2 based on specifying the limiting surface area being fully yielded around the contact.
- 3 Criterion 3 based on taking into consideration the horizontal stresses around the contact.

#### 5.3.2.1 Criterion 1 for classifying the nature of the contact

This is most generalized criterion and is based on just appearance of the equivalent plastic strain required for full yielding (about 0.03) around the contact. According to this criterion, a contact is said to be an elastic contact if the equivalent plastic strain is absent both at the surface and in the bulk as shown in Figure 5.20. If the yielding equivalent plastic strain ( $\sim 0.03$ ) is found in the bulk as well as at the surface at least up to the centre of the sliding tip (Figure 5.21), the contact may be called as a plastic contact. The contact may be considered as an elastic plastic contact if the yielding equivalent plastic strain is present in the bulk but either absent at the surface or is less to be a plastic contact as shown in Figure 5.22. The contact displaying some equivalent plastic strain in the bulk or at the surface but being not sufficient for yielding is also taken as an elastic plastic contact as shown in Figure 5.23. The nature of the contact for different sliding conditions based on this criterion is shown in Table 5.2.



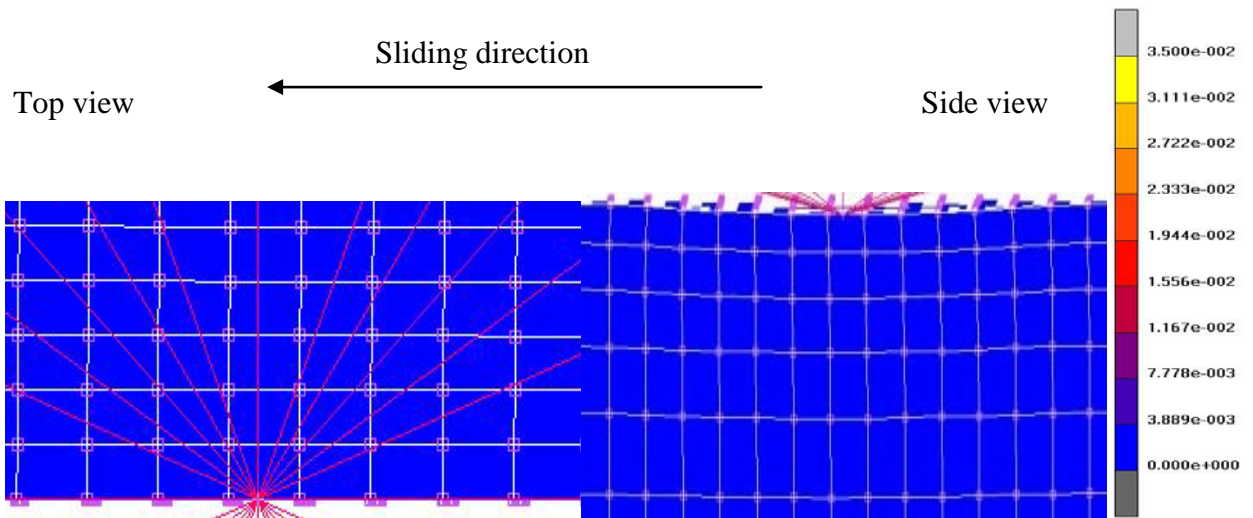


Figure 5.20 Equivalent plastic strain at the surface and in the bulk for  $a/R = 0.075$  and  $\mu_{loc} = 0.4$ . The contact is considered as an elastic one according to first criterion.

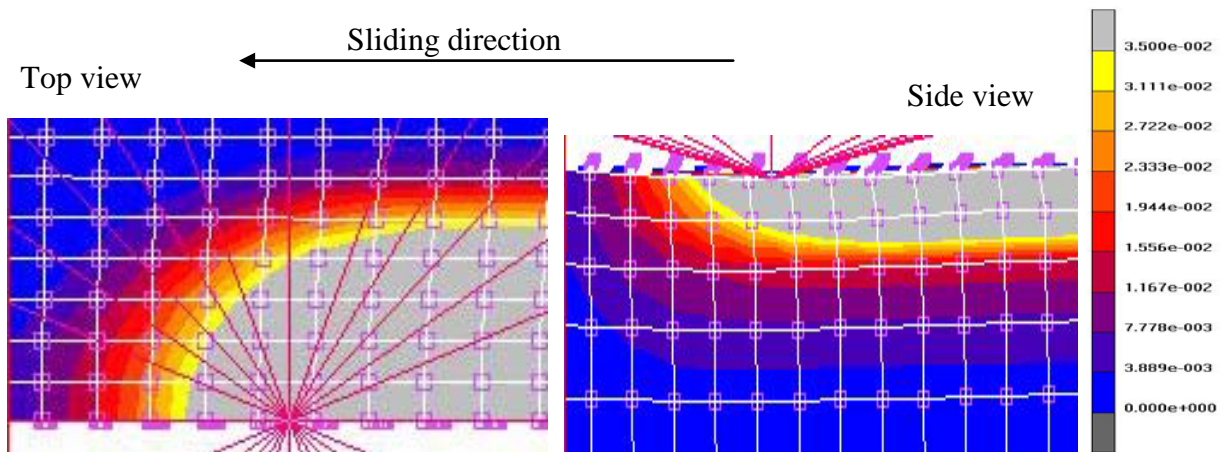


Figure 5.21 Equivalent plastic strain at the surface and in the bulk for  $a/R = 0.075$  and  $\mu_{loc} = 0.5$ . The contact is considered as a plastic one according to first criterion.

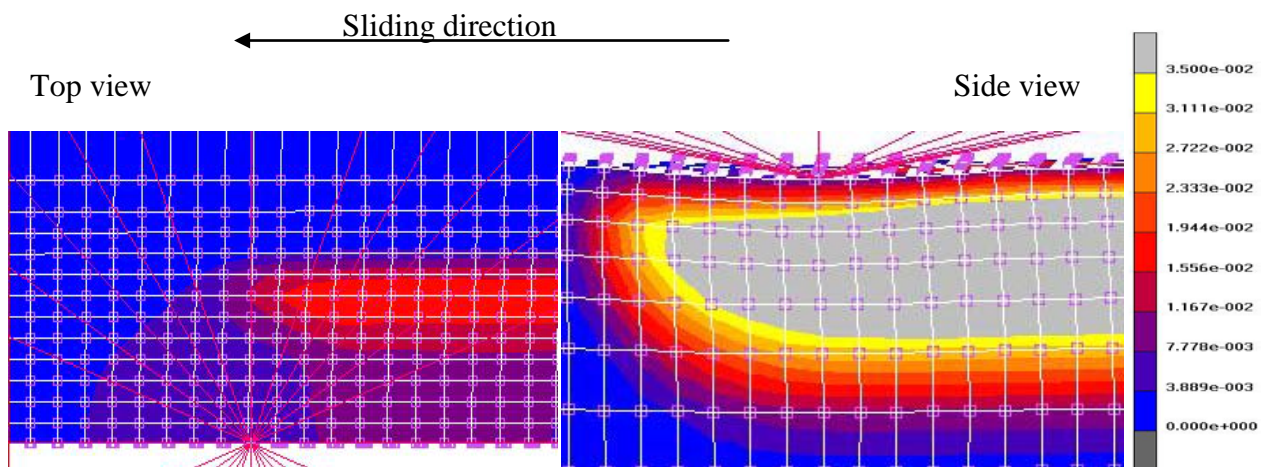


Figure 5.22 Equivalent plastic strain at the surface and in the bulk for  $a/R = 0.15$  and  $\mu_{loc} = 0.1$  displaying no yielding at the contact interface. The contact is considered as an elastic plastic one according to first criterion.

a/R ratio	0.025	0.05	0.075	0.1	0.15	0.2	0.3	0.4	0.5	0.6
$\mu_{loc}$										
0	Elastic	Elastic	Elastic	EP	EP	EP	Plastic	Plastic	Plastic	Plastic
0.05	Elastic	Elastic	Elastic	EP	EP	EP	Plastic	Plastic	Plastic	Plastic
0.1	Elastic	Elastic	Elastic	EP	EP	Plastic	Plastic	Plastic	Plastic	Plastic
0.15	Elastic	Elastic	Elastic	EP	EP	Plastic	Plastic	Plastic	Plastic	Plastic
0.2	Elastic	Elastic	Elastic	EP	EP	Plastic	Plastic	Plastic	Plastic	Plastic
0.25	Elastic	Elastic	Elastic	EP	Plastic	Plastic	Plastic	Plastic	Plastic	Plastic
0.3	Elastic	Elastic	Elastic	EP	Plastic	Plastic	Plastic	Plastic	Plastic	Plastic
0.35	Elastic	Elastic	Elastic	EP	Plastic	Plastic	Plastic	Plastic	Plastic	Plastic
0.4	Elastic	Elastic	Elastic	Plastic	Plastic	Plastic	Plastic	Plastic	Plastic	Plastic
0.45	Elastic	Elastic	EP	Plastic	Plastic	Plastic	Plastic	Plastic	Plastic	Plastic
0.5	Elastic	Elastic	Plastic	Plastic	Plastic	Plastic	Plastic	Plastic	Plastic	Plastic
0.55	Elastic	Elastic	Plastic	Plastic	Plastic	Plastic	Plastic	Plastic	Plastic	Plastic
0.575	Elastic	Elastic	Plastic	Plastic	Plastic	Plastic	Plastic	Plastic	Plastic	Plastic
0.6	Elastic	Elastic	Plastic	Plastic	Plastic	Plastic	Plastic	Plastic	Plastic	Plastic
0.65	Elastic	EP	Plastic	Plastic	Plastic	Plastic	Plastic	Plastic	Plastic	Plastic
0.7	Elastic	Plastic	Plastic	Plastic	Plastic	Plastic	Plastic	Plastic	Plastic	Plastic
0.9	Elastic	Plastic	Plastic	Plastic	Plastic	Plastic	Plastic	Plastic	Plastic	Plastic
1.1	Elastic	Plastic	Plastic	Plastic	Plastic	Plastic	Plastic	Plastic	Plastic	Plastic
1.2	Elastic	Plastic	Plastic	Plastic	Plastic	Plastic	Plastic	Plastic	Plastic	Plastic
1.25	Elastic	Plastic	Plastic	Plastic	Plastic	Plastic	Plastic	Plastic	Plastic	Plastic
1.3	Plastic	Plastic	Plastic	Plastic	Plastic	Plastic	Plastic	Plastic	Plastic	Plastic

Table 5.2 Nature of the contact for different local friction coefficients and different a/R ratios based on first criterion. (EP = Elastic plastic)

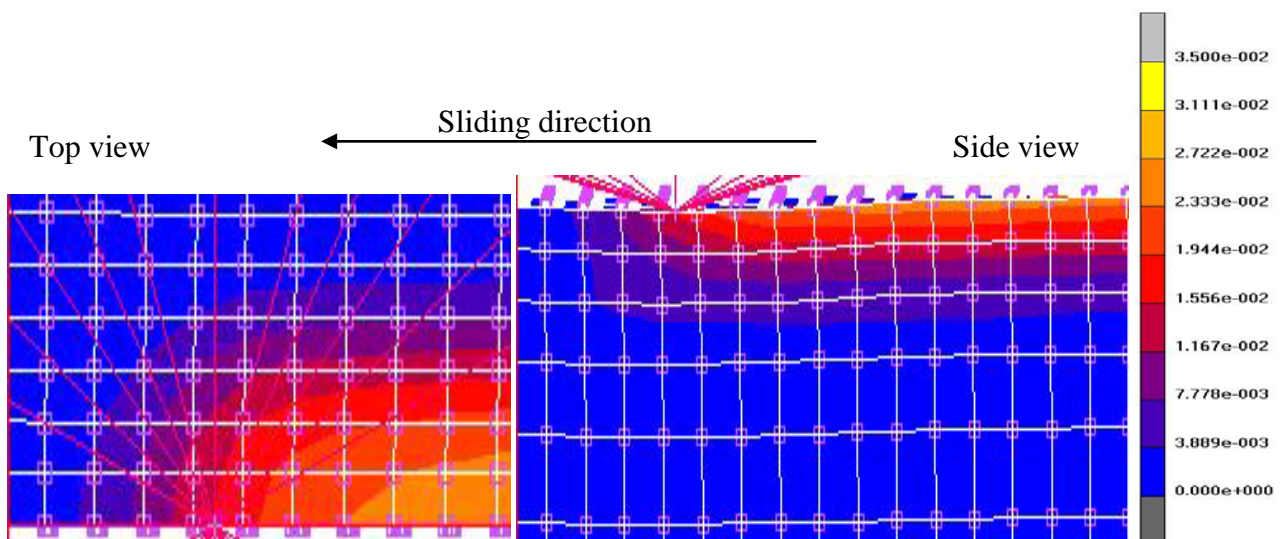


Figure 5.23 Equivalent plastic strain at the surface and in the bulk for  $a/R = 0.075$  and  $\mu_{loc} = 0.45$ . The contact is considered as an elastic plastic one according to first criterion.

### 5.3.2.2 Criterion 2 for classifying the nature of the contact

The basis of this criterion is similar to that of criterion 1 but is somewhat stricter in notifying a plastic contact. According to this criterion, the conditions for declaring the elastic and elastic plastic nature of contact are exactly the same as that in criterion 1. However, in this criterion, a contact will be considered as plastic one only if the yielding equivalent plastic strain at the surface is present in front of the sliding tip over a distance at least equal to the contact radius. The nature of the contact for different sliding conditions depending upon this criterion is shown in Table 5.3. A typical example is shown in the Figure 5.24.

a/R ratio	0.025	0.05	0.075	0.1	0.15	0.2	0.3	0.4	0.5	0.6
$\mu_{loc}$										
0	Elastic	Elastic	Elastic	EP	EP	EP	EP	EP	Plastic	Plastic
0.05	Elastic	Elastic	Elastic	EP	EP	EP	EP	EP	Plastic	Plastic
0.1	Elastic	Elastic	Elastic	EP	EP	EP	EP	EP	Plastic	Plastic
0.15	Elastic	Elastic	Elastic	EP	EP	Plastic	Plastic	Plastic	Plastic	Plastic
0.2	Elastic	Elastic	Elastic	EP	EP	Plastic	Plastic	Plastic	Plastic	Plastic
0.25	Elastic	Elastic	Elastic	EP	Plastic	Plastic	Plastic	Plastic	Plastic	Plastic
0.3	Elastic	Elastic	Elastic	EP	Plastic	Plastic	Plastic	Plastic	Plastic	Plastic
0.35	Elastic	Elastic	Elastic	EP	Plastic	Plastic	Plastic	Plastic	Plastic	Plastic
0.4	Elastic	Elastic	Elastic	EP	Plastic	Plastic	Plastic	Plastic	Plastic	Plastic
0.45	Elastic	Elastic	EP	Plastic	Plastic	Plastic	Plastic	Plastic	Plastic	Plastic
0.5	Elastic	Elastic	EP	Plastic	Plastic	Plastic	Plastic	Plastic	Plastic	Plastic
0.55	Elastic	Elastic	Plastic	Plastic	Plastic	Plastic	Plastic	Plastic	Plastic	Plastic
0.575	Elastic	Elastic	Plastic	Plastic	Plastic	Plastic	Plastic	Plastic	Plastic	Plastic
0.6	Elastic	Elastic	Plastic	Plastic	Plastic	Plastic	Plastic	Plastic	Plastic	Plastic
0.65	Elastic	EP	Plastic	Plastic	Plastic	Plastic	Plastic	Plastic	Plastic	Plastic
0.7	Elastic	Plastic	Plastic	Plastic	Plastic	Plastic	Plastic	Plastic	Plastic	Plastic
0.9	Elastic	Plastic	Plastic	Plastic	Plastic	Plastic	Plastic	Plastic	Plastic	Plastic
1.1	Elastic	Plastic	Plastic	Plastic	Plastic	Plastic	Plastic	Plastic	Plastic	Plastic
1.2	Elastic	Plastic	Plastic	Plastic	Plastic	Plastic	Plastic	Plastic	Plastic	Plastic
1.25	Elastic	Plastic	Plastic	Plastic	Plastic	Plastic	Plastic	Plastic	Plastic	Plastic
1.3	Plastic	Plastic	Plastic	Plastic	Plastic	Plastic	Plastic	Plastic	Plastic	Plastic

Table 5.3 Nature of the contact for different local friction coefficients and different a/R ratios based on second criterion. (EP = Elastic plastic)



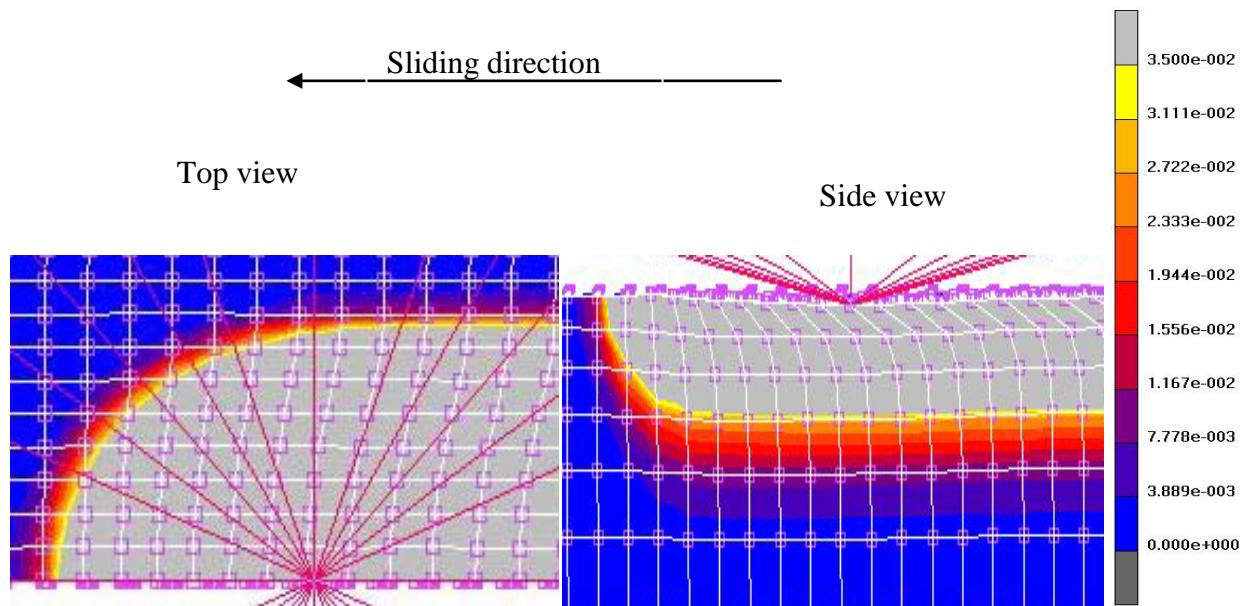


Figure 5.24 Equivalent plastic strain at the surface and in the bulk for  $a/R = 0.075$  and  $\mu_{loc} = 0.55$ . The contact is considered as a plastic one according to second criterion.

### 5.3.2.3 Criterion 3 for classifying the nature of the contact

This criterion differs from the first two criteria in that it takes into account the horizontal stresses around the contact instead of taking into account the equivalent plastic strain. According to this criterion; for an elastic contact, the horizontal stresses for a given  $a/R$  ratio must be equal at the centre of the contact and are located exactly at the same point in the bulk even for different friction conditions as discussed by G M Hamilton [91]. They become almost zero just behind the contact/tip. A typical example is shown in Figure 5.25 and Figure 5.26 for  $a/R = 0.075$ . The value of horizontal stresses for all sliding conditions at  $\mu_{loc} \leq 0.4$  are not only exactly the same near the centre of the contact but also are located exactly at the same point in the bulk. Hence the nature of all the contacts for  $a/R = 0.075$  at  $\mu_{loc} \leq 0.4$  are designated as an elastic one. The horizontal stress around the contact for to be an elastic contact is a characteristic value for each  $a/R$  ratio. This characteristic horizontal stress cannot be defined for  $a/R$  ratio higher than 0.2 as the nature of the contact is elastic plastic even at zero local friction coefficient. A contact is said to be a plastic one if the horizontal stresses are not close to zero behind the contact/tip as is clear for  $\mu_{loc} \geq 0.55$  in Figure 5.25 and Figure 5.26. So the nature of the contact is said to be plastic one for  $a/R = 0.075$  at  $\mu_{loc} \geq 0.55$  according to third criterion. For an elastic plastic contact, the horizontal stresses for a given  $a/R$  ratio are almost equal around the centre of the contact but are located at different location in the bulk for different friction conditions. They are not zero just behind the tip/contact but become almost zero after some time as is clear for  $\mu_{loc} = 0.45$  and  $\mu_{loc} = 0.5$  in Figure 5.25 and Figure 5.26. The nature of the contact for different sliding conditions based upon this criterion is shown Table 5.4. The characteristic values of the horizontal stress and the limiting local friction coefficient for an elastic contact for different  $a/R$  values are shown in Table 5.5.

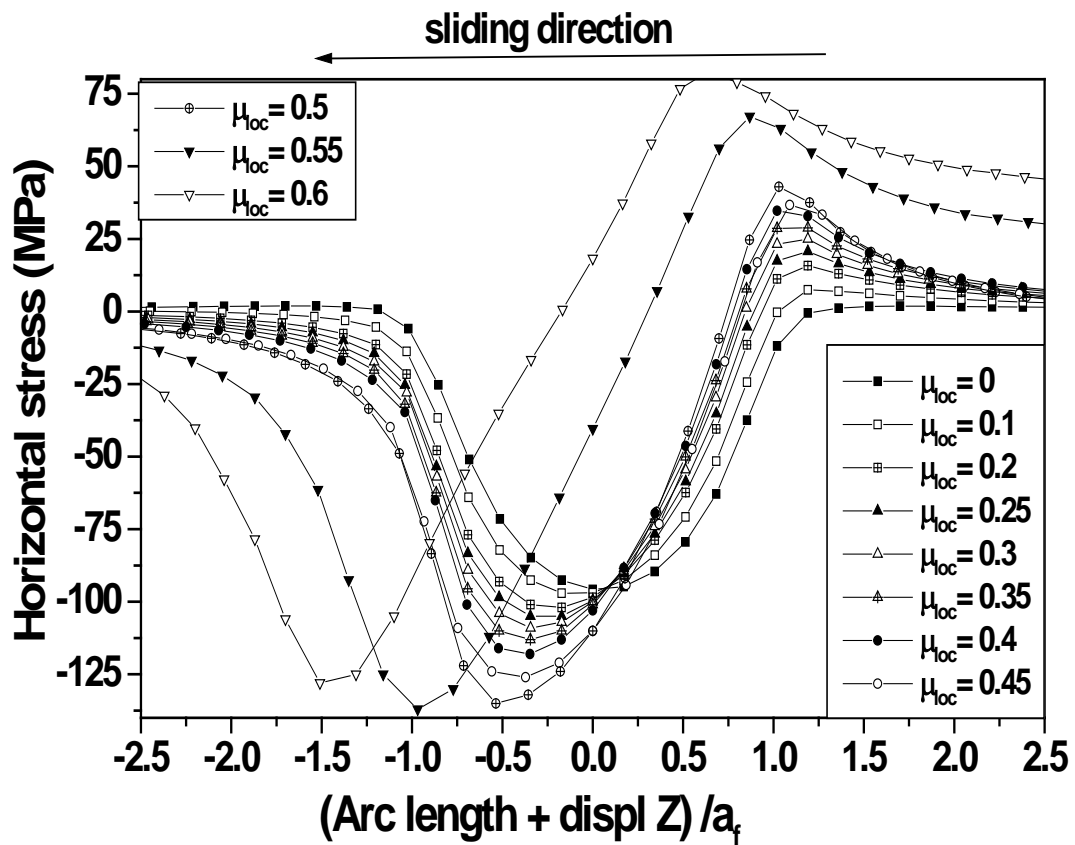


Figure 5.25 Variation of the horizontal stress around the contact for  $a/R = 0.075$  at different conditions of local friction. The centre of the contact lies at 0 on horizontal axis.

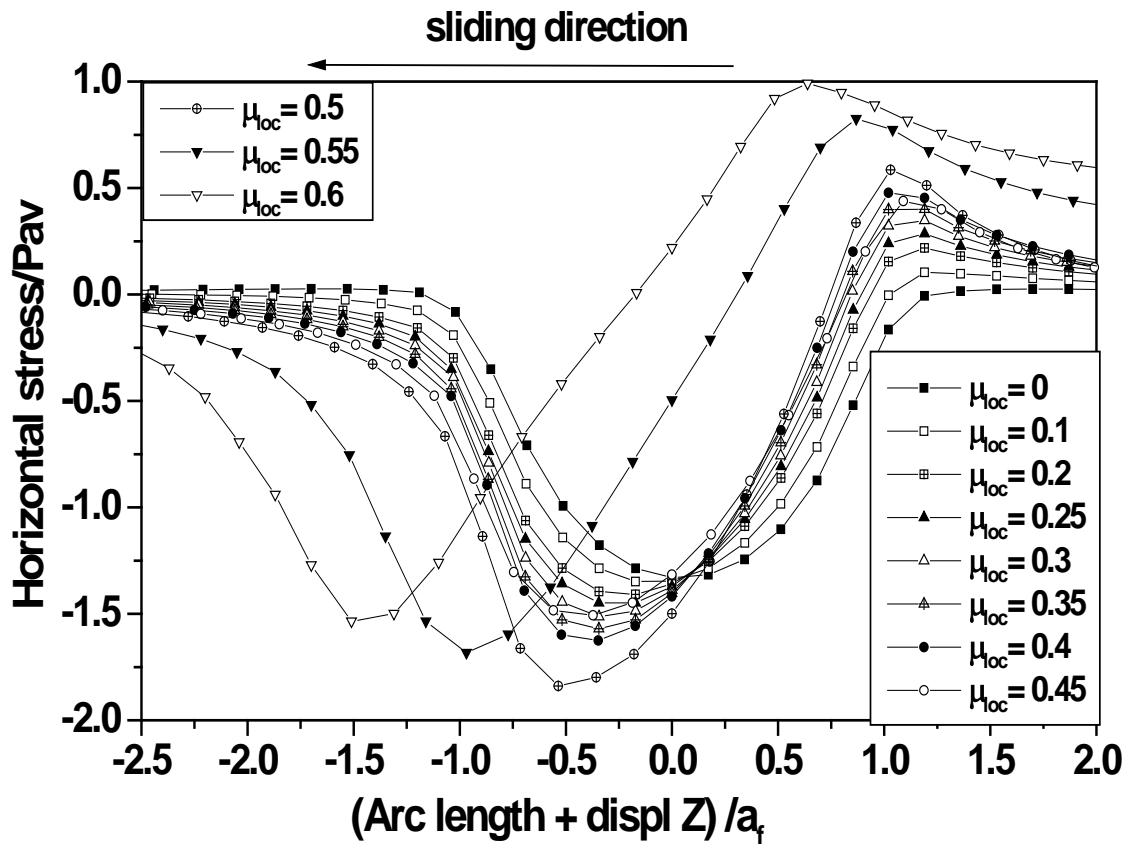


Figure 5.26 Variation of the normalized horizontal stress around the contact for  $a/R = 0.075$  at different conditions of local friction. The centre of the contact lies at 0 on horizontal axis.

a/R ratio	0.025	0.05	0.075	0.1	0.15	0.2	0.3	0.4	0.5	0.6
$\mu_{loc}$										
0	Elastic	Elastic	Elastic	Elastic	Elastic	EP	EP	EP	Plastic	Plastic
0.05	Elastic	Elastic	Elastic	Elastic	Elastic	EP	EP	EP	Plastic	Plastic
0.1	Elastic	Elastic	Elastic	Elastic	Elastic	EP	EP	EP	Plastic	Plastic
0.15	Elastic	Elastic	Elastic	Elastic	EP	EP	EP	Plastic	Plastic	Plastic
0.2	Elastic	Elastic	Elastic	EP	EP	EP	EP	Plastic	Plastic	Plastic
0.25	Elastic	Elastic	Elastic	EP	EP	EP	Plastic	Plastic	Plastic	Plastic
0.3	Elastic	Elastic	Elastic	EP	EP	EP	Plastic	Plastic	Plastic	Plastic
0.35	Elastic	Elastic	Elastic	EP	EP	Plastic	Plastic	Plastic	Plastic	Plastic
0.4	Elastic	Elastic	Elastic	EP	Plastic	Plastic	Plastic	Plastic	Plastic	Plastic
0.45	Elastic	Elastic	EP	Plastic	Plastic	Plastic	Plastic	Plastic	Plastic	Plastic
0.5	Elastic	Elastic	EP	Plastic	Plastic	Plastic	Plastic	Plastic	Plastic	Plastic
0.55	Elastic	Elastic	Plastic	Plastic	Plastic	Plastic	Plastic	Plastic	Plastic	Plastic
0.6	Elastic	Elastic	Plastic	Plastic	Plastic	Plastic	Plastic	Plastic	Plastic	Plastic
0.65	Elastic	EP	Plastic	Plastic	Plastic	Plastic	Plastic	Plastic	Plastic	Plastic
0.7	Elastic	Plastic	Plastic	Plastic	Plastic	Plastic	Plastic	Plastic	Plastic	Plastic
0.8	Elastic	Plastic	Plastic	Plastic	Plastic	Plastic	Plastic	Plastic	Plastic	Plastic
0.9	Elastic	Plastic	Plastic	Plastic	Plastic	Plastic	Plastic	Plastic	Plastic	Plastic
1	Elastic	Plastic	Plastic	Plastic	Plastic	Plastic	Plastic	Plastic	Plastic	Plastic
1.1	Elastic	Plastic	Plastic	Plastic	Plastic	Plastic	Plastic	Plastic	Plastic	Plastic
1.2	Elastic	Plastic	Plastic	Plastic	Plastic	Plastic	Plastic	Plastic	Plastic	Plastic
1.25	Elastic	Plastic	Plastic	Plastic	Plastic	Plastic	Plastic	Plastic	Plastic	Plastic
1.3	Plastic	Plastic	Plastic	Plastic	Plastic	Plastic	Plastic	Plastic	Plastic	Plastic

Table 5.4 Nature of the contact for different local friction coefficients and different a/R ratios based on third criterion. (EP = Elastic plastic)

a/R ratio	0.025	0.05	0.075	0.1	0.15	0.2	0.3	0.4	0.5	0.6
Horizontal stress(MPa)	30	68	95	120	170	215	-	-	-	-
Horizontal stress/ $\sigma_{yield}$	0.3	0.68	0.95	1.20	1.7	2.15	-	-	-	-
Horizontal stress/ $P_{av}$	1.2	1.25	1.3	1.35	1.4	1.4	-	-	-	-
Limiting $\mu_{loc}$	1.25	0.6	0.4	0.15	0.1	0	-	-	-	-

Table 5.5 Characteristic values of the horizontal stresses close to the centre of the contact for different a/R ratio for being a fully elastic contact according to third criterion.

## 5.4 Gratifying findings

- In the elastic region i.e very low contact strain, the apparent friction coefficient depends mainly upon local friction coefficient and for a given local friction coefficient, it remains almost constant for increasing contact strain. However, during elastic plastic and fully plastic, it

depends upon both local friction coefficient and contact strain. It increases with increasing local friction and increasing contact strain.

- For very low and very high values of  $a/R$  ratio, there is no any significant effect of either local friction coefficient or  $a/R$  ratio on the rear contact angle, as the nature of the contact is fully elastic at very low  $a/R$  value (up to 0.1) for all friction coefficients and is fully plastic for high values of  $a/R$  ratios. However, at intermediate contact strains (during the elastic plastic domain of contact), the value of rear contact angle decreases significantly with increasing contact strain. Moreover, the elastic plastic domain is increased by decreasing the friction coefficient.
- The elastic recovery and the pile up height mainly depend upon the contact strain. The elastic recovery decreases and the pile up height increasing with increasing contact strain. Moreover, the effect of contact strain is only significant for moderate contact strains or during elastic plastic nature of contact. For fully elastic or fully plastic contact, the effect of increasing contact strain on elastic recovery and pile up height becomes negligible.
- Both average contact pressure and the maximum contact pressure are found to depend mainly upon the contact strain. They increase with increasing contact strain. The local friction coefficient is found to affect the contact pressure a little bit only at moderate contact strains or only during elastic plastic region. The ratio of maximum to average contact pressure is found to be constant (about 1.6) for all sliding conditions conflicting in local friction and contact strains.
- The maximum shear stress and the shear stress at maximum normal pressure are found to be dependent of only friction coefficient and for a given coefficient friction, they remain almost constant for increasing contact strain.
- The transition from fully elastic to elastic plastic contact is found to be dependent upon the contact pressure and it occurs at the same contact pressure for all friction coefficients but at differing shear stresses for different friction conditions. Interestingly, the transition between elastic plastic to fully plastic contact takes place at almost constant shear stress for all friction coefficients but at different contact pressures depending upon the friction coefficient. The increasing friction coefficient is found to decrease the elastic plastic domain of the contact.
- In elastic region, i.e. for low local friction coefficient and low contact strain, the horizontal stress at maximum contact pressure is almost constant for increasing local friction and depends mainly upon contact strain. However, in elastic plastic and fully plastic regions, it depends upon both local friction coefficient and contact strain. The maximum horizontal stress in front of the contact remains almost same for all sliding conditions during elastic contact. However, for an elastic plastic and fully plastic contact, it depends upon both the contact strain and the friction coefficient, i.e. it increases with both increasing contact strain and increasing friction coefficient. It is valuable to mention that the normalised maximum horizontal stress (by average contact pressure) depends mainly upon friction coefficient during elastic region and for a given friction coefficient, it remains almost constant with increasing contact strain (only in elastic region). However, during elastic plastic and fully plastic region, it depends upon both contact strain and the local friction. It decreases with increasing contact strain and increasing friction coefficient.
- The FE simulation results reveal that with increasing local friction at constant  $a/R$  ratio or/and with increasing  $a/R$  ratio at constant local friction coefficient, there is (a) an increase in the level of plastic strain imposed beneath the moving tip and in the residual groove; (b) a displacement of the location of the maximum plastic strain towards the sub-surface region just beneath the indenter; and (c) an important modification of the shape and size of the plastically deformed volume and hence of the corresponding plastic strain gradient.
- Different criteria may be proposed to classify the nature of contacts under different sliding/scratching conditions conflicting in local friction coefficients and/or in contact strains. These criteria may be based upon taking into account either plastic strain or the horizontal stresses around the contact.

## **Section three**

# **General discussion on results and concluding part**



## 6 General discussion on the results

### 6.1 General discussion on experimental work

As we have discussed in section 3.4 that the process of decreasing the friction coefficient of polymers plasticised by fatty acid amides is time dependent. The rate of decrease is maximum just after the manufacture and the change in friction coefficient with time becomes negligible after a steady state where the maximum amount of the total fatty acid amide is available at the surface. However, it is clear from the experimental results (section 4.2.1.1.2 and section 4.2.1.1.3) that as a result of long time ageing or a short duration heating cycle at higher temperature, the fatty acid amides disappear from the surface of the polymer and consequently the advantage of reduced friction coefficient is also disappeared. Therefore, it can be said that the friction coefficient of plasticised polymers first decreases (when the plasticizer migrates from the bulk to the surface), remains almost stable for a specific duration and then increases again (when the plasticizer evaporates from the surface of the polymer). Therefore the duration of reduced friction coefficient can be extended by minimising the evaporation of plasticizer from the surface. One solution to minimize the evaporation of plasticizer from the surface is to reduce the storage or usage temperature.

As mentioned in sections 2.5.1 and 2.6.4, temperature may rise for higher sliding speeds during scratch test resulting in variation of the bulk mechanical properties of the materials and consequently affecting the scratch test results. As the sliding speed in our case is not very high (only 0.03 mm/s), the resulting temperature rise is less than 1°C as is clear from Figure 6.1 and Figure 6.2 (which are based upon equation 2.16) that is not up to a significant value. This equation, given by Bonne [62] may be written as:

$$\Delta T = \frac{\frac{2}{\pi} \tan \beta \left(\frac{W}{2L}\right) v}{\sqrt{\lambda \rho c v L}} \quad 2.15$$

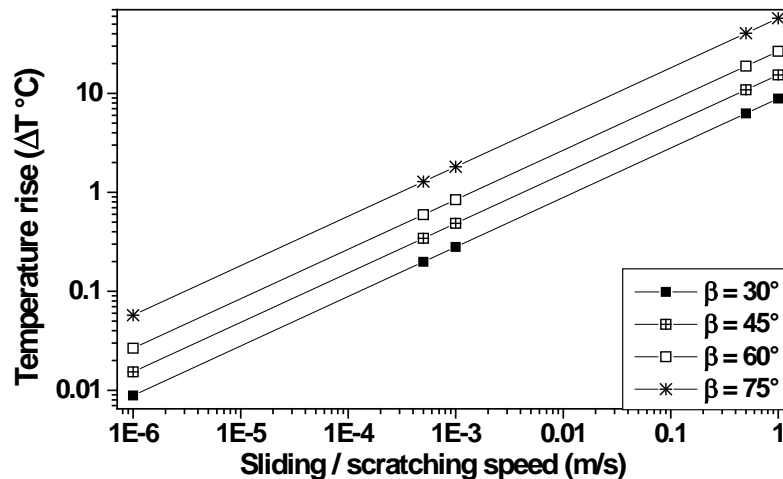


Figure 6.1 Temperature rise ( $\Delta T$ ) for different attack angles ( $\beta$ ) and for different sliding/scratching speeds ( $v$ ) for the contact radius = 10  $\mu\text{m}$  during sliding/scratching test.

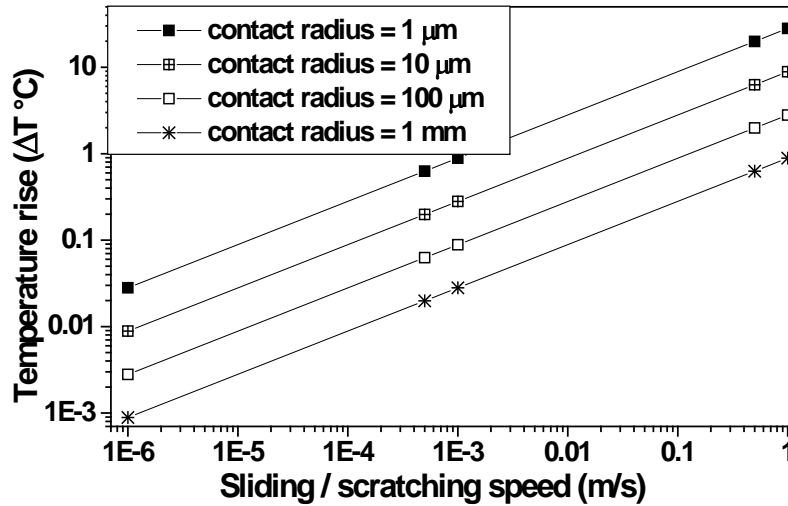


Figure 6.2 Temperature rise ( $\Delta T$ ) during sliding/scratching test for the tip having attack angle ( $\beta$ ) =  $30^\circ$  for different contact radius and different sliding/scratching speeds.

Moreover, it is clear from above plots that the relation between the sliding velocity  $v$  and the temperature rise ( $\Delta T$ ) during a scratch test may be simply shown as:

$$\log \Delta T = m \log v + c \quad 6.1$$

where  $m$  and  $c$  are the constants depending upon the properties of the indenter and of the material being scratched.  $m$  is the slope or temperature gradient with respect to the sliding velocity for a particular system and  $c$  is y-intercept of  $\log \Delta T$  vs  $\log v$  graph.

As discussed in section 2.6.4 that during a scratch test at higher sliding speeds, the temperature may rise to as high as  $100^\circ\text{C}$ . But the master curve of the average contact pressure at lower scratching speeds indicates the right place of the  $T_g$ , so it may be said that self-heating during scratch experiments due to friction may remain to lower values. Moreover, self-heating may illustrate two types of behaviour. It may be either an adiabatic heating or an isothermal scratch where the boundary is directly connected with the velocity. So the self-heating of polymer during scratching either may be limited to the shearing surface (i.e. at the interface of the two surfaces) or may be diffused to the volume.

The surface energy analysis indicates that the changes in friction coefficient brought about by plasticizers cannot be correlated with the surface energies of the PMMA as the surface energy remains almost same for all cases. This is in well agreement with the findings of B. Podgornik et al. [84] showing also that the surface energy data may not be linked with tribology performance of the lubricated surfaces although the changes in surface morphology certainly changes the surface energy. Moreover, the investigations regarding nano-scale lubricated contacts made by H. Berro et al. [85] also showed that the friction coefficient increases initially with increasing surface energy for low friction values ( $\mu \leq 0.09$ ) but for higher friction values, the effect of increasing surface energy on friction becomes negligible. However, the surface energy data is in contrast to the work of M. Minn et al. [21] which shows that the friction coefficient and surface energy are directly proportional to each other. However, they concluded it by studying the changes in surface energy in conjunction with the corresponding changes in friction coefficient brought about by using coatings and by air plasma treatment.



## 6.2 Comparison between experimental and numerical data obtained from FE simulations

Different data obtained from simulations generally holds good as is clear from the comparison of the experimental values of different parameters with those obtained from simulations (Figure 6.3 to Figure 6.6). For example, if we see the relation between the experimental values of the rear contact angle and the mean contact strain for some selected samples differing in friction coefficients and that obtained from the simulations (Figure 6.3), it is almost the same for both cases. For a given value of local friction coefficient, the value of the rear contact angle at a given mean contact strain obtained from experiments as well as that obtained from simulation is almost the same. The transitions between different natures of the contacts are also located at the same mean contact strains assessed from both experimental and simulation methods. For example, the transition from elastic plastic contact to fully plastic contact (the point at which the value of rear contact angle becomes almost constant) for  $\mu_{loc} = 0.4$  obtained from simulations and that for pure PMMA obtained from experiments can be seen in Figure 6.3 at the same mean contact strain equal to about 0.22. Similarly for low friction coefficients, it is about 0.7 for both experimental and the simulation data.

The normalised mean contact pressure-rear contact angle curves (Figure 6.4) for low local friction coefficients ( $\mu_{loc} = 0.1$ ) obtained from experiments and that obtained from simulations are also almost similar. However, for higher friction coefficient ( $\mu_{loc} = 0.4$ ), some discrepancy between the two is found but even then it can be said that both display the similar trend. It is interesting to note that if we look at the normalized mean contact pressure-mean contact strain curve obtained from experiments and that obtained from simulations, the curve for low local friction coefficient like  $\mu_{loc} = 0.1$  may be considered somewhat similar (Figure 6.5) for both cases but for higher local friction coefficients like  $\mu_{loc} = 0.4$ , not only a great disagreement is observed but the trend is also inverted. In the experimental data, the slope of the normalized contact pressure-mean contact strain plot for low friction is lower than that for higher friction. However, surprisingly the data obtained from simulations display an opposite trend. In this case, the slope of the curve for low friction coefficient is higher than that for higher friction coefficient. This deviation between the simulation and experimental data may be attributed due to a number of factors. For example, the complete analysis of the effect of different parameters of the law used in numerical simulations for displaying the mechanical behaviour of the material is very completed and has not been made. Furthermore, during sliding experiments by micro visio scratch apparatus, the same sliding tip geometry was used for all scratch experiments and the mean contact strain was altered mainly by varying the normal load and consequently the contact radius as well as the scratchy/penetration depth was changed correspondingly. On the other hand, in finite element simulations, the contact radius was kept almost constant for all sliding conditions and the contact strain was varied by changing both the tip geometry (mainly tip radius) and the penetration depth. Moreover, the FEM simulations have been made using an absolute spherical tip, while the experimental data have been obtained in fact using a conical tip having a spherical extremity. For low contact strains, it does not affect the results but for higher contact strains (higher than 0.4/0.5), the tip scratches the surface partially with its conical part. So practically it is more difficult to increase the contact strain with such a conical tip having spherical extremity as compared to the case of a perfect and ideal spherical tip. As a result, the imposed normal load on the tip will be largely increased. This finding is also well reflected in the results. The variation of normal load is far less in simulation data for various sliding conditions as compared to that in experiment data. For example, the mean contact strain of about 0.9 is obtained by applying a normal force of about 1.5 N in simulation data whereas in the experimental data, the same level of contact strain is obtained by applying a normal force of about 4 N (Figure 6.6). Similarly the normal load required for a given value of rear contact

angle is dissimilar in simulation data than that in experimental data. Lastly, the consequence of the effect of the friction on the tangential load for these two kinds of contact (large contact strain for a perfect spherical and for a conical tip with spherical extremity) is also not yet well understood.

As the contact radius is kept almost same for all simulated scratch experiments as well as the variation of the normal load is not very high for different sliding conditions, so the variation in mean or maximum contact pressure or in their normalised values for various sliding conditions (differing in local friction coefficients and contact strains) is also far less in simulation data as compared to that obtained from the experimental data.

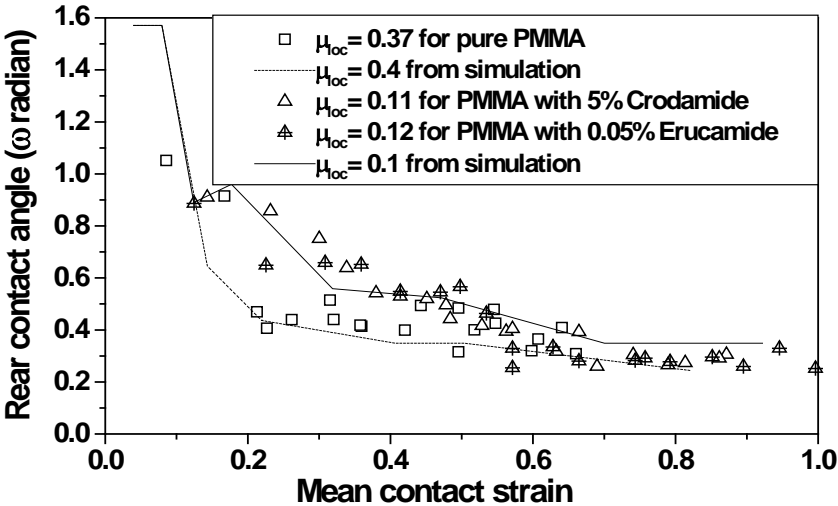


Figure 6.3 The comparison between experimental and the numerical values (obtained from simulations) of rear contact angles for some selected friction coefficients.

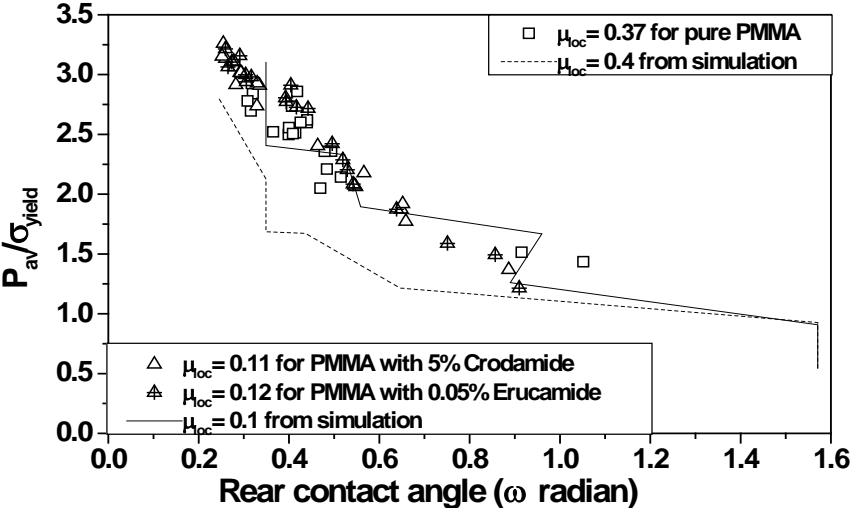


Figure 6.4 The comparison between experimental and the numerical values (obtained from simulations) of normalised average contact pressure for some selected friction coefficients.

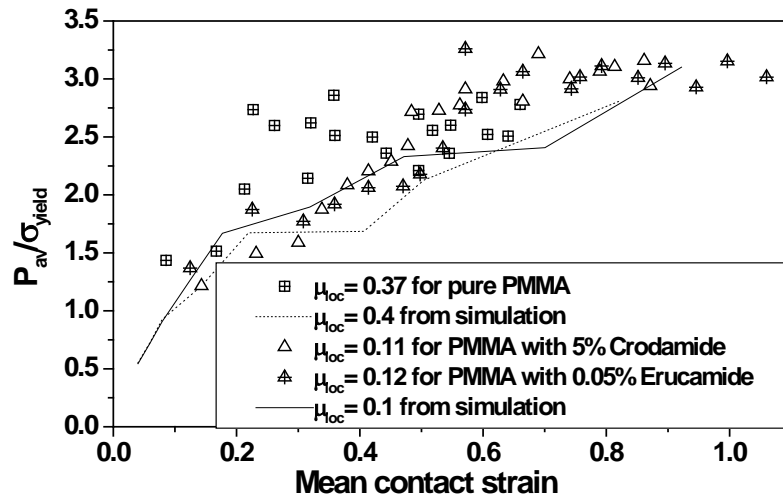


Figure 6.5 The comparison between experimental and the numerical values (obtained from simulations) of normalised average contact pressure for some selected friction coefficients.

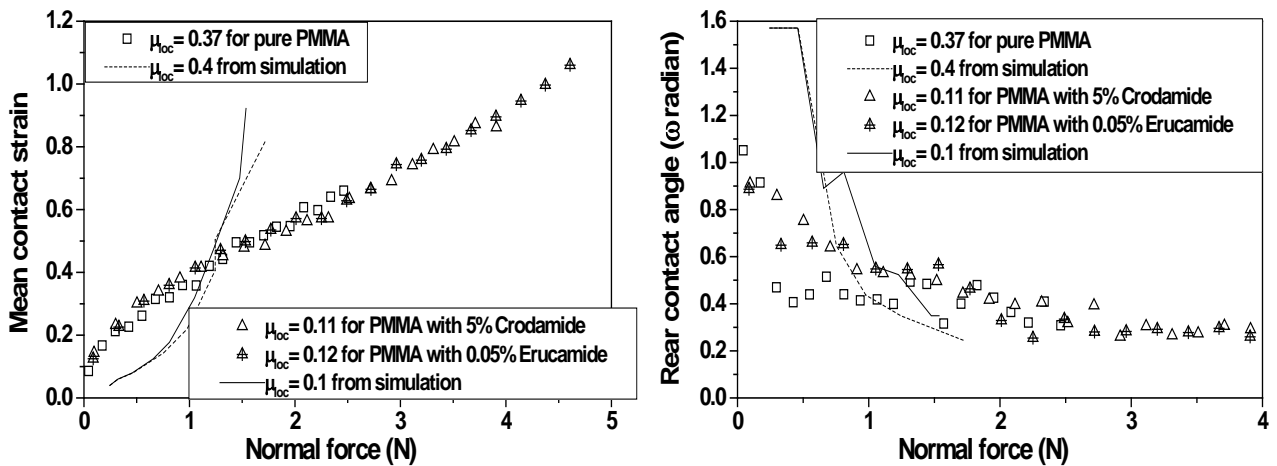


Figure 6.6 Variation of the mean contact strain (on the left) and the rear contact angle (on the right) with increasing normal load for some selected cases from simulation and experimental data.

### 6.3 The best approach to improve the scratch resistance

Three dimensional graphs were drawn based on numerical data in order to associate (i) the rear contact angle, the contact strain and local friction coefficients and (ii) the normalised maximum contact pressure, the contact strain and the local friction coefficient. The purpose was obvious to search out the association of these parameters with each other under different sliding/scratching conditions in order to propose some appropriate technique to improve the scratch resistance of polymers. It is important to mention that the contact strain ( $a/R$ ) mentioned in these plots is the imposed contact strain. The relationship between rear contact angle, contact strain and the local friction coefficient reveals that the maximum effect of local friction coefficient on the rear contact angle mainly lies in the plastic domain of contact (Figure 6.7). The effect of local friction coefficient on the rear contact angle during fully elastic and elastic plastic domain is almost negligible. As the plastic domain of the material depends mainly upon the bulk mechanical properties, therefore in order to improve the scratch resistance of polymers, one should emphasize to modify the bulk behaviour of the materials.

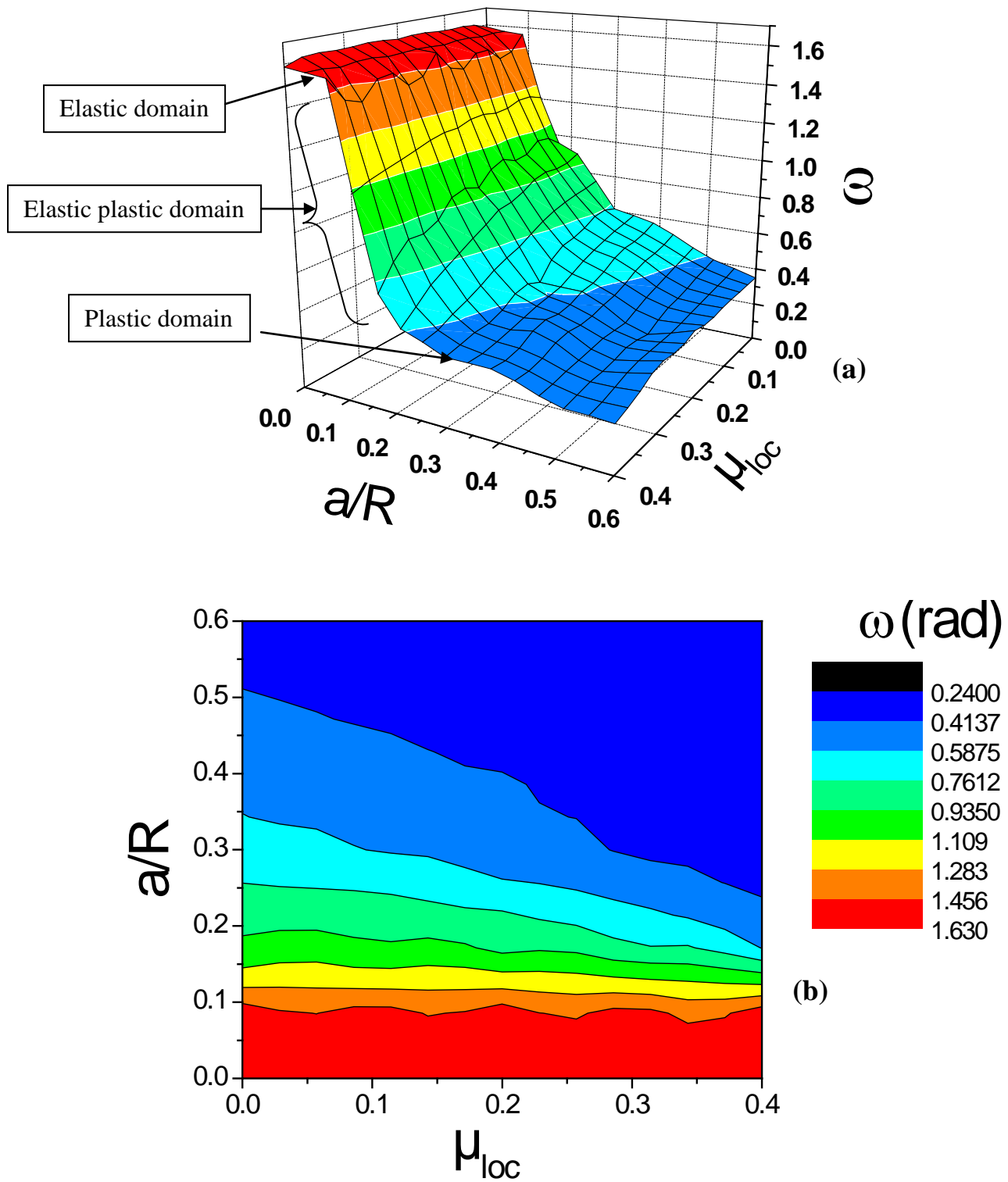


Figure 6.7 The relationship between the rear contact angle  $\omega$ , the imposed contact strain  $a/R$  and the local friction coefficient  $\mu_{loc}$  as obtained from the numerical data.

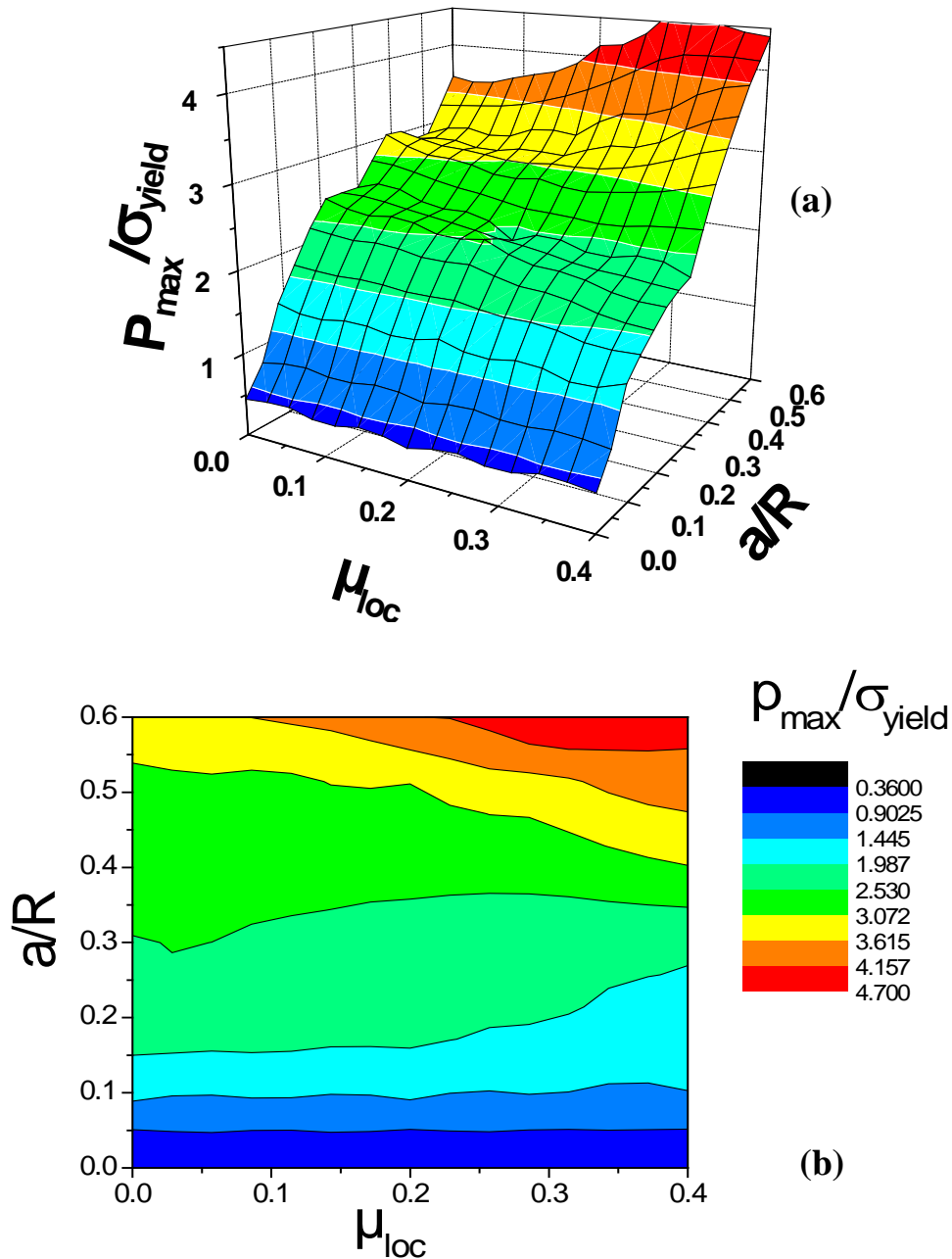


Figure 6.8 The relationship between the normalized maximum contact pressure  $P_{max}/\sigma_{yield}$ , the imposed contact strain  $a/R$  and the local friction coefficient  $\mu_{loc}$  as obtained from the numerical data.

Similar consequence is observed if we see the influence of local friction coefficient on normalised maximum contact pressure. Firstly, in case of frictionless contact, one can find again the well known results, i.e. a linear increase of the normalised contact pressure with increasing contact strain for low range contact strains. The normalised contact pressure also remains almost independent of the increasing friction coefficient during fully elastic contact (Figure 6.8). This is the conformity of the results and discussion mentioned in section 5.3.1.8. It was shown that the transition between elastic and elastic plastic domain mainly depends upon the contact pressure, and that this transition was observed at the same contact pressure for all friction coefficients. It was further shown that the transition from elastic plastic to fully plastic domain is mainly dependent upon shear stress and that this transition was observed at almost same shear stress for all friction

coefficients. The effect of local friction coefficient on the normalised contact pressure appears at the beginning of elastic plastic contact. For example, if we see the normalised contact pressure for contact strain  $a/R=0.15$ , it remains almost same till the local friction coefficient  $\approx 0.3$ . Beyond the local friction coefficient  $\approx 0.3$ , the normalised contact pressure increases with increasing local friction coefficient. The yielding appears in the bulk of the material at  $\mu_{loc} \approx 0.3$  for  $a/R=0.15$ . On further increase in friction coefficient, yielding shifts towards the surface, resulting in subsequent increase in normalised contact pressure. The limiting local friction coefficient (displaying the yielding in the bulk) decreases with increasing contact strain as is clear from Figure 6.8(b). For example, the effect of local friction coefficient on normalised contact pressure for  $a/R=0.3$  appears at about  $\mu_{loc}=0.05$ . These findings are in good accord with experimental values of normalised contact pressure available in the literature for elastic and elastic plastic domains of contact. However, for plastic domain, we do not observe such a high value of normalized contact pressure in the literature. The experimental value of normalized contact pressure remains almost same in the plastic domain even with increasing contact strain and increasing friction coefficient. This discrepancy may be considered due to various phenomena like yielding, crazing and so on that are classically observed during experimental measurements at large contact strains.

## 6.4 Gratifying findings

- As the sliding speed during the scratching test performed is not very high (only 0.03 mm/s), the resulting temperature rise is less than 1°C. This confirms that the self-heating during scratch test was not so high to alter the mechanical behaviour of the polymer and hence its consequence on the scratch test results was negligible.
- The friction coefficient of plasticised polymers first decreases (when the plasticizer migrates from the bulk to the surface), remains almost stable for a specific duration and then increases again (when the plasticizer evaporates from the surface of the polymer).
- The advantage of reduced friction coefficient of a plasticized polymer can be prolonged by decreasing the rate of evaporation of the plasticizer from the polymer. The rate of evaporation of the plasticizer may be decreased by lowering the storage or usage temperature.
- The decrease in friction coefficient given by the plasticizer is not reflected in the surface energy data and so it is difficult to correlate the decrease in friction coefficient with surface energy.
- Generally speaking, the numerical data holds good accord with that obtained from experiments. The rear contact angle-contact strain curve is the example displaying excellent accord of the two data. However, the normal load required to get a given value of rear contact angle or to get a given values of contact strain is not the same in the two cases.
- The relationship between rear contact angle, contact strain and the local friction coefficient reveal that the maximum effect of local friction coefficient on the rear contact angle mainly lies in the plastic domain of contact. The effect of local friction coefficient on the rear contact angle during fully elastic and at the beginning of elastic plastic domain is almost negligible. As the plastic domain of the material depends mainly upon the bulk mechanical properties, therefore in order to improve the scratch resistance of polymers, one should emphasize to modify the bulk behaviour of the materials.

## 7 Conclusion & Perspective

The scratching technique has gained interest in recent times due to its varied applications to a number of engineering materials, especially for the evaluation of surface scratch resistance of plastics. Scratching provides a convenient and reliable means to investigate the mechanical properties of organic polymers under various contact conditions. The method also allows the identification and the assessment of the surface deformation processes and maps defining the scratch deformation modes as a function of contact conditions may be generated. Polymers exhibit a wide range of scratch deformation characteristics and the deformation mechanism is determined by the most efficient energy dissipation process for the particular external constraints [33].

Various physico-chemical processes such as annealing and various ion plantation techniques have been proved very useful for the modification of polymeric surfaces but their applications are limited to some certain polymers due to some disadvantages. Especially, some of them cannot be applied to transparent polymers like PMMA due to their darkening effect. Improvement of the scratch resistance must be investigated primarily as an effect due to decreasing the friction coefficient. The recovery of the groove left increases if the tip is smooth or if the local friction coefficient is low [17]. Investigation of the reduction of friction through use of different plasticizers is an area that has a great potential of research and one might expect a breakthrough in this regard. Discovery of appropriate plasticizers for different polymers to reduce their surface friction is very important in order to improve their scratch resistance.

The effect of various plasticizers on the friction coefficient of PMMA was studied. The experimental results support the nature of action of different fatty acid amides as reported in literature and discussed in section 1.8.6. It was confirmed that the fatty acid amides are generally efficient only in small quantities for reducing the friction coefficient of polymers like PMMA and that their excessive amount affects the friction coefficients adversely probably due to their gumming effect at the surface. The unique exception to this generalisation i.e. stearyl erucamide (Crodamide-212) is also confirmed by the experimental data as the friction coefficient of PMMA decreases directly with its increasing percentage.

It was observed that the yielding contact strain is significantly increased for the samples showing lower friction coefficient. It was also seen that decrease in friction coefficient by the introduction of fatty acid amides is not reflected in the change/increase in surface energy of the PMMA. Moreover, the decrease in friction coefficient is also not reflected in the change in bulk behaviour either on macro or on nano scale. So it may be concluded that the friction is reduced by changing the bulk behaviour only over a very minute area (consisting of only a few tens of nanometres). This area close to the surface (for which the mechanical behaviour is modified) is so small that the modification in mechanical behaviour cannot be detected even by the nano indentation experiments. A spherical tip was chosen to avoid the contact yielding and one may reconsider the choice of the tip to get same or different data.

It is interesting to note that surface free energy of pure Erucamide is much lower than that of the pure PMMA. But when it is added to PMMA in lower amount, it decreases the friction coefficient of PMMA without changing significantly its surface energy.

In short, it can be concluded that the plasticizer reduce the friction coefficient of polymers by;

- modifying the mechanical behaviour over a very minute area close to the surface, mainly increasing the yielding strain at the contact
- broadening the fully elastic and elastic plastic regions during the contact by increasing the yielding strain at the contact
- without altering much the surface free energy and the bulk mechanical properties of the polymer

Moreover, this advantage of plasticizer remains valid as long as the plasticiser remains available at the surface. As most of plasticizers remain in the polymer for limited time, this benefit of decreased friction coefficient is also not durable. More work is required to be done for determining the duration of this advantage for different plasticizer and polymer combinations and discovering the methods to increase this duration in order to get reduced friction coefficient over a sufficient large time period.

Experimental data confirms that the effectiveness of a particular slip additive for reducing the friction coefficient of a particular polymer depends upon their mutual relationship (depending upon their chemical structures). A particular slip additive that is very effective for reducing the friction coefficient of a particular grade of a polymer may not be effective for another grade of the same polymer.

As discussed in section 4.2.4.1.1 that the PMMA containing nano structured PBA displays a different behaviour regarding the effect of high temperature heating on friction coefficient than that of a standard PMMA. This contradictory character may be assumed due to the presence of nano structured elastomeric PBA. For such a nano structured material, we could easily imagine that an annealing step (at 80°C) will change the surface of the material. It can be said that the nano particles of PBA migrate to the surface and cause a decrease in friction coefficient. A measurement of the surface energy and the surface composition (before and after thermal treatment) can verify such "re-organization" of the constituents at the surface.

Experimental results show that there is no any synergy in action found between Erucamide and Behenamide in decreasing the friction coefficient of PMMA. Rather it can be said that there appears some antagonism in the action of Behenamide. Since 0.1% Behenamide when present alone decreases the friction coefficient of PMMA but this decrease in friction coefficient is disappeared in presence of 0.2 % Erucamide. More work may be proposed to find out the best synergetic combination of different fatty acid amides by changing the nature and quantity of different fatty acid amides. Some other materials like nano particles of silica or nanoclay such as laponite may also be tried to find a suitable synergetic combination with Erucamide in order to reduce the friction coefficient of PMMA. The use of some surfactant like SDS (Sodium dodecyl sulfate or sodium laurilsulfate) may also be tried to get reduced friction coefficient of PMMA as it has been used successfully for thin methacrylate films for reducing their friction coefficient.

The results of numerical work employing FE simulation discovered many of the important information regarding material response during different scratch conditions. The transition from fully elastic to elastic plastic contact is found to be dependent upon a critical value of the contact pressure that is almost same for different friction coefficients. However, the shear stresses at this transition are different for different friction conditions. Interestingly, the transition between elastic plastic to fully plastic contact takes place at almost constant shear stress for all friction conditions. This transition takes place, however, at a range of contact pressures depending upon the friction coefficient. The increasing friction coefficient is found to decrease the elastic plastic domain of the contact. For very low and very high values of  $a/R$  ratio, there is no any significant effect of either



local friction coefficient or  $a/R$  ratio on the rear contact angle, as the nature of the contact is fully elastic at very low  $a/R$  value (up to 0.1) for all friction coefficients and is fully plastic for high values of  $a/R$  ratios. However, at intermediate contact strains (during the elastic plastic domain of contact), the value of rear contact angle decreases significantly with increasing contact strain. The elastic recovery and the pile up height mainly depend upon the contact strain. The elastic recovery decreases and pile up height increases with increasing contact strain. Moreover, the effect of contact strain is only significant for moderate contact strains or during elastic plastic nature of contact. For fully elastic or fully plastic contact, the effect of increasing contact strain on elastic recovery and pile up height becomes negligible. Both average contact pressure and the maximum contact pressure are found to depend mainly upon the contact strain. They increase with increasing contact strain. The local friction coefficient is found to affect the contact pressure a little bit only at moderate contact strains or only during elastic plastic region. Fascinatingly, the ratio of maximum to average contact pressure is found to be constant (about 1.6) for all sliding conditions conflicting in local friction and contact strains.

The relationship between rear contact angle, contact strain and the local friction coefficient reveals that the greatest effect of local friction coefficient on the rear contact angle mainly lies in the plastic domain of contact. The effect of local friction coefficient on the rear contact angle during fully elastic and elastic plastic domain is almost negligible. As the plastic domain of the material depends mainly upon the bulk mechanical properties, therefore in order to improve the scratch resistance of polymers, one should emphasize to modify the bulk behaviour of the materials in order to get an increased elastic domain. This can be achieved in a number of ways. One way to increase the elastic domain is to adjust the mechanical bulk properties to get an increased  $\sigma_{\text{yield}}/E$  that is equivalent to an increased elastic strain. The elastic plastic and fully plastic domains can also be shifted to higher contact strains by modifying the strain hardening effect and decreasing the interfacial friction. One solution may also be the developing a mechanical behaviour giving an increased effect of self healing. This can be accomplished by lowering the friction coefficient, avoiding the surface singularities of the material and of the scratching tip or by minimising the effect of these singularities by coating them with elastic surfaces or films.

The numerical work identified the different domains of contact behaviour like elastic contact, elastic plastic contact and plastic contact. The numerical data generally holds good accord with the experimental data. However, more work will be interesting in order to harmonise the sliding conditions in simulation and experimental work so that some discrepancies found can be overcome. It will be also interesting to extend this work to the self-healing of grooves. In addition, the use of different laws concerning elasto visco elastic plastic/visco plastic contacts will allow identifying the relationship between bulk properties and coefficient of friction in order to maximize the scratch resistance.



## 8 References

1. Rodríguez R.J. et al., *Modification of surface mechanical properties of polycarbonate by ion implantation*. Surface and Coatings Technology, 2002. **158-159**: p. 636-642.
2. Pelletier H. et al., *Viscoelastic and elastic-plastic behaviors of amorphous polymeric surfaces during scratch*. Tribology International, 2008. **41**(11): p. 975-984.
3. Jardret V. and P. Morel, *Viscoelastic effects on the scratch resistance of polymers: relationship between mechanical properties and scratch properties at various temperatures*. Progress in Organic Coatings, 2003. **48**(2-4): p. 322-331.
4. Jardret V. et al., *Understanding and quantification of elastic and plastic deformation during a scratch test*. Wear, 1998. **218**(1): p. 8-14.
5. Rahman M. and C.S. Brazel, *The plasticizer market: an assessment of traditional plasticizers and research trends to meet new challenges*. Progress in Polymer Science, 2004. **29**(12): p. 1223-1248.
6. Xiang C. et al., *Scratch behavior and material property relationship in polymers*. Journal of Polymer Science Part B: Polymer Physics, 2001. **39**(1): p. 47-59.
7. Adams M.J. et al., *An experimental study of the nano-scratch behaviour of poly(methyl methacrylate)*. Wear, 2001. **251**(1-12): p. 1579-1583.
8. Tanglumlert W. et al., *Hard-coating materials for poly(methyl methacrylate) from glycidoxypropyltrimethoxysilane-modified silatrane via a sol-gel process*. Surface and Coatings Technology, 2006. **200**(8): p. 2784-2790.
9. Kitova S., M. Minchev and G. Danev, *Soft plasma treatment of polymer surfaces*. Journal of Optoelectronics and Advanced Materials, 2005. **7**(1): p. 249-252.
10. Wong M. et al., *A new test methodology for evaluating scratch resistance of polymers*. Wear, 2004. **256**(11-12): p. 1214-1227.
11. Gauthier C. and R. Schirrer, *Time and temperature dependence of the scratch properties of poly(methylmethacrylate) surfaces*. Journal of Materials Science, 2000. **35**(9): p. 2121-2130.
12. Kopesky E.T., G.H. McKinley and R.E. Cohen, *Toughened poly(methyl methacrylate) nanocomposites by incorporating polyhedral oligomeric silsesquioxanes*. Polymer, 2006. **47**(1): p. 299-309.
13. Lafaye S., C. Gauthier and R. Schirrer, *Analysis of the apparent friction of polymeric surfaces*. Journal of Materials Science, 2006. **41**(19): p. 6441-6452.
14. Felder E. and J.-L. Bucaille, *Mechanical analysis of the scratching of metals and polymers with conical indenters at moderate and large strains*. Tribology International, 2006. **39**(2): p. 70-87.
15. Subhash G. and W. Zhang, *Investigation of the overall friction coefficient in single-pass scratch test*. Wear, 2002. **252**(1-2): p. 123-134.
16. Lafaye S., C. Gauthier and R. Schirrer, *A surface flow line model of a scratching tip: apparent and true local friction coefficients*. Tribology International, 2005. **38**(2): p. 113-127.
17. Gauthier C. et al., *Scratching of a coated polymer and mechanical analysis of a scratch resistance solution*. Tribology International, 2006. **39**(2): p. 88-98.
18. Lafaye S., C. Gauthier and R. Schirrer, *Analyzing friction and scratch tests without in situ observation*. Wear, 2008. **265**(5-6): p. 664-673.
19. Donnet J.-B. and R.-Y. Qin, *Empirical estimation of surface energies of polymers and their temperature dependence*. Journal of Colloid and Interface Science, 1992. **154**(2): p. 434-443.
20. Janczuk B., T. Bialopiotrowicz and W. Wójcik, *The components of surface tension of liquids and their usefulness in determinations of surface free energy of solids*. Journal of Colloid and Interface Science, 1989. **127**(1): p. 59-66.
21. Minn M. and S.K. Sinha, *The frictional behavior of UHMWPE films with different surface energies at low normal loads*. Wear, 2010. **268**(7-8): p. 1030-1036.
22. Piglowski J.M. and M. Bryjak, *Surface studies of poly(methyl methacrylate)/poly(styrene-co-acrylonitrile) blends*. European Polymer Journal, 1998. **34**(11): p. 1669-1673.
23. Janczuk B. and T. Bialopiotrowicz, *Surface free-energy components of liquids and low energy solids and contact angles*. Journal of Colloid and Interface Science, 1989. **127**(1): p. 189-204.

24. Kaminska A., H. Kaczmarek and J. Kowalonek, *The influence of side groups and polarity of polymers on the kind and effectiveness of their surface modification by air plasma action*. European Polymer Journal, 2002. **38**(9): p. 1915-1919.
25. <<http://www.igb.fraunhofer.de/www/gf/grenzflmem/gf-physik/en/GFphys-PolymOberfl.en.html>>.
26. <<http://www.surface-tension.de/solid-surface-energy.htm>>.
27. Arruda E.M. and M.C. Boyce, *Evolution of plastic anisotropy in amorphous polymers during finite straining*. International Journal of Plasticity, 1993. **9**(6): p. 697-720.
28. Richeton J. et al., *A unified model for stiffness modulus of amorphous polymers across transition temperatures and strain rates*. Polymer, 2005. **46**(19): p. 8194-8201.
29. Drozdov A.D., *Viscoelastoplasticity of amorphous glassy polymers*. European Polymer Journal, 2000. **36**(10): p. 2063-2074.
30. Tabor D., *The hardness of solids*. Proceedings of the institute of physics, 1970. **1**(1): p. 145-79.
31. Williams J.A., *Analytical models of scratch hardness*. Tribology International, 1996. **29**(8): p. 675-694.
32. Malzbender J. et al., *Measuring mechanical properties of coatings: A methodology applied to nanoparticle-filled sol-gel coatings on glass*. Materials Science and Engineering: R: Reports, 2002. **36**(2-3).
33. Briscoe B.J. et al., *Scratching maps for polymers*. Wear, 1996. **200**(1-2): p. 137-147.
34. Pane I. and E. Blank, *Role of plasticity on indentation behavior: Relations between surface and subsurface responses*. International Journal of Solids and Structures, 2006. **43**(7-8): p. 2014-2036.
35. Hamouda A.M.S., *The influence of humidity on the deformation and fracture behaviour of PMMA*. Journal of Materials Processing Technology, 2002. **124**(1-2): p. 238-243.
36. Solc K., S.E. Keinath and R.F. Boyer, *Secondary transitions in amorphous polymers. 5. Linear form of the Tait equation applied to isotactic poly(methyl methacrylate)*. Macromolecules, 1983. **16**(10): p. 1645-1652.
37. Rajendran S., M. Sivakumar and R. Subadevi, *Investigations on the effect of various plasticizers in PVA-PMMA solid polymer blend electrolytes*. Materials Letters, 2004. **58**(5): p. 641-649.
38. Cheng J.-Y. et al., *Direct-write laser micromachining and universal surface modification of PMMA for device development*. Sensors and Actuators B: Chemical, 2004. **99**(1): p. 186-196.
39. Subramanian V. et al., *Molecular mechanics studies on polypropylene and polymethylmethacrylate polymers*. Chemical Physics Letters, 2001. **342**(5-6): p. 603-609.
40. Wu H., G. Ma and Y. Xia, *Experimental study of tensile properties of PMMA at intermediate strain rate*. Materials Letters, 2004. **58**(29): p. 3681-3685.
41. Jossierand L., R. Schirrer and P. Davies, *Influence of water on crack propagation in poly methyl methacrylate: craze stress and craze fibril lifetime*. Journal of Materials Science, 1995. **30**(7): p. 1772-1780.
42. Linares A. and J.L. Acosta, *Tensile and dynamic mechanical behaviour of polymer blends based on PVDF*. European Polymer Journal, 1997. **33**(4): p. 467-473.
43. Scott M.P., M. Rahman and C.S. Brazel, *Application of ionic liquids as low-volatility plasticizers for PMMA*. European Polymer Journal, 2003. **39**(10): p. 1947-1953.
44. Zelenev Y.V. and G.M. Bartenev, *Effect of plasticization on the relaxation properties of rubber-like polymers over a broad range of temperatures*. Polymer Science U.S.S.R., 1964. **6**(5): p. 1009-1018.
45. Volynskii A.L. et al., *The nature of fissure formation in polymethyl-methacrylate deformed below the glass temperature*. Polymer Science U.S.S.R., 1975. **17**(3): p. 576-583.
46. Shashkov A.S. et al., *Aspects of the influence of plasticizers of varied nature on the physicomechanical properties and structure of polymethylmethacrylate*. Polymer Science U.S.S.R., 1987. **29**(12): p. 2757-2764.
47. Bajpai R., P. Agrawal and S.C. Datt, *Plasticization in poly (methyl methacrylate) and poly (chlorotrifluoroethylene) blends detected by microhardness measurements*. Polymer Testing, 1994. **13**(2): p. 103-106.
48. Movsum-Zade A.A. et al., *Chemical plasticization of cellulose triacetate by grafting on polymethylmethacrylate*. Polymer Science U.S.S.R., 1964. **6**(7): p. 1481-1488.

49. Mills A., A. Lepre and L. Wild, *Effect of plasticizer-polymer compatibility on the response characteristics of optical thin CO<sub>2</sub> and O<sub>2</sub> sensing films*. *Analytica Chimica Acta*, 1998. **362**(2-3): p. 193-202.
50. Sinko C.M. and G.L. Amidon, *Plasticizer-induced changes in the mechanical rate of response of film coatings: an approach to quantitating plasticizer effectiveness*. *International Journal of Pharmaceutics*, 1989. **55**(2-3): p. 247-256.
51. Markarian J., *Slip and antiblock additives: surface medication for film and sheet*. *Plastics, Additives and Compounding*, 2007. **9**(6): p. 32-35.
52. Wypych G., ed. *HANDBOOK OF ANTIBLOCKING, RELEASE, AND SLIP ADDITIVES*. 2005.
53. Peloso C.W. et al., *Characterising the degradation of the polymer slip additive erucamide in the presence of inorganic antiblock agents*. *Polymer Degradation and Stability*, 1998. **62**(2): p. 285-290.
54. *Croda expansion to boost amide slip additives manufacturing capacity*. *Additives for Polymers*, 2010. **2010**(11): p. 5-6.
55. *Lubricants -- what you need to know to improve your process*. *Plastics, Additives and Compounding*, 2000. **2**(4): p. 18-22.
56. Markarian J., *Additives improve scratch resistance in automotive applications*. *Plastics, Additives and Compounding*, 2009. **11**(2): p. 10-13, 15.
57. Gauthier C., S. Lafaye and R. Schirrer, *Elastic recovery of a scratch in a polymeric surface: experiments and analysis*. *Tribology International*, 2001. **34**(7): p. 469-479.
58. Briscoe B.J. and S.K. Sinha, *Scratch Resistance and Localised Damage Characteristics of Polymer Surfaces - a Review*. *Materialwissenschaft und Werkstofftechnik*, 2003. **34**(10-11): p. 989-1002.
59. Briscoe B.J. et al., *Scratch deformation of methanol plasticized poly(methylmethacrylate) surfaces*. *Polymer*, 1998. **39**(11): p. 2161-2168.
60. Sinha S.K. and D.B.J. Lim, *Effects of normal load on single-pass scratching of polymer surfaces*. *Wear*, 2006. **260**(7-8): p. 751-765.
61. Krichen A., M. Kharrat and A. Chateauminis, *Experimental and numerical investigation of the sliding behaviour in a fretting contact between poly (methylmethacrylate) and a glass counterface*. *Tribology International*, 1996. **29**(7): p. 615-624.
62. Bonne M. et al., *Characterisation of surface abrasion phenomena on poly (methyl methacrylate) surfaces*. *Wear*, 2003. **254**(1-2): p. 55-64.
63. Rittel D., *Experimental investigation of transient thermoplastic effects in dynamic fracture*. *International Journal of Solids and Structures*, 2000. **37**(21): p. 2901-2913.
64. Sakharova N.A. et al., *Comparison between Berkovich, Vickers and conical indentation tests: A three-dimensional numerical simulation study*. *International Journal of Solids and Structures*, 2009. **46**(5): p. 1095-1104.
65. Sujeet K Sinha, B.J.B. *POLYMER TRIBOLOGY*. 2009.
66. Charrault E. et al., *Structural recovery (physical ageing) of the friction coefficient of polymers*. *Journal of Polymer Science, Part B: Polymer Physics*, 2008. **46**(13): p. 1337-1347.
67. Pelletier H., C. Gauthier and R. Schirrer, *Influence of the friction coefficient on the contact geometry during scratch onto amorphous polymers*. *Wear*, 2010. **268**(9-10): p. 1157-1169.
68. Xie Y. and H.M. Hawthorne, *On the possibility of evaluating the resistance of materials to wear by ploughing using a scratch method*. *Wear*, 2000. **240**(1-2): p. 65-71.
69. Bouissou S., J.P. Petit and M. Barquins, *Normal load, slip rate and roughness influence on the PMMA dynamics of sliding 2. Characterisation of the stick-slip phenomenon*. *Wear*, 1998. **215**(1-2): p. 137-145.
70. Cai S. and B. Bhushan, *A numerical three-dimensional contact model for rough, multilayered elastic/plastic solid surfaces*. *Wear*, 2005. **259**(7-12): p. 1408-1423.
71. Karpenko Y.A. and A. Akay, *A numerical model of friction between rough surfaces*. *Tribology International*, 2001. **34**(8): p. 531-545.
72. Bueche A.M. and D.G. Flom, *Surface friction and dynamic mechanical properties of polymers*. *Wear*, 1959. **2**(3): p. 168-182.

73. Ludema K.C. and D. Tabor, *The friction and visco-elastic properties of polymeric solids*. Wear, 1996. **9**(5): p. 329-348.
74. Dann J.R., *Forces involved in the adhesive process : I. Critical surface tensions of polymeric solids as determined with polar liquids*. Journal of Colloid and Interface Science, 1970. **32**(2): p. 302-320.
75. <http://www.atiskimya.com/msds/spect59.pdf>.
76. Markarian J., *Slip and antiblock additives: surface medication for film and sheet*. Plastics, Additives and Compounding, **9**(6): p. 32-35.
77. <http://www.thefreelibrary.com/Lubricants+and+processing+aids.-a0189051619>.
78. Molnar N., *Erucamide*. Journal of the American Oil Chemists' Society, 1974. **51**(3): p. 84-87.
79. *Addcon World '99*. Plastics, Additives and Compounding, 2000. **2**(1): p. 24-28.
80. Janczuk B. and T. Bialopiotrowicz, *The total surface free energy and the contact angle in the case of low energetic solids*. Journal of Colloid and Interface Science, 1990. **140**(2): p. 362-372.
81. Tamai Y., T. Matsunaga and K. Horiuchi, *Surface energy analysis of several organic polymers: Comparison of the two-liquid-contact-angle method with the one-liquid-contact-angle method*. Journal of Colloid and Interface Science, 1977. **60**(1): p. 112-116.
82. Siboni S. et al., *The solid surface free energy calculation: II. The limits of the Zisman and of the "equation-of-state" approaches*. Journal of Colloid and Interface Science, 2004. **271**(2): p. 454-472.
83. Kaminska A., H. Kaczmarek and J. Kowalonek, *The influence of side groups and polarity of polymers on the kind and effectiveness of their surface modification by air plasma action*. European Polymer Journal, 2002. **38**(9): p. 1915-1919.
84. Podgornik B. et al., *Influence of surface energy on the interactions between hard coatings and lubricants*. Wear, 2007. **262**(9-10): p. 1199-1204.
85. Berro H., N. Fillot and P. Vergne, *Molecular dynamics simulation of surface energy and ZDDP effects on friction in nano-scale lubricated contacts*. Tribology International, 2010. **43**(10): p. 1811-1822.
86. Tabor D., *Surface forces and surface interactions*. Journal of Colloid and Interface Science, 1977. **58**(1): p. 2-13.
87. Demmou K. et al., *Temperature effects on mechanical properties of zinc dithiophosphate tribofilms*. Tribology International, 2006. **39**(12): p. 1558-1563.
88. Pelletier H., C. Gauthier and R. Schirrer, *Relationship between contact geometry and average plastic strain during scratch tests on amorphous polymers*. Tribology International, 2010. **43**(4): p. 796-809.
89. G'Sell C. and J.J. Jonas, *Determination of the plastic behaviour of solid polymers at constant true strain rate*. Journal of Materials Science, 1979. **14**(3): p. 583-591.
90. Johnson K.L., *Contact mechanics*. 1985.
91. Hamilton G.M., *Explicit equations for the stresses beneath a sliding spherical contact*. ARCHIVE: Proceedings of the Institution of Mechanical Engineers, Part C: Mechanical Engineering Science 1983-1988 (vols 197-202), 1983. **197**(1983): p. 53-59.

